JAAVSO

Volume 46
Number 1
2018

The Journal of the American Association of Variable Star Observers

Optical Flares and Quasi-Periodic Pulsations on CR Draconis during Periastron Passage

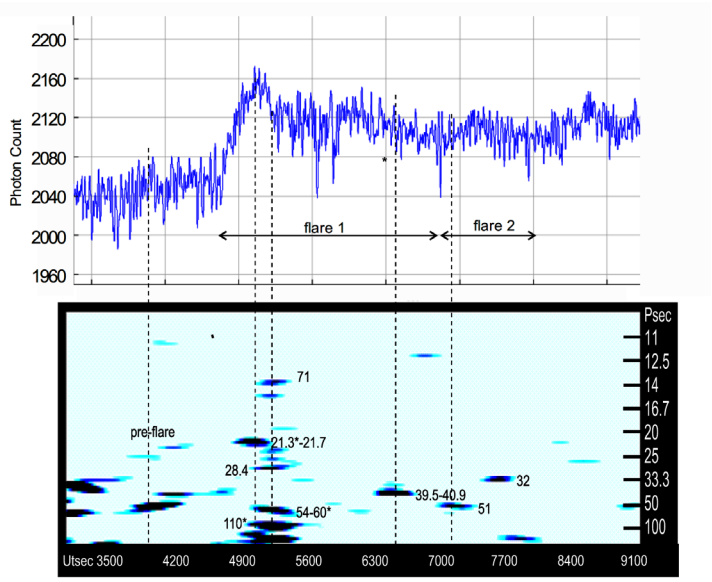

Upper panel: 2017-10-10-flare photon counts, time aligned with FFT spectrogram.

Lower panel: FFT spectrogram shows time in UT seconds versus QPP periods in seconds. Flares cited by Doyle et al. (2018) are shown with (*).

Also in this issue...

Complete table of contents inside...

The American Association of Variable Star Observers
49 Bay State Road, Cambridge, MA 02138, USA

The Journal of the American Association of Variable Star Observers

The Council of the American Association of Variable Star Observers 2017–2018

ISSN 0271-9053 (print)
ISSN 2380-3606 (online)

JAAVSO

The Journal of
The American Association
of Variable Star Observers

Volume 46
Number 1
2018

ISSN 0271-9053 (print)
ISSN 2380-3606 (online)

AAVSO
49 Bay State Road
Cambridge, MA 02138
USA

Publication Schedule

The Journal of the American Association of Variable Star Observers is published twice a year, June 15 (Number 1 of the volume) and December 15 (Number 2 of the volume). The submission window for inclusion in the next issue of JAAVSO closes six weeks before the publication date. A manuscript will be added to the table of contents for an issue when it has been fully accepted for publication upon successful completion of the referee process; these articles will be available online prior to the publication date. An author may not specify in which issue of JAAVSO a manuscript is to be published; accepted manuscripts will be published in the next available issue, except under extraordinary circumstances.

Page Charges

Page charges are waived for Members of the AAVSO. Publication of unsolicited manuscripts in JAAVSO requires a page charge of US $100/page for the final printed manuscript. Page charge waivers may be provided under certain circumstances.

Publication in *JAAVSO*

With the exception of abstracts of papers presented at AAVSO meetings, papers submitted to JAAVSO are peer-reviewed by individuals knowledgable about the topic being discussed. We cannot guarantee that all submissions to JAAVSO will be published, but we encourage authors of all experience levels and in all fields related to variable star astronomy and the AAVSO to submit manuscripts. We especially encourage students and other mentees of researchers affiliated with the AAVSO to submit results of their completed research.

Subscriptions

Institutions and Libraries may subscribe to JAAVSO as part of the Complete Publications Package or as an individual subscription. Individuals may purchase printed copies of recent JAAVSO issues via Createspace. Paper copies of JAAVSO issues prior to volume 36 are available in limited quantities directly from AAVSO Headquarters; please contact the AAVSO for available issues.

Instructions for Submissions

The *Journal of the AAVSO* welcomes papers from all persons concerned with the study of variable stars and topics specifically related to variability. All manuscripts should be written in a style designed to provide clear expositions of the topic. Contributors are encouraged to submit digitized text in MS WORD, LATEX+POSTSCRIPT, or plain-text format. Manuscripts may be mailed electronically to journal@aavso.org or submitted by postal mail to JAAVSO, 49 Bay State Road, Cambridge, MA 02138, USA.

Manuscripts must be submitted according to the following guidelines, or they will be returned to the author for correction:

Manuscripts must be:
1) original, unpublished material;
2) written in English;
3) accompanied by an abstract of no more than 100 words.
4) not more than 2,500–3,000 words in length (10–12 pages double-spaced).

Figures for publication must:
1) be camera-ready or in a high-contrast, high-resolution, standard digitized image format;
2) have all coordinates labeled with division marks on all four sides;
3) be accompanied by a caption that clearly explains all symbols and significance, so that the reader can understand the figure without reference to the text.

Maximum published figure space is 4.5″ by 7″. When submitting original figures, be sure to allow for reduction in size by making all symbols, letters, and division marks sufficiently large.

Photographs and halftone images will be considered for publication if they directly illustrate the text.

Tables should be:
1) provided separate from the main body of the text;
2) numbered sequentially and referred to by Arabic number in the text, e.g., Table 1.

References:
1) References should relate directly to the text.
2) References should be keyed into the text with the author's last name and the year of publication, e.g., (Smith 1974; Jones 1974) or Smith (1974) and Jones (1974).
3) In the case of three or more joint authors, the text reference should be written as follows: (Smith et al. 1976).
4) All references must be listed at the end of the text in alphabetical order by the author's last name and the year of publication, according to the following format: Brown, J., and Green, E. B. 1974, *Astrophys. J.*, **200**, 765.
Thomas, K. 1982, *Phys. Rep.*, **33**, 96.
5) Abbreviations used in references should be based on recent issues of JAAVSO or the listing provided at the beginning of *Astronomy and Astrophysics Abstracts* (Springer-Verlag).

Miscellaneous:
1) Equations should be written on a separate line and given a sequential Arabic number in parentheses near the right-hand margin. Equations should be referred to in the text as, e.g., equation (1).
2) Magnitude will be assumed to be visual unless otherwise specified.
3) Manuscripts may be submitted to referees for review without obligation of publication.

Online Access

Articles published in JAAVSO, and information for authors and referees may be found online at: https://www.aavso.org/apps/jaavso/

The Journal of the American Association of Variable Star Observers
Volume 46, Number 1, 2018

Editorial

Variable Star Research

Variable Star Data

Table of Contents continued on following pages

Review Paper

Abstracts of Papers Presented at the 106th Annual Meeting of the AAVSO, Held in Nashville, Tennessee, November 2–4, 2017

Table of Contents continued on next page

Errata

Editorial

What Use Is Astronomy?

John R. Percy
Editor-in-Chief, *Journal of the AAVSO*

Department of Astronomy and Astrophysics, and Dunlap Institute for Astronomy and Astrophysics, University of Toronto, 50 St. George Street, Toronto, ON M5S 3H4, Canada; john.percy@utoronto.ca

Received May 8, 2018

Why do people such as AAVSOers observe or analyze variable stars? A few readers may simply say that observing is a relaxing, outdoor pastime, like fishing, and that analysis is a way to keep the mind occupied, like solitaire. But most will say "to advance the science of astronomy." But what use is astronomy?

Googling "value of astronomy" usually leads to professional astronomers' websites which emphasize the economic value of astronomy to other sciences, and to engineering, and to society. Often, this is to counter the claim that astronomy is not relevant or useful today. In Canada, an independent study showed that government investment in astronomy repaid itself several times over.

Astronomy has practical value. Almost every civilization has used the sky as a clock, calendar, and compass. Nowadays, we have other technologies for these, but we can intuitively know the time, date, and direction by glancing at the sun or stars. But knowledge of astronomy is now *essential* for understanding space weather, space hazards such as asteroid and comet impacts, and the nature and reality of climate change.

Historically, astronomy spurred the development of mathematics. Now, it spurs the development of high-performance computing, and the analysis of "big data" with artificial intelligence and machine learning. Graduates of astronomy programs are now in demand for a wide range of careers which utilize these powerful skills. Astronomy has led to low-noise radio receivers and other communication technology, and to sensitive detectors and their application to image-processing for fields such as medicine and remote sensing. By providing the ultimate laboratory—the universe—astronomy has also advanced the physical and earth sciences which are the basis of so much of our everyday life.

Over the millennia, astronomy has also occupied a deep spiritual role in society and its culture, and this has led to the relatively new field of "cultural astronomy." Skywatching began as an attempt to understand the nature and cause of earthly and human events—what we now call astrology. The heavens were seen as the abode of the gods, and the sun, moon, and planets represented them in the sky. Buildings, and whole communities were aligned to the sky, especially to the rising and setting points of the sun. For centuries, churches and graves in some Western cultures retained these traditional alignments. The calendar was important for setting the date of religious observances, as it still is today. Eclipses and comets were "omens of disaster." Unfortunately, astrology is still widely accepted, even though there is no evidence for its efficacy, beyond the "placebo effect."

Among the scientific revolutions of history, astronomy and astronomers stand out. Think of Copernicus, Galileo, and Newton. Astronomy continues to resonate deeply with both philosophers and the public. I give numerous non-technical lectures to general audiences. They appreciate learning about the vastness, variety, and beauty of the sky and the universe, and are as excited about black holes as schoolchildren are. In the words of Doug Cunningham, a teacher colleague of mine, astronomy "harnesses curiosity, imagination, and a sense of shared exploration and discovery."

For a 2003 conference of the International Astronomical Union, I outlined the many reasons why astronomy should be part of the school curriculum: www.astro.utoronto.ca/~percy/useful.pdf, and I've been active for many decades in creating curriculum, reviewing textbooks, and providing training and resources for schoolteachers. In addition to the considerations listed earlier, astronomy can be used to illustrate otherwise-boring or difficult topics in math and physics. It requires and enables students to think about vast scales of size, distance, and time. It provides an example of the role of observation and simulation as ways of doing science. It's the ultimate interdisciplinary subject. In my lectures and writings and other outreach activities, I love to explore astronomy's connections to the arts and humanities, and to culture, as well as to other sciences. If properly taught, astronomy can promote rational thinking and an understanding of the nature and value and power of science—something sorely needed in this age of "fake news."

And "the stars belong to everyone." You may have an expensive telescope and CCD camera, but one can still enjoy—and even contribute to—astronomy with binoculars and the naked eye. We need to get young people started as enthusiasts, observers, and "citizen astronomers," to replace the graying, primarily white male observers of today. Astronomy is benign. It is environmentally friendly. It has no borders. It's "one world, one sky." These considerations are important to young people today.

What has this got to do with you, the variable star observer or analyst? First of all: you are adding a brick or two to the wonderful edifice called "the known universe." Astronomy, like other sciences, isn't just big, Nobel-prize-winning discoveries. We all contribute. Your observations help to build the picture which, thanks to popularizers such as Neil deGrasse Tyson,

Stephen Hawking, and Carl Sagan, and Terence Dickinson and Helen Sawyer Hogg in my country, informs and inspires millions. That might include a young student who, attracted to science, will make the discoveries of tomorrow.

And there will be such discoveries. What is the "dark matter" that makes up most of the stuff of the universe? What is the "dark energy" that pushes the universe apart at an accelerating rate? When will we first detect a spectroscopic signature of a biogenic molecule in the atmosphere of an exoplanet?

And in the field of variable stars: what are fast radio bursts (FRBs)? How can we "sharpen" Cepheids and supernovae as tools for determining precise extragalactic distances? And at a more mundane level: what causes the unexplained phenomena in long-period variables—wandering periods, variable amplitudes, and "long secondary periods"—that I and my students study?

But don't leave all the popularizing to the professionals. In addition to your variable star observing and analysis, you can help to advance astronomy through education and public outreach. I've outlined how you can do this, and why (Percy 2017). There are eager audiences out there in your community, from schoolchildren to seniors.

Astronomy has value. Your observations and analyses have value. The AAVSO has value. *JAAVSO* has value—in communicating your contribution to "the known universe" to other AAVSOers and to the rest of the worldwide astronomical community.

Reference

Percy, J. R. 2017, *J. Amer. Assoc. Var. Star Obs.*, **45**, 1.

CCD Photometry and Roche Modeling of the Eclipsing Deep Low Mass, Overcontact Binary Star System TYC 2058-753-1

Kevin B. Alton
UnderOak Observatory, 70 Summit Avenue, Cedar Knolls, NJ; kbalton@optonline.net

Received October 6, 2016; revised February 12, 2018; accepted March 27, 2018

Abstract TYC 2058-753-1 (NSVS 7903497; ASAS 165139+2255.7) is a W UMa binary system (P = 0.353205 d) which has not been rigorously studied since first being detected nearly 15 years ago by the ROTSE-I telescope. Other than the unfiltered ROTSE-I and monochromatic All Sky Automated Survey (ASAS) survey data, no multi-colored light curves (LC) have been published. Photometric data collected in three bandpasses (B, V, and I_c) at Desert Bloom Observatory in June 2017 produced six times-of-minimum for TYC 2058-753-1 which were used to establish a linear ephemeris from the first directly measured Min I epoch (HJD_0). No published radial velocity data are available for this system, however, since this W UMa binary undergoes a very obvious total eclipse, Roche modeling produced a well-constrained photometric value for the mass ratio ($q_{ph} = 0.103 \pm 0.001$). This low-mass ratio binary star system also exhibits a high degree of contact ($f > 56\%$). There is a suggestion from the ROTSE-I and ASAS survey data as well as from the new LCs reported herein that maximum light during quadrature (Max I and Max II) is often not equal. As a result, Roche modeling of the TYC 2058-753-1 LCs was investigated with and without surface spots to address this asymmetry as well as a diagonally-aligned flat bottom during Min I that was observed in 2017.

1. Introduction

The variable behavior of TYC 2058-753-1 was first observed during the ROTSE-I CCD survey (Akerlof *et al.* 2000; Wozniak *et al.* 2004; Gettel *et al.* 2006) and subsequently confirmed from additional photometric measurements taken by the ASAS surrvey (Pojmański *et al.* 2005). The system was classified as an overcontact binary by Hoffman *et al.* (2009). Other than the sparsely sampled photometric readings from the ROTSE-I and ASAS surveys, no other LCs from this binary system were found in the literature. TYC 2058-753-1 is also included in a survey of 606 contact binaries from which accurate colors (BVR_cI_c) were derived (Terrell *et al.* 2012). The paper herein marks the first robust determination of an orbital period and its corresponding linear ephemeris to be published.

Deep, low mass ratio (DLMR) overcontact systems like TYC 2058-753-1 embody a subgroup of W UMa variables with mass ratios (m_2 / m_1) less than 0.25 and degrees of contact (f) greater than 50% (Yang and Qian 2015). Accordingly, these binary systems are approaching a final evolutionary stage before merging into single rapidly-rotating objects such as blue-straggler or FK Com-type stars. DLMR stars are considered an important astrophysical laboratory for studying the dynamical evolution of short-period binary stars in very close contact. In this regard, the Roche-type modeling of TYC 2058-753-1 contained within offers the first published study in which the physical and geometric elements of this system are derived.

2. Observations and data reduction

2.1. Photometry

The equipment at Desert Bloom Observatory (DBO) located in Benson, Arizona, includes a 0.4-m catadioptic telescope mounted on an equatorial fork with an SBIG STT-1603 ME CCD camera installed at the Cassegrain focus. This f/6.7 instrument produces a 17.4 × 11.6 arcmin field-of-view with a 1.36 arcsec/pixel scale (binned 2 × 2). Automated imaging was performed with Astrodon photometric B, V, and I_c filters manufactured to match the Bessell prescription. The computer clock was updated immediately prior to each session and exposure time for all images adjusted to 75 sec. Image acquisition (lights, darks, and flats) was performed using MAXIMDL version 6.13 (Diffraction Limited 2016) or THESKYX version 10.5.0 (Software Bisque 2013) while calibration and registration were performed with AIP4WIN v2.4.0 (Berry and Burnell 2005). MPO CANOPUS v10.7.1.3 (Minor Planet Observer 2015) provided the means for further photometric reduction to LCs using a fixed ensemble of four non-varying comparison stars in the same field-of-view (FOV). Error due to differential refraction and color extinction was minimized by only using data from images taken above 30° altitude (airmass < 2.0). Instrumental readings were reduced to catalog-based magnitudes using the reference MPOSC3 star fields built into MPO CANOPUS (Warner 2007).

2.2. Light curve analyses

Roche type modeling was performed with WDWINT v5.6a (Nelson 2009) and PHOEBE 0.31a (Prša and Zwitter 2005), both of which employ the Wilson-Devinney (W-D) code (Wilson and Devinney 1971; Wilson 1990). Spatial models of TYC 2058-753-1 were rendered with BINARY MAKER 3 (BM3; Bradstreet and Steelman 2002) once W-D model fits were finalized. Times-of-minimum were calculated using the method of Kwee and van Woerden (1956) as implemented in PERANSO v2.5 (Vanmunster 2006).

3. Results and discussion

3.1. Photometry and ephemerides

The four stars in the same FOV with TYC 2058-753-1 (Table 1) which were used to derive MPOSC3-based magnitudes showed no evidence of inherent variability over the interval of image acquisition and stayed within ± 0.007 mag for V–and I_c–and ± 0.017 for B-passbands. Photometric values in B (n = 464), V (n = 478), and I_c (n = 474) were folded by period analysis to generate three LCs that spanned 16 days between June 3 and

Table 1. Astrometric coordinates (J2000) and color indices (B–V) for TYC 2058-0753-1 and four comparison stars used in this photometric study.

Star Identification	*R.A. (J2000)* *h m s*	*Dec. (J2000)* *° ′ ″*	*MPOSC3[a] (B–V)*
TYC 2058-0753-1	16 51 39.43	22 55 43.5	0.822
GSC 2058-0807	16 52 02.94	22 54 10.3	0.743
GSC 2058-0583	16 52 05.65	22 57 16.9	0.674
GSC 2058-0841	16 52 42.02	22 57 16.9	0.463
2MASS 16515918+2256394	16 51 59.06	22 56 39.0	0.387

a. MPOSC3 is a hybrid catalog (Warner 2007) which includes a large subset of the Carlsberg Meridian Catalog (CMC-14) as well as from the Sloan Digital Sky Survey (SDSS).

June 19, 2017 (Figure 1). In total, four primary (p) and two secondary (s) minima were captured during this investigation; the corresponding data (B, V, and I_c) were averaged from each session (Table 2) since no color dependency on the timings was noted. Initially a period determination was made from survey data (ROTSE-I and ASAS) collected between 1999–2009 using PERANSO v2.5 (Vanmunster 2006). The selected analysis method employs periodic orthogonal polynomials (Schwarzenberg-Czerny 1996) to fit observations and analysis of variance (ANOVA) to evaluate fit quality. The resulting orbital period (P = 0.353206 ± 0.000008 d) was very similar to the value cited at the International Variable Star Index website (Watson *et al.* 2014). The Fourier routine (FALC; Harris *et al.* 1989) in MPO CANOPUS provided a comparable period solution (0.353205 ± 0.000001 d) using only the multicolor data from DBO. Finally, after converting magnitude to normalized flux, ROTSE-I, ASAS, and DBO light curve data (HJD; V mag) were then folded together; the best fit was found where the orbital period was 0.353205 ±0.000008 d (Figure 2). As expected with so few data, eclipse timing differences when plotted against period cycle number did not provide any evidence for period change (Figure 3). The first epoch (HJD_0) for this eclipsing binary is therefore defined by the following linear ephemeris equation:

$$\text{Min. I (hel.)} = 2457909.7566\ (3) + 0.353205\ (8)\ E. \quad (1)$$

There is an expectation that while DLMR systems slowly collapse into a higher degree of contact before merger, the orbital period will concomitantly decrease. Since this result is not demonstrably obvious after folding the sparsely sampled survey data (1999–2009) with high cadence LC data acquired in 2017, this hypothesis may not be proven until many more years of eclipse timing data have been collected to determine whether the orbital period of this system undergoes change(s) with time.

3.2. Light curve behavior

LCs (Figure 1) exhibit minima which are separated by 0.5 phase and are consistent with synchronous rotation in a circular orbit typified by W UMa-type variable stars. The flattened bottom at Min I is diagnostic of a binary system that undergoes a total eclipse. Interestingly, LC data from the ROTSE-I and ASAS surveys (Figure 2) exhibit significant variability around Min II suggesting that the deepest minimum likely alternates from time-to-time. The 2017 LCs exhibit asymmetry during

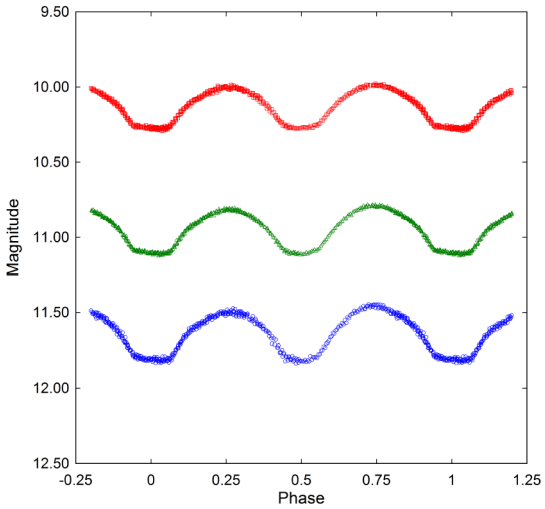

Figure 1. CCD-derived light curves for TYC 2058-753-1 produced from photometric data obtained between June 3 and June 19, 2017. The top (I_c; n = 474), middle (V; n = 478), and bottom curve (B; n =464) shown above were reduced to MPOSC3-based catalog magnitudes using MPO CANOPUS.

Table 2. New times-of-minimum for TYC 2058-753-1 acquired at Desert Bloom Observatory.

ToM HJD–2400000	*UT ± Error*	*Observation Date*	*Type of Minimum[a]*
57909.7566	0.0003	05 June 2017	p
57915.7595	0.0001	11 June 2017	p
57917.6978	0.0002	13 June 2017	s
57921.7631	0.0002	17 June 2017	p
57923.7032	0.0002	19 June 2017	p
57923.8823	0.0002	19 June 2017	s

a. s = secondary; p = primary.

quadrature such that Max I is fainter than Max II (Figure 1). This effect often attributed to O'Connell (1951) has been variously ascribed to the presence of cool starspot(s), hot region(s), gas stream impact on either or both of the binary stars, and/or other unknown phenomena which produce surface inhomogeneities (Yakut and Eggleton 2005). The net result can be unequal heights during maximum light and is often simulated by the introduction of starspots during Roche-type modeling of the LC data.

3.3. Spectral classification

Interstellar extinction (A_V) was estimated using a program (ALEXTIN) developed by Amôres and Lépine (2005) for targets within the Milky Way Galaxy (MWG). In addition to the galactic coordinates (*l, b*) an estimated distance (kpc) to each target is required. The dust maps generated by Schlegel *et al.* (1998) and later adjusted by Schlafly and Finkbeiner (2011) determine extinction based on total dust in a given direction without regard to the target distance. This often leads to an overestimation of reddening within the MWG, most commonly determined as $E(B–V) = A_V / 3.1$. As will be described in section 3.7, the distance to overcontact binary stars can be estimated based on a number of different approaches even in the absence of a directly determined parallax. In this case the adopted

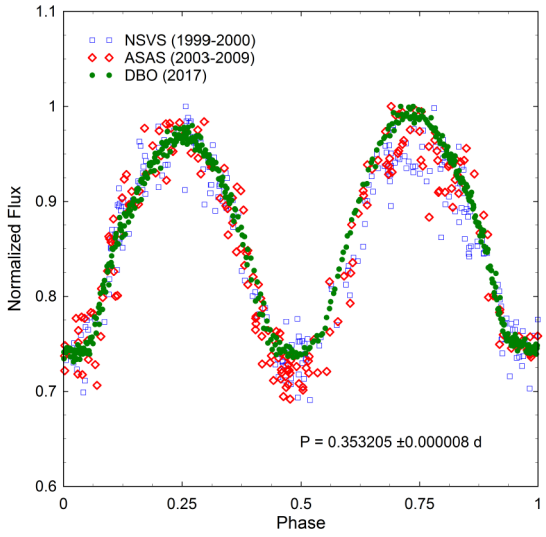

Figure 2. Survey data from the ROTSE-I telescope (NSVS), ASAS Survey, and photometric results (HJD; Vmag) collected at DBO were folded together using period analysis (P = 0.353205 ± 0.000008 d). Greater scatter at phase = 0.50 and 0.75 suggests the presence of an active surface for TYC 2058-753-1.

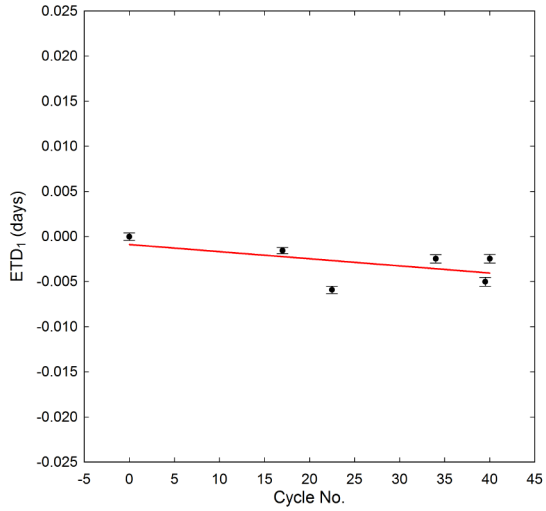

Figure 3. Linear fit of eclipse timing differences (ETD_1) and period cycle number for TYC 2058-0753-1 captured at DBO over 16 days.

Table 3. Spectral classification of TYC 2058-753-1 based upon dereddened (B–V) data from four surveys and the present study.

	Terrell et al. *2005*	*2MASS*	*USNO-A2*	*UCAC4*	*Present Study*
$(B–V)_0$	0.728	0.815	0.774	0.770	0.667
T_{eff1}[a](K)	5506	5282	5353	5370	5703
Spectral Class[a]	G7-G8V	G9-K0V	G8-G9V	G8-G9V	G3-G4V

a. T_{eff1} interpolated and main sequence spectral class assigned from Pecaut and Mamajek (2013). Median value, $(B–V)_0$ = 0.770 ± 0.042, corresponds to a G8V-G9V primary star (T_{eff1} = 5370 K).

distance (~0.190 kpc) results in a reddening value (E(B–V)) of 0.0074±0.0004. Color index (B–V) data collected at DBO and those acquired from an ensemble of four other sources (Table 3) were subsequently dereddened. The median result ($(B-V)_0$ = 0.770±0.042) points to a main sequence primary star with an effective temperature (5370 K) that ranges in spectral type between G8V and G9V (Pecaut and Mamajek 2013).

3.4. Roche modeling approach

Perhaps the greatest obstacle to definitively characterizing the absolute dimensions, geometry, and mass of an eclipsing pair of stars is the general lack of RV data for relatively dim (Vmag > 12) binary systems. This situation is likely to continue until mitigated by the final release of spectroscopic data from the Gaia Mission in 2022. Without RV data, it is not possible to unequivocally determine the mass ratio ($q = m_2/m_1$), total mass or whether TYC 2058-753-1 is an A- or W-type overcontact binary system. Nonetheless, a reliable photometric value for mass ratio (q_{ph}) can be determined but only for those W UMa systems where a total eclipse is observed (Terrell and Wilson 2005). Secondly, in many cases an educated guess about the W UMa subtype (A- or W-) can be made based on general characteristics of each overcontact binary system. Binnendijk (1970) defined an A-type W UMa variable as one in which the deepest minimum (Min I) results from the eclipse of the hotter more massive star by the cooler less massive cohort. By contrast W-types exhibit the deepest minimum when the hotter, but less massive star is eclipsed by its more massive but cooler companion. The published record is very clear that the majority (39 of 46) of DLMR binaries studied thus far appear to be A-type systems (Yang and Qian 2015). By and large, A-type W UMa variables can be characterized by their total mass ($M_T > 1.8\,M_\odot$), spectral class (A-F), orbital period (P > 0.4 d), high degree of thermal contact(f), tendency to totally eclipse due to large size differences, mass ratio (q < 0.3), and the temperature difference ($\Delta T < 100$ K) between the hottest and coolest star (Skelton and Smits 2009). In this case, TYC 2058-753-1 shares attributes from both A- and W-types thereby complicating a definitive assignment without having RV data. Furthermore, LC data from the ASAS (Pojmański *et al.* 2005) and ROTSE surveys survey (Akerlof *et al.* 2000; Gettel *et al.* 2006) suggest that Min I, the deepest minimum, alternates with Min II over time as might be expected from a heavily spotted system. This behavior has been reported for other DMLR overcontact binaries including EM Psc (Qian *et al.* 2008), V1191 Cyg (Ulaş *et al.* 2012), FG Hya (Qian and Yang 2005), and GR Vir (Qian and Yang 2004). Roche modeling of LC data from TYC 2058-753-1 was initially accomplished using the program PHOEBE 0.31a (Prša and Zwitter 2005). The model selected was for an overcontact binary (Mode 3); weighting for each curve was based upon observational scatter. Bolometric albedo ($A_{1,2}$ = 0.5) and gravity darkening coefficients ($g_{1,2}$ = 0.32) for cooler stars (< 7500 K) with convective envelopes were respectively based on the seminal work of Ruciński (1969) and Lucy (1967). The effective temperature of the more massive primary star was fixed (T_{eff1} = 5370 K) according to the earlier designation as spectral type G8V to G9V. Logarithmic limb darkening coefficients (x_1, x_2, y_1, y_2) were interpolated according

to Van Hamme (1993) after any adjustment in the secondary (T_{eff2}) effective temperature. Except for T_{eff1}, $A_{1,2}$, and $g_{1,2}$, all other parameters were allowed to vary during DC iterations. Roche modeling was initially seeded with q = 0.150 and i = 89° based on the similarity between orbital period, effective temperature (T_{eff1}), and light curves for TYC 2058-753-1 and EM Psc (González-Rojas *et al.* 2003; Qian *et al.* 2008). The fit with a slightly higher (+100 K) effective temperature for the secondary was initially investigated since the smaller but potentially hotter star appeared to be occulted at Min I in 2017. This assessment included synthesis of LCs for TYC 2058-753-1 with and without the incorporation of spot(s) to address the negative O'Connell effect (Max II brighter than Max I) and the flattened but diagonally aligned bottom during Min I.

3.5. Roche modeling results

The initial estimates (PHOEBE 0.31a) for q, i, and T_{eff2} converged to a Roche model solution in which the effective temperature of the less massive secondary proved to be slightly higher (> 24 K) than the primary star. Thereafter, final values and errors for T_{eff2}, i, q, $\Omega_{1,2}$, and the spot parameters were determined using WDWINT v5.6a (Table 4). Corresponding unspotted (Figure 4) and spotted (Figure 5) LC simulations revealed that the addition of a cool spot on the primary and a hot spot on the secondary was necessary to achieve the best fit (χ^2) for these multi-color data. Pictorial models rendered (BM3) with both spots using the physical and geometric elements from the 2017 LCs (V-mag) are shown in Figure 6. In this case, these results are consistent with those expected from a W-type overcontact binary system. Nonetheless, it is very clear from the ROTSE-I and ASAS survey data that the deepest minimum for TYC 2058-753-1 can alternate; this most likely occurs due to significant changes in spot location and/or temperature. A subset of LC data (2005–2007) collected during the ASAS survey (Pojmański *et al.* 2005) offers further insight into the challenges faced with trying to unambiguously define this system without supporting RV data. Although the Roche model parameter estimates are more variable (Table 4) from the ASAS survey data, the results suggest that Min I (Figure 7) could arise from a transit of the secondary across the face of the primary star (Figure 8). This scenario is essentially the definition of an A-type W UMa-type system and different from the 2017 findings. Interestingly, the best solution for the 2005–2007 data suggests that the secondary is also hotter (110 K) than the primary, an outcome reported for a large fraction (8/39) of A-type DLMR overcontact binaries (Yang and Qian 2015). The fill-out parameter (f), which is a measure of the shared outer surface volume between each star, was calculated according to Bradstreet (2005) as:

$$f = (\Omega_{inner} - \Omega_{1,2}) / (\Omega_{inner} - \Omega_{outer}), \quad (2)$$

where Ω_{outer} is the outer critical Roche equipotential, Ω_{inner} is the value for the inner critical Roche equipotential, and $\Omega = \Omega_{1,2}$ denotes the common envelope surface potential for the binary system. Since the fill-out value ($f > 0.56$) for TYC 2058-753-1 lies between $0 < f < 1$, the system is defined as an overcontact binary. This high degree of contact in combination with the

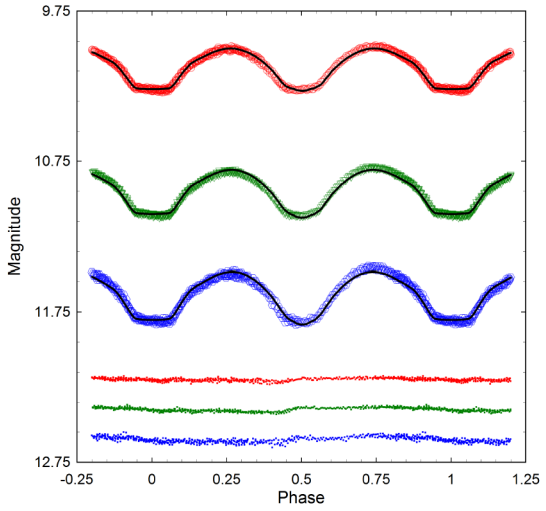

Figure 4. TYC 2058-753-1 Roche model fits (solid-line) of LCs (B-, V-, and I_c-mag) produced from CCD data collected at DBO during 2017. This analysis assumed a W-subtype overcontact binary with no spots; residuals from the model fits are offset at the bottom of the plot to keep the values on scale.

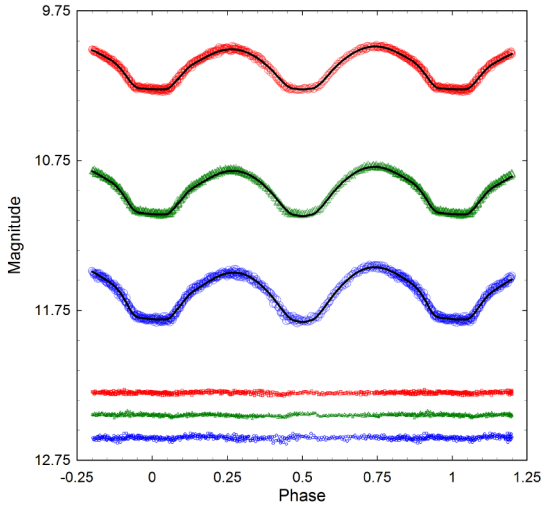

Figure 5. TYC 2058-753-1 Roche model fits (solid-line) of LCs (B-, V-, and I_c-mag) produced from CCD data collected at DBO during 2017. This analysis assumed a W-subtype overcontact binary with a cool spot on the primary and a hot spot on the secondary star; residuals from the model fits are offset at the bottom of the plot to keep the values on scale.

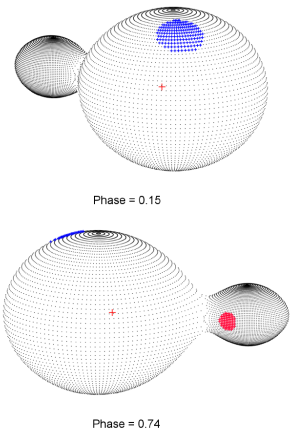

Figure 6. Spatial renderings of TYC 2058-753-1 generated from photometric data (V-mag) acquired in 2017 showing putative locations of a cool spot (blue) on the primary star and a hot spot (red) on the secondary star.

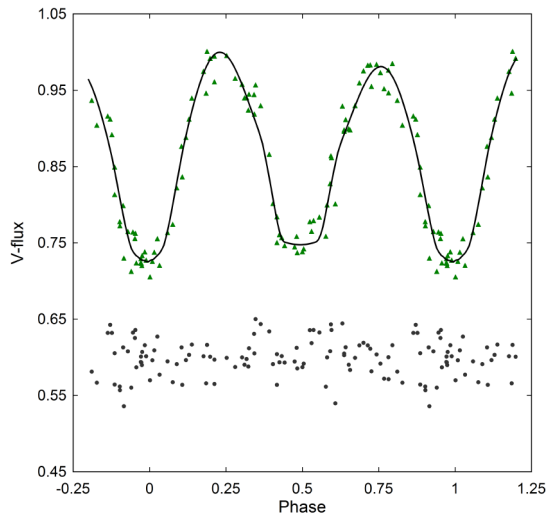

Figure 7. Roche model fit (solid-line) of ASAS survey data for TYC 2058-753-1 acquired between 2005 and 2007. The positive O'Connell effect (Max I > Max II) was simulated by the addition of a cool spot on the less massive secondary component.

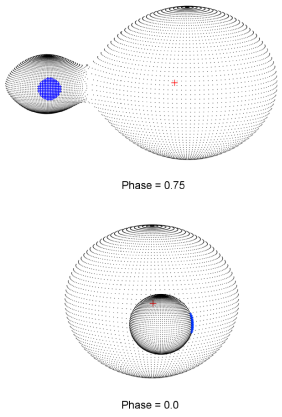

Figure 8. Spatial renderings of TYC 2058-753-1 generated from ASAS photometric data (2005–2007) showing putative location of a cool spot (blue) on the secondary star.

photometrically determined mass ratio ($q_{ph}=0.103\pm0.001$) meets the criteria for what is considered a deep, low mass ratio (DLMR) overcontact binary system. With the exception of AH Cnc, which is a clear outlier, analysis of 23 other DLMR systems (Yang and Qian 2015) shows a strong correlation ($r=0.94$) between spectrophotometric (q_{sp}) and photometric (q_{ph}) mass ratios when both are reported. This is by no means a substitute for having RV data, but it does point out that the q_{ph} value reported herein will likely compare favorably with a more rigorous spectrophotometric determination in the future.

3.6. Absolute parameters

Preliminary absolute parameters (Table 5) were derived for each star in this system using results from the best fit simulation (spotted model) of the 2017 LC. In the absence of RV data, total mass can not be unequivocally calculated; however, stellar mass and radii estimates from binary systems have been tabulated over a wide range of spectral types. This includes a value ($M_1 = 0.98\pm0.05\,M_\odot$) interpolated from Harmanec (1988) and another ($M_1=0.93\pm0.03\,M_\odot$) from Pecaut and Mamajek (2013). Additionally, two different empirical period-mass relationships for W UMa-binaries have been published, by Qian (2003) and later by Gazeas and Stępień (2008). According to Qian (2003) the mass of the primary star (M_1) can be determined from Expression 3:

$$\log M_1 = (0.761\pm0.150)\log P + (1.82\pm0.28), \quad (3)$$

where P is the orbital period in days and leads to $M_1=1.08\pm0.08\ M_\odot$ for the primary. The other mass-period relationship (Equation 4) derived by Gazeas and Stępień (2008):

$$\log M_1 = (0.755\pm0.059)\log P + (0.416\pm0.024), \quad (4)$$

corresponds to a W-type W UMa system where $M_1=1.19\pm0.10\,M_\odot$. The median of all values ($M_1=1.03\pm0.08\ M_\odot$) was used for subsequent determinations of M_2, semi-major axis (a), volume-radius (r_L), bolometric magnitude (M_{bol}), and distance (pc) to TYC 2058-753-1. The semi-major axis, $a(R_\odot)=2.20\pm0.05$, was calculated according to Kepler's third law (Equation 5) where:

$$a^3 = (G\times P^2(M_1+M_2))/(4\pi^2). \quad (5)$$

According to Equation 6 derived by Eggleton (1983), the effective radius of each Roche lobe (r_L) can be calculated to within an error of 1% over the entire range of mass ratios ($0<q<\infty$):

$$r_L = (0.49q^{2/3})/(0.6q^{2/3}+ln(1+q^{1/3})). \quad (6)$$

Volume-radius values were detemined for the primary ($r_1=0.5761\pm0.0003$) and secondary ($r_2=0.2084\pm0.0002$) stars. The absolute solar radii for both binary constituents can then be calculated where $R_1=a\times r_1=1.27\pm0.03\,R_\odot$ and $R_2=a\times r_2=0.46\pm0.01\,R_\odot$. The bolometric magnitude ($M_{bol1,2}$) and luminosity in solar units ($L_\odot$) for the primary and secondary stars were calculated from well-known relationships where:

$$M_{bol1,2} = 4.75 - 5\log(R_{1,2}/R_\odot) - 10\log(T_{1,2}/T_\odot), \quad (7)$$

and

$$L_{1,2} = (R_{1,2}/R_\odot)2\,(T_{1,2}/T_\odot)^4. \quad (8)$$

Assuming that $T_{eff1}=5370\,K$, $T_{eff2}=5394\,K$, and $T_\odot=5772\,K$, the bolometric magnitudes are $M_{bol1}=4.55\pm0.05$ and $M_{bol1}=6.74\pm0.05$, while the solar luminosities for the primary and secondary are $L_1=1.20\pm0.05\,L_\odot$ and $L_2=0.16\pm0.01\,L_\odot$, respectively.

3.7. Distance estimates to TYC 2058-753-1

Using the data generated at DBO, the distance to TYC 2058-753-1 was estimated (183 ± 11 pc) from the distance modulus equation (9) corrected for interstellar extinction:

$$d(pc) = 10^{(m-M_v-A_v+5)/5}, \quad (9)$$

Table 4. Light curve parameters employed for Roche modeling and the geometric elements determined when assuming that TYC 2058-753-1 is an A-type overcontact (2005–2007) or a W-type overcontact binary (2017).

Parameter	*No Spot (2017)*	*Spotted (2017)*	*Spotted (2005–2007)*
T_{eff1} (K)[a]	5370	5370	5370
T_{eff2} (K)[b]	5481 ± 6	5394 ± 4	5511 ± 52
q (m_2 / m_1)[b]	0.102 ± 0.001	0.103 ± 0.001	0.101 ± 0.002
A[a]	0.5	0.5	0.5
g[a]	0.32	0.32	0.32
$\Omega_1 = \Omega_2$[b]	1.928 ± 0.001	1.924 ± 0.002	1.904 ± 0.012
i°[b]	80.13 ± 0.22	78.07 ± 0.16	80.6 ± 3.3
$A_P = T_S / T$[c]	—	0.89 ± 0.01	—
Θ_P (spot co-latitude)	—	35.4 ± 0.3	—
φ_P[c] (spot longitude)	—	133.7 ± 0.5	—
r_P[c] (angular radius)	—	16.2 ± 0.1	—
$A_S = T_S / T$	—	1.18 ± 0.01	0.69 ± 0.21
Θ_S (spot co-latitude)	—	90 ± 2.5	90 ± 20
φ_S (spot longitude)	—	58.3 ± 1.3	270 ± 42
r_S (angular radius)	—	15.0 ± 0.2	20.0 ± 2.1
$L_1 / (L_1 + L_2)_B$[b,d]	0.8575 ± 0.0002	0.8679 ± 0.0001	—
$L_1 / (L_1 + L_2)_V$	0.8639 ± 0.0001	0.8707 ± 0.0001	0.8554 ± 0.0005
$L_1 / (L_1 + L_2)_{I_c}$	0.8689 ± 0.0001	0.8726 ± 0.0001	—
r_1[b] (pole)	0.5452 ± 0.0002	0.5440 ± 0.0001	0.5510 ± 0.0033
r_1 (side)	0.6138 ± 0.0007	0.6118 ± 0.0001	0.6236 ± 0.0057
r_1 (back)	0.6354 ± 0.0008	0.6329 ± 0.0002	0.6467 ± 0.0065
r_2[b] (pole)	0.2068 ± 0.0019	0.2045 ± 0.0008	0.2127 ± 0.0104
r_2 (side)	0.2173 ± 0.0024	0.2146 ± 0.0010	0.2247 ± 0.0131
r_2 (back)	0.2730 ± 0.0078	0.2657 ± 0.0031	0.3060 ± 0.0829
Filling factor	56.5%	64.0%	90%
χ^2 (B)[e]	0.03074	0.01179	—
χ^2 (V)[e]	0.05511	0.01899	0.04609
χ^2 (I_c)[e]	0.14611	0.07703	—

a. Fixed during differential corrections (DC).
b. Error estimates for q_{ph}, i, $\Omega_1 = \Omega_2$, T_{eff2}, $L_1 / (L_1 + L_2)$, spot parameters, r_1, and r_2 (pole, side, and back) from WDWINT v5.6a (Nelson 2009).
c. Primary and secondary spot temperature (A_P; A_S); location (Θ_P,φ_P;Θ_S,φ_S) and size (r_P;r_S)parameters in degrees.
d. Bandpass dependent fractional luminosity; L_1 and L_2 refer to luminosities of the primary and secondary stars, respectively.
e. Monochromatic best Roche model fits (χ^2) from PHOEBE 0.31a (Prša and Zwitter 2005).

Table 5. Preliminary absolute parameters for TYC~2058-753-1 using results from the 2017 spotted Roche model.

Parameter	*Primary*	*Secondary*
Mass ($M_\odot$)	1.03 ± 0.08	0.11 ± 0.01
Radius ($R_\odot$)	1.27 ± 0.03	0.46 ± 0.01
a ($R_\odot$)	2.20 ± 0.05	—
Luminosity ($L_\odot$)	1.20 ± 0.05	0.16 ± 0.01
M_{bol}	4.55 ± 0.05	6.74 ± 0.05
Log(g)	4.25 ± 0.04	4.14 ± 0.04

In this case V_{avg} (m = 10.96 ± 0.11) was used rather than V-mag at Min I since during this time the primary star surface facing the observer is contaminated with a cool spot. M_V is the absolute magnitude derived using the bolometrically corrected magnitude ($M_{bol1} - BC = 4.62 \pm 0.05$), and the interstellar extinction ($A_V = 0.023 \pm 0.001$) was determined as described in section 3.3. Empirical relationships derived from calibrated models for overcontact binaries have also been used to approximate astronomical distances (pc). Mateo and Ruciński (2017) recently developed a relationship between orbital period ($0.275 < P < 0.575$ d) and distance (Tycho-Gaia Astronomic Solution parallax data) from a subset of contact binaries which showed that the absolute magnitude (M_V) can be estimated using expression (10):

$$M_V = (-8.67 \pm 0.65)(\log(P) + 0.4) + (3.73 \pm 0.06). \quad (10)$$

Accordingly the absolute magnitude was calculated to be $M_V = 4.181 \pm 0.069$. Substitution back into Equation 9 yields a distance of 224 ± 14 pc. Another value for distance (167 ± 22 pc) was calculated using Equation 11:

$$\log(d) = 0.2\, V_{max} - 0.18 \log(P) - 1.6\,(J–H) + 0.56, \quad (11)$$

derived by Gettel *et al.* (2006) from a ROTSE-I catalog of overcontact binary stars where d is distance in parsecs, P is the orbital period in days, $V_{max} = 10.81 \pm 0.01$, and (J–H) is the 2MASS color for TYC 2058-753-1. The combined mean distance to this system is therefore estimated to be 191 ± 9 pc.

4. Conclusions

CCD-derived light curves captured in B, V, and I_c passbands produced six new times-of-minimum for the largely ignored W UMa binary system TYC 2058-753-1. A first epoch (HJD_0) linear ephemeris for TYC 2058-753-1 was established, however,

a rigorous assessment of any eclipse timing differences is not possible without many more years of data. There is an expectation that TYC 2058-753-1, like many other DLMR systems, will eventually show a decrease in the orbital period as the binary components collapse into a single rapidly rotating star. An ensemble of reddening corrected (B–V) values from this study and other surveys suggests that the effective temperature of the most luminous star approximates 5370 K, which corresponds to G8V-G9V spectral class. The paucity of published RV data to unambiguously determine a mass ratio (q), total mass, and subtype (A or W) continues to challenge the definitive Roche modeling of newly discovered but relatively dim W UMa binaries. Fortunately this system experiences a clearly defined total eclipse at Min I which helps to constrain a photometrically determined mass ratio result ($q_{ph} = 0.103 \pm 0.001$). Spotted solutions were necessary to achieve the best Roche model fits for TYC 2058-753-1. LCs observed between 1999 and 2009 exhibit similar asymmetry at maximum light in addition to Min I and Min II switching relative to a reference epoch; this suggests that TYC 2058-753-1 has a very active surface. Furthermore, the highly variable nature of these LCs undermines any convincing attempt to define this system as a W-type or A-type overcontact system. Until which time RV data become available, any absolute parameters derived herein for this W UMa binary are subject to greater uncertainty. Public access to the photometric data (B, V, and I_c) acquired in 2017 can be found in the AAVSO International Database at the AAVSO website (https://www.aavso.org/data-download).

5. Acknowledgements

This research has made use of the SIMBAD database, operated at Centre de Données astronomiques de Strasbourg, France, the Northern Sky Variability Survey hosted by the Los Alamos National Laboratory, the All Sky Automated Survey hosted by Astronomical Observatory of the University of Warsaw, and the International Variable Star Index maintained by the AAVSO. The diligence and dedication shown by all associated with these organizations is much appreciated. A special thanks to the *JAAVSO* Editorial staff and the anonymous referee for their support and valuable input.

References

Akerlof, C., *et al.* 2000, *Astron. J.*, **119**, 1901.

Amôres, E. B., and Lépine, J. R. D. 2005, *Astron. J.*, **130**, 650.

Berry, R., and Burnell, J. 2005, *The Handbook of Astronomical Image Processing*, 2nd ed., Willmann-Bell, Richmond, VA.

Binnendijk, L. 1970, *Vistas Astron.*, **12**, 217.

Bradstreet, D. H. 2005, in *The Society for Astronomical Sciences 24th Annual Symposium on Telescope Science*, Society for Astronomical Sciences, Rancho Cucamonga, CA, 23.

Bradstreet, D. H., and Steelman D. P. 2002, *Bull. Amer. Astron. Soc.*, **34**, 1224.

Diffraction Limited. 2016, MAXIMDL version 6.13 image processing software (http://www.cyanogen.com).

Eggleton, P. P. 1983, *Astrophys. J.*, **268**, 368.

Gazeas, K. and Stcępień, K. 2008, *Mon. Not. Roy. Astron. Soc.*, **390**, 1577.

Gettel, S. J., Geske, M. T., and McKay, T. A. 2006, *Astron. J.*, **131**, 621.

González-Rojas, D. J., Castellano-Roig, J., Dueñas-Becerril, M., Lou-Felipe, M., Juan-Samso, J., and Vidal-Sainz, J. 2003, *Inf. Bull. Var. Stars*, No. 5437, 1.

Harmanec, P. 1988, *Bull. Astron. Inst. Czechoslovakia*, **39**, 329.

Harris, A. W., *et al.* 1989, *Icarus*, **77**, 171.

Hoffman, D. J., Harrison, T. E., and McNamara, B. J. 2009, *Astron. J.*, **138**, 466.

Kwee, K. K., and Woerden, H. van 1956, *Bull. Astron. Inst. Netherlands*, **12**, 327.

Lucy, L. B. 1967, Z. Astrophys., **65**, 89.

Mateo, N. M., and Ruciński, S. M. 2017, *Astron. J.*, **154**, 125 (http://arxiv.org/abs/1708.01097v1).

Minor Planet Observer. 2015, MPO Canopus software (http://www.minorplanetobserver.com), BDW Publishing, Colorado Springs, CO.

Nelson, R. H. 2009, WDWINT version 5.6a astronomy software (https://www.variablestarssouth.org/bob-nelson).

O'Connell, D. J. K. 1951, *Publ. Riverview Coll. Obs.*, **2**, 85.

Pecaut, M. J., and Mamajek, E. E. 2013, *Astrophys. J., Suppl. Ser.*, **208**, 9.

Pojmański, G., Pilecki, B., and Szczygiel, D. 2005, *Acta Astron.*, **55**, 275.

Prša, A., and Zwitter, T. 2005, *Astrophys. J.*, **628**, 426.

Qian, S-B. 2003, Mon. Not. R. Astron. Soc., 342, 1260.

Qian, S.-B., He, J.-J., Soonthornthum, B., Liu, L., Zhu, L.-Y., Li, L.-J., Liao, W. P., and Dai, Z.-B. 2008, *Astron. J.*, **136**, 1940.

Qian, S.-B., and Yang, Y.-G. 2004, *Astron. J.*, **128**, 2430.

Qian, S.-B., and Yang, Y.-G. 2005, *Mon. Not. Roy. Astron. Soc.*, **356**, 765.

Ruciński, S. M. 1969, *Acta Astron.*, **19**, 245.

Schlafly, E. F., and Finkbeiner, D. P. 2011, *Astrophys. J.*, **737**, 103.

Schlegel, D. J., Finkbeiner, D. P., and Davis, M. 1998, *Astrophys. J.*, **500**, 525.

Schwarzenberg-Czerny, A. 1996, *Astrophys. J., Lett.*, **460**, L107.

Skelton, P. L., and Smits, D. P. 2009, *S. Afr. J. Sci.*, **105**, 120.

Software Bisque. 2013, THESKYX version 10.5.0 software (http://www.bisque.com).

Terrell, D., and Wilson, R. E. 2005, *Astrophys. Space Sci.*, **296**, 221.

Terrell, D., Gross, J., and Cooney, W. R. 2012, *Astron. J.*, **143**, 1.

Ulaş, B., Kalomeni, B. Keskin, V., Köse, O., and Yakut, K. 2012, *New Astron.*, **17**, 46.

van Hamme, W. 1993, *Astrophys. J.*, **106**, 2096.

Vanmunster, T. 2006, PERANSO v2.5, period analysis software (CBA Belgium Observatory http://www.peranso.com/).

Warner, B. 2007, *Minor Planet Bull.*, **34**, 113.

Watson, C., Henden, A. A., and Price, C. A. 2014, AAVSO International Variable Star Index VSX (Watson+, 2006–2014; http://www.aavso.org/vsx).

Wilson, R. E. 1990, *Astrophys. J.*, **356**, 613.

Wilson, R. E., and Devinney, E. J., 1971, *Astrophys. J.*, **166**, 605.

Wozniak, P. R., *et. al.* 2004, *Astron. J.*, **127**, 2436.

Yakut, K., and Eggleton, P. P. 2005, *Astrophys. J.*, **629**, 1055.

Yang, Y.-G., and Qian, S.-B. 2015, *Astron. J.*, **150**, 69.

A Photometric Study of the Eclipsing Binary NSV 1000

Thomas J. Richards
Pretty Hill Observatory, Kangaroo Ground, Victoria, Australia; tompretttyhill@gmail.com

Colin S. Bembrick
Mount Tarana Observatory, Bathurst, NSW, Australia

Received October 12, 2017; revised December 21, 2017, January 24, 2018; accepted January 24, 2018

Abstract NSV 1000 is an unstudied eclipsing binary in Hydrus. Our photometric research in the period 2014-2016 shows it is a W UMa system with a period of 0.336 579 6(3) d, consistent with the catalogued period. Model fitting to our B, V, and Ic light curves shows the two stars are barely in contact. The parameters derived from the fit satisfy the broadly defined characteristics of a W-type W UMa system.

1. Introduction

NSV 1000 (HV 11909, GSC 9151 0041, ASAS 025619-7431.1, 3UC 031-005816) is a V = 12.75 variable in Hydrus (J2000 02^h 56^m 18.81^s, –74° 31' 03.9"). The GCVS simply lists it as type E (eclipsing) and magnitude 13.5–14.0 (Samus *et al.* 2016). The AAVSO VSX (Watson *et al.* 2014, hereafter VSX) lists it as an EW-type eclipsing binary with a period P = 0.336582 d. Its discovery was reported by Boyce (1943) from a study of photographic plates in the region between the two Magellanic Clouds. That report contains no period or minima timings, simply describing the variable as "Eclipsing or cluster." Except for that one reference, the literature seems to have ignored the star. The ASAS-3 survey (Pojmański 2002) records photometric data for it, folded into a noisy but distinctively EW light curve (Ast. Obs. U. Warsaw 2016) from which S. Otero derived a period and zero epoch which is recorded in the VSX. His elements are E_0 = HJD 2451869.122 (20 November 2000), P = 0.336 582 d, with no uncertainty estimates. The APASS catalogue (Henden *et al.* 2016) gives a color index of 0.727, corresponding to G5-G8 on the Main Sequence.

2. Methods

Richards (AAVSO obscode RIX) carried out 14 nights of time-series observations at Pretty Hill Observatory, Kangaroo Ground, Victoria, Australia (37° 40' 54.0" S, 145° 12' 12.71" E, 163m AMSL), as recorded in Table 1. Instrumentation is an RCOS 41-cm Ritchey-Chrétien reflector equipped with an Apogee U9 camera with a Kodak KAF6303e CCD sensor using Custom Scientific Johnson B, V, and Cousins I_c filters.

All data were calibrated in MUNIWIN (Motl 2007) using bias frames, dark frames and flat-field frames. Photometry was executed in MUNIWIN using comparison and check stars as in Table 2. The APASS catalogue (Henden *et al.* 2016) was used to obtain magnitudes of the Table 2 stars in Johnson B, V, and Sloan *g, r, i* bandpasses, from which I_c magnitudes were derived using the conversions in Munari *et al.* (2014). The comparison star was chosen for having a B–V color index very close to NSV 1000 (0.727 from APASS), eliminating secondary extinction differences; also, being 0.8 magnitude brighter, its contribution to observational errors is reduced.

Table 1. Observations of NSV 1000.

Date (y-m-d)	*Duration (h:m)*	*Filters*
2014-11-11	7:18	B V I_c
2014-11-18	3:49	B V I_c
2014-12-12	2:50	B V I_c
2014-12-13	5:18	B V I_c
2014-12-17	2:22	B V I_c
2014-12-20	3:52	B V I_c
2015-11-22	1:28	B V I_c
2015-11-23	1:23	B V I_c
2015-11-24	6:39	B V I_c
2015-11-26	5:06	B V I_c
2015-12-12	4:54	B V I_c
2016-10-27	1:51	unfiltered
2016-10-28	1:47	V
2016-11-19	6:09	V

3. Results

3.1. Minima and period

Eight of the Table 1 observation sets contained measurable minima—11 minima in all. These times of minima were estimated in PERANSO (Vanmunster 2015) using a fifth-order polynomial fit on un-transformed V data (see Table 3). These are re-measurements since the minima recorded in (Richards *et al.* 2016). Errors are those reported by the fitting algorithm.

Table 2. Comparison (C) and check(K) stars for NSV 1000.

Star	*GSC Ident.*	*R.A. (J2000) h m s*	*Dec. (J2000) ° ′ ″*	*B*	B_{err}	*V*	V_{err}	I_c	$I_{c\,err}$
C	9151 0903	02 55 40.23	-74 29 27.3	13.047	0.011	12.298	0.032	11.543	0.035
K	9151 0875	02 55 08.23	-74 24 52.8	13.752	0.012	13.09	0.0	12.365	0.022

Table 3. NSV 1000, minima estimates. Minima types are primary (P) and secondary (S).

HJD Min.	*Error*	*Type*
2456973.047	0.002	P
2456973.2154	0.0017	S
2457005.022	0.002	P
2457012.090	0.002	P
2457351.026	0.002	P
2457351.1947	0.0017	S
2457353.046	0.002	P
2457369.034	0.002	S
2457690.1305	0.0011	S
2457712.0079	0.0015	S
2457712.1742	0.0015	P

The computer clock was synchronised to a nearby SNTP atomic time service with a variance of < 0.3 sec.

The light elements derived by linear regression from these minima are:

$$En = \text{HJD } 2\,456\,973.0472(4) + 0.336\,579\,6(3)n \text{ d} \quad (1)$$

(Parenthesised numbers are the standard errors in the regression fit, expressed relative to the last digit.)

As a check, we executed a period search in PERANSO using its ANOVA method. This gave $P = 0.336579(5)$ d, which differs from the regression period in equation (1) by 0.1 sigma.

3.2. Light curve

Observations were made of the Southern Landolt field LSE 259 (Landolt 2007) using the same telescope/filter/camera system as for the NSV 1000 observations. From them transformation coefficients were derived to correct raw photometry to the standard system. These had uncertainties, calculated using the standard method of error propagation, of 0.08 magnitude or less. These coefficients were then used to correct the raw instrumental photometric data of NSV 1000.

The 2014 observations were of sufficient quality and coverage to construct complete phased light curves in B, V, and I_c. Later observations were aimed at eclipse phases only. In particular 2015 observations (undertaken in B, V, and I_c in case later observations could be added to give sufficient phase coverage for modelling work) were taken under poor sky conditions with cloud interruptions—too poor in the end for light curve work; further observations were not possible. The 2014 light curves together with the derived color index curves are shown dotted in Figure 2, along with a model fit (solid line, discussed below).

3.3. Light curve analysis

Our B, V, and I_c data were imported into BINARYMAKER3 (hereafter BM3) for light curve analysis (Bradstreet 2005). Input parameters were set as follows. These assume the two stars are in contact. Star 1 is the cooler star.

Effective wavelengths: *B* 4400 Å, *V* 5500 Å, I_c 8070 Å.

Star temperatures: T_1 = 5390 K. This was chosen as the temperature of a main-sequence star with (B–V) = 0.72 (Cox 2000:388). *T*2 is an adjustable parameter.

Gravity brightening: $G_1 = G_2 = 0.32$, the value for convective stars, which have $T_{eff} < 7200$ K (Lucy 1967).

Limb darkening: $X_1 = X_2 = 0.719$, derived from the Van Hamme (1993) tables.

Reflection coefficient: $R_1 = R_2 = \backslash 0.5$, the value for convective stars (Ruciński 1969).

The adjustable parameters are:

T_2, which is adjusted with respect to T_1 to obtain the correct relative depths of the two eclipses.

Inclination *i* of the orbital axis to the observer, which adjusts the absolute depths of the two eclipses.

Fillouts f_1 and f_2, which affect eclipse shapes (equal for stars in contact). There are varying definitions of *f*; we use that of Bradstreet (2005) in which for contact and over-contact binaries (i.e., with surfaces in contact and between the inner and outer Roche surfaces) $0 \le f \le 1$ represents the fractional distance of the surfaces from the inner to the outer Roche surfaces.

Mass ratio $q = m_2/m_1$, where star 1 is the more massive, which affects the relative sizes of the two stars.

These four parameters are not entirely independent of each other, requiring concomitant adjustments of all four to obtain the best match of a computed light curve to an observed one. Of these, T_2 and i are easy to adjust to approximate fits to the light curve. We chose T_2 = 5555 K and $i = 72.5°$ as offering the best initial fits to relative and absolute eclipse depths. Note for W-type W UMa eclipsing binaries the smaller star is hotter and is (partially) occulted in the primary eclipse, so by convention it is star 2. Then we adjusted the two equal fillouts to a value that gave approximate matches to the eclipse shapes, viz. $f = 0.01$. To arrive at the fourth adjustable parameter, *q*, we then conducted a "*q*-search" (see e.g. Liakos and Niarchos 2012) of values of *q* from 0.1 to 0.9 on our V phased data in BM3 to obtain the sum-of-squares residuals for the observed minus calculated (O–C) light curves. Changes to *i* and T_2 invariably made residuals worse—so our initial choices were left as is. These residuals are plotted against *q* in Figure 1.

The *q*-search residuals minimised at $q = 0.3$.Successively finer-grain searches were then executed in a matrix of values of *q* near 0.3 and *f* near 0.01 to find the minimum residual in that region. The best was $q = 0.268$, $f = 0.025$. That same region was then searched in the same way with the *B* and I_c phased data. Small adjustments of all four adjustable parameters were then executed separately in all three bandpasses, resulting in the following best (minimum residuals) values. Table 4 lists the resulting output parameters calculated in BM3 from the assumed parameters and final adjustments of the four adjustable parameters, also listed.

Its last line records the sum-of-squares of residuals in each bandpass.

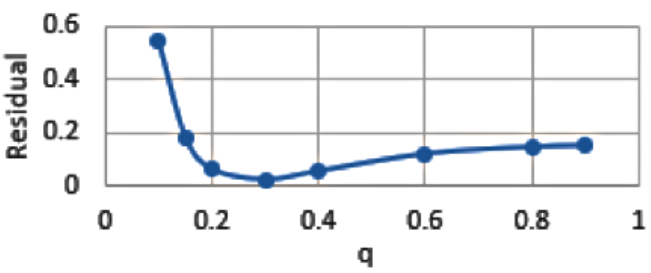

Figure 1. Sum-of-squares residuals plotted against *q* for V-bandpass data.

Table 4. Parameters for NSV 1000. The length unit for the radii, surface area, and volume parameters is orbital major axis = 1.

Parameter	*Bandpass*					
	B		*V*		I_c	
	Star1	*Star2*	*Star1*	*Star2*	*Star1*	*Star2*
			Assumed			
Effective Temperature Teff	5390		5390		5390	
Gravity brightening G			0.32			
Limb darkening coeff. X	0.901		0.719		0.468	
Reflection coefficient R			0.5			
			Adjusted			
Mass ratio m2/m1	0.301		0.269		0.254	
Fillout f	0.024		0.025		0.030	
Inclination i (°)	72.5		72.5		72.5	
Effective Temperature Teff (K)	5555		5555		5485	
			Output			
Omega	7.022		7.538		7.816	
Omega inner	7.037		7.554		7.835	
Omega outer	6.413		6.926		7.205	
Radii: r(back)	0.516	0.307	0.527	0.298	0.532	0.294
r(side)	0.491	0.273	0.502	0.265	0.508	0.261
r(pole)	0.457	0.262	0.465	0.254	0.470	0.250
r(point)	0.620	0.380	0.631	0.369	0.637	0.363
Mean r	0.488	0.281	0.491	0.272	0.503	0.268
Surface area	3.029	1.007	3.153	0.947	3.225	0.920
Volume	0.486	0.093	0.516	0.085	0.533	0.081
Relative luminosity	0.715	0.285	0.742	0.258	0.767	0.233
Sum-of-squares residuals	*0.0501*		*0.0206*		*0.0129*	

The adjusted parameters agree well except the *B* mass ratio is a little higher, as is the I_c fillout. In Figure 2 the resulting model light curves (line) are shown fitted to the observed light curves (dots) in each bandpass. The *B* light curve shows the presence of a slight O'Connell effect, (see e.g. Hilditch 2001:264) Since it is not present in the other light curves, we have not attempted to model it, e.g. by color-sensitive hot or cool spots – which anyway are not likely to be the explanation of the effect.

Figure 3 is a diagram of the system, also showing the inner and outer Roche surfaces, and the centers of mass of each component and the system. Star 1 in the above list is the larger star, on the right in the top diagram of that figure. In accordance with the low fillout, the two stars are joined by a very narrow neck.

The diagram is from the V model – the B and I_c diagrams are indistinguishable from it.

4. Conclusion

From the eleven minima estimates in our data we derived by linear regression the following light elements.

$$En = \text{HJD } 2\,456\,973.0472(4) + 0.336\,579\,6(3)n \text{ d} \qquad (1)$$

Is there evidence of period change? From the VSX light elements, the (*O*–*C*) of the zero epoch E_0 (VSX cycle 15164)

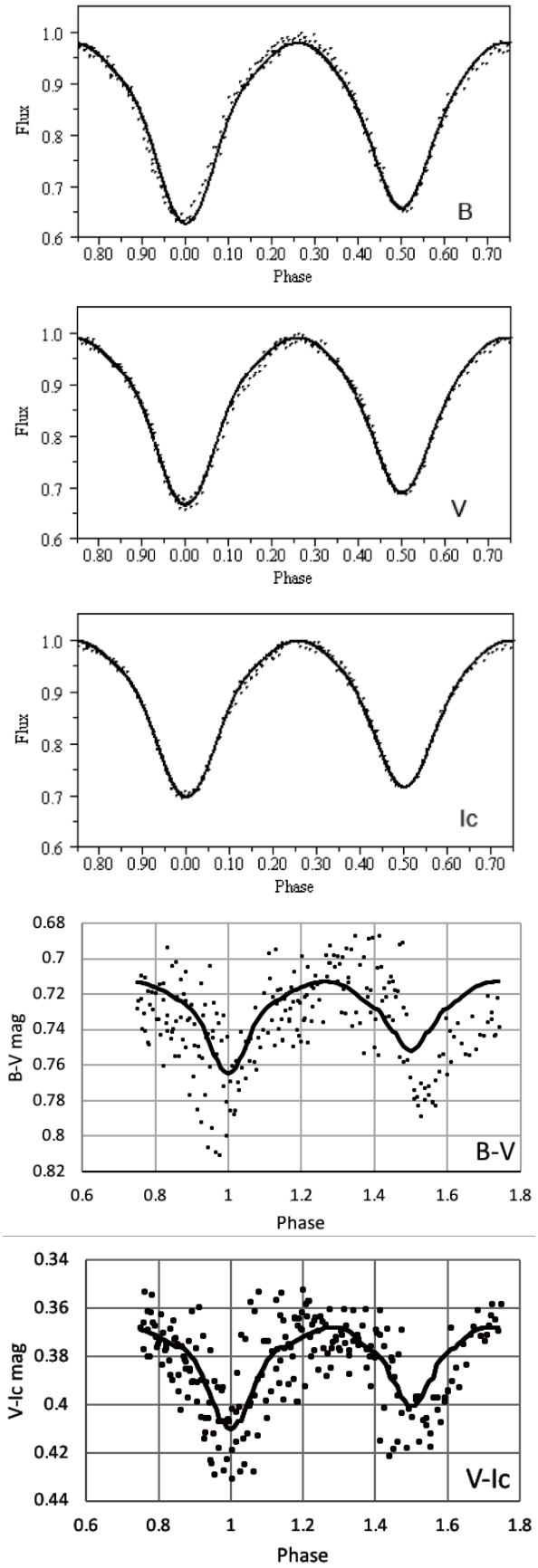

Figure 2. The computed model light curves (line) fitted to the observed phased light curve data points (dots). Top to bottom: B, V, and I_c bandpasses, B–V and V–I_c color indices.

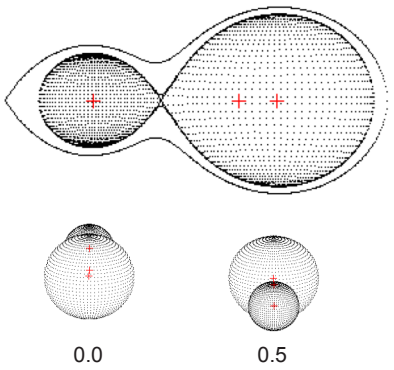

Figure 3. The NSV 1000 system, showing the centers of mass of each star as crosses, and (top) the inner and outer Roche surfaces. Top, phase 0.25 at i = 90.0°. Bottom, phases 0.0 and 0.5 at i = 72.5°.

in Equation 1 is –0.004(2) d. This is ten times the 1-sigma uncertainty on E_0 in Equation 1. The precision error of the VSX E_0 and P is not stated. However a 1-sigma error in the VSX P of 3×10^{-7} d, which is very likely too small since that period is only given to six decimal places, would give an (O–C) error for E_0 in Equation 1 of 0.005 d, sufficient to reconcile calculation with observation. Consequently, within conservatively small error limits, no period change is detected.

The light curve shape (Figure 2) is typical of an EW (W UMa) eclipsing binary. This places the spectral type of the stars as G5 or G8, and temperature ~5390 K (Cox 2000:388). EWs in that temperature range are classified as W-type (Binnendijk 1970). These are characterized by the larger and more massive star being cooler and fainter, unequal eclipse depths of up to 0.1 magnitude, the frequent presence of the O'Connell effect (unequal maxima), mass ratio q = 0.4 to 0.6, slightly over-contact, and both components on or close to the main sequence.

The characteristics of W-type W UMa binaries are satisfied by NSV 1000. Star 1 in the above list is indeed larger, more massive, and cooler. It does have a higher luminosity due to its size, but the unit surface brightness b is less as it must be since it is cooler ($b_1 / b_2 = 0.858$).

When star 1 is placed on the H-R diagram in the position of the (B–V) color index above, it can be seen to be intermediate between spectral classes G5 and G8, very closely similar to the Sun, and with mass 0.85 $M_\odot$ (Cox 2000:389). In that case star 2 at 5555K is G5 and (from q) 0.23 $M_\odot$. (Being less luminous it must be displaced downwards in the H-R diagram and hence to the left of the Main Sequence, as is common with the secondaries of W-types.) Then, from Newton's modification of Kepler's third law, we derive the orbital radius $a = 9.72 \times 10^{-3}$ AU.

Our light curves (Figure 2) show the uneclipsed V magnitude of the system is m = 12.75. Star 1 contributes 0.74 of the luminosity of the entire system, so m_1 = 13.07 in V. The absolute V magnitude of a main sequence star intermediate in G5-G8 spectral class is +5.3, so the distance modulus is 7.77 and distance 358 pc, not allowing for interstellar extinction.

5. Acknowledgements

This research has made use of the International Variable Star Index (VSX) database, operated at AAVSO, Cambridge, Massachusetts, USA; and the AAVSO Photometric All-Sky Survey (APASS), funded by the Robert Martin Ayers Sciences Fund. The authors thank the anonymous referee for suggesting corrections and valuable improvements.

References

Astronomical Observatory of the University of Warsaw. 2016, All-Sky Automated Survey (ASAS; http://www.astrouw.edu.pl/cgi-asas/asas_variable/025619-7431.1,ASAS-3,0.336582,1869.1220,500,0,0, 2016 Nov 24).

Binnendijk, L. 1970, *Vistas Astron.*, **12**, 217.

Boyce, E. H. 1943, *Bull. Harvard. Coll. Obs.*, No. 917, 1.

Bradstreet, D. H. 2005, in *The Society for Astronomical Sciences 24th Annual Symposium on Telescope Science, 23* (http://www.binarymaker.co), Society for Astronomical Sciences, Rancho Cucamonga, California, 23.

Cox, A. N. 2000, *Allen's Astrophysical Quantities*, 4th ed.. Springer, New York.

Henden A. A., *et al.* 2016, The AAVSO Photometric All-Sky Survey, Data Release 9 (http://www.aavso.org/apass).

Hilditch, R. W. 2001, *Introduction to Close Binary Stars*. Cambridge Univ. Press, Cambridge.

Landolt, A. U. 2007, *Astron. J.*, **133**, 2502.

Liakos, A., and Niarchos, P. 2012, *New Astron.*, **17**, 634.

Lucy, L. B. 1967, *Z. Astrophys.*, **65**, 89.

Motl, D. 2007, C-MUNIPACK software (http://c-munipack.sourceforge.net/).

Munari, U., Henden, A., Frigo, A., and Dallaporta, S. 2014, *J. Astron. Data*, **20**, 4.

Pojmański, G. 2002, *Acta Astron.*, **52**, 397.

Richards, T. J., Blackford, M., Butterworth, N., Evans, P., and Jenkins, R. 2016, *Open Eur. J. Var. Stars*, **177**.

Ruciński, S. M. 1969, *Acta Astron.*, **19**, 245.

Samus N. N., Kazarovets, E. V., Durlevich, O. V., Kireeva, N. N., and Pastukhova, E. N. 2016, *General Catalogue of Variable Stars (*GCVS*)*, version 5.1, *Astron. Rep.*, **60**, 1 (http://www.sai.msu.su/gcvs/gcvs/).

van Hamme, W. 1993, *Astron. J.*, **106**, 2096.

Vanmunster, T. 2015, PERANSO light curve and period analysis software (http://www.peranso.com)

Watson, C., Henden, A. A., and Price, C. A. 2014, AAVSO International Variable Star Index VSX (Watson+, 2006–2014; http://www.aavso.org/vsx).

A 1,574-Day Periodicity of Transits Orbiting KIC 8462852

Gary Sacco
3250 SW 195 Terrace, Miramar, FL 33029; gdsacco@hotmail.com

Linh D. Ngo
13980 W 78th Avenue, Arvada, CO 80005; linh@ngo.net

Julien Modolo
Laboratoire Traitement du Signal et de l'Image, 35042 Rennes, France; INSERM, Rennes 1 University, LTSI, Rennes, F-35000, France; julien.modolo@gmail.com

Received November 9, 2017; revised May 8, 2018; accepted May 23, 2018

Abstract Observations of the main sequence F3V star KIC 8462852 (also known as Boyajian's star) revealed extreme aperiodic dips in flux up to 20% during the four years of the *Kepler* mission. Smaller dips (< 3%) were also observed with ground-based telescopes between May 2017 and May 2018. We investigated possible correlation between recent dips and the major dips in the last 100 days of the *Kepler* mission. We compared *Kepler* light curve data, 2017 data from two observatories (TFN, OGG) which are part of the Las Cumbres Observatory (LCO) network, as well as archival data from the Harvard College Observatory (HCO), Sonneberg Observatory, and Sternberg Observatory, and determined that observations appear consistent with a 1,574-day (4.31-year) periodicity of a transit (or group of transits) orbiting Boyajian's star within the habitable zone. Comparison with future observations is required to validate this hypothesis. Furthermore, it is unknown if transits that have produced other major dips as observed during the *Kepler* mission (e.g. D792) share the same orbital period. Nevertheless, the proposed periodicity is a step forward in guiding future observation efforts.

1. Introduction

To identify exoplanetary transits, the *Kepler* mission measured the brightness of objects within a portion of the sky between Cygnus and Lyra over a period of approximately four years (2009 to 2013) with a 30-minute cadence. During this observation period, the mission targeted more than 150,000 stars, finding over 2,300 confirmed exoplanetary transits. Citizen scientists in the Planet Hunters program (2018) helped identify KIC 8462852 via its highly unusual and enigmatic light curve. Yet, additional follow-up ground-based observations reveal an ordinary main sequence F star with no apparent IR excess. The star's light curve exhibits aperiodic irregularly shaped dips ranging from 0.2% to 22.0%. It is intriguing to note that a quasi-periodicity of 24.2 days (between a subset of dips) was identified by Boyajian *et al.* in 2016, and this hypothesized 1,574-day periodicity is equivalent to 24.2×65.0. In that respect, this *Kepler* and Las Cumbres Observatory (LCO) comparison adds additional support to the Boyajian *et al.* (2016) finding. In addition, Boyajian *et al.* (2016) detected a 0.88-day periodicity in the *Kepler* photometric timeseries. They noted that the 0.88-day signal is likely related to the rotation period of the star (84 ± 4 km/s), but a paper published by Makarov and Goldin (2016) suggests this may be due to contamination by another source in the *Kepler* field. It is debatable as to whether this signal originates from a distant companion star.

In the present paper, we examined 2017 ground-based observations and data provided by LCO as they compare to the final set of dips observed in 2013 by the *Kepler* Space Telescope. In addition, we also discuss the possible historical dip detections in October 1978, April 1944, and August 1935. As we detail below, these historical findings align to a 1,574.4-day periodicity.

2. Observations and analysis

2.1. Datasets

Two primary sets were adopted for analysis: The four-year long-cadence *Kepler* photometric time-series and observations from the LCO. First, we used normalized *Kepler* Space Telescope data containing all 1,471 days that the mission observed KIC 8462852 (Figure 1). This photometry is based on subrastered imaging, which are made publicly available as soon as calibration is complete. They can be downloaded from a dedicated data retrieval page at Mikulski Archive for Space Telescopes (MAST; Assoc. Univ. Res. Astron. 2015). It is important also to note that the *Kepler* spacecraft transmitted data once per month, and every three months the spacecraft was rotating to orient its solar cells towards the Sun.

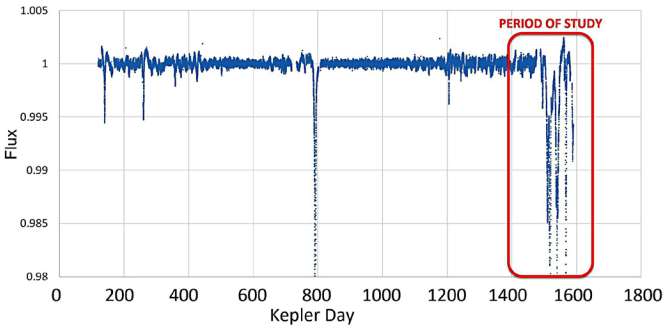

Figure 1. A visual representation of the full *Kepler* light curve for KIC 8462852 (May 1, 2009, to May 11, 2013). The period of study includes a range from D1400 to D1590. Lower limit flux range is limited to 0.98 to allow for clearer illustration of all dip events. Several dips drop significantly deeper, for example, D792, D1519, and D1568 drop by 18%, 22%, and 8%, respectively.

As a result, there are monthly gaps in the observations and a larger gap every three months when the spacecraft was repositioned.

Second, we used r-band daily averages taken by the LCO 0.4-m telescope network as presented in Boyajian *et al.* (2018). The LCO ground-based observations alerted astronomers starting in May 2017 when a nascent dip was observed, later nicknamed Elsie. The Elsie dip was followed by additional dips observed in subsequent LCO observations. For simplicity, we will refer to *Kepler* dips with a "D" followed by the mission day when peak depth was recorded, and we will refer to the 2017 dips by their given names as nominated through Kickstarter contributors (Table 1; note the period (days) between each peak). A mid-July 2017 dip was never named due to its shallow depth. We refer to that dip by the calendar date of peak depth (July 14, 2017) in the remainder of the paper. A comparison of *Kepler* and LCO data is presented in Figure 2.

2.2. Quantifying similarity between 2013 and 2017 dips

In order to quantify the similarity between the dip sequences, which occurred in 2013 (observed by *Kepler*) and in 2017 (observed by the LCO network), we computed different cross-correlograms aiming to identify the periodicity corresponding to an optimal agreement between time-lagged versions of these two signals.

A correlation coefficient measures the extent to which two variables tend to change together. The coefficient describes both the strength and the direction of the relationship. Minitab (2018) offers two different correlation analyses. Correlation coefficients only measure linear (Pearson) or monotonic (Spearman) relationships. We used both cross-correlograms:

• Linear correlation: The Pearson correlation evaluates the linear relationship between two variables. A relationship is linear when there is a change in one variable that is associated with a proportional change in the other.

• Monotonic correlation: The Spearman correlation evaluates the monotonic relationship between two variables. In a monotonic relationship, the variables tend to change together, but not always at a constant rate. This correlation coefficient uses ranked values for each variable.

We note that these cross-correlograms were applied to the raw data, without any detrending or normalization.

Table 1. Comparison of *Kepler* (2013) and LCO (2017) peak dip dates.

Dip	*Observatory*	*Peak (MJD)*	*Period (Days)*
D1487	*Kepler*	56319	—
Elsie	OGG	57893	1574
D1519	*Kepler*	56351	—
Celeste	TFN	57925	1574.6
D1541	*Kepler*	56373	—
Mid-July	OGG	57948	1575
D1568	*Kepler*	56400	—
Skara Brae	TFN	57974	1574.5

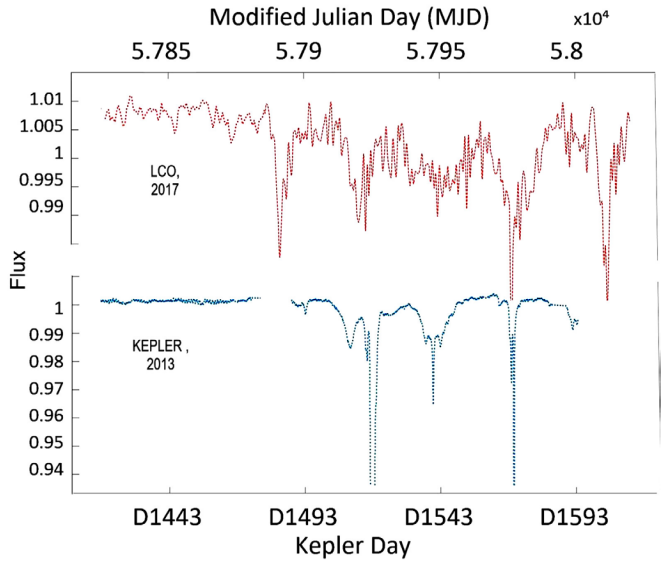

Figure 2. *Kepler* (bottom) light curve for KIC 8462852 (Nov 2, 2012 to May 11, 2013) compared to LCO (top) light curve (Feb 22, 2017, to Sep 19, 2017) using a 1,574-day periodicity. Note that LCO first started observations in February 2017 and recorded no dips prior to Elsie, which is visually consistent with *Kepler* during the same period. Also note that breaks in the *Kepler* line curve represent missing data due to malfunction or changing orientation of the space telescope. LCO data are displayed with an overall moving average applied.

3. **Results**

3.1. Hypothesis

We produced cross-correlograms of data from the LCO network and *Kepler*. Since the amount of data was not sufficiently large, it was not our intent to use correlation tests to establish statistical significance. We used such tests to support our pre-existing goodness of fit hypothesis of 1,574 days periodicity that we found by matching the *Kepler* and LCO light curves. After performing the correlation, we found three plausible dip matchings, but only one (1,572) worked in terms of lining up the *Kepler* Q4 light curve vs the LCO 2017 light curve. Therefore, these tests supported the original hypothesis. However, statistical significance has not been reached yet, which will need further observational data to reach this benchmark.

In the comparison of *Kepler* to LCO data, it is worth pointing out the differences in observation frequency between the two. *Kepler* data have a higher sampling rate (one point every 29.4 minutes). While LCO used two observatories, the rates are significantly lower due to required night coverage and weather conditions. Since *Kepler* has data gaps that might bias results in favor or against non-dips/dips if interpolated, we skipped any comparisons falling within a *Kepler* gap of half a day or more. The results produced by both methods show three potential correlations suggesting a possible periodicity of either: ~1,540 days, ~1,572 days, or ~1,600 days.

A cross-correlogram based on Pearson's Product Moment is presented in Figure 3. Our three matching hypotheses are depicted in the cross-correlogram, corresponding to periods of 1,540, 1,572, and 1,600 days, respectively. Both peaks have similar correlation values; however, the peak corresponding to hypothesis 1 is brief. The peak of hypothesis 2 is broader, suggesting there is greater flexibility in terms of finding a good match and that this periodicity is more robust. A third peak

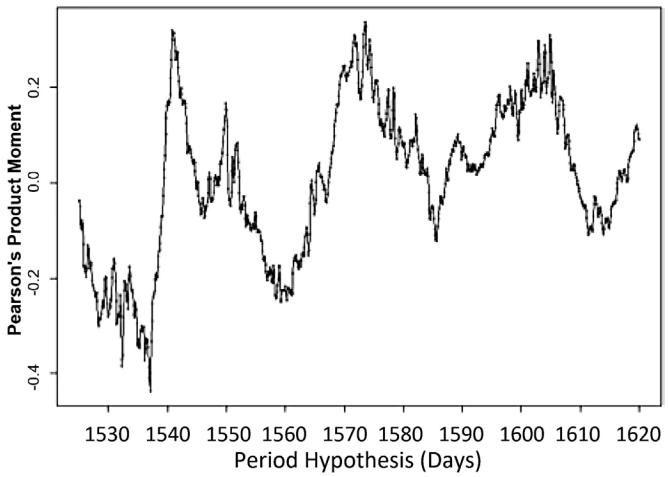

Figure 3. Cross-correlogram between *Kepler* and LCO data based on Pearson's Product Moment. Maximum values suggest a correlation between both datasets.

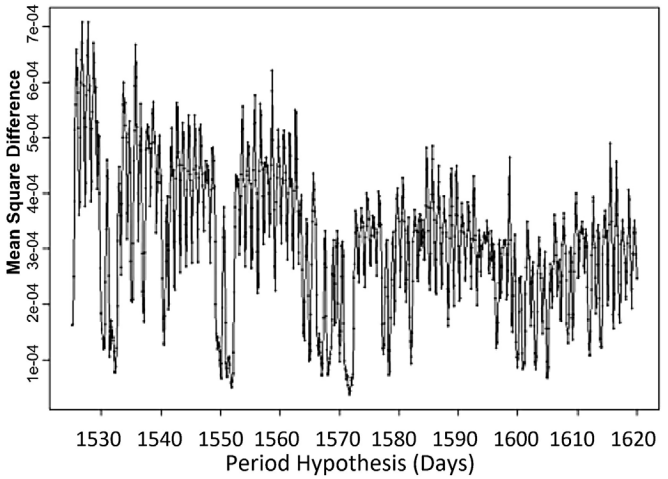

Figure 4. Mean squared error between the *Kepler* and LCO data for different values of hypothetical periodicities. Minimum values suggest a potential correlation between both datasets.

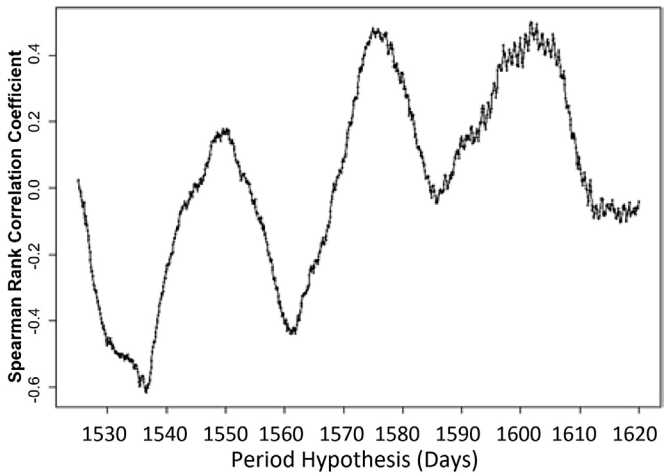

Figure 5. Cross-correlogram computed using Spearman's rank-based correlation. Maximum values suggest a possible correlation between both datasets.

corresponding to 1,600 days, while broad, is clearly shallower than the first two hypotheses.

Since Pearson's Product Moment is a normalized covariance metric, favoring matching between signals of similar phase and frequency but irrespective of amplitude, we also examined the average square differences between the time series for different period hypotheses (Figure 4). In this case, we were looking for minima. While the average of square differences is clearly a less stable metric, it also supports our view that hypothesis 2 appears more plausible than hypothesis 1.

Finally, and most importantly, we found a rank-based correlation in Spearman's decisively favored hypothesis 2, as shown in Figure 5. A rank-based correlation only considers how well the order of observations matches across both time series and does not consider flux values beyond their use in sorting observations.

In summary, in two of the three correlation analyses conducted, hypothesis 2 (1,574 days) had a slightly higher plausibility. Also, the Spearman's rank-based correlation more clearly favors hypothesis 2. In the end, all three methods point to hypothesis 2.

3.2. Hypothesis 2: visual comparison of *Kepler* D1487 to D1590 to LCO May–Sep 2017

The final days of *Kepler* (Figure 1) are an interesting and active period presenting an intriguing result for this analysis. Since there is a series of dips within its last approximately 100 days, it provided an ideal visual test to all three hypotheses. We created three overlay line graphs (1540, 1572, 1600) and found only one with clear visual alignment (1572). Both hypotheses 1 and 3 failed to align visually, and given this, we discontinued consideration of these two results.

Using the favored hypothesis 2 (1,572-day periodicity), our analysis then focused to more precisely refine this by visually inspecting each light curve comparison overlay. We performed this analysis and highlighted each result in the following sections. This review included the same period of *Kepler* days 1,401 to 1,609 with the LCO light curve from 57807 to 58015 (Modified Julian Date). We find that overall a 1,572-day period compares well; however, a slightly refined periodicity of 1,574 provides a more precise visual fit. We examine each dip correlation (*Kepler* vs LCO, Figure 6) in the subsequent sections using a 1,574-day periodicity.

The LCO "Elsie" observation during May of 2017 is an interesting fit because when you subtract 1,574 days, you arrive in the *Kepler* data during a period in which no observations were being made. It turns out that over the four years of the *Kepler* mission, observations were interrupted for a variety of reasons. On a regular basis the spacecraft rotated and recalibrated causing a short down-period of observations. In other cases, mechanical failures caused more extended lapses, as for example between the *Kepler* period 1,477 and 1,489 when no observations were made. Based on a 1,574-day periodicity, we hypothesize that a dip corresponding to Elsie started on *Kepler* day 1,484 and ended on day 1,489 but was not observed by *Kepler* (Figure 6).

We compare the LCO "Celeste" dip to the *Kepler* D1519 dip. We note that there are only about 23 LCO observations to characterize Celeste whereas there are over 900 observations

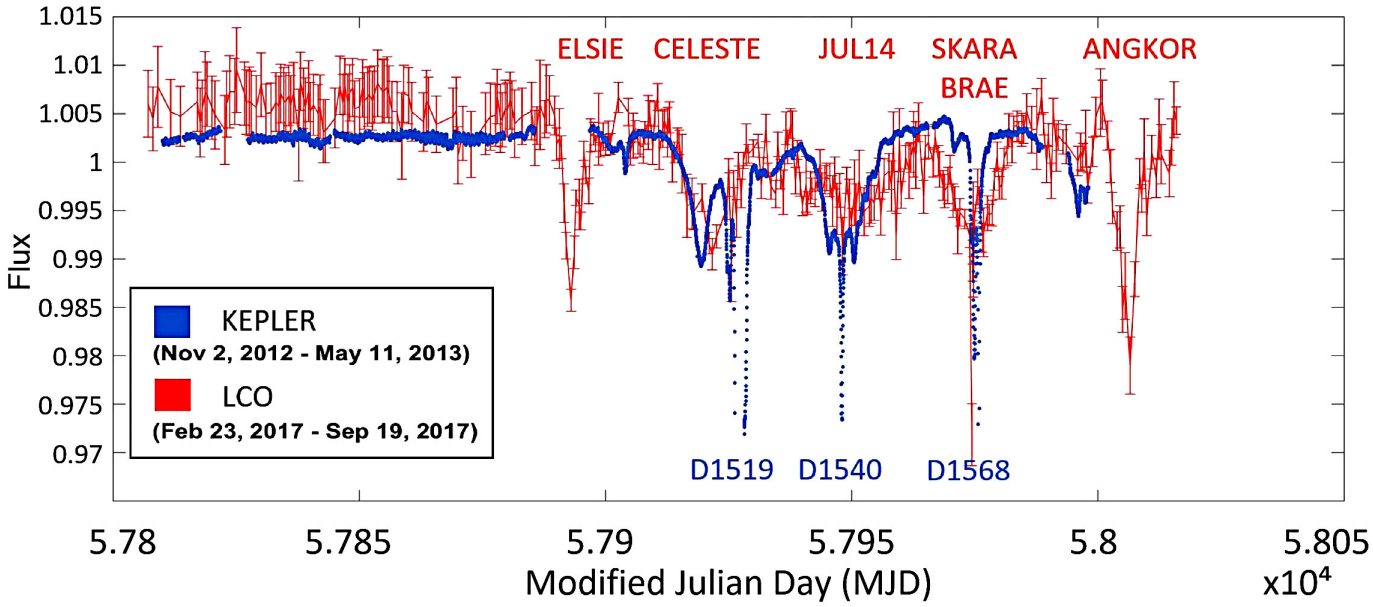

Figure 6. This overlay compares the final *Kepler* dips in 2013 to the more recent ground-based observed dips of 2017. Using the clear favored hypothesis 2 (1,574-day periodicity), we overlaid the *Kepler* light curve from day 1,401 to 1,609 with the LCO light curve from 57807 to 58015 (Modified Julian Date). Missing periods of blue (*Kepler*) light curve are due to lapses of observation from the space telescope.

which depict D1519. Yet, even with the limited number of observations, the depression in the light curve, and timing of both peak and overall duration, during this epoch is clear (Figure 6).

Next, we compared D1540 to the LCO depression that peaked on about July 14, 2017. Both D1540 and the July 14, 2017, event were a complex set of dips and sub-dips (Figure 6). These dips were also the shallowest when compared to the other dips highlighted in the present paper. Ground-based observations in 2017 only detected a maximum depression of 1.12%. However, the timing of dips across what appears to be a complex and lengthy period is correlated. The maximum dip intensity during this period was recorded by LCO on July 14, 2017, and 1,575 days earlier, the maximum intensity of that D1540 dip was recorded.

On August 9, 2017, the Skara Brae dip peaked at almost 3%. 1,574 days prior, *Kepler* D1568 peaked as well (Figure 6, Table 1). Again, there is good agreement in the timing of each event's maximum dip amplitude and duration of the dip.

While a clear matching of duration and peak dip timing between *Kepler* Q4 and LCO 2017 can be seen, the dip intensity is different. Boyajian *et al.* (2018) point out that dip intensity may be expected to change on subsequent orbits if what we are seeing are small dust particle concentrations. This is because such optically thin dust (with a size scale < 1 micrometer) would be quickly blown out of the system. Thus, for each subsequent orbit, the amount of new dust being blown off would likely be different, causing a changing depth of stellar dimming.

3.3. 1,574-day period and a look back at *Kepler*

When we merge *Kepler* with Elsie and Angkor via a 1,574-day period, some symmetry is apparent in both overlaid light curves (Figure 6). Dip D1540, sometimes described as a triplet, might be visualized as the centroid of a group of dips. Similarly, the 2017 LCO dips might be an approximately symmetric group with a centroid around July 14, 2017.

3.4. Other observations and pre-Elsie comparison to *Kepler*

There are no reported and/or confirmed dips detected since the end of the *Kepler* mission and prior to Elsie. Data sources for this period include, but are not limited to: AAVSO, LCO, SWIFT, Spitzer, ASAS (or ASAS-SN), and Bruce Gary's observations (Gary 2017). These sources had various start times of regular observations and differing degrees of accuracy. For example, it is unlikely that AAVSO could detect dip intensities lower than 0.5%. All these other sources are consistent in that no dips were detected prior to Elsie, which is another factor supporting a 1,574-day periodicity. Consequently, it is reasonable to conclude the epoch between August 25, 2016, and May 7, 2017, as consistent with *Kepler* as having nominal flux.

4. Testable predictions

It should be noted that at the time of this paper, no space-borne missions are collecting daily observations of KIC 8462852. Future observations should strive to obtain measurements with night-to-night differential photometry. Consequently, upcoming predictions will need to be monitored closely since they are very small (0.2–0.5%) and might be challenging to detect. On the other hand, a major dip or an attenuated/altered variant might be expected during a hypothesized return of D792 (a 16% dip) on October 17, 2019, assuming this transit is on the same 1,574-day orbit. Table 2 provides a list of all *Kepler* dips with the next occult using a 1,574-day period.

We raise the possibility that a 1,574-day periodicity presents opportunities for confirmation of the largest dips in observatory archival media. As such, we have calculated and identified historical dates in which one of *Kepler*'s deepest dip (D1519 approximately 20% and D1568 approximately 8%) might be observed on such plates (Tables 3 and 4).

The *Kepler* mission made observations of KIC 8462852 every 29.4 minutes from May 1, 2009, up until May 11, 2013,

Table 2. Testable Predictions. A summary of the predicted recurrence of future dips based on the approximate 1,574-day periodicity.

Dip	*Name*	*Depth (%)*	*Date of Next Dip*
1	D140	0.5	3 Jan 2018
2	D260	0.5	3 May 2018
3	D359	0.2	9 Aug 2018
4	D425	0.2	14 Oct 2018
5	D792	16.0	17 Oct 2019
6	D1205	0.4	3 Dec 2020
7	D1487	2.0	10 Sep 2021
8	D1519	21.0	13 Oct 2021
9	D1541	3.0	3 Nov 2021
10	D1568	8.0	1 Dec 2021
11	Angkor	3.2	22 Jan 2022

Note: Only dips associated with the Kepler *light curve between 1,500 and 1,590 can be predicted with high confidence. The remaining dip predictions assumes all objects are on the same 1,574-day orbit.*

when it experienced a fatal mechanical failure involving a second reaction wheel. Therefore, *Kepler* observations covered a total of 1,471 days, a period that is approximately 102 days less than the hypothesized 1,574-day periodicity. Consequently, there is a 102-day period in which no *Kepler* -based predictions can be made.

5. Discussion

We have proposed a 1,574-day periodicity that explains the striking similarity between the complex sequence of dimming events of KIC8462852 observed during the last two quarters of the *Kepler* mission and dips observed more recently from the ground. This result is certainly subject to the poor sampling due to limited number of orbital observations. However, if this hypothesized 1,574-day periodicity is confirmed by further observations, we can calculate the transiting bodies' orbit radius, assuming it is circular. Such a calculation reveals an interesting implication in that orbiting material, causing the complex light curve, would be located at approximately 2.983 AU. This distance is within the habitable zone confined to 2.174 and 3.132 AU, based on an absolute magnitude of 3.08 and a bolometric correction of –0.15 required for an F-star such as KIC 8462852. If this 1,574-day periodicity is verified, one major challenge will be to understand how circumstellar material located at 3 AU from the star can result in such a complex sequence of dimming events. It is however worth pointing out that astronomer Bruce Gary (2018) mentioned that he may have detected a small (~1%) dimming event on May 3, 2018. This date coincides exactly with the expected return of *Kepler* D260 × 2 (Table 2).

While we eagerly await what future observations will bring us, we can already look back at historical results using archived observatory plates. To that end, Castelaz *et al.*'s (2018) examination of KIC 8462852 historical photographic plates archived at the Maria Mitchell Observatory provides evidence in support of a 1,574.4-day periodicity. In their paper, Castelaz *et al.* (2018) identified five possible short term dimming events / dips. As in all observatory archives, there are sporadic historical observations of KIC 8462852 (some not occurring for weeks, months, etc., between observations). However, the identification of five dips presents an excellent opportunity to compare against the *Kepler* and 2017 LCO observations using a 1,574.4-day periodicity. Out of the five historical dips identified, only two of them would have fallen within the same window of time using *Kepler* data from D1487 to D1568, and LCO data from May 2017 to September 2017. For these two dips that did fit our window, our question was, do they align precisely to any

Table 3. Correlation of D1568 to earlier cycles.

Epoch (–D1568)	*1,574-day periodicity*	*1,574.4-day periodicity*
1	9 Aug 2017	9 Aug 2017
0	18 Apr 2013	18 Apr 2013
–1	26 Dec 2008	26 Dec 2008
–2	4 Sep 2004	3 Sep 2004
–3	14 May 2000	13 May 2000
–4	22 Jan 1996	20 Jan 1996
–5	1 Oct 1991	29 Sep 1991
–6	10 Jun 1987	8 Jun 1987
–7	17 Feb 1983	14 Feb 1983
–8	27 Oct 1978	24 Oct 1978
–9	6 Jul 1974	2 Jul 1974
–10	15 Mar 1970	11 Mar 1970
–11	22 Nov 1965	18 Nov 1965
–12	1 Aug 1961	27 Jul 1961
–13	10 Apr 1957	5 Apr 1957
–14	18 Dec 1952	12 Dec 1952
–15	27 Aug 1948	21 Aug 1948
–16	6 May 1944	30 Apr 1944
–17	14 Jan 1940	7 Jan 1940
–18	23 Sep 1935	16 Sep 1935
–19	2 Jun 1931	25 May 1931
–20	9 Feb 1927	1 Feb 1927

Note: The calculated timing of potential past occurrences of D1568 based on an approximate 1,574-day periodicity.

Table 4. Correlation of D1519 to earlier cycles.

Epoch (–D1519)	*1,574-day periodicity*	*1,574.4-day periodicity*
1	21 Jun 2017	21 Jun 2017
0	28 Feb 2013	28 Feb 2013
–1	7 Nov 2008	7 Nov 2008
–2	17 Jul 2004	16 Jul 2004
–3	26 Mar 2000	25 Mar 2000
–4	4 Dec 1995	2 Dec 1995
–5	13 Aug 1991	11 Aug 1991
–6	22 Apr 1987	20 Apr 1987
–7	30 Dec 1982	27 Dec 1982
–8	8 Sep 1978	5 Sep 1978
–9	18 May 1974	14 May 1974
–10	25 Jan 1970	21 Jan 1970
–11	4 Oct 1965	30 Sep 1965
–12	13 Jun 1961	8 Jun 1961
–13	20 Feb 1957	15 Feb 1957
–14	30 Oct 1952	24 Oct 1952
–15	9 Jul 1948	3 Jul 1948
–16	18 Mar 1944	12 Mar 1944
–17	26 Nov 1939	19 Nov 1939
–18	5 Aug 1935	29 Jul 1935
–19	14 Apr 1931	6 Apr 1931
–20	22 Dec 1926	14 Dec 1926

Note: The calculated timing of potential past occurrences of D1519 based on an approximate 1,574-day periodicity.

of the *Kepler* and LCO dips using a 1,574.4-day periodicity? We find that both of the two Castelaz *et al.* identified dips precisely match to the day:

Maria Mitchell Observatory Match 1:
Skara Brae minus 1574 = *Kepler* D1568
Kepler D1568 minus (1574.4 × 9) = October 22,1978

Maria Mitchell Observatory Match 2:
July 2017 dip minus 1574 = *Kepler* D1542
Kepler D1542 minus (1574.4 × 18) = August 21,1935

Castelaz *et al.*'s, other three dips (using 1,574.4) would have fallen outside of the 2017 events historically. This may lend support that other *Kepler* dips (beyond D1487–D1568) are on a different orbit, although this point is completely unclear at this time. That being said, the July 16, 1966, dip is 30 days of D260 and the October 1980 dip is 80 days of D792. It is worth noting that Castelaz *et al.* used eight comparison stars and had a mean uncertainty 0.07 magnitude and the 1978 dip dimmed by at least 10% increasing this sigma result. Furthermore, first identified by Hippke *et al.* (2017), there is a second observation of the October 22, 1978, dip by another observatory (Sternberg, Figure 7). Hippke *et al.*, examined historical plate data from the DASCH digital archive, managed by the Harvard College Observatory (HCO 2016), and from Sonneberg, and Sternberg observatories. Specifically, we reviewed the brightness magnitude (as found by Hippke *et al.*) of KIC 8462852 on the dates as found within Tables 3 and 4, which are the dates that we would expect to find a dip using a 1,574 and 1,574.4-day periodicity and subtracting from both D1519 and D1568. Using these three observatories, there were two observations made of this star during these calculated dates: October 24, 1978 at 8% (Sternberg) and April 30, 1944 at 6% (DASCH).

The Sternberg finding is an intriguing observation because it fits the same data found by Castelaz *et al.* (2018), using completely different plates (Maria Mitchell Observatory). The Sternberg finding was first identified by Hippke *et al.* (2017) and is a potential 8% dip occurring around October 24, 1978 (Table 3, epoch 8 at 1,574.4-day periodicity). Given the two separate observatories, and quality of plates, we believe the 1978 dip to be a multi-sigma detection.

But what about the April 30, 1944, plate within the DASCH archive? Once again using a 1,574.4-day periodicity, we find that D1568 and Skara Brae should have been observable during this exact date in 1944. DASCH records show that indeed this star did dim by 0.07 magnitude (approximately 6%). However, while interesting in itself yet another positive result, there was only one plate and the plate quality is poor. Nonetheless, we are adding this finding within this discussion as it demonstrates our overall effort to determine historical results.

In the original "Where's the Flux" paper, Boyajian *et al.* (2016) noted the apparent occurrence of dip separations that are multiples of 48.4, in some cases at half phase, or 24.2 days. For example, the separation between dips D792 and D1519 is approximately 15 periods of 48.6 days. We note that the proposed period of 1,574 days is equivalent to 65 even periods of 24.2 days, even if the relevance, if any, of this ratio value

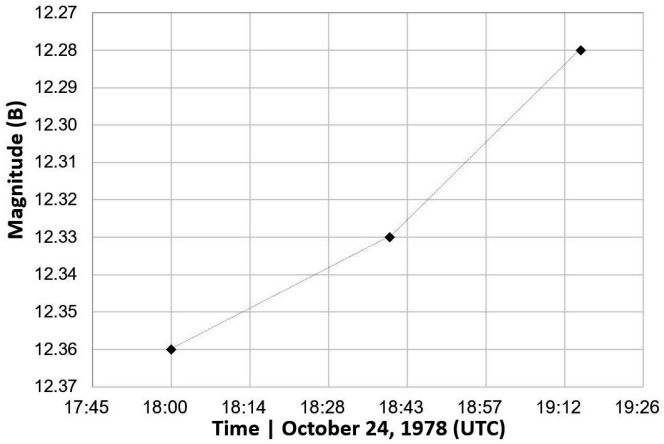

Figure 7. Graph representing depression of light for KIC 8462852 on three separate Sternberg plates from October 24, 1978. This finding of a potential dip was made by Hippke *et al.* (2017).

remains to be determined. Still, this is yet again another apparent result involving 24.2 (1574.0 / 24.2 = 65.0).

Based on this hypothesized periodicity, we provide testable prediction (historical and future) dates of possible dimming events. Should these predictions be verified, this would not only validate this periodicity hypothesis, but it would constitute a new set of extraordinary observations relating to this peculiar star and would be a significant step forward in understanding the underlying mechanisms behind these dimming events.

6. Conclusion

On the basis of several sources of photometric data for KIC 8462852 covering the longest epoch possible, we have provided support for a 1,574-day periodicity of the complex dimming events that have been observed in the light curve by the *Kepler* mission and ground-based telescopes. Based on this periodicity, we formulated testable predictions regarding the exact timing of historical and future events. If confirmed, this periodicity would constrain further the mechanisms at play in this unique and fascinating solar system, notably involving circumstellar material orbiting the star in its habitable zone at approximately 3 AU.

7. Acknowledgements

The authors thank Dr. Tabetha Boyajian for her assistance in both providing access to LCO network data regarding KIC 8462852, and invaluable commentary on this manuscript. We would also like to point out that this paper would not have been possible without her Kick-Starter initiative which ultimately resulted in LCO observations.

We also thank Jose Solorzano for his useful cross correlation suggestions and manuscript comments. We also thank Michael Hippke for his comments on the paper and for providing archival plate data for Sonneberg, DASCH, and Sternberg. Finally, the authors acknowledge the support of the DASCH project at Harvard by partial support from NSF grants AST-0407380, AST-0909073, and AST-1313370.

References

Association of Universities for Research in Astronomy, Inc. (AURA). 2015, Mikulski Archive for Space Telescopes (MAST; https://archive.stsci.edu/).

Boyajian, T. S., *et al.* 2016, *Mon. Not. Roy. Astron. Soc.*, **457**, 3988.

Boyajian, T. S., *et al.* 2018, *Astrophys. J.*, **853**, 8.

Castelaz, M., Barker, T. 2018, arXiv:1803.01943.

Gary, B. L. 2017, KIC8462852 Hereford Arizona Observatory Photometry Observations #3 (http://www.brucegary.net/ts3/).

Gary, B. L. 2018, KIC 8462852 Hereford Arizona Observatory Photometry Observations #6 (http://www.brucegary.net/ts6/).

Harvard College Observatory. 2016, Digital Access to a Sky Century @ Harvard (DASCH) data release 5 (http://dasch.rc.fas.harvard.edu/index.php).

Hippke, M., *et al.* 2017, *Astrophys. J.*, **837**, 85.

Makarov, V. V., and Goldin, A. 2016, *Astrophys. J.*, **833**, 78.

Minitab. 2018, statistical software (http://www.minitab.com/en-US/default.aspx).

Planet Hunters. 2018 Planet Hunters program (https://www.planethunters.org/).

Optical Flares and Quasi-Periodic Pulsations (QPPs) on CR Draconis during Periastron Passage

Gary Vander Haagen
Stonegate Observatory, 825 Stonegate Road, Ann Arbor, MI; garyvh2@gmail.com

Received November 18, 2017; revised February 8, March 1, 2018; accepted March 12, 2018

Abstract The high cadence search at a primary sampling rate of 10 samples/sec of CR Dra revealed six B-band flares totaling 7,574 seconds duration at 26 to 62 mmag peak above the mean. The search for sub-second or spike flares was also conducted with negative results. The study collected 2.5×10^6 photometric measurements over 69.36 hours from 6 July through 10 October 2017. This represents a flare rate of 0.086 flare/hour. The analysis confirmed detection of quasi-periodic pulsations (QPPs) at periods of 71, 51, 39.5–40.9, 32, 28.4, and 21.3–21.7 seconds in the 2017-10-10 flare data within the impulsive and decay phases. Published B-band flare data from 1970–2017 over the binary's two-body separation of 2.96–2.1 AU and through periastron passage were tabulated and analyzed using chi square. The analysis confirmed that there is statistical significance for flaring at periastron verses the more distant separations at better than a 95% probability level. This conclusion should be confirmed with a second more homogeneous photometric study over a similar range of linear two-body separations.

1. Introduction

CR Draconis is one of approximately 100 nearby flare stars within 25 pc, a short period young Me dwarf binary type M5.6V (Wenger *et al.* 2000); B-mag 10.9, HIP 79796. One factor making CR Dra an attractive target for research is its known orbital elements and dynamical mass, making possible correlation of periastron passage with flaring events. Tamazian *et al.* (2008) used speckle measurements to refine the previous work of Blazit *et al.* (1987) to resolve the two-body system. These data revealed a highest probability mass sum of 1.00 Ms, a dynamical parallax of 58.43 mas or 17.4 pc, an orbital period of 4.040 ± 0.005 years, and subsequent ephemeris for the system.

The young Me dwarf star systems such as CR Dra have been of great interest for many years due to their energetic flaring activity. The solar analog has been used as the astrophysical starting point for understanding this star group with recent stellar research refinements. The Me dwarf represents a powerful electromagnetic dynamo with regions of very high magnetic flux interacting with other nearby areas to form magnetic bridges, loops, or tubes, and as the turbulent surface moves causing electromagnetic discontinuities thereby releasing large quantities of energy (Vlahos *et al.* 1995). This process is enhanced by rapid body rotation and very high magnetic fields. The understanding of how these discontinuities form and release their stored energy is under study with numerous theories in play. Vlahos describes the "statistical flare," a sequence whereby many magnetic loops in a highly inhomogeneous region are interacting, with random discontinuities releasing energy and others reforming. This energy release shows up as flares of varying intensity covering a wide range of wavelengths from x-ray to the longer visible wavelengths. This dynamo activity decreases as a star's temperature increases (Candelaresi *et al.* 2014), thereby the greater flaring activity of the young, lower temperature M-stars.

There is another flaring mode that shows up in both Sun and stellar studies, a sequence of fast quasi-periodic pulsations (QPPs) or oscillations (QPOs) that are not confined to either high or low energy flares (Doyle *et al.* 2018). Recent work on magnetically active M stars, including CR Dra, have shown QPPs occurring during both the impulsive and decay phases of flare activity. These pulsations modulate the flare intensity over a widely varying range of 16.2 ± 15.9 min., with the solar counterpart less than 0.1 times the length. The periods of such amplitude pulsation range from 20 to 100 seconds intermixed within the same flare and occur during either the impulsive or decaying phase or both. Doyle *et al.* propose that an understanding of the QPP and MHD modes (magnetohydrodynamic modes) may be linked. The MHD modes are current sheets or tubes with high currents surrounded by a toroidal magnetic field. In solar research these MHD tubes loop into the chromosphere and may exhibit several distinct types of waves: Alfven or magnetic tension components parallel to the magnetic field, slow magneto-acoustic waves with plasma compression and parallel to the magnetic field, or fast magneto-acoustic waves with plasma and magnetic pressure and not oriented to the magnetic field. The relationship between QPP and the MHD modes is still under study with no firm conclusion.

Research by Zalinian and Tovmassian (1987) and further work by Tovmassian *et al.* (1997) reported stellar optical spikes or sub-second flares. These flares are not necessarily associated with any long-duration events and may be single occurrences or several in a cluster ranging from mmag to high-energy events. Similar solar events are reported from x-ray to visible wavelengths, with their mechanism still debated. The most prevalent theory for the solar x-ray to radio emission types is interactions among electromagnetic fields, coronal plasma, and high energy accelerated particles in a synchrotron type process. No literature could be identified on the physical mechanism for optical solar spikes or those on young M dwarfs.

A final related event is coronal mass ejection (CME), a separate but related phenomenon whereby flares and CMEs can occur with or without the other. The CME causes mass loss and a likely change in the local stellar environment. Here, a magnetic flux tube's rapid expansion is theorized to produce shock waves that eject material and energetic particles from the inner corona outward at over 1,000 km/sec to distances as far as 1 AU, thus

producing potential magnetic field interaction between the components of a binary system as distant as two AU. This phenomena and associated flaring activity will be of interest in binaries as they approach periastron (Tamazian *et al.* 2008).

As evidenced from the previous discussion, numerous astrophysical flaring theories have evolved, many as direct extensions of the solar knowledge base, with their extension to stellar flaring still in flux with no cohesive view that unifies the physical mechanisms for flares in the Me dwarf stars.

2. Research objectives

The research objectives were to extend the knowledge of CR Dra by the following means: 1) collect high cadence photometric data for detection of any sub-second or longer flare events; 2) analyze the photometric data looking for QPPs; 3) determine any correlation between orbital phase and flaring activity during periastron passage.

3. Optical system, data collection, and analysis tools

The optical system consisted of a 43-cm corrected Dall-Kirkham scope, a high-speed silicon photomultiplier (SPM), and a data acquisition system capable of sub-millisecond data collection times. The SPM was chosen for this application because it has sensitivity comparable to a standard single channel vacuum photomultiplier yet a more robust mechanical and electrical design with the disadvantage of higher dark counts. The complete optical system and the data collection and reduction pipeline are discussed in detail in Vander Haagen and Owings (2014). The data pipeline produces an integrated file with all constituents ready for analysis, each file containing up to one million data lines containing a GPS synced UT stamp, target photon count, reference, and background data. Using a 500-nm low pass filter combined with the SPM response, the resultant band pass approximates standard B band. The B band was chosen since CR Dra emits greater flare energy at shorter wavelengths (Cristaldi and Longhitano 1979). The U band would have been the best choice for low-level flare detection but the SPM detector has very little response in that region.

The large photometric files from each night's run were analyzed using signal-processing software (SignalLab 2017). SignalLab software, SIGVIEW 3.1, is an analysis program capable of quickly handling files up to 10^6 lines of time-based data. Any portion of the data can be reviewed nearly instantly with a powerful suite of tools: statistical analysis, smoothing, averaging, filtering, resampling, probability distributions, FFTs including spectrograms (FFT segmented over time), and complex calculation capability for correlation and convolution, to mention a few. These data were inspected for potential flares using statistical techniques, resampled for better detection and analysis of longer flares, and viewed using digital filters and FFT for detection of possible periodic occurrences.

4. Flare search and QPP analysis

The first research objective was to collect high cadence photometric data for detection of any sub-second or longer events. The detection of very short or spiky flares is of particular interest to this researcher and represents a potentially fruitful area for better understanding of high speed flaring mechanisms where little data have been collected or research has taken place. Sub-second photometric events have been reported on M dwarfs, MK, and RS CVn stars. Short or spike flares as short as 10 to 100 ms duration have been observed unconnected with longer flaring activity. These very short flares generally consisted of one or more points at 3σ or higher with a peak at 4–10σ. A 50 ms-duration flare was reported on EV Lac in the U–B band by Zhilyaev *et al.* (1990) and simultaneous U- and B-band flares on BY Dra (Zalinian and Tovmassian 1987). Vander Haagen (2013) also reported very short duration flares on AR Lac, II Peg, and UX Ari of 30 to 85 ms duration with peaks 0.29–0.51 mag above the mean.

The criterion was developed to isolate short duration flares in very large sample sizes (Vander Haagen 2015). The flares must consist of a minimum of three consecutive data points, two at or above 3σ and one at or above 5σ. Normal distribution statistics were used since the number of photons always exceeded 100. Statistics were collected 600 seconds prior to the event where possible using digital signal processing software (SignalLab 2017). The probability of this sequence being a random event is 5.2×10^{-13} N, where N is the number of integrations or samples taken during the observing interval and σ is for the positive events only. With N ranging from 1 to 2×10^6 samples during an observing interval the probability of the event sequence being random is appropriately small. This criterion was used for each of the data sets to isolate potential short duration flares.

The search for slower or longer flares with flux change of 100 mmag or less was best served by resampling to a longer gating period, typically 1 to 5 seconds, thereby improving S/N ratios.

Data collection was conducted over a period 6 July 2016 through 10 October 2017. Figure 1 shows the spans in nightly data collection times in UT seconds and the dispersion over the dates. The total data collection time was 69.4 hours or 249.8 Ksec, comprising 2.5×10^6 data points. No sub-second or spike flares were detected using the statistical criteria over the full measurement data set.

Published photometric studies have been conducted on CR Dra over twelve occasions from May 1968 (Cristaldi and Rodono 1970) through October 2016 (Vander Haagen 2017). The historical flare data are summarized in Table 1, which also includes the latest data from this study. The very limited historical flare data were superimposed on the calculated orbital positions (Tamazian *et al.* 2008), and revealed "no plausible correlation between flaring activity and linear distance between components." However, no data had been collected any closer than 2.47 AU separation. During phase one of this study photometric data at two-body linear separations over 2.42–2.75 AU were added to the knowledge base (Vander Haagen 2017), with the full separation ranging 2.1 (periastron) to 2.95 AU. A single flare was identified on 2016-09-27 of 30 mmag, 4.1σ, and 560 seconds duration at a linear separation of 2.48 AU (corrected).

Six long-duration flares were detected as previously summarized in Table 1. The two shown in Figures 2 and 3 were

Table 1. Summary of the published flaring activity on CR Dra over the years 1968 through 2017.

Observation Date(s)	*No. Flares, Band*	*Linear-Distance (AU)*	*Flare Rate (fl/h), Total Hours (h)*	*Reference*
1968 May 28–July 14	0, U, B	2.34–2.59	0	Cristaldi and Rodono (1970)
1970 May 11–June 18	6, U, B	2.45–2.52	[1]	Cristaldi and Longhitano (1979)
1971 July 1	1, U, B	2.95	[2]	Cristaldi and Rodono (1973)
1974 June 7	1, B	2.47	0.025, 39.4	Kareklidis *et al.* (1977)
1974 June	0	2.47	—	Mahmoud (1991)
1975 June–August	0, B	2.93–2.96	0, 46.9	Mahmoud *et al.* (1980)
1978 May 10–17	1	2.41	—	Anderson (1979)
1980 July 19–20	0	2.41	0	Ambruster *et al.* (1987)
1991 June	0 (ROSAT)	2.95	0	Tsikoudi and Kellett (1997)
2007 March–July	0	2.78–2.93	0	Tamazian *et al.* (2008)
2007 April–July	20, U	2.83–2.92	0.69, 29.1	Dal (2012)
2016 May–Oct	1, B	2.42–2.75	0.016, 64.2	Vander Haagen (2017)
2017 July–Oct	6, B	2.17–2.1	0.086, 69.4	this study

Notes: 1. Six flares with estimated total duration of 153 seconds, no total monitoring time cited.
2. One 1,080-second flare, no total monitoring time cited.

detected on 11 September 2017, at 36 mmag peak, 7.9σ, and 1,800 sec duration. Figures 4 and 5 show the second flare series detected on 10 October 2017, separated into four interlaced flares reaching a peak of 62 mmag, 12.2σ at 9,696 sec UT and total duration of 5,774 sec.

The second research objective was to analyze the photometric data looking for possible QPPs. The review of data for QPPs was problematic due to the low S/N and very turbulent atmospheric conditions present. The FFT spectrogram searches employed SIGVIEW 3.1 with the total number of samples set at 16,384 and the number of time analysis segments set to 732. The results were tested for 95% confidence. From work by Doyle *et al.* (2018) the QPP periods prevalent in CR Dra were 20, 43, 60, and 110 secs, with similar Me stars also exhibiting 25- to 39-sec periods. Figure 6 shows the 2017-10-10 flare sequence. During the impulsive phase of flare #1 QPPs were exhibited with a 21-sec period followed by 28.4-, 54-60-, 71-, and 110-sec periods during the decay phase. A second burst in the flare #1 decay phase occurred with a 39.5- to 40.9-sec period. Flare #2 exhibited an impulsive flare of 51-sec period followed by a decay phase event of 32-sec period. The 21-, 39.5–40.9-, 54–60-, and 110-sec QPPs range 492 ± 100 sec in duration. Those reported by Doyle *et al.* (2018) are shown with an (*). Reviewing the spectrogram data of Figure 6, the QPPs longer than 28.4-sec period were not separable from atmospheric noise prevalent prior to the flaring events. The noise contribution was better understood by using the second channel of photometric data, the reference/guide star measurements with a cadence of 10 sec. These data were reviewed using a Sigview FFT-spectrogram as shown in Figure 7. The data show periods from 31 to 250 seconds versus the UT time in seconds. The turbulent regions are noted by the darker blue color with light blue and whites 3 to 15 times lower power spectral density (PSD) than the dark blue. The PSD contrast can be seen in the turbulent regions pre-flare on Figure 6, e.g., at 3800 UT. With these data the periods of 71, 51, 39.5–40.9, 32, 28.4, 21.3–21.7, and 32 seconds are not affected by atmospheric turbulence. However, potential QPP periods of 54–60 and 110 seconds are not separable from the atmospheric noise. There is partial correlation with Doyle's data at periods of 21.3–21.7 and 110 seconds unconfirmed. It is important to note that the body of knowledge of QPPs is very limited and the variability is unknown.

5. Periastron passage and flare activity

The third research objective was to determine any correlation between orbital phase and flaring activity during periastron passage. Figure 8 depicts the two-body phase diagram and data collection range for each study cited in Table 1 where sufficient data were available, e.g., flares detected if any and total time of study is known. It is hypothesized that there is a relationship between flaring and the two-body linear separation, that is, "there is greater flaring at periastron passage than at more distant separations." Assume that alpha = 0.05, or a 5% chance or less is allowed that the hypothesis is incorrect. For normal and ordinal data chi square is used as a test for statistical significance. The observational data are parsed to accommodate use in the chi square contingency table (Table 3). Total flare data collection time will be converted to seconds and divided into 100-sec bins (divide total study monitoring time by 100). Flare durations will be similarly binned into 100-sec segment bins. Observation time or flare durations will be rounded off to the next higher bin, e.g., 2,020 sec will be 21 bins and every flare will generate at least one bin. This gives some weight to shorter flare durations. Using this methodology Table 2 tabulates all the B-band study data from Table 1 and classifies them into two groups, YES flares in bin or NO flares in bin, at two separation distances, one group within 3% or less of periastron and the second more distant than 2.42 AU. It is important to note that these studies were not all of same sensitivity depth, the cadence is not stated in at least one case, and they were conducted over nearly 50 years where equipment and practices differed widely even though they were all B band.

The chi square statistic can be calculated manually or using any number of available web calculators. The data for analysis and binning are shown in Table 2. The chi square results are shown inTable 3 with the input data bins in bold and the expected frequency of occurrence as (xxx) as if there were no relationship between the two-body separation and flaring.

Table 2. B-band flare data tabulation; data from four research studies with CR Dra linear separation greater than 2.42 AU and one study less than 2.12 AU, periastron passage. Binning data is placed in the contingency table (Table 3).

Researcher	*Dates*	*Two-body Separation (AU)*	*Flares, Total Hours*	*Flare Duration (sec.)*	*100s Bins*	*Flare Rate (flares/hour)*
Group over 2.42 AU linear separation						
Christaldi et al.	1970 May–Jun	2.45–2.52	6, —	153	6	—
Kareklidis	1974 Jun	2.47	1, 39.4	326	4	0.025
Mahmoud	1975 Jun–Aug	2.96–2.93	0, 46.9	0	0	0
Vander Haagen	2016 May–Oct	2.75–2.42	1, 64.16	560	6	0.016
			150.5, 541.8 Ksec 5,418 Bins	1,039	16	0.013
Periastron Passage Group						
Vander Haagen	2017 Jul–Oct	2.17–2.1	2, —	1,800	18	
			4, —	5,774	58	
			69.4, 249.8 Ksec 2,498 Bins	7,574	76	0.086

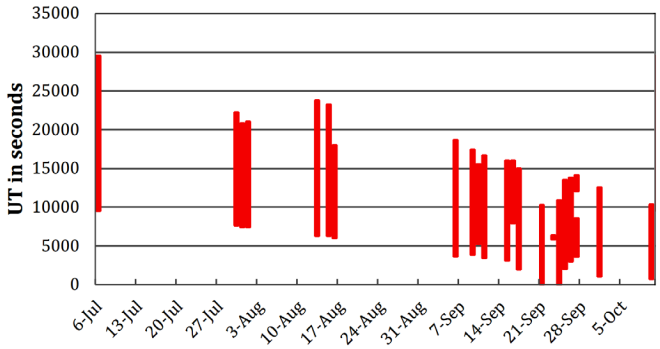

Figure 1. CR Dra photometry 2017 date versus data collection span in UT seconds (e.g., 3,601 sec UT = 01:00:01 UT).

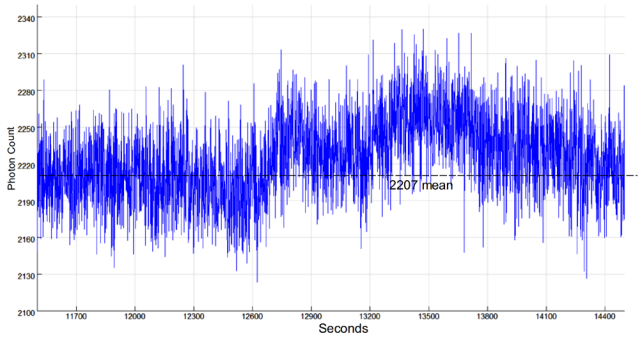

Figure 2. 2017-09-11 flare, time in UT seconds versus photon count, 10 samples/sec flares resampled at 1 sample/sec; 2-flare sequence, pre-flare mean 2,207, σ 28.

Comparing the actual flaring frequency with expected frequency show very significant differences. The [xxx] values are the calculated chi square statistic for each cell. Interpretation of the statistic requires looking up the normal distribution of chi square for a contingency table of two rows and two columns (degree of freedom = 1, (#rows-1) × (#columns-1)), and an alpha of 0.05. The value from the table is 3.841. The contingency tables total (112.3) must exceed the table value for statistical significance. This indicates that there is statistical significance of flaring at periastron verses the most distant data at better than a 95% probability level.

Revisiting Table 1, it is noted that a very high flare rate of 0.69 flare/hr was reported by Dal (2012) at 2.83–2.92 AU, which seems to contradict the results reported at periastron of 0.086 flare/hr. Note that these flares were detected in the U band. Data from Cristaldi and Longhitano (1979) on CR Dra in both U- and B-bands show a U/B flux ratio of 6 and on other similar stars more than 7. This places many of the flares in the Dal study below the detection threshold of this study and does not permit flare rates comparisons.

However, without a reasonable astrophysical flaring model for the Me dwarf and exacerbated by a void of any supporting literature on optical flaring of another Me dwarf of comparable orbital elements during periastron, the meaning of the statistical significance takes on uncertainty. A future study to confirm the statistical significance of flaring at periastron should include collection of homogeneous photometric data, B band with similar depth exposures, and collection system over a large portion of the orbital path. CR Dra and several other shorter-period nearby flaring binaries with resolved orbital elements would be likely candidates, such as CE Boo or EZ Aqr.

6. Conclusions

A high cadence photometric search was undertaken at 10 samples/sec. No sub-second or spike flares were observed in 2.5 × 10^6 photometric measurements over 69.36 hours from 6 July through 10 October 2017. Six long-duration flares were observed producing a flare rate of 0.086 flares/hr: on 2017-09-11, two flares with total of 1,800-sec duration, 36 mmag, 7.9σ, and on 2017-10-10 a second sequence of four flares of 5,774 sec duration peaking at 62 mmag and 12.2σ. The photometric data were further reviewed using FFT spectrograms to determine if QPPs were present during flaring events. The analysis confirmed that components at periods of 71, 51, 21.3–21.7, 28.4,

Table 3. Chi square calculation to determine statistical significance. The contingency table provides the following information: in bold, the input data on flare binning totals from Table 2; from the chi square calculation (the expected cell totals) and [the chi square statistic for each cell].

	Less than 2.17 AU		*Greater than 2.42 AU*		*Marginal Row Totals*
YES flare in 100 sec bin	**76**	(29.03) [75.99]	**16**	(62.97) [35.03]	92
NO flare in 100 sec bin	**2,422**	(2,468.97) [0.89]	**5,402**	(5,355.03) [0.41]	7,824
Marginal Column Totals	**2,498**		**5,418**		7,916 (Grand Total) [112.3]

Note: The sum of the chi square [statistic] from above is 112.3. For significance this calculated chi square statistic must exceed the normal distribution chi square, or 3.841 for an alpha of <0.05. This indicates the result is significant with less than 5% probability of error. This is a pass/fail criterion and does not denote strength of significance.

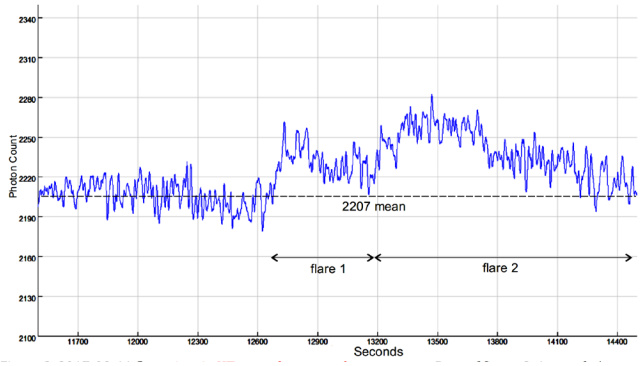

Figure 3. 2017-09-11 flare, time in UT seconds versus photon counts. Figure 2's 1 sample/sec data were smoothed; pre-flare mean 2207, σ 9.6, 1,800 sec total duration; 2-flare sequence, first peak of 2,261 at 12,733 sec, 26 mmag, 5.6σ; second peak of 2,282 at 13,473 sec, 36 mmag, 7.9σ.

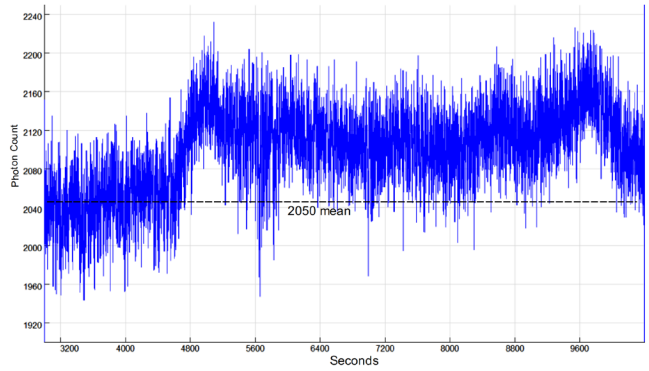

Figure 4. 2017-10-10 flare, time in UT seconds versus photon count, 10 samples/sec, 4-flare sequence resampled at 1 sample/sec; total duration 5,774 sec, pre-flare mean 2,050, σ 32.7.

39.5–40.9, and 32 sec were present in the 2017-10-10 flare data during the impulsive and decay phases. However, potential QPP periods of 54–60 and 110 seconds were not separable from the atmospheric noise. All the reported flare data for CR Dra were tabulated and entered into a chi square Contingency Table to determine the statistical significance of flaring at periastron passage. The chi square analysis confirmed to better than 95% probability that the higher flare rate at periastron was of statistical significance with the caveat previously noted.

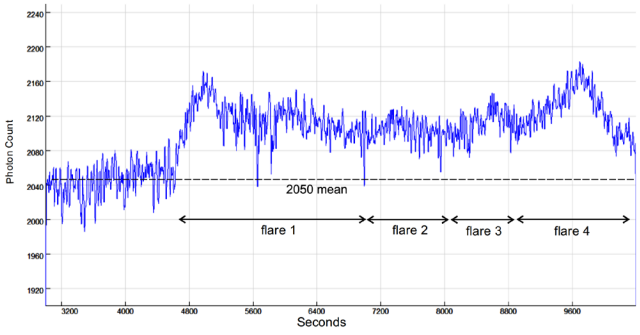

Figure 5. 2017-10-10 flare, time in UT seconds versus photon count. Figure 4's 1 sample/sec, 4-segment flare, smoothed; total duration 5,774 sec, pre-flare mean 2,050, σ 9. See Table 4.

Table 4. 2017-10-10 flare. See Figure 5.

	Peak UT (sec.)	*mmag*	*σ*	*Duration (sec.)*
1st	4,981	55	10.8	2,372
2nd	7,331	34	6.7	1,030
3rd	8,608	42	8.2	878
4th	9,696	62	12.2	1,494
				Total 5,774

7. Acknowledgements

The author expresses his thanks to the referee for the recommendations in linking an astrophysical discussion with research objectives, concern over the photometric variability in the studies cited, and numerous other helpful clarifications.

References

Ambruster, C. W., Sciortino, S., and Golub, L. 1987, *Astrophys. J., Suppl. Ser.*, **65**, 273.

Anderson, C. M. 1979, *Publ. Astron. Soc. Pacific*, **91**, 202.

Blazit, A., Bonneau, D., and Foy, R. 1987, *Astron. Astrophys., Suppl. Ser.*, **71**, 57.

Candelaresi, S., Hillier, A., Maehara, H., Brandenburg, A., and Shibata, K. 2014, *Astrophys. J.*, **792**, 67.

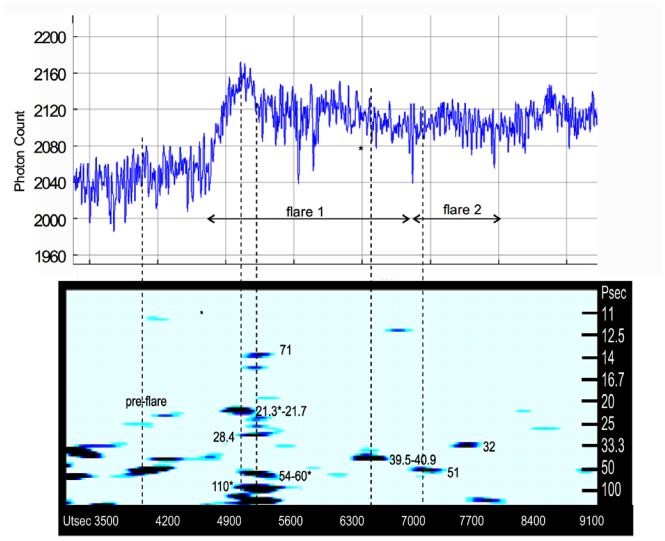

Figure 6. Upper panel: 2017-10-10-flare photon counts, time aligned with FFT spectrogram. Lower panel: FFT spectrogram shows time in UT seconds versus QPP periods in seconds. Flares cited by Doyle *et al.* (2018) are shown with (*). Periods longer than 28.4 sec were typical of the atmospheric noise spectrum just prior to the flare. No QPPs were detected in flares 3 or 4.

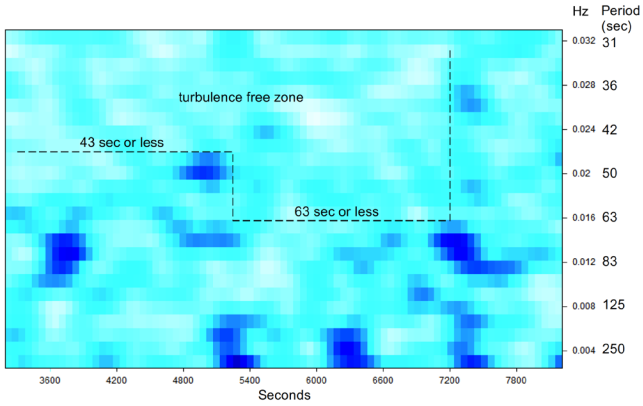

Figure 7. Spectrogram of reference/guiding camera data plotting atmospheric noise with periods between 31 and 250 seconds over the UT (seconds) time span where the QPP data were collected in Figure 6. The darker blue color represents an increase in power spectral density of 3 to 15 times over the background light blue or white, respectively. The periods identified in Figure 6 (71, 51, 39.5–40.9, 32, 28.4, and 21.3–21.7) are outside the atmospheric turbulence zone during this data collection period. Periods 54–60 and 110 seconds shown in Figure 6 are within the turbulence noise zone and are of questionable validity.

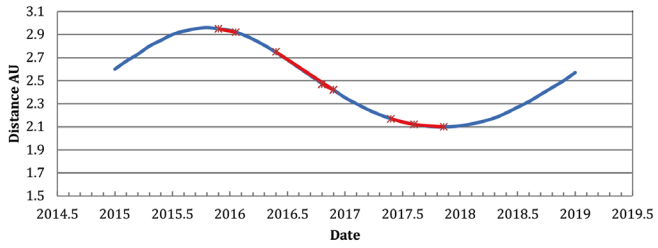

Figure 8. Date versus binary linear body separation in AU; the red-colored segments of the orbital phase are those covered by cited photometric studies. The previous studies by Kareklidis *et al.* (1977) and Mahmoud *et al.* (1980) were phased to fit on the current epoch phase diagram.

Cristaldi, S., and Longhitano, M. 1979, *Astron. Astrophys., Suppl. Ser.*, **38**,175.

Cristaldi, S., and Rodono, M. 1970, *Astron. Astrophys., Suppl. Ser.*, **2**, 223.

Cristaldi, S., and Rodono, M. 1973, *Astron. Astrophys., Suppl. Ser.*, **10**, 47.

Dal, H. A. 2012, *Publ. Astron. Soc. Pacific*, **64**, 82.

Doyle, J. G., *et al.* 2018, *Mon. Not. Roy. Astron. Soc.,* **475**, 2842.

Kareklidis, G., Mavridis, L. N., and Stavridis, D. C. 1977, *Inf. Bull. Var. Stars*, No. 1356, 1.

Mahmoud, F. M. 1991, *Astrophys. Space Sci.*, **186**, 113.

Mahmoud, F. M., Mavridis, L. N., Stavridis, D., and Varvoglis, P. 1980, *Inf. Bull. Var. Stars*, No. 1799, 1.

SignalLab 2017, SIGVIEW 3.1 software for DSP applications (http://www.sigview.com/index.htm).

Tamazian, V. S., Docobo, J. A., Balega, Y. Y., Melikian, N. D., Maximov, A. F., and Malogolovets, E. V. 2008, *Astron. J.*, **136**, 3, 974.

Tovmassian, H. M., Recillas, E., Cardona, O., and Zalinian, V. P. 1997, *Rev. Mex. Astron. Astrofis.*, **33**, 107.

Tsikoudi, V., and Kellett, B. J. 1997, *Mon. Not. Roy. Astron Soc.*, **285**, 759.

Vander Haagen, G. A. 2013, *J. Amer. Assoc. Var. Star Obs.*, **41**, 114.

Vander Haagen, G. A. 2015, *J. Amer. Assoc. Var. Star Obs.*, **43**, 219.

Vander Haagen, G. A. 2017, *J. Amer. Assoc. Var. Star Obs.*, **45**, 36.

Vander Haagen, G. A., and Owings, L. E., 2014, in *The Society for Astronomical Sciences 33rd Annual Symposium on Telescope Science*, Society for Astronomical Sciences, Rancho Cucamonga, CA, 191.

Vlahos, L., Georgoulis, M., Kluiving, R., and Paschos, P. 1995, *Astron. Astrophys.*, **299**, 897.

Wenger, M., *et al.* 2000, *Astron. Astrophys., Suppl. Ser.*, **143**, 9 (http://simbad.u-strasbg.fr/simbad/).

Zalinian, V. P., and Tovmassian, H. M. 1987, *Inf. Bull. Var. Stars*, No. 2992, 1.

Zhilyaev, B. E., Romanjuk, Ya., and Svyatogorov, O. A. 1990, in *Flare Stars in Star Clusters, Associations, and the Solar Vicinity*, eds. L. V. Mirzoyan, B. R. Pettersen, M. K. Tsvetkov, IAU Symp. 137, Kluwer Academic, Dordrecht, 35.

A Photometric Study of the Contact Binary V737 Cephei

Edward J. Michaels
Stephen F. Austin State University, Department of Physics, Engineering and Astronomy, P.O. Box 13044, Nacogdoches, TX 75962; emichaels@sfasu.edu

Received January 8, 2018; revised January 30, 2018; accepted January 30, 2018

Abstract Presented are the first multiband CCD photometry of the eclipsing binary star V737 Cephei. The observations resulted in 22 new times of minimum. New linear and quadratic ephemerides were computed from all available minimum light timings. The orbital period was found to be rapidly decreasing. The light curves were analyzed with the Wilson-Devinney program to find the best-fit stellar model. The model required a large third-light contribution and a cool spot on the larger star to fit light curve asymmetries. A fill-out of 19% is consistent with a W-subtype contact binary.

1. Introduction

The variability of V737 Cephei (NSV 13695) was first reported by Kukarkin *et al.* (1982). Using photometric observations from the ASAS-3, NSVS, and Hipparcos databases, this star was classified as a W-subtype eclipsing binary with an orbital period of 0.298755 d (Otero *et al.* 2005). Gettel *et al.* (2006) gives a maximum visual magnitude of 11.965 and a minimum of 12.370. The parallax measured from the first data release of the Gaia mission gives a distance of 243 ± 51 pc (Gaia 2016). A total of 17 eclipsing timings were reported by Hübscher *et al.* (2012), Hübscher and Lehmann (2012), Hübscher *et al.* (2013), Hübscher (2013, 2017), Hoňková *et al.* (2013), Nelson (2014, 2016) and Juryšek *et al.* (2017). V737 Cep was included in "The 79th Name-List of Variable Stars" (Kazarovets *et al.* 2008).

Presented in this paper is the first photometric study of V737 Cephei. The photometric observations and data reduction methods are presented in section 2, with new times of minima and ephemerides in section 3. Light curve analysis using the Wilson-Devinney model (WD; Wilson and Devinney 1971) is presented in section 4. A discussion of the results and conclusions are given in section 5.

2. Observations

Multi-band photometric observations were acquired at the Waffelow Creek Observatory (http://obs.ejmj.net/index.php) in July 2015 and July 2017. A 0.30-m telescope was used for the 2015 observations and a 0.36-m telescope in 2017. Both instruments had Ritchey-Chrétien optical systems with a robotic mount for automated observing runs. All images were acquired using a SBIG-STXL camera equipped with a cooled KAF-6303E CCD (–30° C). The 2015 data set was obtained in five passbands: 585 images in Johnson B, 962 in Johnson V, 971 in Sloan g', 756 in Sloan r', and 682 in Sloan i'. The 2017 data set includes 1,183 images in Sloan g', 908 in Sloan r', and 1,247 in Sloan i'. Bias, dark, and flat frames were obtained on each night. MIRA software (Mirametrics 2015) was used for image calibration and to perform the ensemble differential aperture photometry of the light images. The coordinates and magnitudes of the comparison and check stars are listed in Table 1 with a finder chart shown in Figure 1. The standard magnitudes of the comparison stars were taken from the AAVSO Photometric All-Sky Survey (APASS) data base (Henden *et al.* 2014) and were used to convert the instrumental magnitudes of V737 Cep to standard magnitudes. The Heliocentric Julian Date of each observation was converted to orbital phase (ϕ) using the following epoch and orbital period: T_o = 2455685.4877 and P = 0.298765 d. Both the 2015 and 2017 data sets provided new times of minima for V737 Cep. The 2017 observations resulted in complete light curves for each observed passband and were also of higher

Table 1. Stars used in this study.

Star	*R.A. (2000) h m s*	*Dec. (2000) ° ′ ″*	*g′*	*r′*	*i′*
V737 Cep	21 23 48.4	+63 33 28			
[1]GSC 04252-00669 (C1)	21 24 34.5	+63 30 04	11.980	11.445	11.275
[1]GSC 04252-00821 (C2)	21 24 45.6	+63 32 03	12.168	11.580	11.361
[1]GSC 04252-00725 (C3)	21 23 39.3	+63 30 31	13.085	12.004	11.560
[1]GSC 04252-01534 (C4)	21 23 53.1	+63 36 10	12.724	12.044	11.835
[2]GSC 04252-00655 (K)	21 23 41.6	+63 40 07	11.413	11.296	11.320

APASS [1]comparison stars (C1–C4) and [2]check star (K) magnitudes.

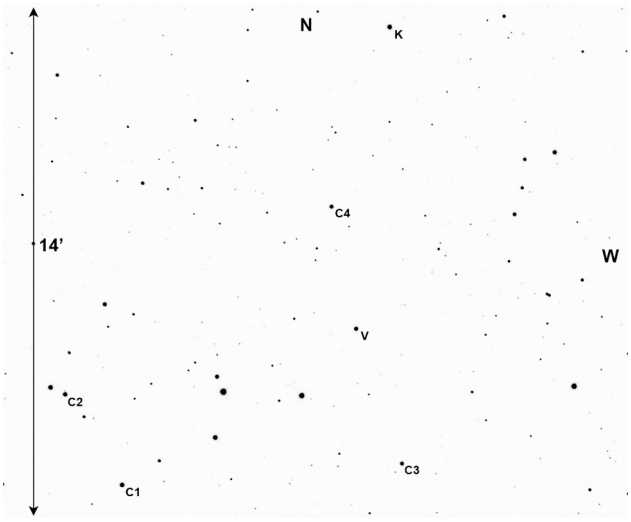

Figure 1. Finder chart for V737 Cep (V), comparison (C1-C4) stars, and check (K) stars.

quality compared to the 2015 data set. This was the result of better seeing conditions in 2017 as well as a higher signal-to-noise ratio provided by the larger telescope. The folded light curves show that both the primary and secondary eclipses are total (Figure 2). All light curves in this paper were plotted from orbital phase –0.6 to 0.6 with negative phase defined as $\phi - 1$. The check star magnitudes were plotted and inspected each night, but no significant variability was noted. The standard deviation of the check star magnitudes (all nights) were 6 mmag for Sloan g', 5 mmag for Sloan r', and 8 mmag for Sloan i'. The Sloan r' check star magnitudes are plotted in the bottom panel of Figure 2. The 2017 observations can be accessed from the AAVSO International Database (Kafka 2017) (https:/www.aavso.org/aavso-international-database).

3. Ephemerides

Table 2 lists 17 times of minima found in the literature along with 22 new minima times from this study. The (O–C) residuals in Table 2 were computed using the following linear ephemeris:

$$\text{HJD Min I} = 2455685.4877 + 0.2987551\text{E}. \quad (1)$$

The epoch for this initial ephemeris uses the first primary minima time shown in Table 2 (Hübscher *et al.* 2012) and the orbital period taken from The International Variable Star Index (VSX; Watson 2006). A new linear ephemeris was computed by least-squares solution using the residuals from Equation 1:

$$\text{HJD Min I} = 2457961.7788(9) + 0.298765(5)\text{E}. \quad (2)$$

Figure 3 shows the residuals of Equation 1 and the best-fit line of Equation 2 (solid line). A second least-squares solution using the Equation 2 residuals yields the following quadratic ephemeris:

$$\text{HJD Min I} = 2457961.7767(7) + 0.298763(5)\text{E} - 3.3(2) \times 10^{-10}\text{E}^2. \quad (3)$$

Figure 4 shows the residuals from Equation 2 and the general trend of the quadratic ephemeris (solid line). The negative curvature indicates a decreasing orbital period, which will be discussed further in section 5.

4. Analysis

4.1. Temperature, spectral type

Pickles and Depagne (2010) using all-sky spectrally matched Tycho 2 stars determined the spectral type of V737 Cep, K0V. A star of this spectral type has an effective temperature of $T_{eff} = 5280$ K and a color of $(B-V)_0 = 0.816$ (Pecaut and Mamajek 2013). To find the observed color, the phase and magnitude of the g' and r' observations were binned with a phase width of 0.01. The phases and magnitudes in each bin interval were averaged. To find the color at quadrature ($\phi = 0.25$), the binned r' magnitudes were subtracted from the linearly interpolated g' magnitudes, giving an observed (g'– r') color of 0.704 ± 0.008. Figure 5 shows the binned r' magnitude light curve with the observed (g'–r') color shown in the bottom panel. The color changes only a small amount over an orbital cycle, which is

Table 2. Times of minima and O-C residuals from Equation 1.

Epoch HJD 2400000+	*Error*	*Cycle*	*O–C*	*References*
55685.4877	0.0006	0.0	0.00000	Hübscher and Lehmann 2012
55692.5070	0.0001	23.5	–0.00148	Hoňková *et al.* 2013
55693.5535	0.0007	27.0	–0.00062	Hoňková *et al.* 2013
55707.4450	0.0001	73.5	–0.00124	Hoňková *et al.* 2013
55787.3664	0.0007	341.0	0.00321	Hübscher and Lehmann 2012
55791.4002	0.0002	354.5	0.00378	Hoňková *et al.* 2013
56072.3892	0.0012	1295.0	0.01365	Hübscher 2013
56072.5405	0.0010	1295.5	0.01557	Hübscher 2013
56421.9450	0.0002	2465.0	0.02598	Nelson 2014
56490.5127	0.0003	2694.5	0.02938	Hübscher 2013
56508.4373	0.0004	2754.5	0.02865	Hoňková *et al.* 2013
56519.3425	0.0002	2791.0	0.02932	Hoňková *et al.* 2013
56519.4923	0.0002	2791.5	0.02973	Hoňková *et al.* 2013
56530.3968	0.0006	2828.0	0.02967	Hoňková *et al.* 2013
57182.8999	0.0001	5012.0	0.05164	Nelson 2016
57217.8561	0.0001	5129.0	0.05345	present paper
57220.8436	0.0001	5139.0	0.05342	present paper
57221.7401	0.0001	5142.0	0.05366	present paper
57222.7864	0.0002	5145.5	0.05436	present paper
57223.8311	0.0001	5149.0	0.05334	present paper
57223.6830	0.0002	5148.5	0.05468	present paper
57224.7273	0.0001	5152.0	0.05327	present paper
57224.8779	0.0002	5152.5	0.05459	present paper
57227.7147	0.0002	5162.0	0.05316	present paper
57227.8652	0.0003	5162.5	0.05428	present paper
57228.7616	0.0002	5165.5	0.05443	present paper
57335.4208	0.0002	5522.5	0.05802	Juryšek 2017
57568.4563	0.0029	6302.5	0.06458	Hübscher 2017
57946.8380	0.0004	7569.0	0.07294	present paper
57952.8131	0.0004	7589.0	0.07291	present paper
57952.6652	0.0004	7588.5	0.07442	present paper
57953.7094	0.0003	7592.0	0.07301	present paper
57953.8602	0.0004	7592.5	0.07442	present paper
57954.7563	0.0002	7595.5	0.07426	present paper
57955.8008	0.0001	7599.0	0.07307	present paper
57955.6525	0.0001	7598.5	0.07418	present paper
57960.8799	0.0001	7616.0	0.07337	present paper
57960.7314	0.0001	7615.5	0.07426	present paper
57961.7762	0.0001	7619.0	0.07343	present paper

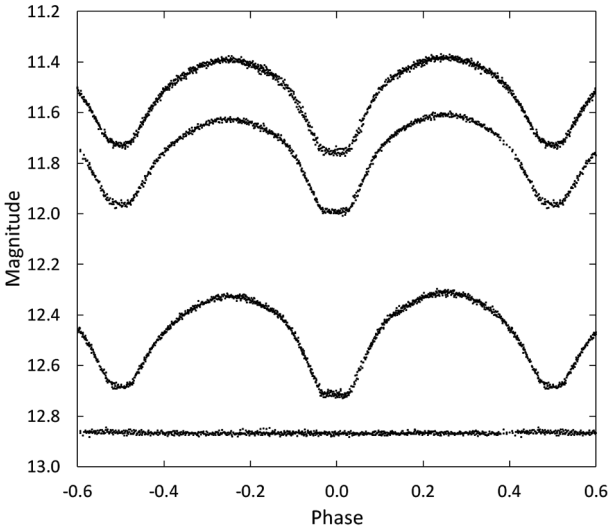

Figure 2. Folded light curves for each observed passband. The differential magnitudes of V737 Cep were converted to standard magnitudes using the calibrated magnitudes of the comparison stars. From top to bottom the light curve passbands are Sloan i', Sloan r', Sloan g'. The bottom curve shows the Sloan r' magnitudes of the check star (offset +1.6 magnitudes). Error bars are not shown for clarity.

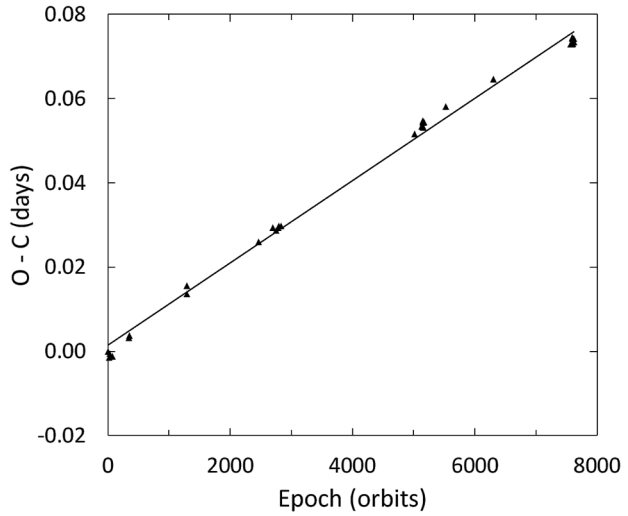

Figure 3. The O–C residuals from Equation 1 with the solid line as the linear ephemeris fit of Equation 2.

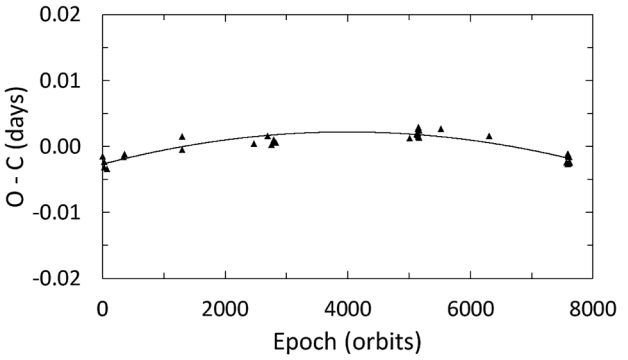

Figure 4. The O–C residuals from Equation 2 with the solid line as the quadratic ephemeris fit of Equation 3.

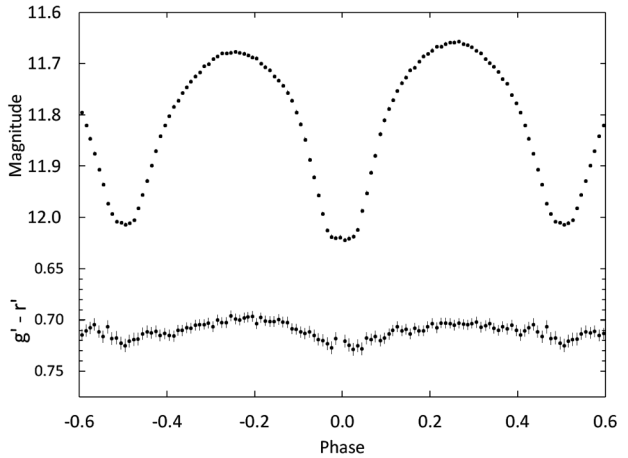

Figure 5. Light curve of all Sloan r'-band observations in standard magnitudes (top panel). The observations were binned with a phase width of 0.01. The errors for each binned point are about the size of the plotted points. The g'- r' colors were calculated by subtracting the linearly interpolated binned Sloan g' magnitudes from the linearly interpolated binned Sloan r' magnitudes.

expected for a contact binary. Using the Bilir *et al.* (2005) transformation equation,

$$(B-V) = \frac{(g'-r') + 0.25187}{1.12431}\ , \qquad (4)$$

gives an observed (B–V) color of 0.850 ± 0.008. The color excess was determined by differencing the observed color and the standard color for a star of spectral type K0. The approximate color excess and interstellar extinction values are $E(B-V) = 0.03 \pm 0.06$ and $A_V = 0.1 \pm 0.2$, respectively. The small values for these two quantities are reasonable given the proximity of V737 Cep to Earth.

4.2. Synthetic light curve modeling

The Sloan g', r', and i' passband data acquired in 2017 were used for light curve modeling. The observations were binned in both phase and magnitude as described in section 4.1. The average number of observations per bin for the g', r', and i' passbands was 12, 9, and 12, respectively. The binned magnitudes were converted to relative flux for modeling. Preliminary fits to the light curves were attained using the program BINARY MAKER3.0 (BM3) (Bradstreet and Steelman 2002). Standard convective parameters were employed in the model with the limb darkening coefficients taken from Van Hamme's (1993) tabular values. A good fit was not possible until a third light contribution was added for all three passbands. There were asymmetries in the light curve as well, but they were not modeled with BM3 in this initial solution attempt. When a good fit was obtained between the synthetic and the observed light curves, the resulting stellar parameters for each passband were averaged. These values were used as the input parameters for computation of a simultaneous three-color light curve solution with the WD program (Wilson and Devinney 1971; Van Hamme and Wilson 1998). The light curve morphology of this star indicates a contact configuration, with the stars having a common convective envelope. The WD program was configured for overcontact binaries (Mode 3). Each binned input data point was assigned a weight equal to the number of observations forming that point. The Method of Multiple Subsets (MMS) was used to minimize strong correlations of parameters (Wilson and Biermann 1976) and the Kurucz stellar atmosphere model was applied. The fixed inputs included standard convective parameters: gravity darkening, $g_1 = g_2 = 0.32$ (Lucy 1968) and albedo value $A_1 = A_2 = 0.5$ (Ruciński 1969). The temperature of the hotter primary star, T_1, was fixed at a 5280 K (see section 4.1). The program calculated linear limb darkening coefficients from tabulated values using the method of Van Hamme (1993). The solution's adjustable parameters include the inclination (i), mass ratio ($q = M_2/M_1$), potential ($\Omega_1 = \Omega_2$), temperature of the secondary star (T_2), the normalized flux for each wavelength (L), third light (l), and phase shift. The best-fit solution parameters with errors are shown in column 2 of Table 3 (Solution 1). The filling-factor in Table 3 was computed using the method of Lucy and Wilson (1979) given by:

$$f = \frac{\Omega_{inner} - \Omega}{\Omega_{inner} - \Omega_{outer}}\ . \qquad (5)$$

For solution 1, $\Omega_{inner} = 5.94$, $\Omega_{outer} = 5.33$, and $\Omega = 5.82$, which gives a fill-out of f = 0.20. Figure 6 shows the normalized light curves overlaid by the synthetic solution curves with the residuals shown in Figure 7.

4.3. Spot model

Low mass, rapidly revolving contact binaries are often magnetically active and thus spotted. The asymmetries seen in the light curves (Figure 6) and in the residuals (Figure 7) are an indication of cool spots or hot regions such as faculae on the star surfaces. The light curves also show an O'Connell effect with Max I ($\phi = 0.25$) brighter than Max II ($\phi = 0.75$), which is also indicative of spotting. The residual plots (Figure 7) show a light loss between orbital phase $\phi = 0.4$ and $\phi = 0.8$, indicating a possible under-luminous region on the larger secondary star. Using the stellar parameters from solution 1, a single cool spot was modeled with BM3. The spot's latitude, longitude, size, and temperature were adjusted until a good fit was obtained between the synthetic and observed light curves. The spot parameters were then incorporated into a new WD solution attempt. The resulting best-fit WD spotted solution parameters are shown in column 3 of Table 3 (Solution 2). Figure 8 shows the final spotted model fit (solid line) overlaid onto the observed light curves with the residuals shown in Figure 9. Solution 2 gave an improved fit with the residuals 2.3 times smaller compared to solution 1. The single large spot on the secondary star was sufficient to model most of the asymmetries in the observed light curves. A graphical representation of solution 2 is shown in Figure 10.

5. Discussion and conclusions

V737 Cep is a W-subtype eclipsing binary with the more massive cooler secondary at a lower surface brightness than its companion. The primary minimum is an occultation. The best-fit spotted WD solution gives a fill-out of 19%, which is consistent with a contact binary. The total eclipses provide the necessary constraints for an accurate determination of the mass ratio (q) in the WD solution (Wilson 1978) (Terrell and Wilson 2005). Provisional absolute stellar parameters can now be calculated using this mass ratio and the secondary star's mass (M_2). M_2 was estimated from the period-mass relation for contact binaries (Gazeas and Stępień 2008):

$$\log M_2 = (0.755 \pm 0.059) \log P + (0.416 \pm 0.024) . \quad (6)$$

The calculated stellar masses are $M_2 = 1.05 \pm 0.09\, M_\odot$ and $M_1 = 0.42 \pm 0.04\, M_\odot$. Kepler's Third Law gives the distance between the mass centers of the two stars, $2.14 \pm 0.05\, R_\odot$. The WD light curve program (LC) computed the stellar radii, surface gravities, and bolometric magnitudes. The mean stellar densities were calculated from the following equations:

$$\bar{\rho}_1 = \frac{0.0189}{r_1^3 (1 + q) P^2} \quad \text{and} \quad \bar{\rho}_2 = \frac{0.0189q}{r_2^3 (1 + q) P^2} , \quad (7)$$

where the stellar radius is normalized to the semi-major axis and P is in days (Mochnacki 1981). All the calculated stellar parameter values are collected in Table 4. A spectroscopic study of this system would provide the radial velocity measurements required to confirm the provisional masses and orbital radii presented here.

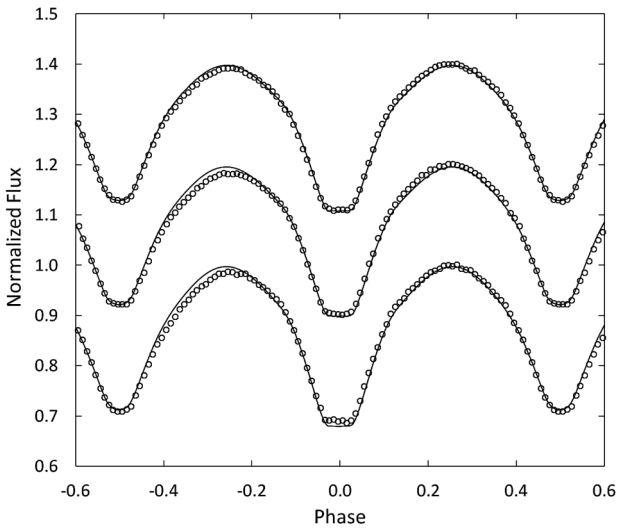

Figure 6. The WD model fit without spots (solid curve) to the observed normalized flux curves for each passband. From top to bottom the passbands are Sloan i', Sloan r', and Sloan g'. Each curve is offset by 0.2 for this combined plot. The best-fit parameters are given in column 2 of Table 3. Error bars are omitted from the points for clarity.

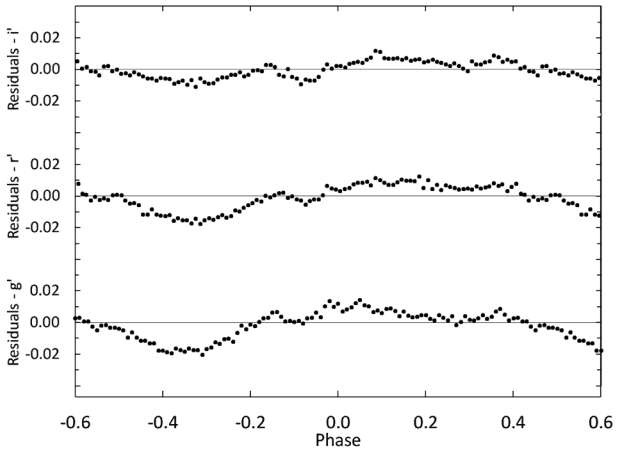

Figure 7. The residuals for the best-fit WD model without spots. Error bars are omitted from the points for clarity.

The (O–C) residuals shown in Figure 4 indicate the orbital period of V737 Cep is decreasing. The quadratic least-squares solution gives the rate of period change as $dP/dt = -8.0\,(4) \times 10^{-7}$ d yr^{-1}, or 6.9 seconds per century. If the decreasing orbital period is the result of a secular period change, then conservative mass exchange is occurring from the larger more massive secondary star to the primary star at a rate of $dM/dt = 6.3\,(2) \times 10^{-7}\, M_\odot$/yr. It is also possible that the period change results from a light-time effect. The (O–C) curve may be a small part of longer sinusoidal ephemeris caused by a third body orbiting the contact binary on a wide orbit. The light curve solution may support the second possibility, given the considerable third-light found, reaching about 37 percent in each passband. A field star could also be responsible for the third-light contribution. Careful examination of the best images

Table 3. Results derived from light curve modeling.

Parameter	*Solution 1 (no spots)*	*Solution 2 (1 spot)*
phase shift	–0.0017 ±0.0002	–0.0036 ±0.0001
filling factor	20%	19%
i (°)	89.8 ± 4	88.1 ± 1
T_1 (K)	[1] 5280	[1] 5280
T_2 (K)	4984 ± 8	4982 ± 6
$\Omega_1 = \Omega_2$	5.82 ± 0.03	5.83 ± 0.02
$q(M_2 / M_1)$	2.50 ± 0.02	2.50 ± 0.01
$L_1 / (L_1 + L_2)$ (g')	0.3918 ± 0.0017	0.3924 ± 0.0007
$L_1 / (L_1 + L_2)$ (r')	0.3679 ± 0.0016	0.3683 ± 0.0007
$L_1 / (L_1 + L_2)$ (i')	0.3581 ± 0.0012	0.3585 ± 0.0006
l_3 (g′)	[2] 0.376 ± 0.005	[2] 0.374 ± 0.003
l_3 (r′)	[2] 0.373 ± 0.005	[2] 0.371 ± 0.003
l_3 (i′)	[2] 0.370 ± 0.004	[2] 0.369 ± 0.003
r_1 side	0.301 ± 0.001	0.303 ± 0.001
r_2 side	0.488 ± 0.004	0.479 ± 0.002
$\sum res^2$	0.14	0.06
Spot Parameters		*Star 2—cool spot*
colatitude (°)		107 ± 14
longitude (°)		318 ± 3
spot radius (°)		24 ± 6
Temp.-factor		0.95 ± 0.02

[1] *Assumed.*
[2] *Third lights are the percent of light contributed at orbital phase 0.25.*

The subscripts 1 and 2 refer to the star being eclipsed at primary and secondary minimum, respectively.

Note: The errors in the stellar parameters result from the least-squares fit to the model. The actual uncertainties of the parameters are considerably larger (T_1 and T_2 have uncertainties of about ± 200 K).

Table 4. Estimated absolute parameters for V737 Cep.

Parameter	*Symbol*	*Value*
Stellar masses	M_1 ($M_\odot$)	0.42 ± 0.04
	M_2 ($M_\odot$)	1.05 ± 0.09
Semi-major axis	a ($R_\odot$)	2.14 ± 0.05
Mean stellar radii	R_1 ($R_\odot$)	0.67 ± 0.02
	R_2 ($R_\odot$)	1.01 ± 0.02
Stellar luminosity	L_1 ($L_\odot$)	0.32 ± 0.08
	L_2 ($L_\odot$)	0.57 ± 0.24
Bolometric magnitude	$M_{bol,1}$	6.0 ± 0.3
	$M_{bol,2}$	5.4 ± 0.5
Surface gravity	log g_1 (cgs)	4.40 ± 0.04
	log g_2 (cgs)	4.45 ± 0.04
Mean density	$\overline{\rho}_1$ (g cm^{-3})	1.92 ± 0.06
	$\overline{\rho}_2$ (g cm^{-3})	1.42 ± 0.08

The calculated values in this table are provisional. Radial velocity observations are necessary for direct determination of M_1, M_2, and a.

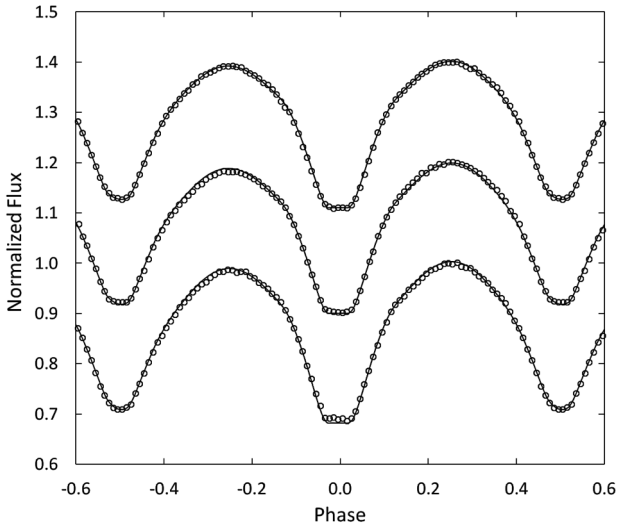

Figure 8. The WD model fit with spots (solid curve) to the observed normalized flux curves for each passband. From top to bottom the passbands are Sloan i', Sloan r', and Sloan g'. Each curve is offset by 0.2 for this combined plot. The best-fit parameters are given in column 3 of Table 3. Error bars are omitted from the points for clarity.

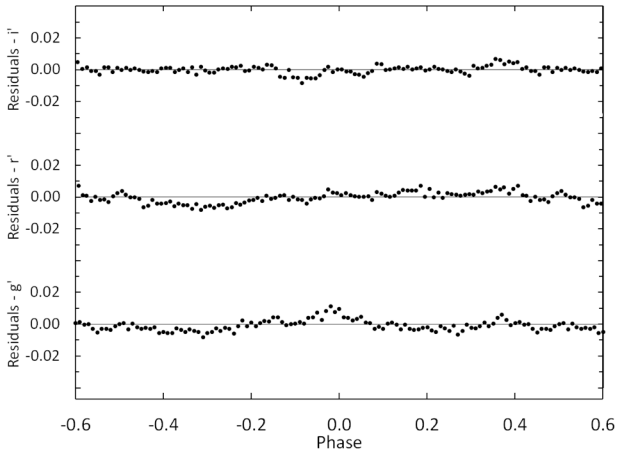

Figure 9. The residuals for the spotted WD model in each passband. Error bars are omitted from the points for clarity.

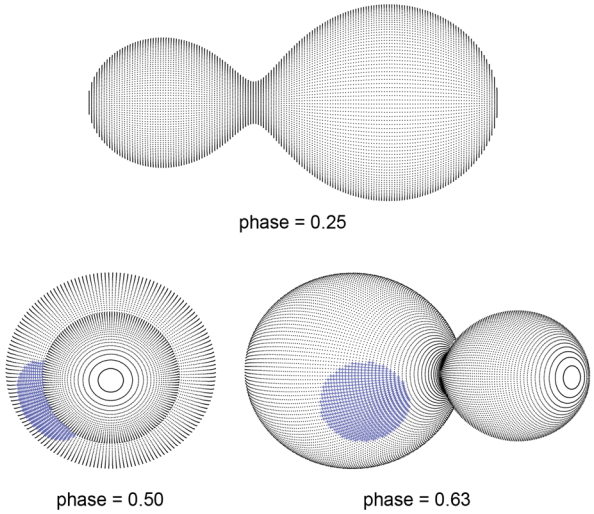

Figure 10. Roche Lobe surfaces of the best-fit wd spot model with orbital phase shown below each diagram.

acquired in this study as well as a Digitized Sky Survey (DSS) image showed no evidence of a field star. Additional precision times of minima spanning several years will be necessary to confirm whether V737 Cep is a trinary system.

6. Acknowledgements

This research was made possible through the use of the AAVSO Photometric All-Sky Survey (APASS), funded by the Robert Martin Ayers Sciences Fund. This research has made use of the SIMBAD database and the VizieR catalogue access tool, operated at CDS, Strasbourg, France. This work has made use of data from the European Space Agency (ESA) mission Gaia (https://www.cosmos.esa.int/gaia), processed by the Gaia Data Processing and Analysis Consortium (DPAC, https://www.cosmos.esa.int/web/gaia/dpac/consortium). Funding for the DPAC has been provided by national institutions, in particular the institutions participating in the Gaia Multilateral Agreement.

References

Bilir, S., Karaali, S., and Tunçel, S. 2005, *Astron. Nachr.*, **326**, 321.

Bradstreet, D. H., and Steelman, D. P. 2002, *Bull. Amer. Astron. Soc.*, **34**, 1224.

Gaia Collaboration: Prusti, T., *et al.* 2016, *Astron. Astrophys.*, **595A**, 1 (Gaia Data Release 1).

Gazeas, K., and Stępień, K. 2008, *Mon. Not. Roy. Astron. Soc*., **390**, 1577.

Gettel, S. J., Geske, M. T., and McKay, T. A. 2006, *Astron. J.*, **131**, 621.

Henden, A. A., *et al.* 2014, AAVSO Photometric All-Sky Survey, data release 9, (http:www.aavso.org/apass).

Hoňková, K., *et al.* 2013, *Open Eur. J. Var. Stars*, No. 160, 1.

Hübscher, J. 2013, *Inf. Bull. Var. Stars*, No. 6084, 1.

Hübscher, J. 2017, *Inf. Bull. Var. Stars*, No. 6196, 1.

Hübscher, J., and Lehmann, P. 2012, *Inf. Bull. Var. Stars*, No. 6026, 1.

Hübscher, J., and Lehmann, P. B. 2013, *Inf. Bull. Var. Stars*, No. 6070, 1.

Hübscher, J., Lehmann, P. B., and Walter, F. 2012, *Inf. Bull. Var. Stars*, No. 6010, 1.

Juryšek, J., *et al.* 2017, *Open Eur. J. Var. Stars*, No. 179, 1.

Kafka, S. 2017, variable star observations from the AAVSO International Database (https://www.aavso.org/aavso-international-database).

Kazarovets, E. V., Samus, N. N., Durlevich, O. V., Kireeva, N. N., and Pastukhova, E. N. 2008, *Inf. Bull. Var. Stars*, No. 5863, 1.

Kukarkin, B. V., and Kholopov, P. N. 1982, *New Catalogue of Suspected Variable Stars*, Nauka, Moscow.

Lucy, L. B. 1968, *Astrophys, J.*, **151**, 1123.

Lucy, L. B., and Wilson, R. E. 1979, *Astrophys, J.*, **231**, 502.

Mirametrics. 2015, Image Processing, Visualization, Data Analysis, (http://www.mirametrics.com).

Mochnacki, S. W. 1981, *Astrophys. J.*, 245, 650.

Nelson, R. H. 2014, *Inf. Bull. Var. Stars*, No. 6092, 1.

Nelson, R. H. 2016, *Inf. Bull. Var. Stars*, No. 6164, 1.

Otero, S., Wils, P., and Dubovsky, P. A. 2005, *Inf. Bull. Var. Stars*, No. 5586, 1.

Pecaut, M. J., and Mamajek, E. E. 2013, *Astrophys. J., Suppl. Ser.*, **208**, 9, (http://www.pas.rochester.edu/~emamajek/EEM_dwarf_UBVIJHK_colors_Teff.txt).

Pickles, A., and Depagne, E. 2010, *Publ. Astron. Soc. Pacific*, **122**, 1437.

Ruciński, S. M. 1969, *Acta Astron.*, **19**, 245.

Terrell, D., and Wilson, R. E. 2005, *Astrophys. Space Sci.*, **296**, 221.

van Hamme, W. 1993, *Astron. J.*, **106**, 2096.

van Hamme, W., and Wilson, R. E. 1998, *Bull. Amer. Astron. Soc.*, **30**, 1402.

Watson, C., Henden, A. A., and Price, C. A. 2014, AAVSO International Variable Star Index VSX (Watson+, 2006–2014; http://www.aavso.org/vsx).

Wilson, R. E. 1978, *Astrophys. J.*, **224**, 885.

Wilson, R. E., and Biermann, P. 1976, *Astron. Astrophys.*, **48**, 349.

Wilson, R. E., and Devinney, E. J. 1971, *Astrophys. J.*, **166**, 605.

KIC 8462852: Maria Mitchell Observatory Photographic Photometry 1922 to 1991

Michael Castelaz
Division of Science and Mathematics, Brevard College, Brevard, NC 28712; michael.castelaz@brevard.edu

Thurburn Barker
Astronomical Photographic Data Archive, Pisgah Astronomical Research Institute, Rosman, NC 28772; tbarker@pari.edu

Received January 23, 2018; revised February 20, 2018; accepted February 23, 2018

Abstract A new study of the long-term photometric behavior of the the unusual star KIC 8462852 (Boyajian's Star) has been carried out using archival photographic plates from 1922–1991 taken at the Maria Mitchell Observatory (MMO). We find five episodes of sudden, several day, decreases in magnitude occurring in 1935, 1966, 1978, and two in 1980. Episodes of sudden increase in magnitude appear to occur in 1967 and 1977. Inspection of archival light curves of KIC 8462852 from two previous studies based on the Harvard and the Sonneberg plate collections finds apparent corresponding events to these observed episodes in the MMO light curve. Also, a general trend of 0.12 ± 0.02 magnitude per century decrease is observed in the MMO light curve, significant, but less than the trend of 0.164 ± 0.013 observed in the Harvard light curve.

1. Introduction

KIC 8462852 (Boyajian's star; R. A. (J2000) $20^h\ 06^m\ 15.455^s$ Dec. (J2000) +44° 27' 24.793") is an F3V star which underwent several aperiodic dimming events lasting several days (hereafter referred to as dips) in the Kepler bandpass by 16% in 2011 and again in 2013 by 21%, 3%, and 8%, in addition to six other dips of 0.5% and less during the Kepler mission (Boyajian *et al* 2016). A series of dips in 2013 were separated by a total of about 50 days. The star dipped again a few percent in May 2017 (Waagen 2017). Using 800 days of photometry from the All-Sky Automated Survey for Supernovae (ASAS-SN; Shappee *et al.* 2014) and 4,000 days of photometry from the All-Sky Automated Survey (ASAS; Pojmański 2002), Simon *et al.* (2017) find two brightening episodes lasting several hundred days and a steady decrease in magnitude of 6.3 ± 1.4 mmag yr^{-1}. Kiefer *et al.* (2017) reanalyzed the Kepler data and found 22 dips, with two dip events separated by 928.25 days, each lasting ~2 days and dropping 1010 ± 40 ppm. Furthermore, Gary and Bourne (2017) observe U-shaped fading separated in time by 4.4 years. Besides dips and brightening episodes, Montet and Simon (2016) found cumulative fading of 3% over the four year Kepler mission which is similar to the dimming observed by Simon *et al.* (2017).

Explanations for long term dimming and brightening and dips include models of obscuration that could result from the catastrophic destruction of a planet, large comet fields impacting the star, asteroids, and planetary/massive object transits (for various scenerios see Boyajian *et al.* 2018). One transit model includes Trojan-like asteroids and a ringed planet (Ballesteros *et al.* 2018) and makes the prediction that large decreases will occur again in the year 2021 based on a ≈12-year orbital period of a ringed planet. Another transit model indicates a 4.31-year period attributed to a transit or groups of transits (Sacco *et al.* 2017). The transit model of Neslušan and Budaj (2017) shows that the light curve can be explained with four massive objects where each massive object is surrounded by a dust cloud and all four objects are in similar eccentric orbits. Metzger *et al.* 2017) develop models of planetary consumption where the dips are due to obscuration by planetary debris from the disruption of a Jupiter-mass planet. This study also explains the slow long term dimming of KIC 8462852. Boyajian *et al.* (2018) observed 4 dips from 1% to 4% beginning in May 2017 until the end of 2017. Their observations are consistent with obscuration by ordinary dust.

Internal mechanism models used to describe the variations of KIC 8462852 were originally proposed by Wright and Sigurdsson (2016). Foukal (2017) explains the long and short term variability of KIC 8462852 with a model of star spots where the stellar convective zone stores the heat flux. Dips in the magnitude of KIC 8462852 may be the star storing its radiative flux. Sheikh *et al.* (2016) modeled the small few tenths of a percent dips in the Kepler light curve of KIC 8462852 as intrinsic transitions, but this model does not explain the deep, sudden dips like those observed in 2011 and 2013. Clearly, continued observations are needed to constrain the external and intrinsic mechanism models developed to explain the light curve.

Photometry from archival photographic plates can provide data useful for testing models by searching for long term variations and dips looking back in time many decades. Photometric studies extending back more than 100 years have been conducted from historic data archived in photographic plate collections. Schaefer (2016) presents a light curve from 1,338 Harvard College Observatory plates over the period 1890 to 1989. The digitization and photometry were provided by the Digital Access to a Sky Century @ Harvard project (DASCH; Grindlay *et al.* 2009). The light curve from the Harvard data suggests KIC 8462852 is dimming 0.164 ± 0.013 magnitude per century.

Hippke *et al.* (2016) accessed the Sonneberg Observatory photographic plate collection (Bräuer and Fuhrmann 1992) to produce light curves from 861 B magnitudes (Sonnberg—pv data) and 397 V magnitudes (Sonneberg-pg data) covering the period from 1934 to 1995. The light curve shows constant magnitude to within 0.03 magnitude per century, or about a 3% decrease in brightness, consistent with the ASAS light curve and Kepler data. The same study also used some plates

from the Sternberg Observatory and Pulkovo Observatory plate collections.

The Astronomical Photographic Data Archive at the Pisgah Astronomical Research Institute (Castelaz 2009; Barker 2014) contains a set of astronomical photographic plates consistently taken with the same telescope from the Maria Mitchell Observatory (MMO; Strelnitski 2009) from 1922 to 1991. The plates were taken by astronomers at Maria Mitchell Observatory for a study of DF Cygni (Belserene 1984), an RV Tau variable, and the field of view of the plates fortunately encompasses KIC 8462852. KIC 8462852 is located ~4.5° from DF Cygni. Throughout the period multiple plates were taken during single nights for several nights, providing the opportunity to search for sudden dimming (dips) and brightening (flare) events that last only several days. We have extracted the photographic magnitudes of KIC 8462852 from 835 MMO plates dating from 1922 to 1991. The light curve of KIC 8462852 is used to search for such events, as well as the reported long-term dimming.

2. Data

Figure 1 shows the number of MMO plates that contain KIC 8462852 taken per year from 1920 to 2000. Also shown are the histograms for the Harvard plates (Schaefer 2016) and Sonneberg plates (Hippke *et al.* 2016) that also contain KIC 8462852. The coverage of the MMO plates is more heavily weighted towards the 1930s whereas the Sonneberg collection is more heavily weighted towards the 1960s. The MMO, Harvard, and Sonneberg collections complement each other. Harvard plates before 1920 are not included in the histogram because we are interested in the comparison of the MMO plates with the other collections. Note the MMO and Sonneberg collections fill in the Harvard "Menzel gap" from 1952 to 1965.

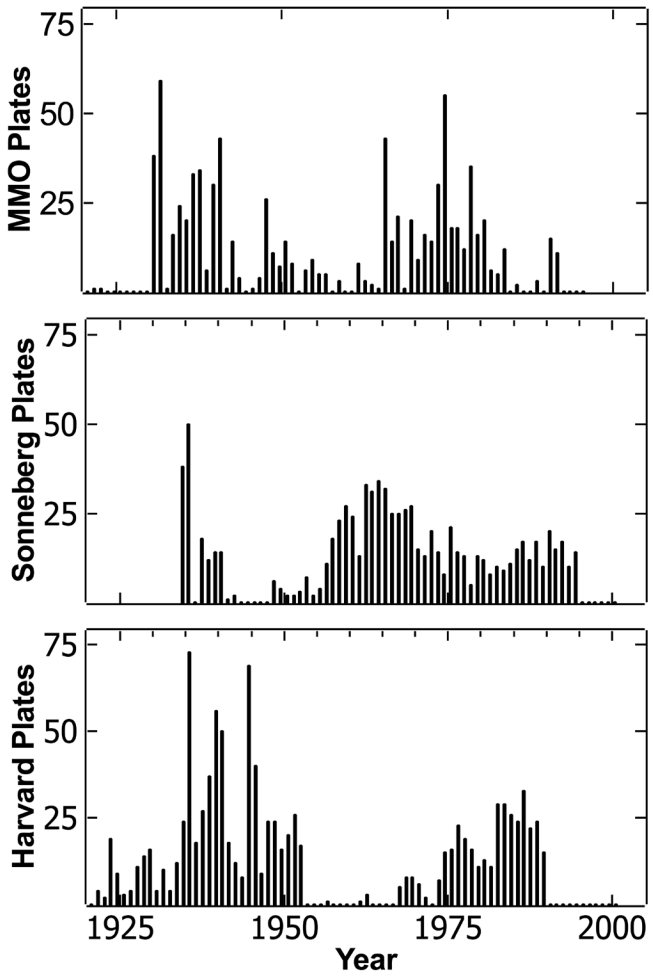

Figure 1. Histogram showing the number of plates that contain KIC 8462852 taken per year for the MMO, Harvard, and Sonneberg collections.

2.1. The Maria Mitchell plate collection

The Maria Mitchell Observatory (Strelnitsky 2009) photographic plate collection began in 1913 with the installation of the 7.5-inch Cooke/Clarke telescope. Plates are 8 × 10 inches with a plate scale of 240"/mm and a field size of 13.5° × 17° providing a uniform set of images. A large majority of plates are blue sensitive (Friel 1992). Exposure times for the plates in this study vary from 5 minutes to 60 minutes, with two plates (plate index numbers NA 468 and NA 487) with exposure times of 180 minutes taken in 1922 (Figure 2).

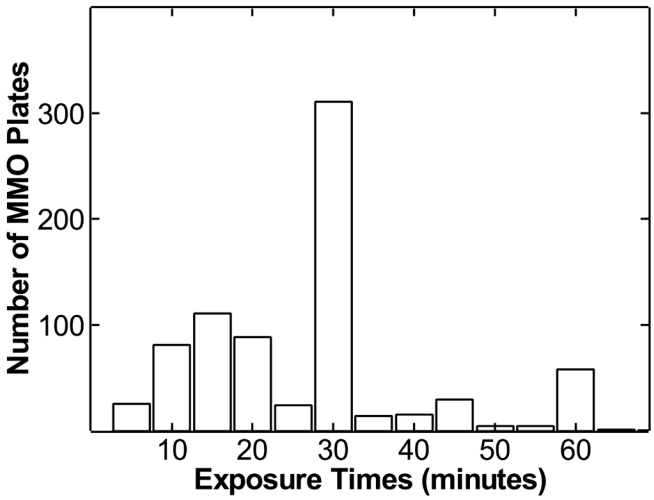

Figure 2. Histogram of exposure times of the plates used in this study. The two MMO plates taken in 1922 with exposure times of 180 minutes are not plotted.

2.2. KIC 8462852 photometry

A 40' × 68' area around KIC 8462852 was digitized and eight comparison stars in that area were selected. The criteria for comparison star selection was adopted from Schaefer (2016), although the stars themselves are not necessarily the same comparison stars used in the Harvard study because of the much smaller field of view used for the MMO photometry. Comparison stars are within one spectral subclass, and within 0.5 visual magnitude of KIC 8462852. The comparison stars are also selected because they are not identified as variables after a search through literature. Eight stars meet these criteria. The comparison stars are listed in Table 1. Figure 3 is the finding chart for the KIC 8462852 field of comparison stars. In this paper, to be consistent with the Harvard photometry of KIC 8462852 (Schaefer 2016), the comparison star photometric magnitudes are taken from the AAVSO Photometric All-Sky Survey (APASS; Henden and Munari 2014). Prior to 1950,

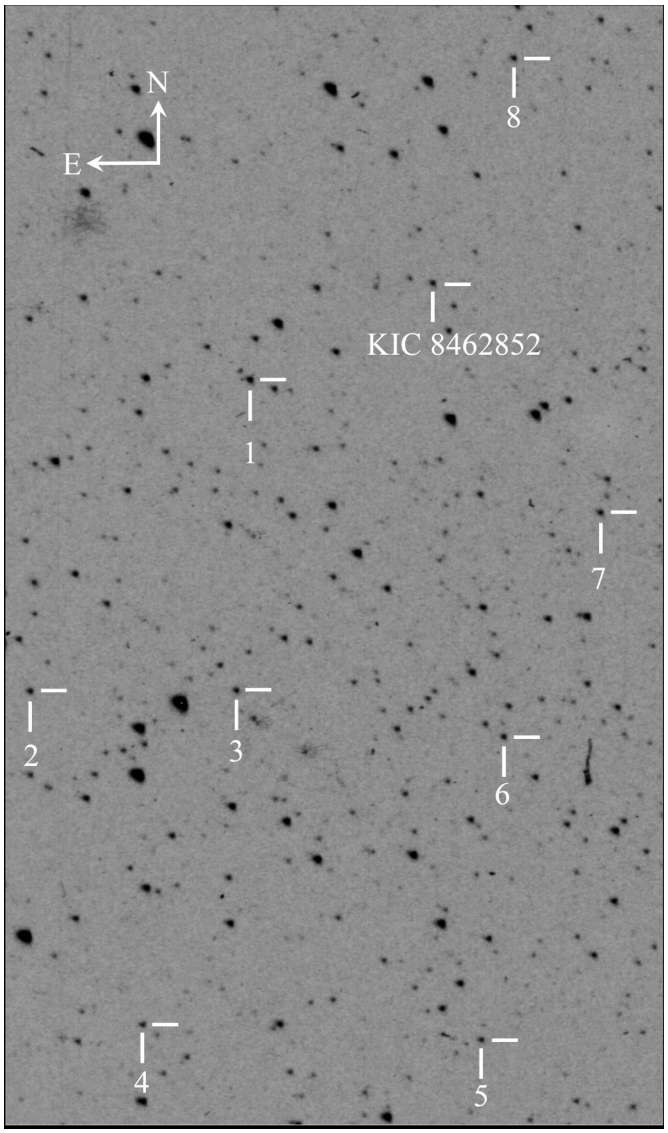

Figure 3. Finding chart. This field of view is from plate NA1143 taken 25 February 1931. The digitized image size is 10 mm × 17 mm (40' × 68'). KIC 8462852 and comparison stars are indicated in the figure and the comparison star names, coordinates, and APASS magnitudes are given in Table 1.

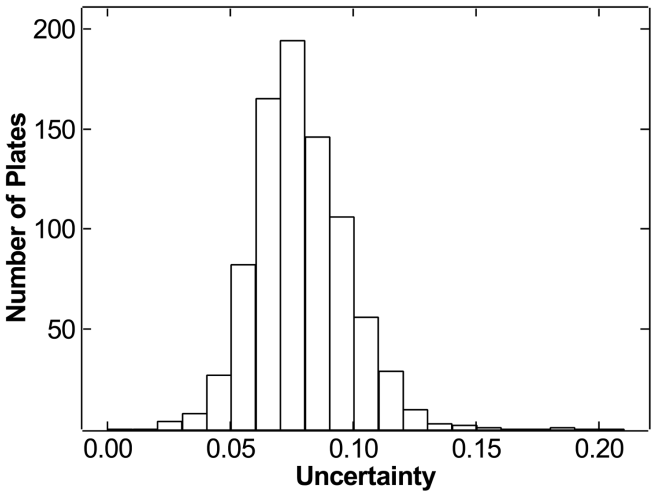

Figure 4. Histogram of uncertainties of the MMO Photometry.

Table 1. Comparison Stars. Figure 3 shows the field-of-view with these comparison stars.

Star No.	*TYC 3162-*	*R.A. (2000) h m s*	*Dec. (2000) ° ′ ″*	*APASS Magnitude*
1	1320-1	20 07 09.068	44 20 17.06	12.133
2	1698-1	20 08 28.312	44 00 36.23	12.108
3	488-1	20 07 16.759	44 01 24.86	12.158
4	964-1	20 07 42.879	43 40 14.10	12.478
5	420-1	20 05 45.801	43 40 28.10	12.604
6	462-1	20 05 43.265	43 59 27.68	12.351
7	316-1	20 05 13.017	44 13 41.71	12.125
8	509-1	20 05 50.997	44 41 43.34	12.107

three emulsion types were used that included Speedway, Cramer Presto, and Cramer Hispeed, and after 1950, only Eastman Kodak 103aO and IIaO emulsions were used (Davis 2004). All of these emulsions are blue sensitive, and the APASS magnitudes are closest in bandpass to the emulsions. However, because the MMO plates do have a variety of emulsion types, we refer to the MMO photometric results as photographic magnitudes (m_{pg}).

The photometry follows the method used by the Harvard DASCH project (Grindlay *et al.* 2009; Tang *et al.* 2013). Stars are extracted using the Source Extractor routine in the MIRA PRO photometry software (Walker *et al.* 2007). We set the threshold to 10 sigma above the background and measure the effective area of the eight selected comparison stars. This approach is more similar to iris photometry, where stellar magnitudes are measured by a density-weighted image diameter, than today's more common aperture photometry using total flux through a fixed measurement aperture. Every digitized image was visually inspected for defects like scratches on the emulsion. A total of 867 plates were found in the MMO collection with images of KIC 8462852. Of these, 32 were rejected because of defects or faint stellar images due to exposure times less than 5 minutes. A linear fit between the comparison star magnitudes and effective areas provides the calibration for KIC 8462852. This method deviates from the DASCH method where all stars in the field from the brightest to the faintest are used for calibration which requires a more robust fitting algorithm between magnitude and effective area. Because all of our comparison stars are within 0.5 mag of KIC 8462852, we used a linear fit.

From the linear fit of magnitude versus effective area we derive the magnitude of KIC 8462852. The mean residual is a measure of the uncertainty of the magnitude of KIC 8462852. Figure 4 is a histogram of uncertainties of all measured plates. The mean uncertainty is 0.07 mag and 81% of the plates have uncertainties ≤0.1 mag. Figure 5 shows the resulting MMO light curve of KIC 8462852.

For reproducibility and independent re-analysis, we release the data used to produce the figures (https://github.com/castelaz/kic8462852-MMO-data).

3. Results

3.1. Long term variation

For perspective, Figure 6 shows the light curves of KIC 8462852 and the comparison stars. A linear fit to each

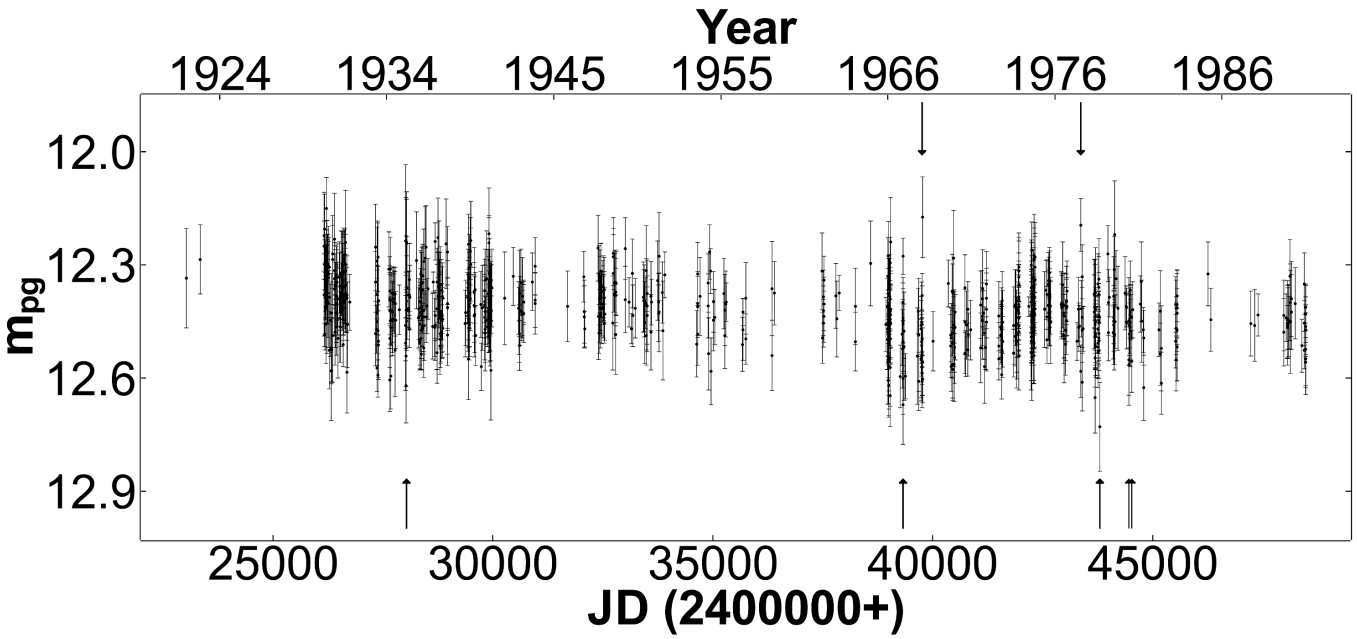

Figure 5. Light curve of KIC 8462852 from MMO photographic plates from 1922 to 1991. The up arrows point to dip events and the down arrows point to flare events. Two up arrows are blended for dip events which occurred between JD2444464 and 2444522 in 1980. For details see section 3.2, and Table 3.

light curve is included in Figure 6. Table 2 shows the slopes from the linear fits for KIC 8462852 and the comparison stars. The absolute values of the slopes of six of the eight comparison stars are $\leq 0.04 \pm 0.03$ mag/century. One comparison star has a slope of $+0.06 \pm 0.03$, and another has a slope of -0.07 ± 0.03 mag/century. In contrast, the derived slope of KIC 8462852 is $+0.11 \pm 0.04$ mag/century, larger than any of the comparison stars.

The MMO light curves (Figures 5 and 6) indicate a decrease in magnitude trend of $+0.11 \pm 0.04$ mag/century. Although not as steep as the 0.164 ± 0.013 mag/century slope measured by Schaefer (2016), the slope measured from the 70-year MMO light curve is consistent with the Harvard data. Schaefer (2016) had binned the Harvard data in five-year intervals, and doing the same with the MMO data, the linear fit indicates a decrease of $+0.12 \pm 0.02$ mag/century (Figure 7). The decrease in magnitude from 1922 to 1991 shown in Figure 7 clearly indicates that KIC 8462852 is slowly fading. These results contrast with the analysis of Hippke *et al.* (2016) who cite a slope of 0.046 ± 0.040 mag/century from all of the available Sternberg data and 0.09 ± 0.02 from Sternberg Astrograph data alone. However, the Astrograph data are not well-sampled, and only 17 measurements exist between 1960 and 1990. The MMO light curve supports the observation of slow fading of KIC 8462852.

3.2. Episodes of dip and flare events

Several photometric data points in the light curve of KIC 8462852 appear to stand out either as much dimmer (dips) or much brighter (flares) than most data points in the light curve. These anomalous data points are designated in Figure 5 with arrows. Table 3 lists the Julian Dates, dates, and magnitudes of these apparent dip and flare events in the MMO light curve. The photographic magnitudes of these events are fainter than 12.6 and brighter than 12.2, ~15% different than the average magnitude of 12.4, or 2- to 3-sigma difference based on the range of uncertainties of 0.06 magnitude to 0.11 magnitud of the measurements.

If the MMO events listed in Table 3 are real, then we would expect light curves from other data sets (Harvard, Sonneberg, and Sternberg) to show dip and flare events during the same time periods. Because the Kepler 2013 light curve shows a number of dips over a 50-day period, we also search a time window of ±50 days around each MMO event for dips and flares in the other data sets (Harvard and Sonneberg plate collections). Also, keeping in mind that the observations conducted in each data set were not synchronized with each other, and in most cases data may have been taken for several nights, and then gaps of days or weeks before the next set, we would not expect to find dip or flare events between data sets to match exactly. In fact, the dip and flare events may not actually be the faintest or brightest variation. Only regular, multiple observations over a long time frame, like the Kepler data, will measure the true dip or flare event magnitude. With these caveats in mind, comparison to Harvard (Schaefer 2016), Sonneberg and Sternberg (Hippke *et al.* 2016) light curves with dip events within ±50 days of the corresponding MMO events are given in Table 3. The Harvard, Sonneberg, and Sternberg magnitudes are each

Table 2. Slopes of light curves of KIC 8462852 and comparison stars.

Star	*Slope (mag/century)*
KIC 8462852	+0:11 ± 0:04
TYC 3162-1320-1	–0:02 ± 0:03
TYC 3162-1698-1	–0:04 ± 0:03
TYC 3162-488-1	–0:04 ± 0:03
TYC 3162-964-1	+0:03 ± 0:03
TYC 3162-420-1	+0:06 ± 0:03
TYC 3162-462-1	+0:03 ± 0:03
TYC 3162-316-1	+0:04 ± 0:03
TYC 3162-509-1	–0:07 ± 0:03

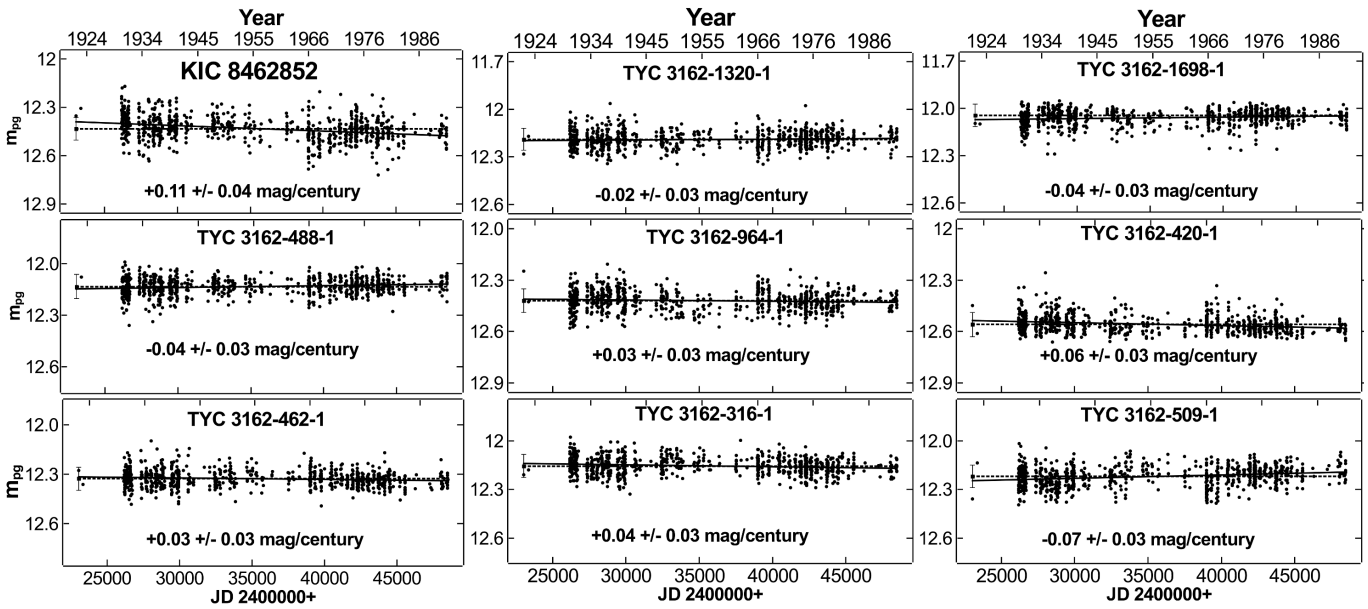

Figure 6. The light curve of KIC 8462852 and the comparison stars with linear fits to each light curve (solid lines). The slopes are given for each linear fit. A dotted line is drawn horizontally across each plot using the mean magnitude of each star, and a typical error bar is shown for reference on the left of each light curve.

Table 3. Dip and Flare events detected in the MMO light curve (Figure 5). Because the 2013 Kepler data show dips separated by up to 50 days, the nearest minima that appear in the Harvard, Sonneberg, and Sternberg data are given when the extrema are within 50 days of the MMO extrema. The Sonneberg data are dierential magnitudes in the two color bands pv (red) and pg (blue) (Hippke *et al.* 2016). Blanks are given where photographic data do not exist.

	MMO	*Harvard*	*Sonneberg pv*	*Sonneberg pg*	*Sternberg*
Average Mag.	12.43	12.34	–0.01	0.00	12.26
Dips					
JD	2428036	2428017	—	2428054	—
Date	21 Aug 1935	02 Aug 1935	—	8 Sep 1935	—
Mag.	12.61 ± 0.11	12.87 ± 0.26	—	0.39 ± 0.23	—
JD	2439323	—	2439363	—	—
Date	16 Jul 1966	—	25 Aug 1966	—	—
Mag.	12.66 ± 0.09	—	0.49 ± 0.13	—	—
JD	2443803	2443792	—	—	2443806
Date	21 Oct 1978	10 Oct 1978	—	—	24 Oct 1978
Mag.	12.68 ± 0.11	12.69 ± 0.21	—	—	12.36 ± 0.10
JD	2444464	2444467	—	—	—
Date	12 Aug 1980	15 Aug 1980	—	—	—
Mag.	12.69 ± 0.07	12.45 ± 0.14	—	—	—
JD	2444522	2444523	2444521	2444521	—
Date	09 Oct 1980	10 Oct 1980	08 Oct 1980	8 Oct 1980	—
Mag.	12.56 ± 0.07	12.61 ± 0.12	0.25 ± 0.19	0.42 ± 0.15	—
Flares					
JD	2439764	2439733	2439735	2439735	—
Date	30 Sep 1967	30 Aug 1967	01 Sep 1967	01 Sep 1967	—
Mag.	12.20 ± 0.09	12.29 ± 0.11	-0.29 ± 0.16	-0.13 ± 0.11	—
JD	2443366	2443371	2443372	2443372	—
Date	10 Aug 1977	15 Aug 1977	16 Aug 1977	16 Aug 1977	—
Mag.	12.22 ± 0.06	12.20 ± 0.11	-0.48 ± 0.13	-0.10 ± 0.10	—

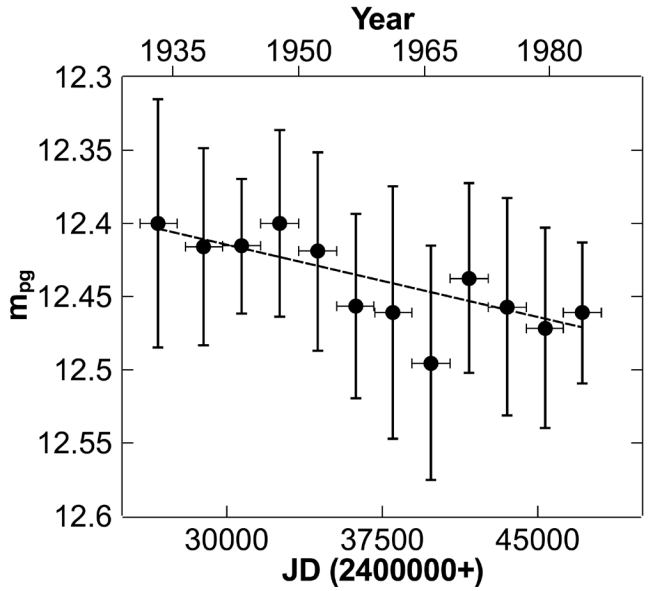

Figure 7. The light curve of KIC 8462852 binned in five-year intervals. The slope of the light curve is 0.12±0.02 magnitude/century (dashed line). The x-axis error bars show the five-year span for each data point. The y-axis error bars are the average residuals to the fit.

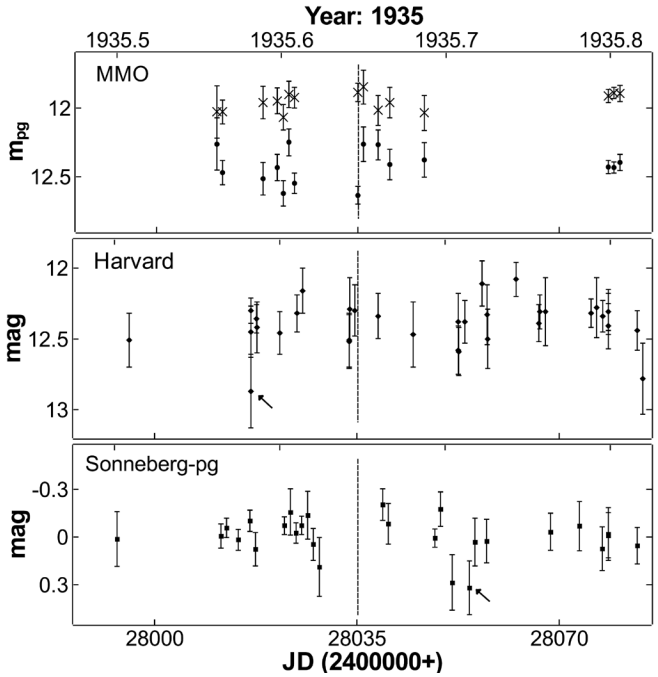

Figure 8. MMO light curve showing a dip event in 1935. The time spans 50 days before the MMO dip to 50 days after the MMO dip. The median comparison star magnitudes (denoted by "x"), offset by mpg = −0.25, don't show a dip. The MMO dip occurs on 21 August 1935 (1935.638, JD 2428036). Harvard and Sonneberg-pg data exist and those data are also shown. A dip in the Harvard data appears to occur on 2 August 1935 (arrow), and three dips appear to occur in the Sonneberg data with the deepest on 8 September 1935 (arrow). Sonneberg-pv data do not exist in 1935. The central vertical line marks the MMO dip event in each plot. See Table 3 for dates and magnitudes.

0.2 magnitude fainter or brighter than their respective average magnitudes, and represent ~15% differences. Figures 8, 9, 10, and 11 show the dip events detected in 1935, 1966, 1978, and 1980, respectively.

The observed dip and flare events could be due to factors related to the night sky, image quality, and exposure time, for example, and should not be dismissed. However, visual inspection of the MMO plates does not show defects or dirt near KIC 8462852 or any of the comparison stars. Also, the effects of sky conditions and image quality on the photometry are minimized because the eight comparison stars are near KIC 8462852 and would be affected in the same way. So, the dip and flare light curves shown in Figures 8–12 and given in Table 3 are taken as real.

Figure 8 shows the MMO light curve for a dip event that occurs on 21 August 1935 (Table 3). Data on the Harvard light curve were taken two days before the MMO dip event and do not show a dip. However, a dip event appears to occur in the Harvard data on 2 August 1935. The Sonneberg-pg data shows three possible dip events near the MMO dip event, two occurring on 8 September 1935 with relative magnitudes of 0.39±0.23 and 0.31±0.16. The third possible dip event in the Sonneberg-pg data occurs at 0.19±0.19. Because of the irregular spacing in time, none of these events correlate with any others, but do occur within 50 days of each other, and may be similar to events observed in the Kepler 2013 light curve that shows multiple dip events.

The 16 July 1966 dip event observed in the MMO light curve (Figure 9; Table 3) is m_{pg} = 12.66 ± 0.09 and seems to continue with m_{pg} = 12.61 ± 0.09 on 17 July 1966. But, by 20 July 1966, the MMO light curve no longer shows a dip. The Sonneberg-pv and Sonneberg-pg light curves have data on 12 July 1966 and 19 July 1966, and neither of these data show dip events similar to the July dates in the MMO light curve where no dips occur. Note the dip in the Sonneberg-pv data on 25 August 1966, 39 days after the MMO dip. A similar dip event would be expected in the Sonneberg-pg data taken on the same date, but one is not observed. MMO data do not exist for 25 August 1966. So, the nature of the apparent Sonneberg-pv dip event on 25 August 1966 is unclear.

The dip event of ~10% shown in Figure 10 and given in Table 3 on 22 October 1978 occurs in the last set of plates (plate index numbers NA6114, NA6115, and NA6116) taken at the end of the 1978 season. Photometry for the next season beginning 23 April 1979 shows the magnitude is once again like that from earlier in 1978 (see Figure 5). The fact that the Sternberg data show a drop on 24 October 1978 (Hippke *et al.* 2016), and the Harvard data drop on 10 October 1978 suggests the event is real. Sonneberg data do not exist during this time period. Being aware that the photographic plates were taken with a non-periodic cadence, with several plates taken one night followed by several nights of no imaging, the 1978 event may be near a minimum, but is not necessarily the minimum.

We observe two dip events in 1980 separated by 57 days (Figure 11; Table 3). One occurs on 12 August 1980. Three MMO photographic plates were taken on 12 August 1980 (JD 2444464.69, JD 2444464.80, and JD 2444464.83). Photometry from the first two plates, separated by 158 minutes,

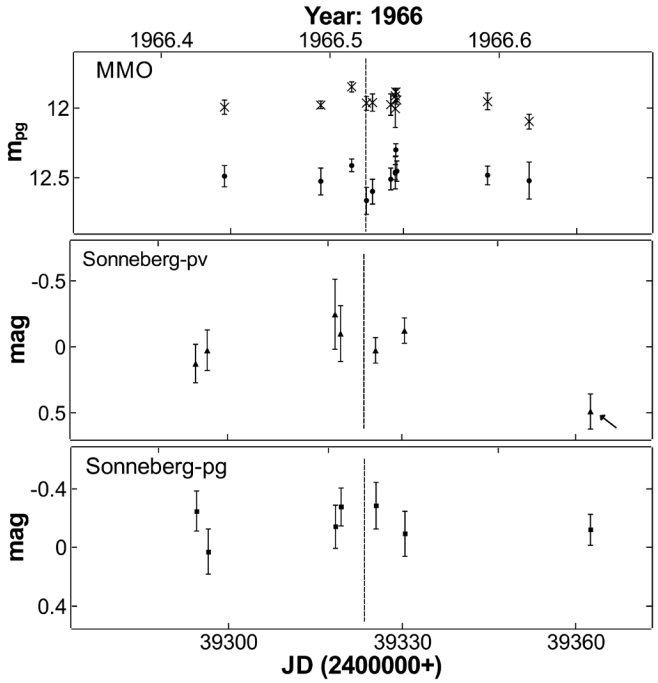

Figure 9. MMO light curve showing a dip event in 1966. The time spans 50 days before the MMO dip to 50 days after the MMO dip event. The median comparison star magnitudes (denoted by "x"), offset by mpg = –0.25, don't show a dip. The MMO dip occurs on 16 July 1966 (1966.512, JD 2439323). Sonneberg-pv and Sonneberg-pg data exist and those data are also shown. A dip event appears to occur in the Sonneberg-pv data on 25 August 1966 data (arrow), but the Sonneberg-pg data do not show a dip event on or around 25 August 1966. The central vertical line marks the MMO dip event in each plot. See Table 3 for dates and magnitudes.

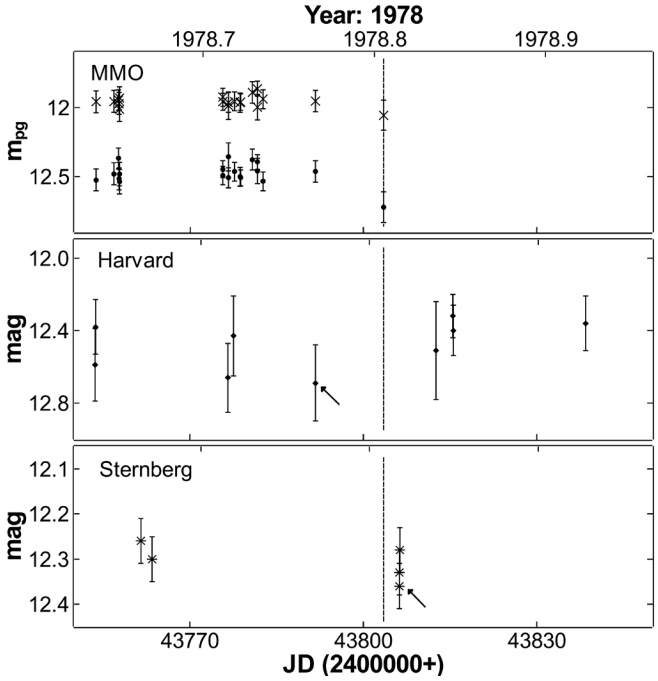

Figure 10. MMO light curve showing a dip event in 1978. The time spans 50 days before the MMO dip to 50 days after the MMO dip event. The median comparison star magnitudes (denoted by "x"), offset by mpg = –0.25, don't show a dip. The MMO dip occurs on 21 October 1978 (1978.805, JD 2443803). Harvard and Sternberg data exist and those data are also shown. A dip appears to occur in the Harvard data a few days before on 10 October 1978 (arrow), and a few days after in the Sternberg data on 24 October 1978 (arrow). Sonneberg-pv and Sonneberg-pg data do not exist for this time period. The central vertical line marks the MMO dip event in each plot. See Table 3 for dates and magnitudes.

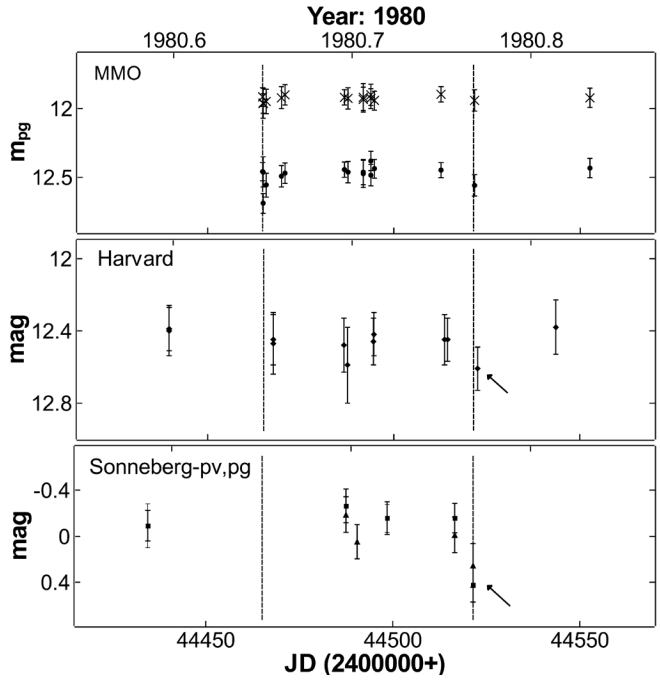

Figure 11. MMO light curve showing two dip events in 1980. The time spans 50 days before the first MMO dip to 50 days after the second MMO dip event. The median comparison star magnitudes (denoted by "x"), offset by mpg = –0.25, don't show a dip. The MMO dips occur on 13 August 1980 (1980.617, JD 2444465) and 9 October 1980 (1980.773, JD 2444522). Harvard, Sonneberg-pv (triangles), and Sonneberg-pg (rectangles) are also shown. An apparent dip in the Harvard data on 10 October 1980 (arrow) occurs one day after the second MMO dip event. The Sonneberg-pv and Sonneberg-pg data only exist in October and dips appear on 8 October 1980 (arrow). The central vertical lines mark the MMO dip events in each plot. See Table 3 for dates and magnitudes.

gives m_{pg} = 12.45 ± 0.07 and m_{pg} = 12.46 ± 0.10, respectively. The third in the sequence for that night of observing, 45 minutes after the second, gives m_{pg} = 12.69 ± 0.07. The next observations were on 13 August 1980 and 17 August 1980 and these give m_{pg} = 12.56 ± 0.08 and m_{pg} = 12.49 ± 0.08, respectively, indicating a return to an average MMO magnitude. The nearest Harvard datum is mag = 12.45 ± 0.21 on 15 August 1980, which does not appear to be significantly different from the Harvard average magnitude of 12.34, and is consistent with the 17 August 1980 MMO magnitude returning to an average magnitude. This suggests the 12 August 1980 dip event lasted only a few days.

The second MMO dip in 1980 occurred on 9 October. Note that Harvard and Sonneberg light curves have data on 10 October 1980 and 8 October 1980, respectively, so a comparison in magnitudes can be made between the data sets separated by only two days. The MMO dip is ~5% below the average, whereas the Harvard and Sonneberg magnitudes are ~10% below their averages. This dip event around 8–10 October 1980 is one of the stronger cases for a sudden decrease in brightness over a short period of just a few days.

Two events where KIC 8462852 appears to have flared in the MMO light curve occur on 30 September 1967 and 10 August 1977. These events are listed in Table 3 and are shown in Figure 12. In both cases, the increase in the MMO magnitude is ~10% above the normal scatter of ± 0.07 magnitude. Three MMO photographic plates were taken on 30 September 1967 (JD 2439764.6, JD 2439764.638, and JD 2439764.694).

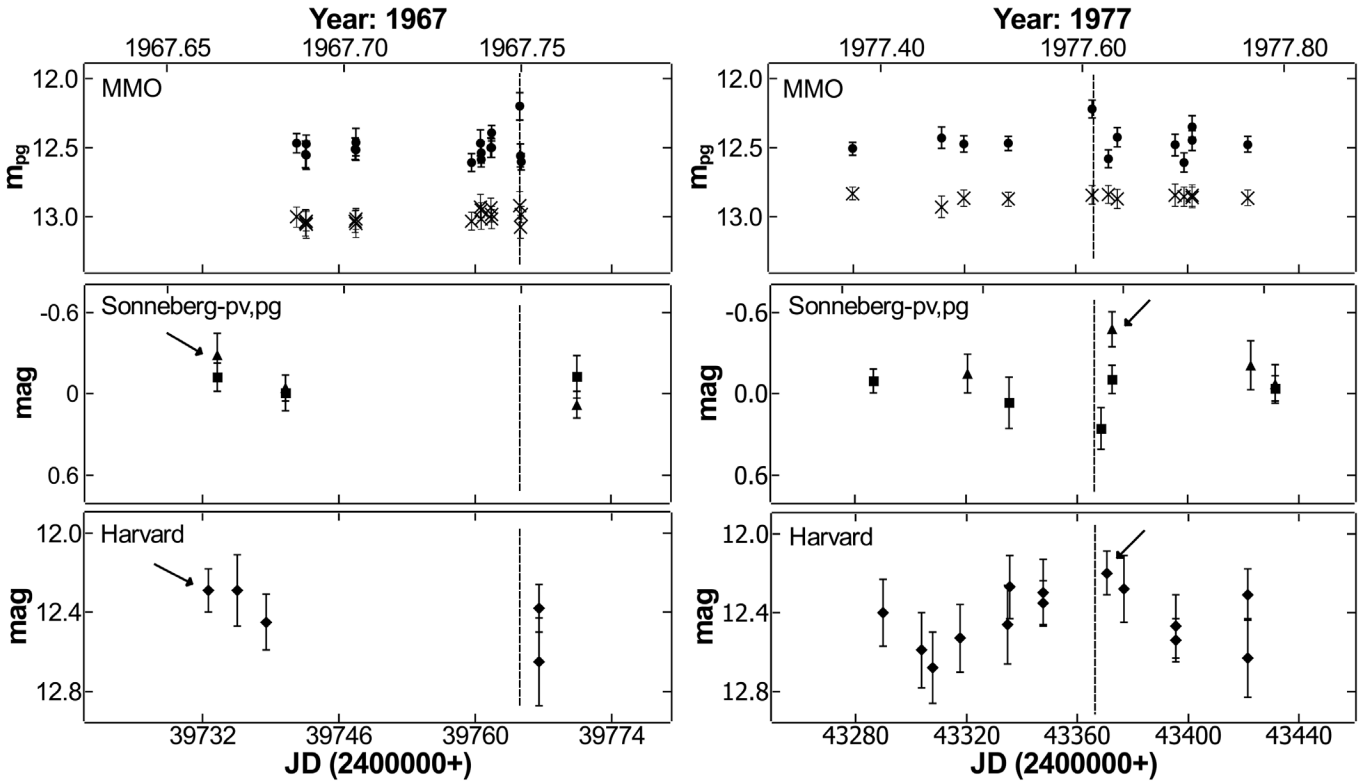

Figure 12. MMO, Harvard, Sonneberg-pv (triangles), and Sonneberg-pg (rectangles) light curves of observed flares over the period 30 August–30 September 1967, and again 10–16 August 1977. The dotted vertical line marks the MMO flare events in each plot. Flares observed in the Harvard and Sonneberg light curves are indicated by arrows. Sternberg data do not exist for these dates. The median MMO comparison star magnitudes (x; top frame), with magnitudes offset by mpg = +0.7, do not show the increase seen in KIC 8462852. See Table 3 for dates and magnitudes.

Photometry from the first gives m_{pg} = 12.20 ± 0.09 whereas the next two plates taken in sequence give m_{pg} = 12.56 ± 0.09 and 12.60 ± 0.06, 55 minutes and 155 minutes after the first plate, respectively. The next closest MMO photographic plate recorded was three nights before on 27 September 1977, where m_{pg} = 12.50 ± 0.07. The Sonneberg light curve does not have data taken near the MMO flare event. Harvard data taken within two days of the MMO flare do not show a flare event. Note that both the Sonneberg and Harvard light curves appear to have corresponding flare events on 30 August–1 September 1967, but MMO data do not exist for that date.

On 10 August 1980, the MMO magnitude was 12.22 ± 0.06, brighter than the average MMO magnitude of 12.43, and is considered a flare event. Photometry from Harvard plates suggests the the star is gradually increasing from mag = 12.35 ± 0.11 over 20 days to a peak of 12.20 ± 0.11 on 10 August 1977, then gradually decreasing for about 15 days to mag = 12.47 ± 0.16. The Harvard peak is within two days of the MMO flare event. The gradual brightening and fading over ~35 days in the Harvard light curve is reminiscent of the brightening episodes reported by Simon *et al.* (2017), but which in that case lasted several hundred days. The Sonneberg light curve shows an increase in magnitude from 12 August 1977 to 16 August 1977, consistent with the MMO and Harvard data. The flare events observed from the three different photographic plate collections coincide in 1977 and present a strong case for a KIC 8462852 flare event.

4. Discussion

The Kepler dip events with dips ≳10% occurred in March 2011 and about 720 days later in March 2013. Note that the 1978 MMO dip event is followed by another dip event in 1980, about 720 days later. The similarity in timing between the 2011–2013 and 1978–1980 light curve dip events is enticing. Neither the 1935 nor the 1966 dip events appears to have corresponding dip events occurring within 720 days. The lack of observed dip events separated by 720 days in the 1930s and 1960s may be due to the irregularity in observing times, resulting in gaps in data. However, these times are fairly well observed as seen in the light curve (Figure 5), so we might expect to see other dips. But, if the dips are ≲10%, we may not see the dip events in the MMO photographic data where typical uncertainty is ± 0.07 mag. As such, we cannot be certain the 720 days between MMO dip events 1978–1980 is a repetition of the 2011–2013 events. In any case, five apparent dip events were observed between 1922 and 1991 in the MMO light curve. Models like those of Ballesteros *et al.* (2018) which are based on periodic events cannot be ruled out, and attempts to fit such models to the MMO data may find a period that works. However, at the same time, debris models like those of Metzger *et al.* (2017) or models of internal mechanisms (e.g. Wright and Sigurdsson 2016; Foukal 2017; Sheiky *et al.* 2016), may also fit the MMO dip events.

The 1967 and 1977 MMO flare events occur within one year of the 1966 and 1978 dip events. The same does not occur in

1935 or 1980. Even though 23 MMO photographic plates were taken between 9 July and 11 December 1934, a year before the 1935 MMO dip event, no flare is observed. The same is true one year after, when 36 MMO photographic plates were taken between 3 April and 18 December 1936. Also, a year before the 1980 MMO dip events, 16 MMO photographic plates were taken between 23 April and 22 October 1979, and no flares were observed. Only six MMO photographic plates were taken between 26 April and 8 July 1981, a year after the 1980 MMO dip event, and no flare event was observed. As such, the flare events cannot be confidently connected to dip events. As pointed out in Section 3.2, the 1977 MMO flare event may be more of a gradual brightening over tens of days. The 1967 MMO flare lacks data and corresponding data in the Harvard and Sonneberg light curves to say the same. Without more evidence, we cannot say for certain whether the flares are sudden events or more gradual brightening of the star over tens of days. The 1967 and 1977 data seem to support both claims.

5. Conclusions

Our data indicate KIC 8462852 gradually decreased in magnitude over 70 years from 1922 to 1991. From binned five-year intervals of the light curve, our derived rate is $+0.12 \pm 0.02$ magnitude/century. This is consistent with the trend of slow fading first pointed out by Schaefer (2016), who found $+0.164 \pm 0.013$ from Harvard plates.

Five dip events and two flare events are observed, but the photographic data are too sparse to firmly establish any periodicity to the occurrence of the events. Also, the uncertainty in magnitude is large enough that perhaps other smaller dip or flare events may be lost in the noise. Constraints on either periodic transit models, debris models, and intrinsic mechanism models depend on future observations. However, observations from the past 100 years, like those from the MMO photographic plates, complement new observations and provide important tests for the models.

We point out that the use of archival photographic data to explore events in the light curve of KIC 8462852 can be expanded. In this paper we started with observed dips and flares in the MMO light curve and then looked for corresponding evidence of similar events from photometry from other photographic plate collections. An interesting study might be to begin with the identification of potential dips and flares in the Harvard collection, for example, and look for corresponding evidence in the Sonneberg and MMO light curves.

6. Acknowledgements

We acknowledge Terry Jednaszewski and Sheldon Kagel for digitizing the photographic plates. We gratefully acknowledge Don Cline and his efforts to secure our astronomical heritage by storing and archiving astronomical photographic plate collections in APDA at the Pisgah Astronomical Research Institute. We also gratefully acknowledge support from those who contributed to the crowdfunding project called The Astronomy Legacy Project, who helped fund the digitizing equipment that was used in this study. We also acknowledge the countless hours at the Maria Mitchell Observatory telescope by several generations of astronomers who took the photographic plates used in this study. We thank the anonymous referee for many helpful comments for improvements which helped clarify and focus this paper.

References

Ballesteros, F. J., Arnalte-Mur, P., Fernandez-Soto, A., and Martnez, V. J. 2018, *Mon. Not. Roy. Astron. Soc.*, **473**, L21.

Barker, T. H. 2014, in *Astroplate 2014*, eds. L. Mišková, S. Vitek, Institute of Chemical Technology, Prague, 4.

Belserene, E. P. 1984, *J. Amer. Assoc. Var. Star Obs.*, **13**, 62.

Boyajian, T. S., *et al.* 2016, *Mon. Not. Roy. Astron. Soc.*, **457**, 3988.

Boyajian, T. S., *et al.* 2018, ArXiv e-prints, arXiv:1801.00732 (https://arxiv.org/abs/1801.00732).

Bräuer, H.-J., and Fuhrmann, B. 1992, *Sterne*, **68**, 19.

Castelaz, M. W. 2009, in *Preserving Astronomy's Photographic Legacy: Current State and the Future of North American Astronomical Plates*, eds. W. Osborn, L. Robbins, ASP Conf. Ser. 410, Astronomical Society of the Pacific, San Francisco, 70.

Davis, A. 2004, *J. Amer. Assoc. Var. Star Obs.*, **32**, 126.

Foukal, P. 2017, *Astrophys. J., Lett.*, **842**, L3.

Friel, E. D. 1992, *J. Amer. Assoc. Var. Star Obs.*, **21**, 99.

Gary, B., and Bourne, R. 2017, *Res. Notes Amer. Astron.Soc.*, **1**, 22.

Grindlay, J., Tang, S., Simcoe, R., Laycock, S., Los, E., Mink, D., Doane, A., and Champine, G. 2009, in *Preserving Astronomy's Photographic Legacy: Current State and the Future of North American Astronomical Plates*, eds. W. Osborn, L. Robbins, ASP Conf. Ser. 410, Astronomical Society of the Pacific, San Francisco, 101.

Henden, A., and Munari, U. 2014, Contrib. Astron. Obs. Skalnate Pleso, **43**, 518.

Hippke, M., Angerhausen, D., Lund, M. B., Pepper, J., and Stassun, K. G. 2016, *Astrophys. J.*, **825**, 73.

Kiefer, F., Lecavelier des Etangs, A., Vidal-Madjar, A., Hébrard, G., Bourrier, V., and Wilson, P.-A. 2017, ArXiv e-prints, arXiv:1709.01732 (https://arxiv.org/abs/1709.01732).

Metzger, B. D., Shen, K. J., and Stone, N. 2017, *Mon. Not. Roy. Astron. Soc.*, **468**, 4399.

Montet, B. T., and Simon, J. D. 2016, *Astrophys. J., Lett.*, **830**, L39.

Neslusan, L., and Budaj, J. 2017, *Astron. Astrophys.*, **600**, A86.

Pojmański, G. 2002, *Acta Astron.*, **52**, 397.

Sacco, G., Ngo, L., and Modolo, J. 2017, ArXiv e-prints, arXiv:1710.01081 (https://arxiv.org/abs/1710.01081).

Schaefer, B. E. 2016, *Astrophys. J., Lett.*, **822**, L34.

Shappee, B. J., *et al.* 2014, *Astrophys. J.*, **788**, 48.

Sheikh, M. A., Weaver, R. L., and Dahmen, K. A. 2016, *Phys. Rev. Lett.*, **117**, i.d. 261101 (https://link.aps.org/doi/10.1103/PhysRevLett.117.261101).

Simon, J. D., Shappee, B. J., Pojmański, G., Montet, B. T., Kochanek, C. S., van Saders, J., Holoien, T. W.-S., and Henden, A. A. 2017, ArXiv e-prints, arXiv:1708.07822 (https://arxiv.org/abs/1708.07822).

Strelnitski, V. 2009, in *Preserving Astronomy's Photographic Legacy: Current State and the Future of North American*

Astronomical Plates, eds. W. Osborn, L. Robbins, ASP Conf. Ser. 410, Astronomical Society of the Pacific, San Francisco, 96.

Tang, S., Grindlay, J., Los, E., and Servillat, M. 2013, *Publ. Astron. Soc. Pacific*, **125**, 857.

Waagen, E. O. 2017, *AAVSO Alert Not.*, No. 579, 1.

Walker, R. G., Weaver, W. B., Shane, W. W., and Babcock, A. 2007, *Icarus*, **187**, 285.

Wright, J. T., and Sigurdsson, S. 2016, *Astrophys. J., Lett.*, **829**, L3.

Observations, Roche Lobe Analysis, and Period Study of the Eclipsing Contact Binary System GM Canum Venaticorum

Kevin B. Alton
UnderOak Observatory, 70 Summit Avenue, Cedar Knolls, NJ; kbalton@optonline.net

Robert H. Nelson
Mountain Ash Observatory, 1349 Garvin Street, Prince George, BC V2M 3Z1, Canada
Guest Investigator, Dominion Astrophysical Observatory Herzberg Institute of AstrophysicsNational Research Council of Canada

Received January 24, 2018; revised March 23, 2018; accepted March 28, 2018

Abstract GM CVn is an eclipsing W UMa binary system (P = 0.366984 d) which has been largely neglected since its variability was first detected during the ROTSE-I campaign (1999–2000). Other than a single unfiltered light curve (LC) no other photometric data have been published. LC data collected in three bandpasses (B, V, and R_c) at UnderOak Observatory (UO) produced three new times of minimum for GM CVn. These along with other eclipse timings from the literature were used to update the linear ephemeris. Roche modeling to produce synthetic LC fits to the observed data was accomplished using BINARY MAKER 3, WDWINT56A, and PHOEBE v.31a. Newly acquired radial velocity data were pivotal to defining the absolute and geometric parameters for this partially eclipsing binary system. An unspotted solution achieved the best Roche model fits for the multi-color LCs collected in 2013.

1. Introduction

The variable behavior of GM CVn (GSC 2545-0970) was first observed during the ROTSE-I CCD survey (Akerlof *et al.* 2000); these photometric determinations are available on the Northern Sky Variable Survey website (Wozniak *et al.* 2004). The same data were analyzed later in more detail by Gettel *et al.* (2006), while an ephemeris was reported by Blättler and Diethelm (2006) based on new unfiltered light curve (LC) results. Although times of minimum light have been sporadically published since 2005, this paper marks the first detailed period analysis, spectroscopic study, and multi-color Roche model assessment of LCs for this system in the literature.

2. Observations and data reduction

2.1. Photometry

Photometric collection dates (UTC) at UnderOak Observatory (UO) included seven sessions between 05 May 2013 and 31 May 2013, with an additional imaging run captured on 05 June 2013. Equipment included a 0.2-m Schmidt-Cassegrain telescope with an SBIG ST-8XME CCD camera mounted at the Cassegrain focus. Automated imaging was performed with photometric B, V, and R_c filters sourced from SBIG and manufactured to match the Bessell prescription; the exposure time for all dark- and light-frames was 60 seconds. The computer clock was updated automatically via the U.S. Naval Observatory Time Server immediately prior to each session. Image acquisition (lights, darks, and flats) was performed using CCDSOFT v5 (Software Bisque 2011) while calibration and registration were performed with AIP4WIN v2.4.0 (Berry and Burnell 2005). Images of GM CVn were plate-solved using the standard star fields (MPOSC3) provided in MPOCANOPUS v10.7.1.3 (Minor Planet Observer 2015) in order to obtain the magnitude (B, V, and R_c) assignments for each comparison star. Reduction to magnitudes was accomplished using aperture photometry on a fixed ensemble of five non-varying comparison stars in the same field-of-view (FOV). Only images taken above 30° altitude (airmass < 2.0) were accepted in order to minimize the effects of differential refraction and color extinction.

2.2. Light curve analyses

Roche-type modeling was initially performed using BINARY MAKER 3.03 (BM3; Bradstreet and Steelman 2002). Thereafter, WDWINT56A (Nelson 2009) and PHOEBE v.31a (Prša and Zwitter 2005), both of which employ the Wilson-Devinney (WD) code (Wilson and Devinney 1971; Wilson 1990), were used to refine the fit and estimate parameter errors. A rendering of the Roche surface from GM CVn was produced by BM3 once model fitting was finalized. Times of minimum were calculated using the method of Kwee and van Woerden (1956) as featured in PERANSO v2.5 (Paunzen and Vanmunster 2016).

2.3. Spectroscopic observations

A total of ten medium-resolution (mean R ~ 10,000) spectra of GM CVn were acquired at the Dominion Astrophysical Observatory (DAO) in Victoria, British Columbia, Canada, between 09 April and 18 April 2017. For this study a Cassegrain spectrograph with a grating (#21181; 1,800 lines / mm) blazed at 5000 Å was installed on the 1.85-m "Plaskett" telescope. This provided a reciprocal first order linear dispersion of 10 Å / mm that approximately covered a wavelength region between 5000 and 5260 Å. Other specifics regarding the instrument and data processing are detailed elsewhere (Nelson 2010a).

3. Results and discussion

3.1. Photometry and ephemerides

A summary of the five stars in the same FOV with GM CVn used to derive catalog-based (MPOSC3) magnitudes in MPOCANOPUS is provided in Table 1. During each image acquisition session comparison stars typically stayed within ±0.014 mag for V and R_c filters and ±0.03 mag for B passband.

Table 1. Astrometric coordinates (J2000) and color indices (B–V) for GM CVn and five comparison stars used in this photometric study.

Star Identification	*R. A. h m s*	*Dec. ° ′ ″*	*MPOSC3[a] (B–V)*
GM CVn	14 02 46.63	32 08 47.9	0.618
TYC 2545-0240-1	14 02 05.69	32 08 01.8	0.521
TYC 2545-1027-1	14 02 05.69	32 11 49.1	0.598
TYC 2545-0285-1	14 01 22.44	32 17 24.9	1.131
TYC 2545-0235-1	14 01 04.29	32 16 04.8	0.502
GSC 02545-0759	14 01 58.48	32 06 24.1	0.660

a. MPOSC3 is a hybrid catalog which includes a large subset of the Carlsberg Meridian Catalog *(CMC-14) as well as data from the* Sloan Digital Sky Survey *(SDSS). Stars with BVR$_c$ magnitudes derived from 2MASS J–K magnitudes have an internal consistency of ± 0.05 mag. for V, ± 0.08 mag. for B, ± 0.03 mag. for Rc , and ± 0.05 mag. for B–V (Warner 2007).*

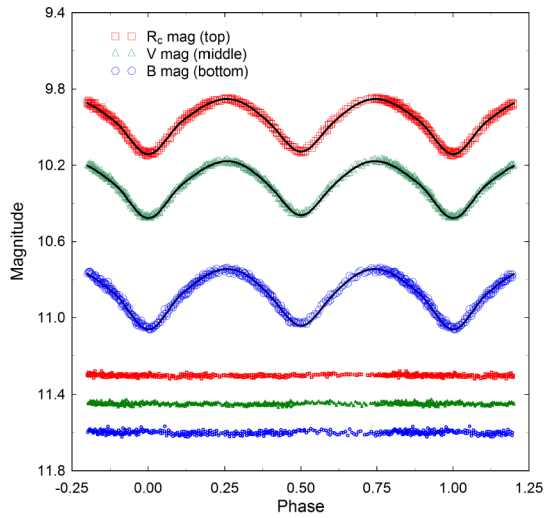

Figure 1. Folded CCD light curves for GM CVn produced from photometric data obtained between 05 May and 05 June 2013. The top (R$_c$), middle (V), and bottom (B) curves shown above were reduced to MPOSC3-based catalog magnitudes using MPOCANOPUS. The light curves are shallow and lack a total eclipse so the WD solution required simultaneous modeling with radial velocity data. In this case, the Roche model assumed a W-subtype contact binary with no spots; residuals from the model fits are offset at the bottom of the plot to keep the values on scale.

Photometric values in B (n = 332), V (n = 341), and R$_c$ (n = 345) passbands were separately processed to produce LCs that spanned 31 days in between 05 May and 05 June 2013 (Figure 1). These determinations included three new times of minimum for each filter and since there was no obvious color dependency on the timings, all data were averaged (Table 2) from each session. The Fourier routine (FALC; Harris *et al.* 1989) in MPOCANOPUS produced a slightly longer period solution (0.366996 ± 0.000001 d) after initially seeding the analysis with the orbital period (0.366986 d) from the ephemeris (Equation 1) derived by Blättler and Diethelm (2006). An independent verification of all period determinations was performed using PERANSO v2.5 (Paunzen and Vanmunster 2016) by applying periodic orthogonals (Schwarzenberg-Czerny 1996) to fit observations and analysis of variance (ANOVA) to assess fit quality. In this case a similar period solution (0.366995 ± 0.000012 d) was obtained. Finally, folding together (time span = 5,173 d) the sparsely sampled ROTSE-I data with those (V-mag) acquired at UO yielded a period at 0.366984 ± 0.000012 d. New minima acquired at UO along with published values starting in 2005 (Table 2) were used to analyze eclipse timings through 2016 when the latest time of minimum was reported in the literature. The reference epoch (Blättler and Diethelm 2006) employed for calculating ET differences (ETD) was defined by the following linear ephemeris Equation 1:

Table 2. Calculated differences (ETD)$_1$ following linear least squares fit of observed times-of-minimum for GM CVn and cycle number between 12 Jan 2005 and 17 Mar 2016.

HJD = 2400000+	*Cycle No.*	*ETD$_1$[a]*	*Reference*
53382.5390	–327	–0.004378	Diethelm 2006
53382.7261	–326.5	–0.000771	Diethelm 2006
53445.4833	–155.5	0.001823	Diethelm 2006
53463.4644	–106.5	0.000609	Diethelm 2006
53502.3652	–0.5	0.000893	Diethelm 2006
53502.5476	0	–0.000200	Diethelm 2006
53502.5478	0	0.000000	Blättler and Diethelm 2006
53515.3925	35	0.000190	Diethelm 2006
53515.5758	35.5	–0.000003	Diethelm 2006
53517.4118	40.5	0.001067	Diethelm 2006
53936.5091	1182.5	0.000355	Diethelm 2007
54174.4923	1831	–0.006866	Diethelm 2007
54856.9018	3690.5	–0.007833	Nelson 2010b
54857.0824	3691	–0.010726	Nelson 2010b
54936.7183	3908	–0.010788	Nelson 2010b
55015.4361	4122.5	–0.011485	Diethelm 2010
55560.9579	5609	–0.014374	Nelson 2011
56014.7339	6845.5	–0.016563	Nelson 2013a
56069.4179	6994.5	–0.013477	Hübscher and Lehmann 2013
56408.5114	7918.5	–0.015041	Hübscher 2013
56418.4159	7945.5	–0.019163	Hübscher 2013
56418.5992	7946	–0.019314	This study
56439.6980	8003.5	–0.022247	This study
56448.6917	8028	–0.019749	This study
57021.0020	9587.5	–0.024075	Nelson 2015
57115.4993	9845	–0.025670	Bahar *et al.* 2017
57119.5361	9856	–0.025716	Hübscher 2017
57352.0223	10489.5	–0.025147	Nelson 2016
57464.5003	10796	–0.028356	Hübscher 2017

a. (ETD)$_1$ = Eclipse Time Difference between observed time-of-minimum and that calculated using the reference ephemeris (Blättler and Diethelm 2006).

$$Min.\ I\ (HJD) = 2453502.5478 + 0.366986\ E. \quad (1)$$

Variations in orbital period over time can potentially be uncovered by plotting the difference between the observed eclipse times and those predicted by the reference epoch against cycle number (Figure 2). Thus far, all of the calculated ETD values basically describe a straight line relationship and suggest that little or no change to the period has occurred since 2005. The improved ephemeris (Equation 2) based on eclipse timing data available through March 2016 is as follows:

$$Min.\ I\ (HJD) = 2457464.5020(5) + 0.3669835(1)\ E. \quad (2)$$

Given that these data cover a relatively short span of time (~12 yr) there is always the possibility that significant orbital

period changes in the system had not occurred within this interval. Future times of minimum could potentially reveal residuals consistent with the gravitational influence of a third (or more) body, star-spot cycles (Applegate 1992), or periodic mass transfer between either star.

3.2. Light curve behavior

The phasing of the light curves reveals that GM CVn is tidally locked as expected for a W UMa eclipsing binary (Figure 1). The primary and secondary maxima are equal; this classically indicates that there are no major spots at the present (Yakut and Eggleton 2005). In contrast to the 2013 LCs, unfiltered photometric data taken during the ROTSE-I CCD survey and later by Blätter and Dielthelm (2006) did exhibit unequal heights (Max I > Max II), which indicates that this system like most other contact binaries is photospherically active (Figure 3).

3.3. Spectral classification

The interstellar extinction (A_V) was estimated for GM CVn according to the approach described by Amôres and Lépine (2005). This model, which is simulated in a companion program (ALEXTIN: http://www.galextin.org/explain.html) for targets within the Milky Way Galaxy, requires the galactic coordinates (*l, b*) and an estimated distance in kpc. In this case the value for A_V (0.024) corresponds to a target positioned at l = 55.348° and b = +73.936° which is located within 200 pc (see section 3.8). The dust maps rendered by Schlegel *et al.* (1998) and later refined by Schlafly and Finkbeiner (2011) determine extinction based on total dust in a given direction and not extinction within a certain distance. Therefore, reddening values for objects like GM CVn closer than 1 kpc tend to be overestimated ($A_V = 0.045$; $E(B–V) = 0.0145$) particularly as they approach the galactic plane. Color index (B–V) data collected at UO and those acquired from an ensemble of eight other sources (Table 3) were corrected using the reddening value estimated by factoring in distance. The median result ($(B–V)_0 = 0.588 \pm 0.027$) which was adopted for Roche modeling indicates a primary star with an effective temperature (5920 K) that ranges in spectral type between F9V and G0V.

3.4. Spectroscopic observations

A log of all spectra captured between 09 April and 18 April 2017 is provided in Table 4, while two representative sample spectra are illustrated in Figure 4. Spectral reduction was performed using the application RAVERE (Nelson 2010c). This software includes the ability to manually remove trace cosmic hits, produce a median background fit for each column (or wavelength), perform aperture summation and background subtraction for each column, and normalize the continuum. Final extraction of the RV data employed broadening functions (BROAD; Nelson 2013b) to improve peak resolution. Further details regarding the advantage of using wavelength broadening functions for contact binary systems rather than cross-correlation

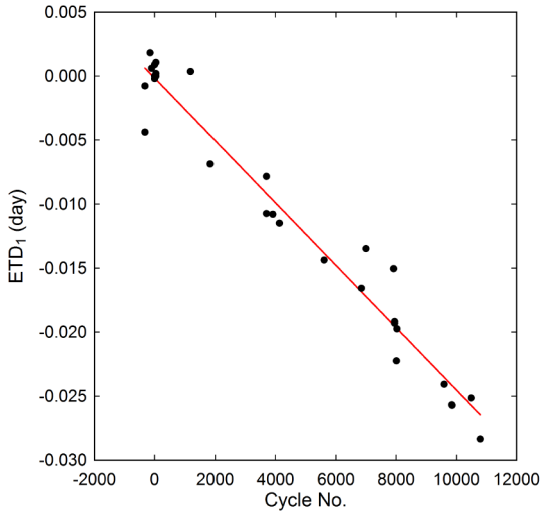

Figure 2. Straight line fit (ETD vs. period cycle number) suggesting that little or no change to the orbital period of GM CVn had occurred between 2005 and 2016.

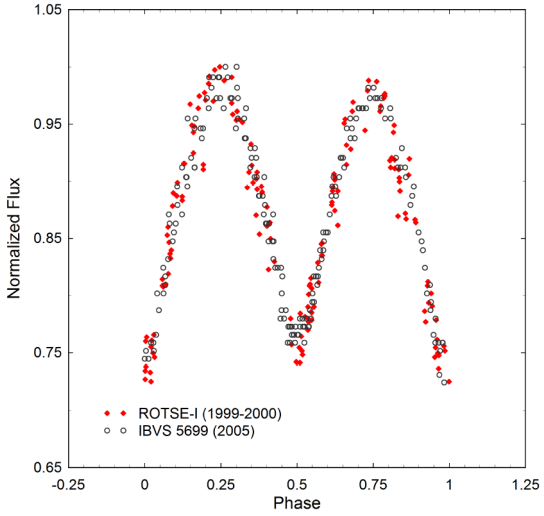

Figure 3. Folded (unfiltered) light curves (P = 0.366986 ± 0.000045 d) for GM CVn illustrating peak asymmetry (Max I > Max II) observed during quadrature in 1999–2000 (ROTSE-I; Akerlof *et al.* 2000) and in 2005 (Blättler and Diethelm 2006).

Table 3. Spectral classification of GM CVn based upon dereddened (B–V) data from eight surveys and the present study.

	USNO-B1.0	*All Sky Combined*	*2MASS*	*USNO A2*	*SDSS-DR9*	*Tycho*	*UCAC4*	*HIP/ Tycho*	*Present Study*
$(B–V)_0$	0.515	0.611	0.610	0.500	0.621	0.588	0.542	0.609	0.561
T_{effl} [a] (K)	6218	5863	5865	6278	5839	5921	6089	5867	6009
Spectral Class[a]	F7-F8V	G1-G2V	G1-G2V	F6-F7V	G1-G2V	F9-G0V	F8-F9V	G1-G2V	F9-G0V

a. T_{effl} interpolated and spectral class assigned from Pecaut and Mamajek (2013). Median value, $(B–V)_0 = 0.588 \pm 0.027$, corresponds to an F9V-G0V primary star ($T_{effl} = 5920$ K).

Table 4. A log of spectral observations at the DAO in April 2017.

DAO Image #	*Mid-time (HJD = 2400000+)*	*Exposure (s)*	*Phase at Mid-exp.*	*V_2 (km/s)*	*V_1 (km/s)*
3921	57852.8978	1748	0.370	-208.6 ± 2.0	37.70 ± 1.8
3938	57854.7431	157	0.398	-172.5 ± 3.6	25.95 ± 5.3
3958	57854.8960	1800	0.815	196.2 ± 3.7	-97.5 ± 3.7
3998	57859.8229	1800	0.240	-254.7 ± 1.7	56.0 ± 0.6
4032	57861.8914	600	0.876	149.0 ± 3.2	-87.8 ± 2.5

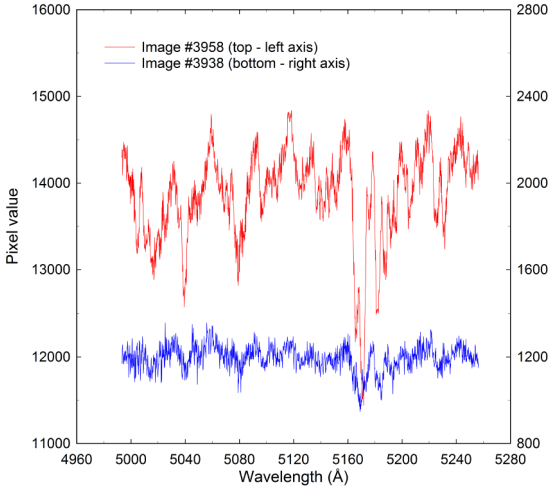

Figure 4. Representative spectra collected at DAO to determine radial velocities for GM CVn at φ = 0.398 (Image # 3938) and φ = 0.815 (Image # 3958).

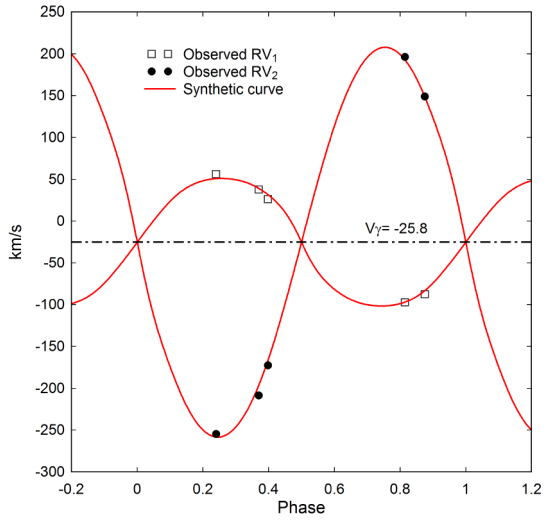

Figure 5. Best fit radial velocity curve produced following simultaneous WD modeling (WDWINT56A) with LC data. RMS error (2.72 km/s) for the synthetic RV curve indicated a good fit to the observed velocity data.

is described elsewhere (Ruciński 2004). Arguably, more data might dispel concerns about the robustness of the RV model fits; however, we feel confident about the final results from these ten values given the high precision of the velocity determinations and the relatively low rms (2.72 km/s) calculated for the model fits.

3.5. Roche modeling approach

The newly acquired radial velocity (RV) data reported herein (Table 4; Figures 4 and 5) for the first time were necessary to obtain a unique solution for the mass ratio (m_2/m_1), determine a value for the total mass, and unequivocally determine whether GM CVn is an A-type or W-type contact binary system. Aside from initial modeling with BM3 (Bradstreet and Steelman 2002), Roche modeling of LC data from GM CVn was primarily accomplished using the programs PHOEBE v.31a (Prša and Zwitter 2005) and WDWINT56A (Nelson 2009), both of which feature a user-friendly interface to the Wilson-Devinney (WD) code (Wilson and Devinney 1971; Wilson 1990). WDWINT56A makes use of Kurucz's atmosphere models (Kurucz 2000) which are integrated over UBV$R_c I_c$ optical passbands. In both cases, the selected model was Mode 3 for an over-contact binary. Bolometric albedo ($A_{1,2}$ = 0.5) and gravity darkening coefficients ($g_{1,2}$ = 0.32) for cooler stars (7500 K) with convective envelopes were respectively assigned according to Ruciński (1969) and Lucy (1967). Logarithmic limb darkening coefficients (x_1, x_2, y_1, y_2) were interpolated (van Hamme 1993) following any change in the effective temperature (T_{eff2}) of the secondary star during model fit optimization. According to the putative classification of GM CVn as spectral type F9V to G0V the effective temperature of the more massive star was fixed (T_{eff1} = 5920 K). Direct least-squares sinusoidal curve fitting of the RV data was initially carried out with an EXCEL spreadsheet designed by RHN using a custom macro and the Solver add-in. These preliminary results led to values for the radial velocities (v_{1r} = 241.05 km/s and v_{2r} = 82.93 km/s), q = 0.344, and the systemic velocity (V_γ = –24.41 km/s). Subsequently, RV and LC data (V-mag only) were simultaneously modeled using WDWINT56A in order to obtain initial estimates for K_1, K_2, q, the semi-major axis (SMA), and V_γ. All but the temperature of the more massive star (T_{eff1}), orbital period (P = 0.366984 d), $A_{1,2}$, and $g_{1,2}$ were allowed to vary during DC iterations. In general, the best fits for T_{eff2}, i, and Roche potentials ($\Omega_1 = \Omega_2$) were collectively refined (method of multiple subsets) by DC before attempts were made to simultaneously optimize $\Omega_{1,2}$, i, T_{eff2}, q, V_γ, and the SMA. Once the Roche model fit was optimized using the monochromatic LC data, the other LCs (B and R_c) were added to the model. Hereafter T_{eff1} remained fixed while simultaneously varying T_{eff2}, i, q, V_γ, SMA, and the Roche potential ($\Omega_1 = \Omega_2$) to obtain a best fit for the multicolor data. Synthesis of light curves for GM CVn with good fits during quadrature (Max I ~ Max II) and around minimum light (Min I and Min II) were possible without the incorporation of a spot.

3.6. Roche modeling results

According to the convention employed herein, the primary star (m_1) is considered the more massive, thus, the best fit for the mass ratio (m_2/m_1) was observed at q = 0.341 ± 0.001. In order to accommodate this definition, the LC phase had to be shifted (φ ± 0.5) to properly align the RV and LC data. Simultaneous Roche modeling of RV and LC data demonstrates that GM CVn is a W-type contact binary system (Figure 1) in which the smaller but slightly hotter star is eclipsed (in this case partially) by its cooler but larger orbital partner. These results are consistent with the general observation (Csizmadia and Klagyivik 2004; Skelton and Smits 2009) that W-type eclipsing binaries have a mass ratio $m_2/m_1 > 0.3$, are equal to or cooler than the Sun with spectral types ranging from G to K, and orbit each other

with periods varying between 0.22 to 0.4 day. A pictorial model rendered with BM3 using the physical and geometric elements from the best fit Roche model is shown in Figure 6. The LC parameters and geometric elements determined for each of these model fits are summarized in Table 5. It should be noted that the listed errors only reflect the model fit to the observations which assumed exact values for all fixed parameters.

The fill-out parameter (f), which corresponds to a volume percent of the outer surface shared between each star, was calculated according to Equation 3 (Kallrath and Malone 1999; Bradstreet 2005) where:

$$f = (\Omega_{inner} - \Omega_{1,2} / (\Omega_{inner} - \Omega_{outer}), \quad (3)$$

Ω_{outer} is the outer critical Roche equipotential, Ω_{inner} is the value for the inner critical Roche equipotential, and $\Omega = \Omega_{1,2}$ denotes the common envelope surface potential for the binary system. In this case the constituent stars are in shallow contact (f < 15%) as defined by He and Qian (2009). The evolutionary track for GM CVn is probably similar to that described for V608 Cas (Liu *et al.* 2016), another W-type shallow-contact binary system with a mass ratio (q = 0.343) similar to GM CVn. Shallow-contact W UMa variables are believed to be in an evolutionary path between deep contact and near contact binary stars. When a semi-detached binary evolves inward as a result of mass transfer and/or angular momentum loss (Bradstreet and Guinan 1994) it can evolve into a contact system. Others have argued (Liu *et al.* 2010) that deep-contact binaries may evolve to shallow-contact systems by thermal relaxation oscillation (TRO) and could ultimately reach a broken-contact phase. Additional photometric studies on GM CVn could prove invaluable to understanding the evolutionary status of this system.

3.7. Absolute parameters

Absolute parameters (Table 6) were derived for each star in this W-type W UMa binary system using results from the unspotted model simulation. Apart from a spectroscopic mass ratio (q_{sp}), the other critical values provided by RV data are the orbital speeds ($v_{1r} + v_{2r}$). As such, the total mass can be calculated according to Equation 4 when the orbital inclination (i) is known:

$$(m_1 + m_2) sin^3 i = (P / 2\pi G)(v_{1r} + v_{2r})^3. \quad (4)$$

From the simultaneous fit of LC and RV data, $V_\gamma = -25.8 \pm 0.29$ km/s, $v_{2r} = 236.9 \pm 5.45$ km/s, $v_{1r} = 76.55 \pm 6.16$ km/s, and $i° = 63.07 \pm 0.06$. The total mass of the system was determined to be $1.65 \pm 0.09\ M_\odot$ and since q = 0.341, the primary mass = $1.23 \pm 0.06\ M_\odot$ and the secondary mass = $0.42 \pm 0.02\ M_\odot$. A stand-alone star with a mass similar to the secondary would likely be classified as an early M-type. The semi-major axis, $a(R_\odot) = 2.55 \pm 0.04$, was calculated from Newton's version (Equation 5) of Kepler's third law where:

$$a^3 = (G \times P^2 (M_1 + M_2)) / (4\pi^2). \quad (5)$$

The effective radii of each Roche lobe (r_L) can be calculated to over the entire range of mass ratios ($0 < q < \infty$) according to the expression (6) derived by Eggleton (1983):

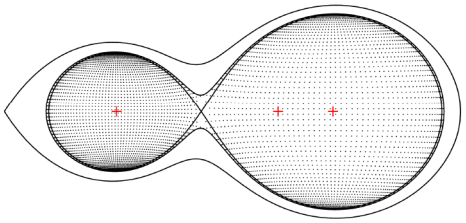

Figure 6. Surface model (φ = 0.25) of GM CVn showing the Roche lobe outlines for this shallow contact W-type W UMa eclipsing binary system.

Table 5. Synthetic light curve parameters employed for Roche modeling and the geometric elements determined for GM CVn, a W-type W UMa variable.

Parameter	*Value*
T_{eff1} (K)[b]	5920
T_{eff2} (K)	6004 ± 4
q (m_2 / m_1)	0.341 ± 0.001
A[b]	0.5
g[b]	0.32
$\Omega_1 = \Omega_2$	2.528 ± 0.001
i°	63.07 ± 0.06
$L_1 / (L_1 + L_2)_B$[c]	0.7016 ± 0.0001
$L_1 / (L_1 + L_2)_V$	0.7071 ± 0.0001
$L_1 / (L_1 + L_2)_{Rc}$	0.7095 ± 0.0001
r_1 (pole)	0.4510 ± 0.0004
r_1 (side)	0.4846 ± 0.0005
r_1 (back)	0.5124 ± 0.0006
r_2 (pole)	0.2764 ± 0.0011
r_2 (side)	0.2888 ± 0.0014
r_2 (back)	0.3259 ± 0.0025
Fill-out factor	13.1%
RMS (B)[d]	0.00982
RMS (V)[d]	0.00699
RMS (R_c)[d]	0.00636

a. All error estimates from WDWINTV5.6A (Nelson 2009).
b. Fixed during DC.
c. L_1 and L_2 refer to luminosities of the primary (cooler) and secondary stars, respectively.
d. Monochromatic root mean square deviation of model fit from observed values (mag).

Table 6. Mean absolute parameters (±SD) for GM CVn using mass ratio (q = m_2 / m_1) and total mass results from the simultaneous Roche model fits of LC and RV data.

Parameter	*Primary*	*Secondary*
Mass ($M_\odot$)	1.23 ± 0.06	0.42 ± 0.02
Radius ($R_\odot$)	1.21 ± 0.02	0.74 ± 0.01
a ($R_\odot$)	2.55 ± 0.04	—
Luminosity ($L_\odot$)	1.62 ± 0.06	0.64 ± 0.02
M_{bol}	4.23 ± 0.04	5.23 ± 0.04
Log (g)	4.36 ± 0.03	4.32 ± 0.03

$$r_L = (0.49q^{2/3}) / (0.6q^{2/3} + ln(1 + q^{1/3})), \quad (6)$$

from which values for r_1 (0.4739 ± 0.0003) and r_2 (0.2908 ± 0.0002) were determined for the primary and secondary stars, respectively. Since the semi-major axis and the volume radii are known, the solar radii for both binary constituents can be calculated where $R_1 = a \cdot r_1 = (1.21 \pm 0.02\ R_\odot)$ and $R_2 = a \cdot r_2 = (0.74 \pm 0.01\ R_\odot)$.

3.8. Distance estimates to GM CVn

The bolometric magnitudes ($M_{bol1,2}$) and luminosity in solar units ($L_\odot$) for the primary (L_1) and secondary stars (L_2) were calculated from well-known relationships where:

$$M_{bol1,2} = 4.75 - 5 \log (R_{1,2} / R_\odot) - 10 \log (T_{1,2} / T_\odot), \quad (7)$$

and

$$L_{1,2} = (R_{1,2} / R_\odot)^2 (T_{1,2} / T_\odot)^4. \quad (8)$$

Assuming that $T_{eff1} = 5920$ K, $T_{eff2} = 6004$ K, and $T_\odot = 5772$ K, the solar luminosities for the primary and secondary are $L_1 = 1.62 \pm 0.06$ and $L_2 = 0.64 \pm 0.02$, respectively. Bolometric magnitudes were calculated to be $M_{bol1} = 4.23 \pm 0.04$ and $M_{bol2} = 5.23 \pm 0.04$. Combining the bolometric magnitudes resulted in an absolute value ($M_V = 3.95 \pm 0.04$) when adjusted with the bolometric correction (BC = –0.090) interpolated from Pecaut and Mamajek (2013). Substituting into the Equation 9, the distance modulus:

$$d(pc) = 10^{(m - M_V - A_V + 5) / 5)}, \quad (9)$$

where $m = V_{max}$ (10.18 ± 0.01) and $A_V = 0.024$, leads to an estimated distance of 174 ± 3 pc to GM CVn. This value is about 10% lower than the distance (191 ± 9 pc) calculated directly from the first release (DR-1) of parallax data from the Gaia mission (Lindegren *et al.* 2016). The distance to GM CVn was also estimated using two different empirical relationships derived from calibrated models for contact binaries. Mateo and Ruciński (2017) recently developed a relationship between orbital period ($0.275 < P < 0.575$ d) and distance (Tycho-Gaia Astronomic Solution parallax data) from a subset of contact binaries which showed that the absolute magnitude (M_V) can be estimated with the expression:

$$M_V = (-8.67 \pm 0.65) (\log(P) + 0.4) + (3.73 \pm 0.06). \quad (10)$$

Using this relationship the absolute magnitude was calculated to be $M_V = 4.04 \pm 0.06$, which upon substitution into Equation 9 yielded a distance of 168 ± 5 pc. A third value for distance (169 ± 33 pc) was derived from a ROTSE-1 catalog of contact binary stars (Gettel *et al.* 2006) in accordance with the empirically derived expression:

$$\log (d) = 0.2 V_{max} - 0.18 \log(P) - 1.6 (J-H) + 0.56, \quad (11)$$

where d is distance in parsecs, P is the orbital period in days, and (J–H) is the 2MASS color for GM CVn. Collectively, the mean distance to this system is therefore estimated to be 175 ± 9 pc.

4. Conclusions

Three new times of minimum were observed based on CCD data collected through B, V, and R_c filters; these along with other published values led to an updated linear ephemeris for GM CVn. Potential changes in orbital periodicity were assessed using eclipse timings which unfortunately only cover a 12-year time period. A straight line relationship between the observed and predicted times of minimum suggests that since 2005 no significant change in the orbital period has occurred. The intrinsic color, $(B-V)_0$, determined from this study and eight surveys indicates that the effective temperature for the primary is ~5920 K, which corresponds to spectral class F9V-G0V. Radial velocity findings are reported for the first time herein and resulted in a robust solution for the mass ratio ($q = 0.341 \pm 0.001$) after simultaneously modeling with the 2013 LC data. Furthermore, these Roche model simulations revealed that GM CVn is a shallow contact W-type W UMa variable. This system is a worthy candidate for further study to advance our knowledge about the evolutionary track of shallow contact binary systems.

5. Acknowledgements

This research has made use of the SIMBAD database operated at Centre de Données astronomiques de Strasbourg, France. Time-of-minima data from the IBVS website proved invaluable to the assessment of potential period changes experienced by this variable star. In addition, the Northern Sky Variability Survey hosted by the Los Alamos National Laboratory and the International Variable Star Index maintained by the AAVSO (Watson *et al.* 2014) were mined for valuable information. The diligence and dedication shown by all associated with these organizations is very much appreciated. R.H.N. wishes to thank the staff members at the DAO (Dmitry Monin, David Bohlender, and the late Les Saddlmyer) for their usual splendid help and assistance. We very much appreciate the critical review and useful commentary provided by the referee assigned to this paper.

References

Akerlof, C., *et al.* 2000, *Astron. J.*, **119**, 1901.

Amôres, E. B., and Lépine, J. R. D. 2005, *Astron. J.*, **130**, 659.

Applegate, J. H. 1992, *Astrophys. J.*, **385**, 621.

Bahar, E., *et al.* 2017, *Inf. Bull. Var. Stars*, No. 6209, 1.

Berry, R., and Burnell, J. 2005, "Astronomical Image Processing for Windows," version 2.4.0, provided with *The Handbook of Astronomical Image Processing*, 2nd ed., Willmann-Bell, Richmond, VA.

Blättler, E., and Diethelm, R. 2006, *Inf. Bull. Var. Stars*, No. 5699, 1.

Bradstreet, D. H. 2005, in *The Society for Astronomical Sciences 24th Annual Symposium on Telescope Science*, The Society for Astronomical Sciences, Rancho Cucamonga, CA, 23.

Bradstreet, D. H., and Guinan, E. F. 1994, in *Interacting Binary Stars*, ed. A. W. Shafter, ASP Conf. Ser. 56, Astronomical Society of the Pacific, San Francisco, 228.

Bradstreet, D. H., and Steelman, D. P. 2002, *Bull. Amer. Astron. Soc.*, 34, 1224.

Csizmadia, Sz., and Klagyivik, P. 2004, *Astron. Astrophys.*, **426**, 1001.

Diethelm, R. 2006, *Inf. Bull. Var. Stars*, No. 5713, 1.

Diethelm, R. 2007, *Inf. Bull. Var. Stars*, No. 5781, 1.

Diethelm, R. 2010, *Inf. Bull. Var. Stars*, No. 5920, 1.

Eggleton, P. P. 1983, *Astrophys. J.*, **268**, 368.
Gettel, S. J., Geske, M. T., and McKay, T. A. 2006, *Astron. J.*, **131**, 621.
Harris, A. W., *et al.* 1989, *Icarus*, **77**, 171.
He, J.-J., and Qian, S.-B. 2009, in *The Eighth Pacific Rim Conference on Stellar Astrophysics: A Tribute to Kam-Ching Leung*, eds. B. Soonthornthum, S. Komonjinda, K.S. Cheng, K.C. Leung, ASP Conf. Ser. 404, Astronomical Society of the Pacific, San Francisco, 194.
Hübscher, J. 2013, *Inf. Bull. Var. Stars*, No. 6084, 1.
Hübscher, J. 2017, *Inf. Bull. Var. Stars*, No. 6196, 1.
Hübscher, J., and Lehmann, P. B. 2013, *Inf. Bull. Var. Stars*, No. 6070, 1.
Kallrath, J., and Milone, E. F. 1999, *Eclipsing Binary Stars: Modeling and Analysis*, Springer, New York.
Kurucz, R. L. 2000, Baltic Astron., 11, 101.
Kwee, K. K., and van Woerden, H. 1956, *Bull. Astron. Inst. Netherlands*, **12**, 327.
Lindegren, L., *et al.* 2016, *Astron. Astrophys.*, **595A**, 4.
Liu, L., Qian, S.-B., He, J.-J., Li, L.-J., and Liao, W.-P. 2010, *Publ. Astron Soc. Japan*, **62**, 81.
Liu, L., Qian, S.-B., He, J.-J., Li, L.-J., Zhao, E.-G., Jiang, L.-Q., and Han, Z.-T. 2016, *New Astron.*, **43**, 1.
Lucy, L. B. 1967, *Z. Astrophys.*, 65, 89.
Mateo, N. M., and Ruciński, S. M. 2017, *Astron. J.*, **154**, 125.
Minor Planet Observer. 2015, MPO Software Suite (http://www.minorplanetobserver.com), BDW Publishing, Colorado Springs.
Nelson, R. H. 2009, WDWINT56A: Astronomy Software by Bob Nelson (https://www.variablestarssouth.org/bob-nelson).
Nelson, R. H. 2010a, in *The Alt-Az Initiative, Telescope Mirror & Instrument Developments*, eds. R. M. Genet, J. M. Johnson, V. Wallen, Collins Foundation Press, Santa Margarita, CA.
Nelson, R. H. 2010b, *Inf. Bull. Var. Stars*, No. 5929, 1.
Nelson, R. H. 2010c, RAVERE: Astronomy Software by Bob Nelson (https://www.variablestarssouth.org/bob-nelson/).
Nelson, R. H. 2011, *Inf. Bull. Var. Stars*, No. 5966, 1.
Nelson, R. H. 2013a, *Inf. Bull. Var. Stars*, No. 6050, 1.
Nelson, R. H. 2013b, BROAD: Astronomy Software by Bob Nelson (https://www.variablestarssouth.org/bob-nelson/).
Nelson, R. H. 2015, *Inf. Bull. Var. Stars*, No. 6131, 1.
Nelson, R. H. 2016, *Inf. Bull. Var. Stars*, No. 6164, 1.
Paunzen, E. and Vanmunster, T. 2016, *Astron. Nachr.*, **337**, 239.
Pecaut, M. J., and Mamajek, E. E. 2013, *Astrophys. J., Suppl. Ser.*, **208**, 1.
Prša, A., and Zwitter, T. 2005, *Astrophys. J.*, **628**, 426.
Ruciński, S. M. 1969, *Acta Astron.*, **19**, 245.
Ruciński, S. M. 2004, in *Stellar Rotation*, Proc. IAU Symp. 215, eds. A. Maeder, P. Eenens, Astronomical Society of the Pacific, San Francisco, 17.
Schlafly, E. F., and Finkbeiner, D. P. 2011, *Astrophys. J.*, **737**, 103.
Schlegel, D. J., Finkbeiner, D. P., and Davis, M. 1998, *Astrophys. J.*, **500**, 525.
Schwarzenberg-Czerny, A. 1996, *Astrophys. J., Lett.*, **460**, L107.
Skelton, P. L., and Smits, D. P. 2009, *S. Afr. J. Sci.*, **105**, 120.
Software Bisque. 2011, CCDSOFT CCD control software (http://www.bisque.com).
Van Hamme, W. 1993, *Astrophys. J.*, **106**, 2096.
Warner, B. 2007, *Minor Planet Bull.*, **34**, 113.
Watson, C., Henden, A. A., and Price, C. A. 2014, AAVSO International Variable Star Index VSX (Watson+, 2006-2014; http://www.aavso.org/vsx).
Wilson, R. E. 1990, *Astrophys. J.*, **356**, 613.
Wilson, R. E., and Devinney, E. J., 1971, *Astrophys. J.*, **166**, 605.
Wozniak, P. R., *et al.* 2004, *Astrophys. J.*, **127**, 2436.
Yakut, K., and Eggleton, P. P. 2005, *Astrophys. J.*, **629**, 1055.

The Dwarf Nova SY Cancri and its Environs

Arlo U. Landolt
Department of Physics and Astronomy, Louisiana State University, Baton Rouge, LA 70803-4001; landolt@phys.lsu.edu

Visiting astronomer, Kitt Peak National Observatory, National Optical Astronomical Observatory, which is operated by the Association of Universities for Research in Astronomy, Inc., under contract with the National Science Foundation.

James L. Clem
Department of Physics and Astronomy, Louisiana State University, Baton Rouge, LA 70803-4001 (Current address: Department of Physics, Grove City College, Grove City, PA 16127); jclem@phys.lsu.edu

Visiting astronomer, Kitt Peak National Observatory, National Optical Astronomical Observatory, which is operated by the Association of Universities for Research in Astronomy, Inc., under contract with the National Science Foundation.

Received February 22, 2018; revised April 4, 2018; accepted April 4, 2018

Abstract Multicolor UBVRI photometry, collected intermittedly over a period of 22 years, is presented for the dwarf nova SY Cancri. Additional UBVRI photometry for a handful of sequence stars in the vicinity of SY Cancri is also presented.

1. Introduction

The dwarf nova SY Cancri (R. A. = $09^h\ 01^m\ 03.23^s$, Dec. = +17° 53' 56.2"; J2000) was discovered to be variable by Mme. L. Ceraski as announced by S. Blažko (1929). She observed a light variation between photographic magnitude 9.5 and 12.5, based on 14 photographic plates taken in the time frame 1912–1928. The star initially designated as AN 401.1929 also is known as BD+18° 2101, GSC 01397-00817, 2MASS J09010332+1753561, PG 0858+181, SV 228, AAVSO AUID 000-BBQ-187, and UCAC4 540-048343.

Selected references for SY Cnc and its variable star cousins are illustrative for readers new to this kind of variable star. The characteristics of cataclysmic variable stars (CVs), a sub-group within the CVs called dwarf novae, and a further sub-division within the dwarf novae sub-group called Z Cam stars, is described extensively in Warner (1995). Sterken and Jaschek (1996) illustrate characteristic light curves for these variable stars, essentially all interacting binary systems. Dwarf novae brightnesses may increase by as much as six magnitudes (Percy 2007). The Z Cam variable star sub-group features frequent outbursts (Warner 1995), and "have a defining characteristic of a 'still stand' or halt [in the decline of] their light curve on the way down from maximum [brightness] (Percy 2007)." Words added by the authors are indicated within square brackets. A recent summary of the Z Cam subset was given by Simonsen (2011) and by Simonsen *et al.* (2014), wherein SY Cnc was included as a bona fide Z Cam class variable star.

Additional information useful in understanding these variable stars may be found in the following papers. Kraft and Luyten (1965) derived the mean absolute magnitudes of dwarf novae at minimum light to be $M_V = +7.5 \pm 0.7$, based on proper motions and radial velocities. Early AAVSO observations for this class variable star, including SY Cnc, were reported by Mayall (1968) and by Mattei (1974). An initial review of the structure of cataclysmic variables was written by Robinson (1976). A discussion of a variety of observational characteristics for dwarf novae, including SY Cnc, and taken from the AAVSO archives, appeared in Szkody and Mattei (1984). BVRI photometry was published by Spogli (1993). Secondary standards in the field of SY Cnc were provided by Henden and Honeycutt (1997). Bruch and Engel (1994) reported a color excess for SY Cnc of $E_{(B-V)} = 0.0$.

Shafter *et al.* (2005) determined, from AAVSO data, a recurrence time versus orbital period relation for variable stars of the Z Cam type. SY Cnc has the longest orbital period, at 0.380 day, in the group that they considered. Smith *et al.* (2005) conclude that the secondary companion in the SY Cnc binary system is a non-main-sequence star which fills its Roche lobe.

2. Observations

Data were obtained for SY Cnc intermittently in the time frame 1984 November through 2005 April, a period of 22 years, as primary observing programs permitted. Consequently, a variety of telescopes, detectors, and filter sets was employed for the data acquisition. A listing of telescopes, detectors, and filter sets is given in Table 1. The first column lists the UT date during which data were taken. The observatory site and telescope utilized are given next. The KPNO 0.9-m telescope used on 1993 March 16 UT, which is the 0.9-m currently on site, resulted from a combination of the two original 0.9-m telescopes on Kitt Peak, namely the No.1 0.9-m and No.2 0.9-m. The third column indicates that photomultipliers were the detector of choice except for the night of 2002 March 12 UT. Normally a 14-arc second diaphragm was used for the photoelectric observations. A description of the different filter sets used in the data acquisition process is presented in the last column. The identification includes the filter and the filter's identification number in the KPNO and CTIO filter databases. The UBVRI set of filters used at the Lowell Perkins 1.8-m telescope was the KPNO J filter set of UBVRI filters.

The majority of the data herein was taken as part of AUL's standard star programs. An overview of data acquisition procedures and reduction techniques may be found in Landolt

Table 1. Telescopes, Detectors, and Filters.

UT mmddyy	*Observatory Telescope*	*Detector Set-up*	*Filter Identifications*
111284	KPNO #1 0.9-m	1P21; cold box 10	V, 232; B, 233; U, 974 + solid CuSO4
111484	KPNO #1 0.9-m	1P21; cold box 10	V, 232; B, 233; U, 974 + solid CuSO4
121885	KPNO #2 0.9-m	1P21; cold box 10	V, 232; B, 233; U, 974 + solid CuSO4
121985	KPNO #2 0.9-m	1P21; cold box 10	V, 232; B, 233; U, 974 + solid CuSO4
111588	KPNO 1.3-m	RCA 31034A-02; coldbox 51	J filter set: I, 1114; R, 1113; V, 1112; B, 1111; U-234+CuSO4
011790	KPNO #2 0.9-m	1P21; cold box 10	V, 232; B, 233; U, 974 + solid CuSO4
032490	KPNO 1.3-m	RCA 31034A-02; cold box 51	J filter set: I, 1114; R, 1113; V, 1112; B, 1111; U-234+CuSO4
031693	KPNO 0.9-m	RCA 31034A-02; cold box 51	J filter set: I, 1114; R, 1113; V, 1112; B, 1111; U-234+CuSO4
030996	CTIO 1.0-m	RCA 31034A-02; cold box 60	Landolt (1983), Table III
031896	CTIO 1.5-m	RCA 31034A-02; cold box 60	Landolt (1983), Table III
031202	CTIO 1.5-m	CCD, Tek 2K #3	CCD Tek set #3
041205	Lowell 1.8-m	RCA 31034A-02	J filter set: I, 1114; R, 1113; V, 1112; B, 1111; U-234+CuSO4

(2007). Since the data were acquired over a twenty-two year period, several different combinations of detectors, coldboxes, mountain tops, and filter sets were involved. The UBVRI photometry taken under differing circumstances was standardized through use of different editions of standard stars (Landolt 1983, 1992). There were too few data in common between the ten observing runs to tie the final magnitudes and color indices together as tightly as could be done, say in the definition of standard star lists, e.g., Landolt (1992, 2009). The resulting photometric errors for a given star therefore are somewhat larger than one might like. An indication of the errors for the measured photoelectric-based magnitudes and color indices is listed in Table 2. The errors in Table 2 are the average errors of a single observation for the recovered magnitudes and color indices of the standard stars used to calibrate the nightly photometry into the UBVRI photometric system as defined by Landolt (1983, 1992). Since, on occasion, SY Cnc was somewhat fainter than the standard stars, those fainter observations' errors may be a percent or two larger.

Table 2. RMS Photometric Errors per Night.

UT	*HJD*	*RMS Errors Recovered Standards*					
mmddyy	*2400000.0+*	*V*	*(B–V)*	*(U–B)*	*(V–R)*	*(R–I)*	*(V–I)*
111284	46016.5	0.009	0.006	0.023	—	—	—
111484	46018.5	0.005	0.006	0.017	—	—	—
121885	46417.5	0.007	0.009	0.012	—	—	—
121985	46418.5	0.010	0.004	0.015	—	—	—
111588	47480.5	0.010	0.005	0.009	0.004	0.004	0.004
011790	47908.5	0.009	0.010	0.023	—	—	—
032490	47974.5	0.013	0.008	0.016	0.006	0.004	0.008
031693	49062.5	0.007	0.006	0.013	0.004	0.006	0.005
030996	50151.5	0.009	0.012	0.024	—	—	—
031896	50160.5	0.008	0.011	0.023	0.006	0.004	0.007
031202	52345.5	—	—	—	—	—	—
041205	53472.5	0.007	0.005	0.020	0.011	0.015	0.021
	ave	0.009	0.007	0.018	0.006	0.007	0.009
	±	0.002	0.003	0.005	0.003	0.005	0.007

3. Discussion

Two finding charts, each with a separate purpose, are provided. SY Cnc and photoelectrically observed sequence stars in its vicinity, similar to standard AAVSO charts, are identified in Figure 1. The numerous stars with CCD measurements preclude identifying each star. Identifications for several brighter stars observed with the CCD detector are shown in Figure 2. The accuracy of the coordinates in Table 3 enable the identification in Figure 2 of the remaining stars observed with the CCD. When the photoelectric observational program was begun in 1984 November, the finding chart employed was an AAVSO chart dated 17 December 1968 (revised). The selection of sequence stars that was observed photoelectrically at the telescope was based on the identification numbers on that chart. Those numbers actually were the then-adopted brightness of each AAVSO sequence star. Consequently, our identification numbers for the photoelectrically-observed stars in the SY Cnc field, presented in column one of Table 4, are cross-identified with the identification numbers from the 1968 AAVSO chart in column two. The UCAC4 catalogue identification, Zacharias *et al.* (2013), is in the third column, and that catalogue's right ascension and declination for J2000 are presented in the last

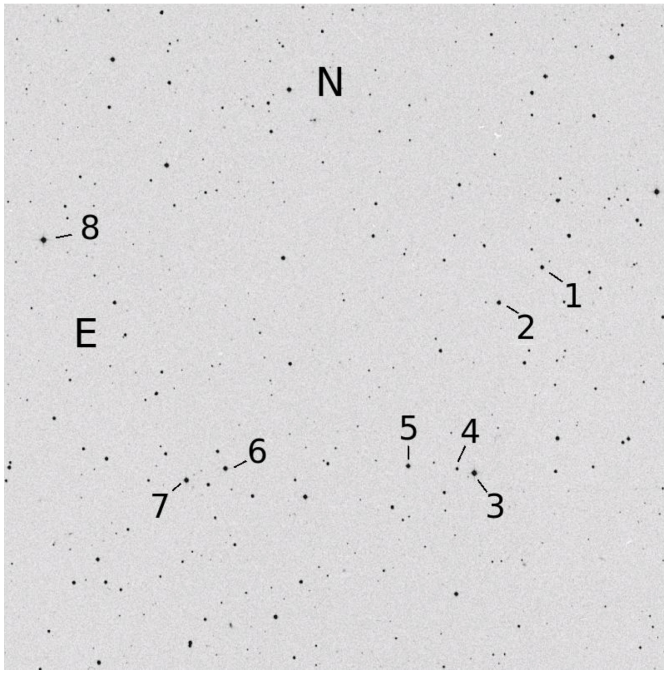

Figure 1. Finding chart for photoelectric measurements of SY Cnc and sequence stars (Tables 4 and 5). SY Cnc is star 3. The field of view is approximately 30 arc minutes on a side.

Table 3. CCD Photometry of Nearby Stars.

Ident.	UCAC4	R.A.(J2000.0) h m s	Dec.(J2000.0) ° ′ ″	V	(B–V)	(U–B)	(V–R)	(R–I)	(V–I)	V	(B–V)	(U–B)	(V–R)	(R–I)	(V–I)
										Observation Errors					
1	540–048331	09 00 34.31	17 55 32.9	13.414	0.715	0.328	0.377	0.404	0.781	0.0069	0.0075	0.0047	0.0072	0.0025	0.0071
2	540–048332	09 00 35.00	17 55 19.9	13.716	1.052	0.905	0.605	0.649	1.254	0.0082	0.0096	0.0156	0.0096	0.0056	0.0086
3	540–048333	09 00 40.62	17 57 48.1	15.168	0.724	0.355	0.387	0.404	0.791	0.0046	0.0076	0.0099	0.0057	0.0086	0.0091
4	540–048334	09 00 40.92	17 54 17.3	15.333	0.766	0.299	0.408	0.433	0.841	0.0040	0.0076	0.0102	0.0079	0.0079	0.0057
5	—	09 00 41.66	17 51 00.9	18.217	0.667	0.209	0.451	0.482	0.933	0.0311	0.0880	0.1057	0.0437	0.0507	0.0509
6	541–047626	09 00 42.45	18 00 23.4	16.775	0.920	0.755	0.472	0.563	1.035	0.0097	0.0475	0.0594	0.0175	0.0175	0.0137
7	—	09 00 44.11	17 56 07.3	18.522	0.408	–0.036	0.417	0.370	0.787	0.0454	0.0672	0.0762	0.0580	0.0628	0.0686
8	—	09 00 45.57	17 53 10.6	18.816	0.524	–0.273	0.278	0.175	0.453	0.0540	0.0916	0.2125	0.0914	0.1787	0.1715
9	540–048335	09 00 46.51	17 59 29.1	16.078	1.266	1.264	0.714	0.753	1.467	0.0060	0.0169	0.1044	0.0107	0.0103	0.0080
10	540–048336	09 00 47.55	17 58 55.7	15.851	1.324	1.171	0.948	1.304	2.252	0.0113	0.1255	0.1289	0.0136	0.0079	0.0116
11	540–048337	09 00 47.65	17 55 32.1	12.612	0.903	0.667	0.494	0.494	0.988	0.0015	0.0039	0.0046	0.0021	0.0020	0.0021
12	540–048338	09 00 47.96	17 54 01.8	14.545	0.399	–0.196	0.246	0.321	0.567	0.0056	0.0067	0.0052	0.0062	0.0043	0.0065
13	540–048339	09 00 48.35	17 57 56.7	15.850	0.627	0.018	0.342	0.398	0.740	0.0058	0.0152	0.0297	0.0079	0.0083	0.0086
14	540–048341	09 00 53.30	17 59 28.0	15.541	0.760	0.385	0.396	0.413	0.809	0.0100	0.0139	0.0134	0.0108	0.0073	0.0117
15	540–048342	09 00 54.17	17 58 54.9	14.072	0.630	0.165	0.347	0.364	0.711	0.0030	0.0051	0.0054	0.0039	0.0042	0.0045
16	—	09 00 54.21	17 50 02.4	17.013	0.680	0.131	0.445	0.318	0.763	0.0116	0.0239	0.0312	0.0857	0.0880	0.0260
17	539–047119	09 00 54.56	17 47 04.2	14.486	1.005	1.221	0.560	0.546	1.106	0.0028	0.0087	0.0131	0.0037	0.0050	0.0052
18	—	09 00 58.11	17 49 59.2	17.100	0.638	0.118	0.363	0.361	0.724	0.0125	0.0228	0.0307	0.0171	0.0415	0.0417
19	—	09 00 59.02	17 55 57.9	17.575	0.433	–0.259	0.275	0.394	0.669	0.0183	0.0297	0.0320	0.0265	0.0314	0.0308
20	541–047637	09 00 59.14	18 01 36.4	12.450	0.963	0.851	0.499	0.537	1.036	0.0037	0.0044	0.0038	0.0039	0.0049	0.0060
21	—	09 00 59.79	17 49 57.2	17.237	0.642	0.103	0.364	0.399	0.763	0.0138	0.0266	0.0345	0.0191	0.0217	0.0221
22	—	09 01 01.64	18 01 37.4	16.961	1.026	1.014	0.558	0.542	1.100	0.0124	0.0615	0.1240	0.0157	0.0144	0.0164
23	540–048343	09 01 03.32	17 53 56.1	13.621	0.528	–0.474	0.380	0.474	0.854	0.0048	0.0073	0.0111	0.0053	0.0029	0.0051
24	540–048344	09 01 06.67	17 48 28.3	12.680	0.828	0.556	0.446	0.439	0.885	0.0037	0.0045	0.0042	0.0041	0.0024	0.0041
25	540–048345	09 01 06.70	17 54 07.1	14.238	0.642	0.154	0.345	0.373	0.718	0.0037	0.0077	0.0081	0.0044	0.0035	0.0045
26	—	09 01 06.91	17 51 07.3	17.896	0.664	–0.116	0.344	0.441	0.785	0.0248	0.0724	0.0801	0.0412	0.0497	0.0448
27	540–048346	09 01 07.87	17 55 44.0	16.897	1.229	1.033	0.673	0.648	1.321	0.0211	0.0418	0.0747	0.0233	0.0143	0.0235
28	540–048347	09 01 08.81	17 52 13.8	16.727	0.784	0.270	0.417	0.416	0.833	0.0094	0.0342	0.0421	0.0158	0.0173	0.0150
29	540–048348	09 01 09.07	17 53 02.9	14.996	0.637	0.071	0.355	0.404	0.759	0.0056	0.0076	0.0079	0.0066	0.0048	0.0066
30	540–048349	09 01 10.06	17 59 24.9	13.575	0.821	0.434	0.440	0.465	0.905	0.0021	0.0048	0.0060	0.0031	0.0058	0.0057
31	540–048350	09 01 11.00	17 59 57.3	16.924	0.755	0.292	0.400	0.455	0.855	0.0152	0.0327	0.0396	0.0180	0.0200	0.0232
32	540–048351	09 01 11.09	17 54 22.3	16.905	0.599	–0.024	0.321	0.373	0.694	0.0108	0.0459	0.0483	0.0161	0.0265	0.0260
33	540–048352	09 01 12.53	17 50 35.8	16.542	1.240	1.162	0.711	0.691	1.402	0.0120	0.0247	0.0566	0.0140	0.0131	0.0162
34	540–048353	09 01 15.72	17 51 55.8	16.434	1.056	0.743	0.593	0.581	1.174	0.0092	0.0214	0.0368	0.0112	0.0097	0.0117
35	540–048354	09 01 15.89	17 54 12.1	12.821	0.213	0.035	0.104	0.142	0.246	0.0037	0.0061	0.0054	0.0041	0.0025	0.0041
36	540–048355	09 01 16.86	17 51 44.9	15.236	1.358	0.983	0.796	0.836	1.632	0.0048	0.0160	0.0230	0.0056	0.0040	0.0056
37	540–048356	09 01 18.77	17 52 20.8	14.005	0.571	–0.022	0.323	0.372	0.695	0.0023	0.0041	0.0069	0.0072	0.0071	0.0032
38	—	09 01 18.99	17 58 37.7	17.690	0.910	0.218	0.444	0.523	0.967	0.0192	0.0450	0.0685	0.0257	0.0279	0.0292
39	540–048357	09 01 20.33	17 49 30.0	16.041	0.502	–0.055	0.308	0.356	0.664	0.0060	0.0102	0.0133	0.0086	0.0105	0.0104
40	540–048358	09 01 21.62	17 57 43.3	16.969	1.418	1.094	1.033	1.363	2.396	0.0108	0.0378	0.1517	0.0131	0.0107	0.0133
41	540–048360	09 01 23.63	17 58 29.0	15.795	1.186	1.140	0.661	0.649	1.310	0.0106	0.0236	0.0366	0.0119	0.0074	0.0117
42	—	09 01 24.90	17 52 40.7	17.982	0.871	0.597	0.411	0.515	0.926	0.0499	0.0735	0.1043	0.0552	0.0449	0.0629
43	540–048361	09 01 25.63	17 55 58.3	16.280	1.452	1.232	0.886	0.919	1.805	0.0067	0.0214	0.0583	0.0387	0.0384	0.0080
44	—	09 01 27.23	17 50 41.8	18.479	0.801	0.192	0.373	0.324	0.697	0.0491	0.1453	0.2365	0.0599	0.1096	0.1151
45	540–048362	09 01 29.75	17 54 58.4	16.555	0.892	0.551	0.497	0.529	1.026	0.0098	0.0381	0.0481	0.0150	0.0150	0.0139
46	540–048363	09 01 30.90	17 49 14.2	16.768	0.624	–0.086	0.402	0.458	0.860	0.0219	0.0314	0.0275	0.0244	0.0236	0.0303
47	540–048364	09 01 31.16	17 54 16.5	14.662	0.533	0.145	0.321	0.372	0.693	0.0082	0.0718	0.0715	0.0086	0.0043	0.0089
48	540–048365	09 01 31.92	17 54 23.8	16.717	0.803	0.477	0.432	0.446	0.878	0.0093	0.0280	0.0388	0.0123	0.0130	0.0138
49	—	09 01 32.59	17 49 36.7	17.081	1.028	1.020	0.552	0.577	1.129	0.0464	0.0808	0.0912	0.0479	0.0389	0.0593

two columns. The UBVRI photoelectric photometry for these comparison stars appears in Table 5.

Observations were downloaded from the AAVSO photometric database in the Julian Day (JD) time interval $2445700.5 \leq JD \leq 2453736.5$ to encompass the time frame for the new data described in this paper. These AAVSO data between 1984 January 1 and 2006 January 1 UT cover 8,036 days, or 22.0 years. Visual observations indicating "fainter than" and those taken through filters other than "Johnson *V*" then were eliminated from the listing. The remaining 13,349 AAVSO observations have been displayed in Figure 3 as black filled circles.

The new photoelectric data herein for SY Cnc, tabulated in Table 6, are illustrated in Figures 3, 4, and 5. The photoelectric *V*-magnitude data have been overlaid, as red filled circles, onto the AAVSO database points in Figure 3. Figures 4 and 5 illustrate the photoelectric data as a function of Heliocentric Julian Day (HJD) (one is reminded that the AAVSO database observations are in Julian Days (JDs), whereas the authors' are in Heliocentric Julian Days (HJDs)). While appearing somewhat redundant, the presentation of the *V* photoelectric data again in Figure 4 shows the behavior of those data free of the clutter of Figure 3, as well as permitting a more clear picture of the behavior of the *V* photoelectric data concurrent with the photoelectric color data plotted in Figure 5.

These data show a range in brightness of $11.21 \leq V \leq 13.62$ and in color index of $-0.02 \leq (B-V) \leq +0.53$. The times of

observation found SY Cnc either near its brightest, $V \sim 11$, or its faintest, $V \sim 13$ magnitude. The average of seven observations near its brightest found $(U–B) = –0.80 \pm 0.04$ and $(B–V) = +0.04 \pm 0.04$. The average of ten observations near SY Cnc's faintest found $(U–B) = –0.72 \pm 0.11$, and $(B–V) = +0.40 \pm 0.07$. There appears to be a trend, following HJD 2452000 and shown in Figure 5, in all color indices, except perhaps $(U–B)$, by more than a couple tenths of a magnitude toward redder colors.

CCD observations of the SY Cnc field in Table 3 were obtained on the photometric night of 2002 March 12 UT at the CTIO 1.5-m telescope. The detector was CTIO's Tek2k No.6, and the filter set was CTIO's Tek No.3, all 3 × 3 inch filters. A 14-arc second equivalent aperture was used in the reduction of the CCD data (Clem and Landolt) 2013, thereby ensuring that both the standard and program stars were reduced with the same aperture size as was employed in the definition of the standard stars. These data were calibrated with standards defined in Landolt (1992). Similar observation and reduction procedures have been described in Clem and Landolt (2013). Two successive frames were taken of the SY Cnc field, with exposures of 180, 30, 20, 20, and 30 seconds through the *U, B, V, R,* and *I* filters, respectively.

A running number for the CCD data for these 49 stars is given in the first column of Table 3. The corresponding identification in the second column, together with the coordinates in columns three and four, are from the UCAC4 catalogue (Zacharias *et al.* 2013). In instances where UCAC4 identifications did not exist, coordinates were derived from this CCD image material [see Clem and Landolt (2013), section 3.3 for details]. The *UBVRI* photometry based on the CCD data is given in columns five through ten. Since the CCD photometry came from two exposures on one telescope setting on one night, the errors indicated are a combination of instrumental errors combined with errors resulting from the calibration of the instrumental photometry to the standard system. These errors are labeled as observation errors for each star's data as presented in columns eleven through sixteen. The single CCD-based photometric data point for SY Cnc from Table 3 falls at HJD 2452345.60401 in Figures 3, 4, and 5.

The errors in the CCD *V* magnitudes in Table 3 as a function of the CCD *V* magnitude are illustrated in Figure 6. They are on the order of ≤ 0.01 magnitude for stars brighter than $V = 16.5$, and less than two percent down to $V \sim 16.8$. Figure 7, using data in Table 3, shows the scale to be linear when intercomparing the APASS *V* magnitude with our CCD *V* magnitude. The difference APASS *V* magnitudes minus the CCD *V* magnitudes in Table 3

Table 4. Comparsion Stars for SY Cnc.

Ident.	*Old Ident.*	*UCAC4*	*R. A. (J2000.0) h m s*	*Dec. (J2000.0) ° ′ ″*
1	var	541-047633	09 00 50.936	+18 03 12.58
2	124	541-047637	09 00 59.139	+18 01 36.32
3	SY	540-048343	09 01 03.314	+17 53 56.03
4	142	540-048345	09 01 06.693	+17 54 07.07
5	130	540-048354	09 01 15.888	+17 54 12.14
6	122	540-048376	09 01 50.541	+17 53 59.07
7	126	540-048382	09 01 57.892	+17 53 27.85
8	115	541-047674	09 02 25.595	+18 04 09.39

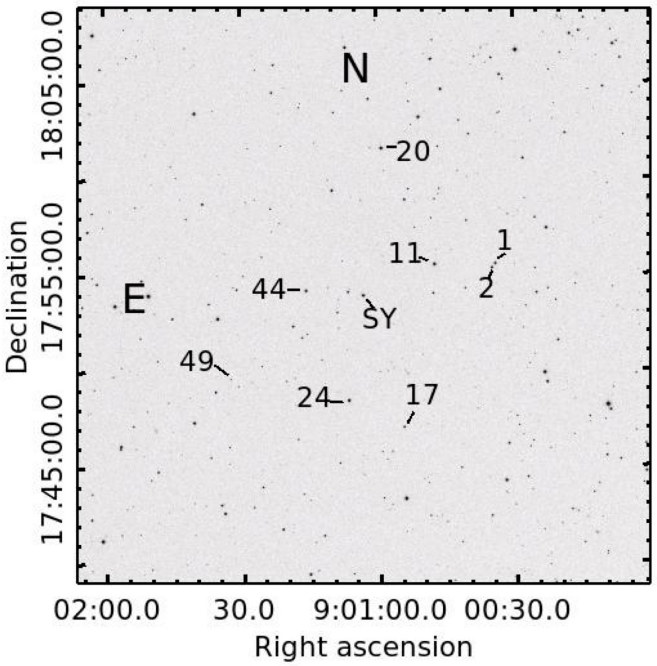

Figure 2. Finding chart for SY Cnc and CCD measured sequence stars from Table 3. The field of view is approximately 25 arc minutes on a side.

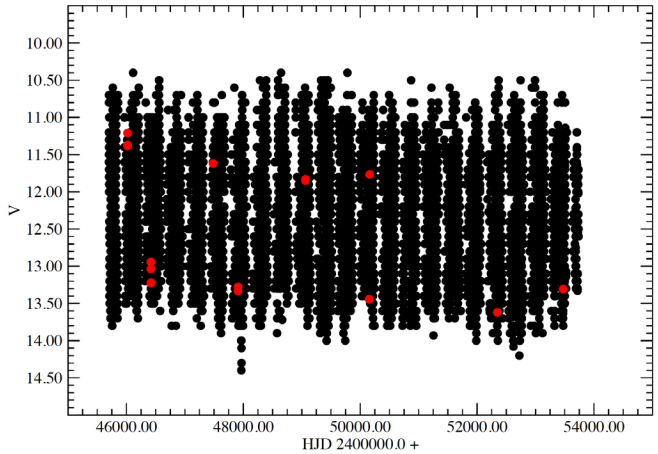

Figure 3. Visual AAVSO database V magnitudes plus V photoelectric and CCD magnitudes from this paper for SY €nc. Black color coding indicates AAVSO data; red color coding illustrates photoelectric data from Table 6 and CCD data from Table 3.

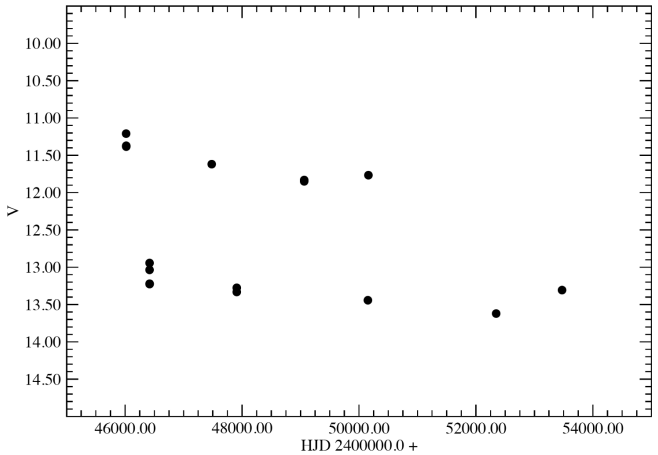

Figure 4. Photoelectric *V* magnitudes for SY Cnc from Table 6 as a function of HJD.

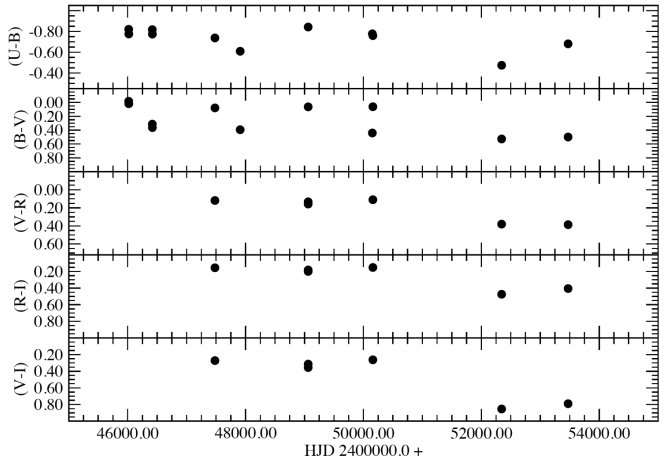

Figure 5. Photoelectric *UBVRI* color indices for SY Cnc from Table 6 as a function of HJD.

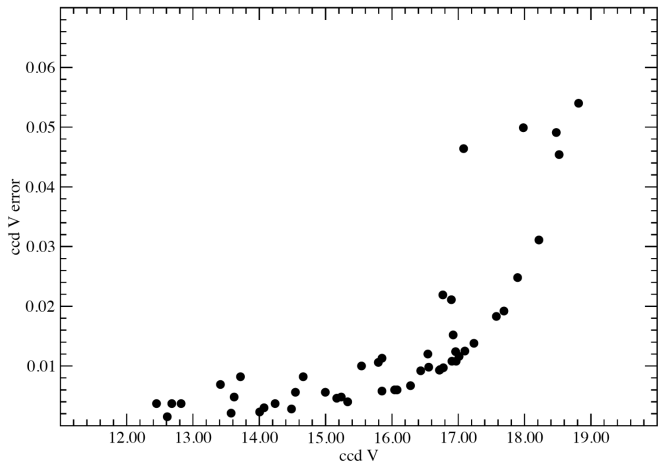

Figure 6. CCD *V* magnitude errors as a function of the CCD *V* magnitude from Table 3.

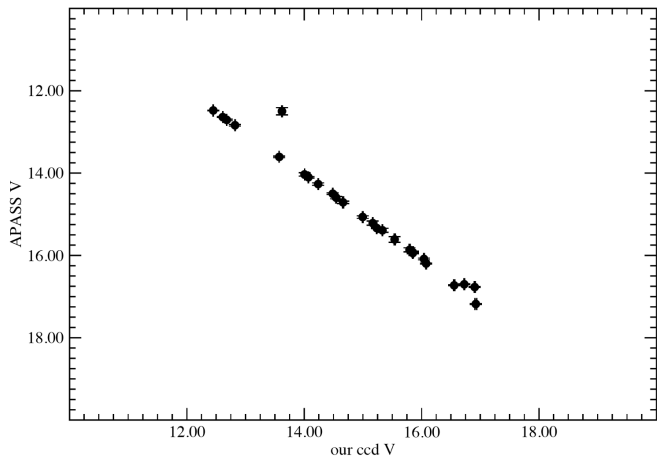

Figure 7. The APASS *V* magnitude plotted against the CCD *V* magnitude in Table 3. The outlier is SY Cnc.

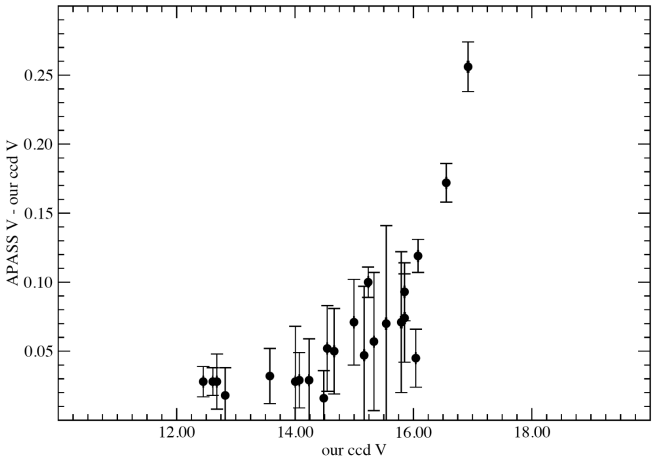

Figure 8. The difference between APASS *V* magnitude and the CCD *V* magnitudes in Table 3 versus the CCD *V* magnitudes in Table 3.

is +0.054 ± 0.069, for the 25 stars for which there are UCAC4 data. Consideration of stars brighter than *V* = 15th magnitude gives a difference of +0.034 ± 0.016. The outlier star in Figure 7 is SY Cnc, which has been excluded from these comparisons.

Figure 8 compares, for stars in the vicinity of SY Cnc, the difference between the UCAC4 *V* magnitudes, taken from APASS, and the CCD *V* magnitudes, with the CCD *V* magnitudes from Table 3. A divergence beginning about *V* = 15th magnitude becomes much stronger for stars fainter than *V* = 16.2, near the effective faint limit for both data sets.

It would be of interest to determine whether SY Cnc, as an object, shows any long term overall light variation. An examination of Figure 3 by eye is not sufficient. Consequently, the AAVSO data that were plotted in Figure 3 were subdivided by year. Each year's data provided an average magnitude and associated error. The associated mid-year Julian Day was taken to be 30 June. This resulted in a table of 22 mid-year Julian Days and associated average *V* magnitudes and associated errors. A linear regression was performed on these twenty-two pairs of Julian Date and magnitude, providing a relation:

$$\overline{V} = 12.72 \pm 0.56 - 6.142 \times 10^{-6} \pm 1.130 \times 10^{-5}\ \text{JD}. \qquad (1)$$

Application of this relation to an interval of 10,000 days, 2445000 < JD < 2455000 encompassing the data herein, indicates an overall increase in brightness of 0.06 magnitude. While there does appear to be a slight brightening, the size of the errors associated with the coefficients indicates low significance.

Table 4 contains GSC 01397-00509, also known as UCAC4 541-047633, a star in the field of SY Cnc. The star has a moderate proper motion of $\mu_\alpha = -40.8 \pm 2.7$ mas yr^{-1} and $\mu_\delta = -21.0 \pm 1.5$ mas yr^{-1}. Its APASS magnitude and color index are *V* = 12.730 and (*B*–*V*) = +0.829. When AUL initially began observations of SY Cnc and stars in its vicinity, GSC 01397-00509 was marked "var." on the AAVSO chart dated 17 December 1968 (revised), a possible variable star. Cook (1984) noted that the sequence for SY Cnc of that era was not in good shape. Hence, several random observations of this star also were obtained over the next years, and are presented in Table 7. While one might expect smaller errors for a star of GSC 01397-00509's brightness and

Table 5. Comparison Stars' UBVRI Photoelectric Data.

Ident.	V	(B–V)	(U–B)	(V–R)	(R–I)	(V–I)	*n*	V	(B–V)	(U–B)	(V–R)	(R–I)	(V–I)
										RMS Errors			
SY 115	10.813	+0.556	+0.015	+0.343	+0.340	+0.680	7	0.018	0.019	0.017	0.000	0.002	0.001
SY 122	11.704	+0.995	+0.766	+0.538	+0.508	+1.044	8	0.011	0.010	0.021	0.004	0.007	0.003
SY 124	12.491	+0.989	+0.762	—	—	—	1	—	—	—	—	—	—
SY 126	12.035	+0.499	-0.015	+0.306	+0.297	+0.602	8	0.006	0.012	0.019	0.001	0.003	—
SY 130	12.841	+0.204	+0.055	+0.104	+0.142	+0.246	3	0.017	0.009	0.081	—	—	—
SY 142	14.283	+0.604	+0.199	+0.345	+0.373	+0.718	3	0.043	0.033	0.041	—	—	—

Table 6. UBVRI Photoelectric Data for SY Cnc.

UT	*HJD*	*V*	*(B–V)*	*(U–B)*	*(V–R)*	*(R–I)*	*(V–I)*
mmddyy	*2400000.0+*	*m*	*m*	*m*	*m*	*m*	*m*
111284	46017.03000	11.210	–0.017	–0.820	—	—	—
111484	46018.98586	11.384	+0.019	–0.775	—	—	—
111484	46019.00338	11.372	+0.016	–0.794	—	—	—
121885	46418.03016	13.036	+0.313	–0.817	—	—	—
121885	46418.04486	12.944	+0.345	–0.778	—	—	—
121985	46418.98997	13.221	+0.363	–0.774	—	—	—
121985	46419.00078	13.224	+0.325	–0.814	—	—	—
121985	46419.00878	13.226	+0.363	–0.792	—	—	—
111588	47480.98158	11.619	+0.079	–0.737	+0.119	+0.156	+0.272
011790	47908.93623	13.276	+0.394	–0.609	—	—	—
011790	47908.95925	13.332	+0.418	–0.635	—	—	—
031693	49062.66303	11.849	+0.064	–0.842	+0.133	+0.182	+0.314
031693	49062.66567	11.831	+0.075	–0.846	+0.158	+0.200	+0.356
030996	50151.60221	13.443	+0.441	–0.777	—	—	—
031896	50160.55609	11.767	+0.062	–0.759	+0.110	+0.152	+0.263
031202	52345.60401	13.621	+0.528	–0.474	+0.380	+0.474	+0.854
041205	53472.70440	13.307	+0.499	-0.680	+0.386	+0.406	+0.791

Table 7. Multi-color Photometry for GSC 01397-00509.

UT	*HJD*	*V*	*(B–V)*	*(U–B)*	*(V–R)*	*(R–I)*	*(V–I)*
mmddyy	*2400000.0+*	*m*	*m*	*m*	*m*	*m*	*m*
121885	46418.03844	12.689	+0.900	+0.485	—	—	—
121985	46418.99833	12.739	+0.842	+0.630	—	—	—
111588	47480.99760	12.728	+0.826	+0.562	+0.474	+0.403	+0.874
011790	47908.95287	12.715	+0.875	+0.523	—	—	—
032490	47974.79669	12.731	+0.841	+0.575	+0.460	+0.405	+0.865
031693	49062.66892	12.721	+0.854	+0.577	+0.465	+0.388	+0.854
n = 6 (UBV)	3 (RI)	12.720	+0.856	+0.559	+0.466	+0.399	+0.864
	rms error	0.018	0.027	0.050	0.007	0.009	0.010

color together with the equipment involved in acquiring those data, the errors are not large enough to indicate variability. Upon comparison with tables in Drilling and Landolt (2000), the UBV color indices of GSC 01397-00509 indicate it to be an early K dwarf, or a G5 star if a giant. The *R,I* colors appear too blue, by 0.2 magnitude in (*V–R*), though, for these spectral types. The (*V–I*) color together with the (*J–K*) color of +0.447 from Cutri *et al.* (2003) also indicates a star of spectral type late G dwarf, or early G giant (Bessell and Brett 1988).

The star marked 115 on the 17 December 1968 (revised) chart is UCAC4 541-047674 (Table 4). Correspondence between AUL and Cook (1984) agreed that its magnitude was in error. Its magnitude and color index in Table 5 herein compares well with $V = 10.798$ and $(B–V) = +0.547$, APASS magnitudes, in the UCAC4 catalog (Zacharias *et al.* 2013).

4. Summary

Calibrated *UBVRI* photometric photoelectric and CCD data for SY Cnc were obtained by the authors over a period of 22 years. The color indices of the photoelectric sequence stars encompass the colors of SY Cnc as shown in Figure 5. Although each CCD sequence star only was observed twice, there are sufficient such stars to permit appropriate calibration of CCD images. The CCD measured sequence stars also encompass the known color variations of SY Cnc. A search for a long term trend in SY Cnc's longterm average brightness was inconclusive.

5. Acknowledgements

It is a pleasure to thank the staffs of the KPNO, CTIO, and Lowell Observatory for their help in making the observing runs a success. The authors recognize with gratitude the long term observation efforts of the AAVSO community. They acknowledge with thanks comments from the referee.

Acquisition of these data has been funded under the aegis of AFOSR grant 82-0192, Space Telescope Science Institute (STScI) grant CW-0004-85, and NSF grants AST 91-14457, AST 95-28177, AST 00-97895, AST 05-03871, and AST-0803158.

References

Bessell, M. S., and Brett, J. M. 1988, *Publ. Astron. Soc. Pacific*, **100**, 1134.

Blažko, S., *Astron. Nachr.*, No. 236, 279.

Bruch, A., and Engel, A. 1994, *Astron. Astrophys., Suppl. Ser.*, **104**, 79.

Clem, J. L., and Landolt, A.U. 2013, *Astron. J.*, **146**, 88.

Cook, L. M. 1984, private communication.

Cutri, R. M., *et al.* 2003, *2MASS All Sky Catalog of Point Sources*, NASA/IPAC Infrared Science Archive (http://irsa.ipac.caltech.edu/applications/Gator/), VizieR II/246/out.

Drilling, J. S., and Landolt, A. U. 2000, in *Allen's Astrophysical Quantities*, 4th ed., ed. A. N. Cox, AIP Press, Springer, New York, 381.

Henden, A. A., and Honeycutt, R. K. 1997, *Publ. Astron. Soc. Pacific*, **109**, 441.

Kraft, R. P., and Luyten, W. J. 1965, *Astrophys. J.*, **142**, 1041.

Landolt, A. U. 1983, *Astron. J.*, **88**, 439.

Landolt, A. U. 1992, *Astron. J.*, **104**, 340.

Landolt, A. U. 2007, in *The Future of Photometric, Spectrophotometric, and Polarimetric Standardization*, ed. C. Sterken, ASP Conf. Ser. 364, Astronomical Society of the Pacific, San Francisco, 27.

Landolt, A. U. 2009, *Astron. J.*, **137**, 4186.

Mattei, J. A. 1974, *J. Roy. Astron. Soc. Canada*, **68**, 169.

Mayall, M. W. 1968, *J. Roy. Astron. Soc. Canada*, **62**, 141.

Percy, J. R. 2007, *Understanding Variable Stars*, Cambridge University Press, Cambridge.

Robinson, E. L. 1976, *Annu. Rev. Astron. Astrophys*., **14**, 119.

Shafter, A. W., Cannizzo, J. K., and Waagen, E. O. 2005, *Publ. Astron. Soc. Pacific*, **117**, 931.

Simonsen, M. 2011, *J. Amer. Assoc. Var. Star Obs.*, **39**, 66.

Simonsen, M., *et al.* 2014, *J. Amer. Assoc. Var. Star Obs.*, **42**, 177.

Smith, R. C., Mehes, O., Vande Putte, D., and Hawkins, N. A. 2005, *Mon. Not. Roy. Astron. Soc.*, **360**, 364.

Spogli, C., Fiorucci, M., and Tosti, G. 1993, *Inf. Bull. Var. Stars*, No. 3949, 1.

Sterken, C., and Jaschek, C. 1996, in *Light Curves of Variable Stars*, eds. C. Sterken, C. Jaschek, Cambridge University Press, Cambridge, 148.

Szkody, P., and Mattei, J. A. 1984, *Publ. Astron. Soc. Pacific*, **96**, 988.

Warner, B. 1995, in Cataclysmic Variable Stars, Cambridge University Press, Cambridge, 126, 163.

Zacharias, N., Finch, C. T., Girard, T. M., Henden, A., Bartlett, J. L., Monet, D. G., and Zacharias, M. I. 2013, *Astron. J.*, **145**, 44.

First Precision Photometric Observations and Analyses of the Totally Eclipsing, Solar Type Binary V573 Pegasi

Ronald G. Samec
Faculty Research Associate, Pisgah Astronomical Research Institute, 1 PARI Drive, Rosman, NC 28772; ronaldsamec@gmail.com

Daniel B. Caton
Dark Sky Observatory, Department of Physics and Astronomy, Appalachian State University, 525 Rivers Street, Boone, NC 28608

Danny R. Faulkner
Johnson Observatory, 1414 Bur Oak Court, Hebron, KY 41048

Received April 26, 2018; revised May 25, 2018; accepted May 28, 2018

Abstract. CCD VR_cI_c light curves of V573 Peg were taken 26 and 27 September and 2, 4, and 6 October, 2017, at the Dark Sky Observatory in North Carolina with the 0.81-m reflector of Appalachian State University. Five times of minimum light were calculated, two primary and three secondary eclipses, from our present observations. The following quadratic ephemeris was determined from all available times of minimum light: JD Hel MinI = 2456876.4958 (2) d + 0.41744860 (8) × E –2.74 (12) × 10^{-10} × E^2, where the parentheses hold the ± error in the last two digits of the preceding value. A 14-year period study (covered by 24 times of minimum light) reveals a decreasing orbital period with high confidence, possibly due to magnetic braking. The mass ratio is found to be somewhat extreme, $M_2/M_1 = 0.2629 \pm 0.0006$ ($M_1/M_2 = 3.8$). Its Roche Lobe fill-out is ~25%. The solution had no need of spots. The component temperature difference is about 130 K, with the less massive component as the hotter one, so it is a W-type W UMa Binary. The inclination is 80.4 ± 0.1°. Our secondary eclipse shows a time of constant light with an eclipse duration of 24 minutes. More information is given in the following report.

1. Introduction

Studies of solar-type eclipsing binaries continue to yield important information on their evolution and nature of orbits. These investigations possibly link detached configurations to semidetached V1010 Oph types (Angione and Sievers 2013) and Algol types to contact binaries, to overcontact binaries, and to red novae (Tylenda and Kamiński 2016) and fast rotating A-type (Guinan and Bradstreet 1988) and FK Comae single stars. Many O–C plots of these binaries are found to be sinusoidal indicating the presence of an orbiting third body. A parabolic O–C plot indicates a continuously decreasing (decaying) or increasing orbital period. V573 Pegasi is a binary in the later case in a near extreme mass ratio configuration with a decaying orbital period.

2. History and observations

The variable was discovered by Maciejewski *et al.* (2004) in a list of 28 new variable stars (SAVS 231034+314253). Their light curve is shown as Figure 1.

They give a V-magnitude of 12.34, an amplitude of V = 0.51 mag, and the ephemeris:

$$\text{JD Hel MinI} = 2452885.2469 + 0.417461\,(3)\,\text{d} \times \text{E}, \quad (1)$$

was given as well as an EW designation. This variable was listed in "A Catalog of 1022 Bright Contact Binary Stars" (Gettel *et al.* 2006). Timings of minimum light have been given by Gürol *et al.* (2007), Paschke (2009), Nelson (2009), Gökay *et al.* (2012), Demircan *et al.* (2012), and Hübscher (2014). The system was listed in "The 80th Name-List of Variable Stars" (Kazarovets *et al.* 2013).

This system was observed as a part of our professional collaborative studies of interacting binaries at Pisgah Astronomical Research Institute from data taken from Dark Sky Observatory (DSO) observations. The observations were taken by D. Caton. Reduction and analyses were done by Ron Samec. Our 2017 VR_cI_c light curves were taken at Dark Sky Observatory 26 and 27 September and 2, 4, and 6 October 2017 with a thermoelectrically cooled (–35° C) 2KX2K FLI camera and VR_cI_c filters. Individual observations included 328 in V, 338 in R_c, and 348 in I_c. The probable error of a single observation was 7 mmag in R_c and I_c, as well as 8 mmag in V. The nightly Comparison—Check star values stayed constant throughout the observing run with a precision of 3 mmag in V and R_c, and 3.5 mmag in I_c. Exposure times varied from 25-30s in V and 25s in R_c and I_c. To produce the images, nightly images were calibrated with 25 bias frames, at least five flat frames in each filter, and ten 300-second dark frames.

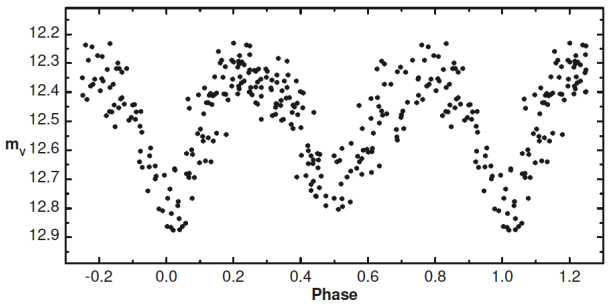

Figure 1. SAVS discovery light curve of SAVS 231034+314253 (V573 Peg). From Maciejewski *et al.* (2004).

The VR_cI_c observations are given in Table 1 as HJD vs Magnitude. Figures 2a and b show two sample light curves taken September 27 and October 2, 2017.

3. Finding chart

The finding chart, given here for future observers, is shown as Figure 3. The coordinates and magnitudes of the variable star, comparison star, and check star are given in Table 2.

4. Period Study

Five mean times (from VR_cI_c data) of minimum light were calculated from our present observations, three primary and two secondary eclipses:

HJD Min I = 2456876.49380 ± 0.0006, 2458023.6420 ± 0.0011, 2458028.65221 ± 0.0021

HJD Min II = 2458022.5991 ± 0.0011, 2458023.8510 ± 0.0010, 2458028.86081 ± 0.0005.

A least squares minimization method (Mikulášek *et al.* 2014) was used to determine the minima for each curve. VR_cI_c results were averaged to determine each time of minimum light. All minima were weighted as 1.0 in the period study.

In addition, nineteen times of minimum light were collected from literature and listed in Table 3. A weighted least squares program was used to determine linear and quadratic ephemerides from these data:

$$\text{MinI} = \text{JD Hel}\, 2456876.4944\,(11) + 0.41745021\,(25)\,\text{d} \times \text{E} \quad (2)$$

$$\text{MinI} = \text{JD Hel}\, 2456876.4958\,(3) + 0.41744860\,(12)\,\text{d} \times \text{E} - [2.7\,(2) \times 10^{-10}] \times \text{E}^2 \quad (3)$$

The residuals from the linear term of Equation 3 is shown with the quadratic fit in Figure 4.

This period study covers a time interval of over 14 years and shows an orbital period that is decreasing (at the 13-sigma level). A possible cause of this effect is magnetic braking that occurs as plasma winds leave the system on stiff, but rotating and spreading, dipole magnetic field lines. This causes a continuous angular momentum loss. This scenario is typical for overcontact binaries which eventually coalesce, albeit, in a catastrophic way, producing red novae (Tylenda and Kamiński 2016). The residuals from the linear term of Equation 3 is shown with the quadratic fit in Figure 4. Both the linear and quadratic O–C residuals are given in Table 3.

5. Light curve characteristics

The VR_c and I_c curves and $V–R_c$, $V–I_c$ color curves are shown in Figures 5a and b. These are phased with Equation 2. Light curve amplitudes and the differences in magnitudes at various quadratures are given in Table 4. The curves are of good precision, averaging somewhat better than 1% photometric precision. The amplitude of the light curve varies from

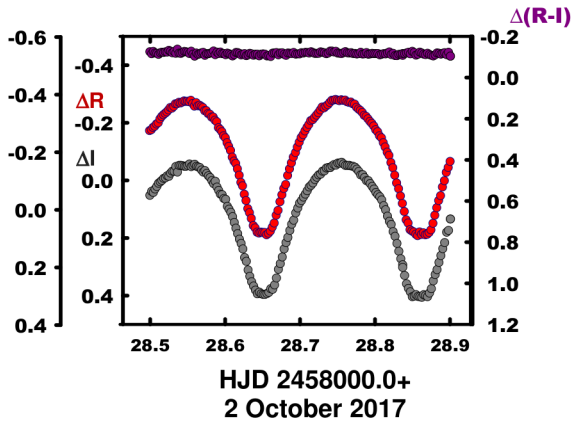

Figure 2a. V573 Peg. Observations taken 2 October 2017.

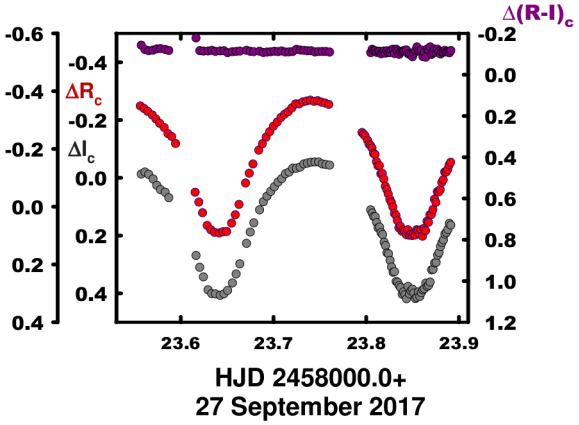

Figure 2b. V573 Peg. Observations taken 27 September 2017.

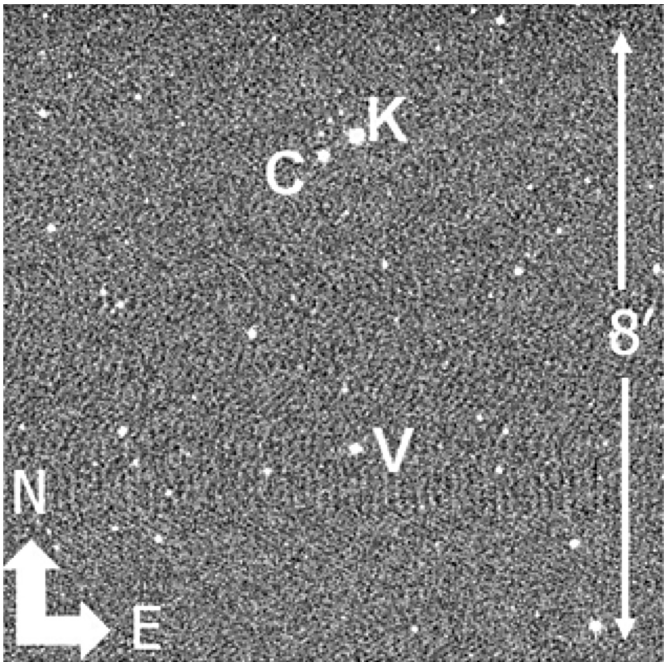

Figure 3. Finding chart, V573 Peg (V), Comparison (C), and Check (K).

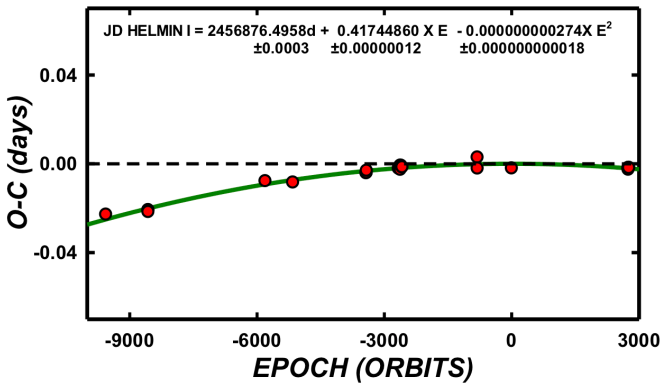

Figure 4. The residuals from the quadratic term of Equation 3 in the period study of V573 Peg.

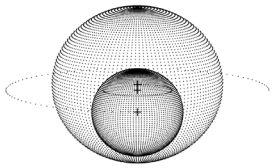

Figure 6a. V573 Peg, geometrical representation at phase 0.00.

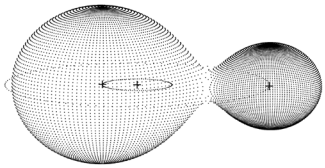

Figure 6b. V573 Peg, geometrical representation at phase 0.25.

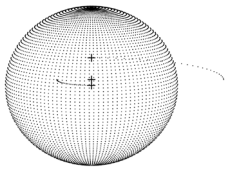

Figure 6c. V573 Peg, geometrical representation at phase 0.50.

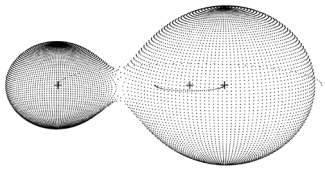

Figure 6d. V573 Peg, geometrical representation at phase 0.75.

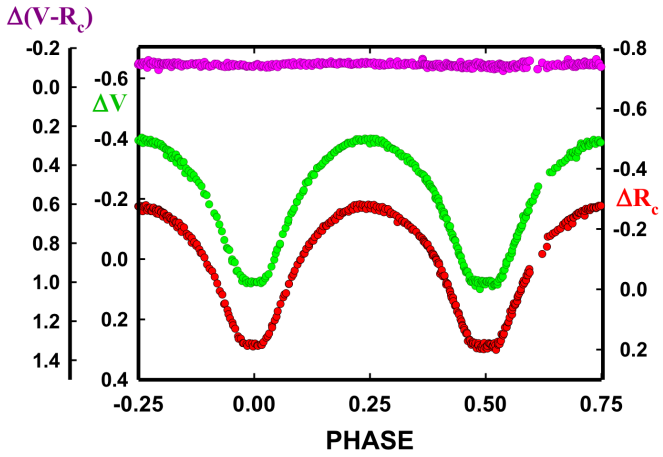

Figure 5a. VR_c magnitude light curves of V573 Peg phased by Equation 2.

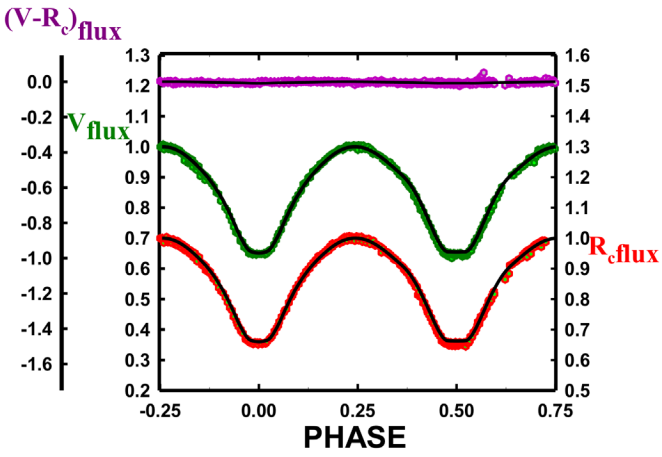

Figure 7a. V573 Peg, V, R_c normalized fluxes overlaid by our solution.

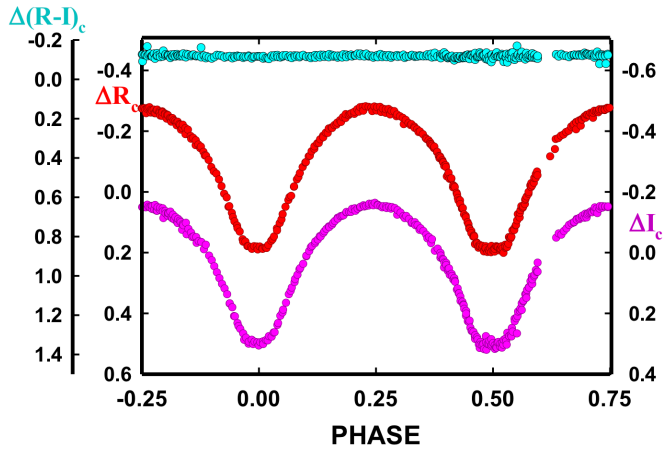

Figure 5b. R_cI_c magnitude light curves of V573 Peg phased by Equation 2.

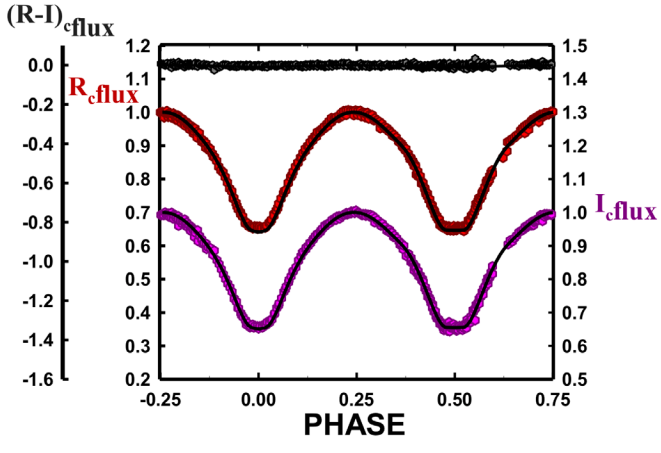

Figure 7b. V573 Peg, R_c, I_c normalized fluxes overlaid by our solution.

0.47–0.46 mag in V to I_c. The O'Connell effect, an indicator of spot activity, averages less than the noise level, 0.002–0.004 mag, not necessarily indicating the presence of star spots. The differences in minima are negligible, 0.005–0.008 mag, indicating overcontact light curves in thermal contact. A time of constant light, a total eclipse, occurs at our secondary minima.

6. Temperature

The 2MASS J–K equals 0.314 ± 0.049 for the binary. The APASS B–V equals 0.59. These correspond to a ~F7 ± 2V spectral type, which yields a temperature of 6250 K ± 300 K. Fast rotating binary stars of this type are noted for having convective atmospheres, so the binary is of solar type.

7. Light curve solution

The VR_cI_c curves were pre-modeled with BINARY MAKER 3.0 (Bradstreet and Steelman 2002). Fits were determined in VR_cI_c filter bands which were very stable. The solution was that of an overcontact eclipsing binary. The parameters were then averaged and input into a three-color simultaneous light curve calculation using the Wilson-Devinney Program (Wilson and Devinney 1971; Wilson 1990, 1994; Van Hamme and Wilson 1998). The computation was computed in Mode 3 and converged to a solution. Convective parameters, g = 0.32, A = 0.5 were used.

An eclipse duration of ~24 minutes was determined for our secondary eclipse (phase 0.5) and the light curve solution. The less massive component is the hottest, making the system a W-type W UMa contact binary. Since the eclipses were total, the mass ratio, q, is well determined with a fill-out of 24.5 (1)%. The light curve solution is given in Table 5. The Roche Lobe representation at quarter orbital phases is shown in Figures 6a, b, c, and d and the normalized fluxes overlaid by our solution of V573 Peg in VR_cI_c are shown in Figures 7a and b.

8. Discussion

V573 Peg is an overcontact W U Ma binary. The system has a rather extreme mass ratio of ~0.26, and a component temperature difference of ~130 K. No spots were needed in the modeling. The Roche Lobe fill-out of the binary is ~24.5% with an inclination of ~80 degrees. Its photometric spectral type indicates a surface temperature of ~6250 K for the primary component, making it a solar type binary. Such a main sequence star would have a mass of ~1.25 $M_\odot$ and the secondary (from the mass ratio) would have a mass of ~0.33 $M_\odot$, making it very much undersized. The W-type configuration is thought to be due to a surface saturated with solar phenomena on the primary component, suppressing its temperature. The secondary component has a temperature of ~6379 K.

9. Conclusion

The period study of this overcontact W UMa binary has a 14-year duration. The orbital period is found to be increasing at about the 13-sigma level. The system is of solar type and this is hinted at by the fact that the smaller component is the hotter one. This "W-type" phenomena is probably due to spots saturating the primary component with its deep convective envelope. The strong period decrease is probably due to magnetic braking. If this is the case, the system will slowly coalesce over time with the mass ratio becoming more extreme, as it loses angular momentum. In time, if this continues, one would expect that the binary will become a rather normal, fast rotating, single ~F2V type field star after a red nova coalescence event and some mass loss (Tylenda and Kamiński 2016).

10. Acknowledgement

Dr. Samec wishes to thank Dr. Danny Faulkner for his continued help and friendship through the years.

References

Angione, R. J., and Sievers, J. R. 2013, *Publ. Astron. Soc. Pacific*, **125**, 41.

Bradstreet, D. H., and Steelman, D. P. 2002, *Bull. Amer. Astron. Soc.*, **34**, 1224.

Demircan, Y., *et al.* 2012, *Inf. Bull. Var. Stars*, No. 6041, 1.

Gettel, S. J., Geske, M. T., and McKay, T. A. 2006, *Astron. J.*, **131**, 621.

Gökay, G., *et al.* 2012, *Inf. Bull. Var. Stars*, No. 6039, 1.

Guinan, E. F., and Bradstreet, D. H. 1988, in *Formation and Evolution of Low Mass Stars*, eds. A. K. Dupree, M. T. V. T. Lago, NATO Advanced Science Institutes (ASI) Ser. C, Vol. 241, Kluwer, Dordrecht, Netherlands, 345–375.

Gürol, B., *et al.* 2007, *Inf. Bull. Var. Stars*, No. 5791, 1.

Høg, E., *et al.* 2000, *Astron. Astrophys.*, **355**, L27.

Hübscher, J. 2014, *Inf. Bull. Var. Stars*, No. 6118, 1.

Kazarovets, E. V., Samus, N. N., Durlevich, O. V., Kireeva, N. N., and Pastukhova, E. N. 2013, *Inf. Bull. Var. Stars*, No. 6052, 1.

Maciejewski, G., Czart, K., and Niedzielski, A. 2004, *Inf. Bull. Var. Stars*, No. 5518, 1.

Mikulášek, Z., Chrastina, M., Liška, J., Zejda, M., Janík, J., Zhu, L.-Y., and Qian, S.-B. 2014, *Contrib. Astron. Obs. Skalnaté Pleso*, **43**, 382.

Nelson, R. H. 2009, *Inf. Bull. Var. Stars*, No. 5875, 1.

Paschke, A. 2009, *Open Eur. J. Var. Stars*, **116**, 1.

Skrutskie, M. F., *et al.* 2006, *Astron. J.*, **131**, 1163.

Tylenda, R., and Kamiński, T. 2016, *Astron. Astrophys.*, **592A**, 134.

U.S. Naval Observatory. 2012, UCAC-3 (http://www.usno.navy.mil/USNO/astrometry/optical-IR-prod/ucac).

Van Hamme, W. V., and Wilson, R. E. 1998, *Bull. Amer. Astron. Soc.*, **30**, 1402.

Wilson, R. E., and Devinney, E. J. 1971, *Astrophys. J.*, **166**, 605.

Wilson, R. E. 1990, *Astrophys. J.*, **356**, 613.

Wilson, R. E. 1994, *Publ. Astron. Soc. Pacific*, **106**, 921.

Table 1. V573 Peg observations, ΔV, ΔR_c, and ΔI_c, variable star minus comparison star.

ΔV	*HJD 2458000+*	ΔV	*HJD 2458000+*	ΔV	*HJD 2458000+*	ΔV	*HJD 2458000+*	ΔV	*HJD 2458000+*
–0.365	22.5156	–0.385	23.7271	–0.391	23.7350	–0.190	23.8924	0.070	28.6446
–0.350	22.5224	–0.382	23.7311	–0.391	23.7390	–0.192	23.8940	0.077	28.6472
–0.323	22.5285	–0.391	23.7350	–0.393	23.7430	–0.210	23.8956	0.075	28.6497
–0.316	22.5321	–0.391	23.7390	–0.382	23.7470	–0.222	23.8972	0.077	28.6523
–0.310	22.5356	–0.393	23.7430	–0.385	23.7510	–0.240	23.8988	0.077	28.6548
–0.280	22.5425	–0.382	23.7470	–0.385	23.7549	–0.287	28.5012	0.072	28.6574
–0.258	22.5458	–0.385	23.7510	–0.381	23.7589	–0.287	28.5035	0.076	28.6599
–0.239	22.5491	–0.385	23.7549	–0.368	23.7629	–0.301	28.5058	0.058	28.6625
–0.199	22.5541	–0.381	23.7589	–0.262	23.7969	–0.303	28.5081	0.051	28.6650
–0.175	22.5574	–0.368	23.7629	–0.255	23.7985	–0.317	28.5104	0.026	28.6676
–0.141	22.5606	–0.262	23.7969	–0.247	23.8001	–0.319	28.5127	0.003	28.6701
–0.108	22.5670	–0.255	23.7985	–0.236	23.8028	–0.326	28.5150	–0.031	28.6727
–0.062	22.5712	–0.247	23.8001	–0.227	23.8044	–0.335	28.5173	–0.047	28.6752
–0.012	22.5754	–0.236	23.8028	–0.202	23.8060	–0.344	28.5196	–0.082	28.6778
0.045	22.5813	–0.227	23.8044	–0.196	23.8076	–0.351	28.5219	–0.102	28.6803
0.076	22.5855	–0.202	23.8060	–0.190	23.8092	–0.347	28.5242	–0.130	28.6829
0.090	22.5897	–0.196	23.8076	–0.173	23.8108	–0.354	28.5265	–0.150	28.6854
0.073	22.5957	–0.190	23.8092	–0.157	23.8124	–0.373	28.5287	–0.167	28.6880
0.074	22.5999	–0.173	23.8108	–0.148	23.8140	–0.367	28.5310	–0.189	28.6905
0.082	22.6041	–0.157	23.8124	–0.135	23.8156	–0.374	28.5333	–0.207	28.6931
0.083	22.6095	–0.148	23.8140	–0.113	23.8172	–0.379	28.5356	–0.222	28.6960
0.055	22.6137	–0.135	23.8156	–0.100	23.8188	–0.382	28.5379	–0.252	28.6985
0.013	22.6179	–0.113	23.8172	–0.085	23.8204	–0.392	28.5402	–0.255	28.7010
–0.028	22.6229	–0.100	23.8188	–0.068	23.8220	–0.381	28.5425	–0.276	28.7036
–0.076	22.6271	–0.085	23.8204	–0.061	23.8236	–0.388	28.5448	–0.278	28.7061
–0.103	22.6313	–0.068	23.8220	–0.041	23.8252	–0.386	28.5471	–0.302	28.7087
–0.155	22.6365	–0.061	23.8236	–0.019	23.8269	–0.389	28.5494	–0.307	28.7112
–0.338	22.6766	–0.041	23.8252	–0.009	23.8285	–0.384	28.5517	–0.317	28.7138
–0.335	22.6808	–0.019	23.8269	0.010	23.8301	–0.392	28.5540	–0.330	28.7163
–0.383	22.6850	–0.009	23.8285	0.028	23.8317	–0.385	28.5563	–0.335	28.7189
–0.376	22.6918	0.010	23.8301	0.040	23.8335	–0.395	28.5586	–0.345	28.7214
–0.374	22.6922	0.028	23.8317	0.042	23.8351	–0.385	28.5609	–0.353	28.7240
–0.395	22.6964	0.040	23.8335	0.069	23.8367	–0.389	28.5632	–0.361	28.7265
–0.386	22.7022	0.042	23.8351	0.077	23.8383	–0.384	28.5655	–0.368	28.7291
–0.402	22.7064	0.069	23.8367	0.077	23.8398	–0.374	28.5678	–0.372	28.7316
–0.383	22.7148	0.077	23.8383	0.069	23.8414	–0.373	28.5700	–0.378	28.7341
–0.343	23.5637	0.077	23.8398	0.078	23.8430	–0.363	28.5723	–0.382	28.7367
–0.334	23.5676	0.069	23.8414	0.080	23.8446	–0.361	28.5746	–0.386	28.7392
–0.319	23.5725	0.078	23.8430	0.101	23.8462	–0.356	28.5769	–0.390	28.7418
–0.308	23.5765	0.080	23.8446	0.076	23.8478	–0.333	28.5792	–0.397	28.7443
–0.284	23.5804	0.101	23.8462	0.074	23.8494	–0.346	28.5815	–0.397	28.7469
–0.268	23.5854	0.076	23.8478	0.085	23.8510	–0.334	28.5838	–0.395	28.7494
–0.033	23.6188	0.074	23.8494	0.075	23.8526	–0.321	28.5861	–0.399	28.7520
0.009	23.6228	0.085	23.8510	0.078	23.8542	–0.321	28.5884	–0.397	28.7545
0.041	23.6267	0.075	23.8526	0.073	23.8558	–0.300	28.5907	–0.399	28.7571
0.074	23.6317	0.078	23.8542	0.092	23.8574	–0.292	28.5930	–0.398	28.7596
0.081	23.6357	0.073	23.8558	0.086	23.8590	–0.285	28.5953	–0.398	28.7621
0.082	23.6396	0.092	23.8574	0.084	23.8606	–0.277	28.5976	–0.392	28.7647
0.078	23.6448	0.086	23.8590	0.086	23.8622	–0.263	28.5999	–0.393	28.7672
0.081	23.6488	0.084	23.8606	0.067	23.8637	–0.252	28.6022	–0.386	28.7698
0.065	23.6527	0.086	23.8622	0.065	23.8653	–0.241	28.6045	–0.378	28.7723
–0.017	23.6620	0.067	23.8637	0.059	23.8669	–0.216	28.6068	–0.369	28.7749
–0.050	23.6660	0.065	23.8653	0.037	23.8685	–0.211	28.6091	–0.363	28.7774
–0.121	23.6732	0.059	23.8669	0.009	23.8701	–0.181	28.6114	–0.360	28.7800
–0.157	23.6772	0.037	23.8685	–0.002	23.8733	–0.151	28.6160	–0.348	28.7825
–0.189	23.6811	0.009	23.8701	–0.018	23.8749	–0.139	28.6183	–0.339	28.7851
–0.228	23.6873	–0.002	23.8733	–0.044	23.8765	–0.114	28.6206	–0.339	28.7876
–0.258	23.6913	–0.018	23.8749	–0.058	23.8781	–0.091	28.6229	–0.337	28.7902
–0.281	23.6953	–0.044	23.8765	–0.067	23.8797	–0.062	28.6251	–0.327	28.7927
–0.300	23.6993	–0.058	23.8781	–0.090	23.8813	–0.036	28.6274	–0.316	28.7952
–0.311	23.7032	–0.067	23.8797	–0.107	23.8829	–0.029	28.6297	–0.300	28.7978
–0.326	23.7072	–0.090	23.8813	–0.112	23.8844	0.002	28.6321	–0.288	28.8003
–0.338	23.7112	–0.107	23.8829	–0.129	23.8860	0.012	28.6345	–0.282	28.8029
–0.353	23.7152	–0.112	23.8844	–0.143	23.8876	0.039	28.6370	–0.276	28.8054
–0.364	23.7191	–0.129	23.8860	–0.156	23.8892	0.054	28.6396		
–0.374	23.7231	–0.143	23.8876	–0.181	23.8908	0.063	28.6421		

Table continued on following pages

Table 1. V573 Peg observations, ΔV, ΔR_c, and ΔI_c, variable star minus comparison star, cont.

ΔR_c	*HJD 2458000+*	ΔR_c	*HJD 2458000+*	ΔR_c	*HJD 2458000+*	ΔR_c	*HJD 2458000+*	ΔR_c	*HJD 2458000+*
–0.248	22.5129	–0.141	23.6921	0.049	23.8783	0.132	28.6349	–0.148	28.8085
–0.222	22.5195	–0.160	23.6960	0.041	23.8799	0.157	28.6375	–0.131	28.8110
–0.219	22.5256	–0.179	23.7000	0.016	23.8815	0.165	28.6400	–0.116	28.8135
–0.210	22.5292	–0.193	23.7040	0.007	23.8831	0.180	28.6426	–0.098	28.8161
–0.196	22.5327	–0.209	23.7080	–0.020	23.8847	0.183	28.6451	–0.087	28.8186
–0.173	22.5398	–0.220	23.7119	–0.020	23.8863	0.180	28.6477	–0.062	28.8212
–0.162	22.5431	–0.229	23.7159	–0.029	23.8879	0.181	28.6502	–0.044	28.8237
–0.143	22.5464	–0.242	23.7199	–0.045	23.8895	0.181	28.6528	–0.018	28.8263
–0.110	22.5514	–0.256	23.7239	–0.054	23.8911	0.189	28.6553	0.009	28.8288
–0.096	22.5547	–0.256	23.7278	–0.173	28.4993	0.184	28.6579	0.029	28.8314
–0.050	22.5579	–0.263	23.7318	–0.176	28.5016	0.176	28.6604	0.054	28.8339
–0.021	22.5636	–0.266	23.7358	–0.184	28.5039	0.162	28.6630	0.080	28.8365
0.021	22.5678	–0.265	23.7438	–0.188	28.5062	0.148	28.6655	0.108	28.8390
0.055	22.5720	–0.267	23.7477	–0.196	28.5085	0.121	28.6681	0.137	28.8415
0.120	22.5779	–0.262	23.7517	–0.200	28.5108	0.104	28.6706	0.148	28.8441
0.145	22.5821	–0.259	23.7557	–0.214	28.5131	0.074	28.6732	0.171	28.8466
0.179	22.5863	–0.254	23.7597	–0.222	28.5154	0.050	28.6757	0.176	28.8492
0.187	22.5923	–0.157	23.7955	–0.228	28.5177	0.028	28.6783	0.179	28.8517
0.187	22.5965	–0.151	23.7972	–0.233	28.5200	0.014	28.6808	0.187	28.8543
0.189	22.6007	–0.145	23.7988	–0.238	28.5223	–0.017	28.6834	0.192	28.8568
0.188	22.6060	–0.130	23.8015	–0.245	28.5246	–0.040	28.6859	0.179	28.8594
0.185	22.6102	–0.117	23.8031	–0.253	28.5269	–0.061	28.6885	0.188	28.8619
0.153	22.6144	–0.112	23.8047	–0.251	28.5292	–0.081	28.6910	0.182	28.8645
0.111	22.6194	–0.103	23.8063	–0.257	28.5315	–0.097	28.6939	0.189	28.8670
0.061	22.6236	–0.085	23.8079	–0.266	28.5337	–0.116	28.6964	0.187	28.8696
0.027	22.6278	–0.081	23.8095	–0.266	28.5360	–0.133	28.6990	0.181	28.8721
–0.015	22.6331	–0.056	23.8111	–0.271	28.5383	–0.149	28.7015	0.172	28.8746
–0.058	22.6373	–0.042	23.8127	–0.269	28.5406	–0.159	28.7041	0.149	28.8772
–0.116	22.6501	–0.042	23.8143	–0.272	28.5429	–0.172	28.7066	0.121	28.8797
–0.140	22.6543	–0.014	23.8158	–0.276	28.5452	–0.184	28.7092	0.095	28.8823
–0.205	22.6732	–0.015	23.8174	–0.274	28.5475	–0.194	28.7117	0.070	28.8848
–0.217	22.6774	0.004	23.8190	–0.275	28.5498	–0.208	28.7143	0.053	28.8874
–0.243	22.6816	0.029	23.8206	–0.273	28.5521	–0.211	28.7168	0.023	28.8899
–0.243	22.6883	0.041	23.8222	–0.278	28.5544	–0.219	28.7194	0.001	28.8925
–0.261	22.6930	0.056	23.8238	–0.267	28.5567	–0.227	28.7219	–0.028	28.8950
–0.270	22.6988	0.075	23.8256	–0.258	28.5590	–0.235	28.7244	–0.045	28.8976
–0.276	22.7030	0.085	23.8272	–0.270	28.5613	–0.245	28.7270	–0.066	28.9001
–0.258	22.7072	0.101	23.8288	–0.259	28.5636	–0.255	28.7295	–0.217	30.6022
–0.260	22.7114	0.123	23.8304	–0.261	28.5659	–0.252	28.7321	–0.229	30.6048
–0.258	22.7156	0.130	23.8321	–0.257	28.5682	–0.258	28.7346	–0.234	30.6073
–0.250	22.7198	0.148	23.8337	–0.253	28.5704	–0.263	28.7372	–0.237	30.6099
–0.249	23.5564	0.173	23.8353	–0.242	28.5727	–0.271	28.7397	–0.248	30.6124
–0.240	23.5604	0.168	23.8369	–0.242	28.5750	–0.278	28.7423	–0.253	30.6149
–0.230	23.5644	0.185	23.8385	–0.232	28.5773	–0.279	28.7448	–0.259	30.6175
–0.218	23.5693	0.181	23.8401	–0.230	28.5796	–0.281	28.7473	–0.259	30.6200
–0.204	23.5732	0.185	23.8417	–0.220	28.5819	–0.279	28.7499	–0.263	30.6225
–0.189	23.5772	0.197	23.8433	–0.220	28.5842	–0.277	28.7524	–0.267	30.6251
–0.174	23.5822	0.180	23.8449	–0.209	28.5865	–0.280	28.7550	–0.271	30.6276
–0.153	23.5862	0.199	23.8465	–0.204	28.5888	–0.278	28.7575	–0.268	30.6302
–0.143	23.5902	0.196	23.8481	–0.183	28.5911	–0.279	28.7601	–0.273	30.6328
–0.119	23.5944	0.200	23.8497	–0.177	28.5934	–0.273	28.7626	–0.273	30.6353
0.050	23.6155	0.193	23.8513	–0.169	28.5957	–0.271	28.7652	–0.270	30.6379
0.084	23.6195	0.198	23.8529	–0.155	28.5980	–0.272	28.7677	–0.276	30.6404
0.121	23.6235	0.180	23.8544	–0.148	28.6003	–0.266	28.7703	–0.269	30.6429
0.165	23.6285	0.183	23.8560	–0.131	28.6026	–0.265	28.7728	–0.270	30.6455
0.180	23.6324	0.194	23.8576	–0.118	28.6049	–0.254	28.7753	–0.268	30.6480
0.189	23.6364	0.180	23.8592	–0.104	28.6072	–0.248	28.7779	–0.264	30.6506
0.191	23.6416	0.202	23.8608	–0.081	28.6095	–0.243	28.7804	–0.264	30.6531
0.187	23.6455	0.175	23.8624	–0.067	28.6118	–0.236	28.7830	–0.254	30.6556
0.186	23.6495	0.183	23.8640	–0.059	28.6141	–0.226	28.7855	–0.251	30.6582
0.157	23.6548	0.150	23.8656	–0.040	28.6164	–0.222	28.7881	–0.240	30.6607
0.128	23.6588	0.154	23.8672	–0.018	28.6187	–0.214	28.7906	–0.235	30.6633
0.092	23.6628	0.128	23.8688	0.007	28.6210	–0.205	28.7932	–0.227	30.6658
0.018	23.6699	0.127	23.8704	0.019	28.6233	–0.198	28.7957	–0.222	30.6683
–0.016	23.6739	0.110	23.8720	0.048	28.6256	–0.189	28.7983	–0.210	30.6709
–0.048	23.6779	0.074	23.8736	0.070	28.6279	–0.176	28.8008		
–0.096	23.6841	0.085	23.8752	0.098	28.6302	–0.169	28.8034		
–0.118	23.6881	0.048	23.8767	0.112	28.6325	–0.155	28.8059		

Table continued on following pages

Table 1. V573 Peg observations, ΔV, ΔR_c, and ΔI_c, variable star minus comparison star, cont.

ΔI_c	*HJD 2458000+*	ΔI_c	*HJD 2458000+*	ΔI_c	*HJD 2458000+*	ΔI_c	*HJD 2458000+*	ΔI_c	*HJD 2458000+*
–0.124	22.5137	–0.133	23.7208	0.064	23.8913	0.296	28.6507	0.042	28.8191
–0.113	22.5204	–0.133	23.7248	–0.048	28.4997	0.296	28.6532	0.053	28.8216
–0.096	22.5265	–0.137	23.7288	–0.062	28.5020	0.293	28.6558	0.078	28.8242
–0.089	22.5300	–0.148	23.7328	–0.058	28.5043	0.289	28.6583	0.094	28.8267
–0.074	22.5336	–0.151	23.7367	–0.070	28.5066	0.276	28.6609	0.119	28.8293
–0.046	22.5406	–0.154	23.7407	–0.079	28.5089	0.278	28.6634	0.146	28.8318
–0.030	22.5439	–0.155	23.7447	–0.090	28.5112	0.263	28.6660	0.172	28.8344
–0.005	22.5472	–0.155	23.7487	–0.095	28.5135	0.239	28.6685	0.193	28.8369
0.018	22.5522	–0.148	23.7527	–0.100	28.5158	0.209	28.6711	0.202	28.8369
0.050	22.5555	–0.146	23.7566	–0.107	28.5181	0.189	28.6736	0.230	28.8395
0.061	22.5588	–0.144	23.7606	–0.109	28.5204	0.166	28.6762	0.259	28.8420
0.085	22.5646	0.011	23.8049	–0.116	28.5227	0.138	28.6787	0.275	28.8446
0.135	22.5688	0.022	23.8065	–0.114	28.5250	0.116	28.6813	0.287	28.8471
0.174	22.5730	0.034	23.8081	–0.125	28.5273	0.098	28.6838	0.304	28.8497
0.248	22.5789	0.035	23.8097	–0.132	28.5296	0.074	28.6864	0.302	28.8522
0.285	22.5831	0.055	23.8113	–0.132	28.5319	0.052	28.6889	0.297	28.8547
0.315	22.5873	0.074	23.8129	–0.148	28.5342	0.038	28.6915	0.303	28.8573
0.321	22.5933	0.071	23.8145	–0.129	28.5364	0.013	28.6943	0.304	28.8598
0.308	22.5975	0.090	23.8161	–0.152	28.5387	–0.004	28.6969	0.306	28.8624
0.313	22.6017	0.097	23.8177	–0.152	28.5410	–0.021	28.6994	0.297	28.8649
0.314	22.6071	0.123	23.8193	–0.151	28.5433	–0.030	28.7020	0.300	28.8675
0.304	22.6113	0.135	23.8209	–0.149	28.5456	–0.042	28.7045	0.304	28.8700
0.277	22.6155	0.160	23.8225	–0.149	28.5479	–0.052	28.7071	0.291	28.8726
0.267	22.6205	0.163	23.8241	–0.152	28.5502	–0.064	28.7096	0.276	28.8751
0.190	22.6247	0.186	23.8258	–0.157	28.5525	–0.077	28.7122	0.249	28.8777
0.150	22.6289	0.209	23.8274	–0.148	28.5548	–0.083	28.7147	0.227	28.8802
0.104	22.6341	0.227	23.8290	–0.152	28.5571	–0.091	28.7173	0.210	28.8827
0.065	22.6383	0.225	23.8306	–0.156	28.5594	–0.103	28.7198	0.185	28.8853
–0.115	22.6826	0.259	23.8324	–0.149	28.5617	–0.111	28.7224	0.161	28.8878
–0.137	22.6894	0.262	23.8340	–0.147	28.5640	–0.119	28.7249	0.137	28.8904
–0.143	22.7124	0.273	23.8356	–0.145	28.5663	–0.122	28.7275	0.116	28.8929
–0.137	22.7166	0.280	23.8372	–0.136	28.5686	–0.132	28.7300	0.080	28.8955
–0.113	23.5574	0.303	23.8388	–0.129	28.5709	–0.133	28.7325	0.074	28.8980
–0.120	23.5614	0.295	23.8403	–0.134	28.5731	–0.143	28.7351	0.034	28.9006
–0.112	23.5654	0.305	23.8419	–0.124	28.5754	–0.145	28.7376	–0.098	30.6027
–0.096	23.5702	0.319	23.8435	–0.116	28.5777	–0.144	28.7402	–0.110	30.6052
–0.074	23.5742	0.276	23.8451	–0.110	28.5800	–0.150	28.7427	–0.114	30.6078
–0.059	23.5782	0.302	23.8467	–0.099	28.5823	–0.155	28.7453	–0.121	30.6103
–0.050	23.5832	0.291	23.8483	–0.089	28.5846	–0.153	28.7478	–0.127	30.6129
–0.031	23.5871	0.286	23.8499	–0.097	28.5869	–0.160	28.7504	–0.129	30.6154
–0.025	23.5953	0.299	23.8515	–0.077	28.5892	–0.160	28.7529	–0.135	30.6179
0.169	23.6165	0.318	23.8531	–0.065	28.5915	–0.163	28.7555	–0.139	30.6205
0.210	23.6205	0.314	23.8547	–0.052	28.5938	–0.157	28.7580	–0.144	30.6230
0.243	23.6244	0.295	23.8563	–0.050	28.5961	–0.152	28.7605	–0.144	30.6256
0.288	23.6294	0.311	23.8579	–0.037	28.5984	–0.152	28.7631	–0.147	30.6281
0.301	23.6334	0.298	23.8595	–0.034	28.6007	–0.152	28.7656	–0.151	30.6307
0.302	23.6374	0.288	23.8611	–0.010	28.6030	–0.150	28.7682	–0.151	30.6332
0.307	23.6425	0.284	23.8627	0.011	28.6076	–0.149	28.7707	–0.148	30.6358
0.302	23.6465	0.265	23.8642	0.026	28.6099	–0.146	28.7733	–0.148	30.6383
0.290	23.6505	0.276	23.8658	0.046	28.6122	–0.139	28.7758	–0.150	30.6409
0.264	23.6557	0.272	23.8674	0.066	28.6145	–0.131	28.7784	–0.153	30.6434
0.233	23.6597	0.261	23.8690	0.085	28.6168	–0.119	28.7809	–0.141	30.6459
0.198	23.6637	0.219	23.8706	0.104	28.6191	–0.120	28.7835	–0.137	30.6485
0.127	23.6709	0.217	23.8722	0.119	28.6214	–0.110	28.7860	–0.140	30.6510
0.088	23.6749	0.195	23.8738	0.138	28.6237	–0.099	28.7886	–0.135	30.6536
0.056	23.6788	0.193	23.8754	0.168	28.6260	–0.099	28.7911	–0.128	30.6561
0.011	23.6850	0.168	23.8770	0.181	28.6283	–0.089	28.7936	–0.129	30.6587
–0.017	23.6890	0.159	23.8786	0.211	28.6306	–0.079	28.7962	–0.115	30.6612
–0.036	23.6930	0.138	23.8802	0.233	28.6329	–0.070	28.7987	–0.108	30.6637
–0.053	23.6970	0.124	23.8818	0.252	28.6354	–0.058	28.8013	–0.100	30.6663
–0.069	23.7010	0.115	23.8833	0.267	28.6380	–0.050	28.8038	–0.104	30.6688
–0.085	23.7049	0.095	23.8849	0.281	28.6405	–0.043	28.8064	–0.092	30.6713
–0.097	23.7089	0.089	23.8865	0.294	28.6430	–0.012	28.8115		
–0.114	23.7129	0.079	23.8881	0.288	28.6456	0.002	28.8140		
–0.120	23.7169	0.058	23.8897	0.294	28.6481	0.024	28.8166		

Table 2. Information on the stars used in this study.

Star	*Name*	*R.A. (2000)* h m s	*Dec. (2000)* ° ′ ″	*V*	*J–K*
V	V573 Peg GSC 2751-1007 SAVS 231034+314253 CRTS J231034.2+314254 NSVS 9014625 3UC167-320333	23 10 34.2395	31 42 53.744[1]	12.59[2]	0.314 ± 0.049[2]
C	GSC 2751-01803 3UC244-290293	23 10 32.1420	31 46 54.821[1]	12.55[2]	0.48[2]
K (Check)	GSC 2751-0129 3UC167-320353	23 10 34.2599	31 47 10.500[3]	11.263[2]	0.277 ± 0.046[2]

[1] *UCAC-3 (USNO 2012).* [2] *2Mass (Skrutskie* et al. *2006).* [3] *TYCHO (Høg, E.,* et al. *2000).*

Table 3. O–C Residuals for V573 Peg.

	Epoch 2400000+	*Cycles*	*Linear Residuals*	*Quadratic Residuals*	*Reference*
1	52885.2469	–9561.0	–0.0060	0.0022	VSX
2	53300.4014	–8566.5	–0.0057	–0.0008	Gürol *et al.* 2007
3	53301.2365	–8564.5	–0.0055	–0.0007	Gürol *et al.* 2007
4	53301.4443	–8564.0	–0.0064	–0.0016	Gürol *et al.* 2007
5	54452.3640	–5807.0	0.0030	0.0015	Paschke 2009
6	54723.7050	–5157.0	0.0014	–0.0011	Nelson 2008
7	55445.4778	–3428.0	0.0028	–0.0010	Gökay *et al.* 2012
8	55448.4001	–3421.0	0.0029	–0.0008	Gökay *et al.* 2012
9	55449.4447	–3418.5	0.0039	0.0001	Gökay *et al.* 2012
10	55764.4106	–2664.0	0.0036	–0.0002	Demircan *et al.* 2012
11	55778.3963	–2630.5	0.0047	0.0009	Demircan *et al.* 2012
12	55781.5255	–2623.0	0.0030	–0.0007	Demircan *et al.* 2012
13	55783.4059	–2618.5	0.0049	0.0011	Demircan *et al.* 2012
14	55790.5024	–2601.5	0.0048	0.0010	Demircan *et al.* 2012
15	55799.2681	–2580.5	0.0040	0.0002	Demircan *et al.* 2012
16	55799.4769	–2580.0	0.0041	0.0003	Demircan *et al.* 2012
17	56539.4090	–807.5	0.0057	0.0031	Hübscher 2014
18	56539.6127	–807.0	0.0007	–0.0019	Hübscher 2014
19	56876.4938	0.0	–0.0006	–0.0020	Hübscher 2014
20	58022.5991	2745.5	–0.0048	0.0003	This paper
21	58023.6420	2748.0	–0.0056	–0.0005	This paper
22	58023.8510	2748.5	–0.0053	–0.0002	This paper
23	58028.6522	2760.0	–0.0047	0.0004	This paper
24	58028.8608	2760.5	–0.0049	0.0002	This paper

Calculated from the light curve data given in the reference.
The quadratic ephemeris yields a $\dot{P} = -4.79 \times 10^{-7}$ d/yr.

Table 4. Averaged light curve characteristics of V573 Peg.

Filter	*Phase*	*Magnitude Min. I*	*Phase*	*Magnitude Max. I*
	0.0		0.25	
V		0.075 ± 0.002		–0.393 ± 0.007
Rc		0.184 ± 0.005		–0.274 ± 0.007
Ic		0.298 ± 0.006		–0.157 ± 0.004
Filter	*Phase*	*Magnitude Min. II*	*Phase*	*Magnitude Max. II*
	0.5		0.75	
V		0.080 ± 0.009		–0.392 ± 0.006
Rc		0.192 ± 0.007		–0.271 ± 0.006
Ic		0.303 ± 0.009		–0.153 ± 0.018

Filter	*Min. I – Max. I*	*Max. I – Max. II*	*Min. I – Min. II*
V	0.468 ± 0.009	–0.002 ± 0.013	–0.005 ± 0.011
Rc	0.458 ± 0.011	–0.004 ± 0.013	–0.008 ± 0.011
Ic	0.455 ± 0.010	–0.004 ± 0.022	–0.005 ± 0.015

Filter	*Max. II – Max. I*	*Filter*	*Min. II – Max. I*
V	0.002 ± 0.013	V	0.472 ± 0.016
Rc	0.004 ± 0.013	Rc	0.463 ± 0.013
Ic	0.004 ± 0.022	Ic	0.456 ± 0.013

Table 5. VR_cI_c solution parameters for V573 Peg.

Parameter	*Overcontact Solution*	*Parameter*	*Overcontact Solution*
l_V, l_{Rc}, l_{Ic} (nm)	440, 550, 640, 790	$q(m_2/m_1)$	0.2629 ± 0.0003
$x_{bol1,2}$, $y_{bol1,}2$	0.640 0 .640, 0.232, 0.232	Fill–outs: $F_1 = F_2$ (%)	24.5 ± 1.0
$x_{1Ic,2Ic}$, $y_{1Ic,2I}$c	0.569, 0.569, 0.271, 0.271	$L_1/(L_1+L_2)_{Ic}$	0.7554 ± 0.0003
$x_{1Rc,2Rc}$, $y_{1Rc,2Rc}$	0.652, 0.652, 0. 278, 0.278	$L_1/(L_1+L_2)_{Rc}$	0.7531 ± 0.0003
$x_{1V,2V}$, $y_{1V,2V}$	0.725, 0.725, 0.266, 0. 266	$L_1/(L_1+L_2)_V$	0.7023 ± 0.0003
g_1 , g_2	0.320, 0.320	JD_o (days)	2458028.65131 ± 0.00006
A1 , A_2	0.5, 0.5	Period (days)	0.417454 ± 0.000007
Inclination (°)	80.43 ± 0.06	r_1, r_2 (pole)	0.4751 ± 0.0003, 0.2613 ± 0.0006
T_1, T_2 (K)	6250, 6379 ± 1	r_1, r_2 (side)	0.5152 ± 0.0005, 0.2733 ± 0.0008
$\Omega_1 = \Omega_2$ pot	2.3421 ± 0.0005	r_1, r_2 (back)	0.5426 ± 0.0006, 0.3146 ± 0.0016

Sparsely-Observed Pulsating Red Giants in the AAVSO Observing Program

John R. Percy
Department of Astronomy and Astrophysics, and Dunlap Institute of Astronomy and Astrophysics, University of Toronto, Toronto ON M5S 3H4, Canada

Received May 16, 2018; revised June 14, 2018; accepted June 14, 2018

Abstract This paper reports on time-series analysis of 156 pulsating red giants (21 SRa, 52 SRb, 33 SR, 50 Lb) in the AAVSO observing program for which there are no more than 150–250 observations in total. Some results were obtained for 68 of these stars: 17 SRa, 14 SRb, 20 SR, and 17 Lb. These results generally include only an average period and amplitude. Many, if not most of the stars are undoubtedly more complex; pulsating red giants are known to have wandering periods, variable amplitudes, and often multiple periods including "long secondary periods" of unknown origin. These results (or lack thereof) raise the question of how the AAVSO should best manage the observation of these and other sparsely-observed pulsating red giants.

1. Introduction

Red giants are unstable to radial pulsation. As they expand and cool, the period and amplitude of pulsation increase. Pulsating red giants (PRGs) are classified as Mira if they have well-pronounced periodicity and visual range greater than 2.5, as SRa if they have smaller amplitudes and persistent periodicity, as SRb if the periodicity is poorly expressed, and Lb if the variability is irregular. These classes are arbitrary; there is a spectrum of behavior from strictly periodic to completely irregular, and of amplitudes from millimagnitudes up to 10 magnitudes.

The AAVSO International Database contains observations of thousands of PRGs. Some are well-studied, especially the brighter Miras; see Templeton *et al.* (2005) for a study of the periods and period changes in 547 of them. There are many, however, which have not been studied, often because the number of observations is insufficient. A few years ago, my students and I undertook a study of some PRGs for which there were only a few hundred observations: SRa/SRb/SR stars (Percy and Tan 2013; Percy and Kojar 2013) and Lb stars (Percy and Long 2010; Percy and Terziev 2011).

The present paper describes a study of several dozen more SR and Lb stars for which there were a total of 150–250 observations, and for which analysis might be possible. I thank Elizabeth Waagen, at AAVSO HQ, for compiling lists of these sparsely-observed SRa, SRb, SR, and Lb stars. Although the primary purpose of this study was to determine the basic variability parameters of as many of these stars as possible, an equally-important purpose was, more generally, to determine whether sparsely-observed PRGs can yield any meaningful results.

2. Data and analysis

Observations were taken from the AAVSO International Database (Kafka 2018). They ranged from all visual for some stars, to all Johnson V (photoelectric or CCD) for others. Periods were determined (or searched for) using the Fourier routine in the VSTAR software package (Benn 2013). Some of the stars had been studied with the All-Sky Automated Survey (ASAS: Pojmański 1997), and a period had been derived. In many cases, the ASAS light curve showed that the variability was complex, and occurred on two or more periods or time scales. This may be true for most of our stars.

3. Results

Tables 1–4 list results for the stars classified as SRa, SRb, SR, and Lb, respectively. Columns list: the star; the period in the VSX catalog (PVSX); the mean period and semi-amplitude obtained in the present study; and notes about the star. Visual amplitudes are denoted v, Johnson V amplitudes as V. The notes are as follows: 1: new period gives a better phase curve than PVSX; 2: new period and PVSX give equally good phase curves; 3: PVSX gives a poor phase curve; 4: neither new period or PVSX gives a good phase curve; *: see note in section 3.1. Figure 1 gives one example of an SR star (EQ And) which shows a quite acceptable phase curve.

Many of the Lb stars in Table 4 were observed primarily in Johnson V, and produce acceptable results with only a few dozen observations.

The following are the number of stars analyzed, and the number and percent which produced results, and which appear in Tables 1–4: SRa: 21, 17, 81%; SRb: 52, 14, 27%; SR: 33, 20, 61%; Lb: 50, 17, 34%.

3.1. Notes on individual stars

These notes on individual SRa, SRb, SR, and Lb stars are combined, and are listed in order of constellation. Many of the 156 stars in the input list also have observations from other sources, such as ASAS, *Hipparcos*, DIRBE (Smith *et al.* 2002), AFOEV, etc., but, unless they helped in the analysis or interpretation of the AAVSO data, they are not discussed here.

KW Cep the Fourier spectrum is complex; the dominant cycle lengths are about 150 days.

UZ Cet the ASAS period is 80.9 days, but the average cycle length is about 117 days. PVSX, the new period, and the ASAS period produce equally unsatisfactory phase curves, but PVSX is probably the best.

RU CrB the V observations show cycle lengths of about 60 days, but the early visual observations give a period of 436 days, which may possibly be a long secondary period.

VY Eri the ASAS light curve is very complex; irregular or multiperiodic star?

TZ Hor there is also a peak at 23.41 days, but the cycle lengths are 35 days.

DV Lac the Fourier spectrum is complex, with cycle lengths in the range of 150 to 180 days.

RS LMi complex; cycle lengths about 110 days; there may be a long secondary period.

V360 Peg the *General Catalogue of Variable Stars* (Samus *et al.* 2017) classifies this star as possibly RV Tauri type, but we find no evidence for this.

SW Pic the V observations show periods of about 25 and 35 days.

TW Ret the *General Catalogue of Variable Stars* (Samus *et al.* 2017) classifies this star as possibly RV Tauri type, but we find no evidence for this.

BN Ser there are several peaks of comparable height in the Fourier spectrum. There appears to be a long secondary period.

4. Discussion

In the AAVSO observing program, there are 155 PRGs which are designated as "legacy stars," and recommended for regular observation. Over the last decade, they have averaged about 375 observations *per year* (Pearce 2018). These dense, sustained observations enable astronomers to follow their wandering periods, variable amplitudes, multiperiodicity, and long secondary periods (LSPs).

For the 156 stars in the present study, there are less than 250 observations *in total*. As a result, less than half the stars yield any meaningful result, that usually being only an estimate of the average period and amplitude. There are some stars which have only a few dozen V observations obtained on a single night (!). For others, sparse observations are spread over many decades. For others, the Fourier spectra showed many comparable peaks, with none of them prominent. Some PRGs are known to pulsate in both the fundamental and first-overtone modes. There may be some stars for which the derived period is actually an LSP, with the shorter pulsation period hidden in the noise. Some stars, especially the Lb stars, may be truly irregular.

A few of the Lb stars in Table 4 had only one or two cycles of V observations, so it was not possible to say whether they showed any strict periodicity. A few others had more V observations, but not enough to say whether they were multiperiodic or irregular. A few, such as OR Cep (Figure 2), RU Leo, and Z LMi, showed good phase curves, and may be SR. Some of the stars in Tables 1–4 may, of course, have been misclassified as to variable star type because of limited observations.

5. Conclusions

Of the 156 stars that were examined, less than half yielded any useful information, that being an average period and amplitude. In many cases, that information was uncertain. It is noteworthy, however, that about a third of the Lb (irregular) variables showed some periodicity.

It is not clear that continued *sparse* observation of the stars in this study will yield better results. And there are many more PRGs in the AAVSO observing program with *less* than 150 observations in total, and which were therefore not included in the present study. AAVSO might wish to think seriously about how to manage these PRGs in its observing program. If it is decided that these stars should continue to be observed, then it might be best if observers "adopted" stars for a year or two (or three), to ensure that they were observed sufficiently regularly.

Another important development is the ASAS-SN (All-Sky Automated Survey for Supernovae) project, based at Ohio State University. In the near future, it will have pre-computed light curves for all the stars in the VSX catalog at https://asas-sn.osu.edu/variables.

Thus, the management of the AAVSO observing programs will have to be done in the context of ASAS-SN and other large all-sky surveys.

6. Acknowledgements

I thank the AAVSO observers who made the observations on which this project is based, the AAVSO staff who archived them and made them publicly available, and the developers of the VSTAR package which was used in the analysis. Special thanks to Elizabeth Waagen. I thank Professor Christopher Kochanek for helpful information about ASAS-SN. This project made use of the SIMBAD database, maintained in Strasbourg, France. The Dunlap Institute is funded through an endowment established by the David Dunlap family, and the University of Toronto.

References

Benn, D. 2013, VSTAR data analysis software (http://www.aavso.org/vstar-overview).

Kafka, S. 2018, variable star observations from the AAVSO International Database: (https://www.aavso.org/aavso-international-database).

Pearce, A. 2018, *AAVSO Newsletter*, No. 75 (January), 15.

Percy, J. R., and Kojar, T. 2013, *J. Amer. Assoc. Var. Star Obs.*, **41**, 15.

Percy, J. R., and Long, J. 2010, *J. Amer. Assoc. Var. Star Obs.*, **38**, 161.

Percy, J. R., and Tan, P. J. 2013, *J. Amer. Assoc. Var. Star Obs.*, **41**, 1.

Percy, J. R., and Terziev, E. 2011, *J. Amer. Assoc. Var. Star Obs.*, **39**, 1.

Pojmański, G. 1997, *Acta Astron.*, **47**, 467.

Samus, N. N., *et al.* 2017, *General Catalogue of Variable Stars*, Sternberg Astronomical Institute, Moscow (GCVS database: http://www.sai.msu.ru/gcvs/gcvs/index.htm).

Smith, B. J., Leisawitz, D., Castelaz, M. W., and Luttermoser, D. 2002, *Astron. J.*, **123**, 948.

Templeton, M. R., Mattei, J. A., and Willson, L. A. 2005, *Astron. J.*, **130**, 776.

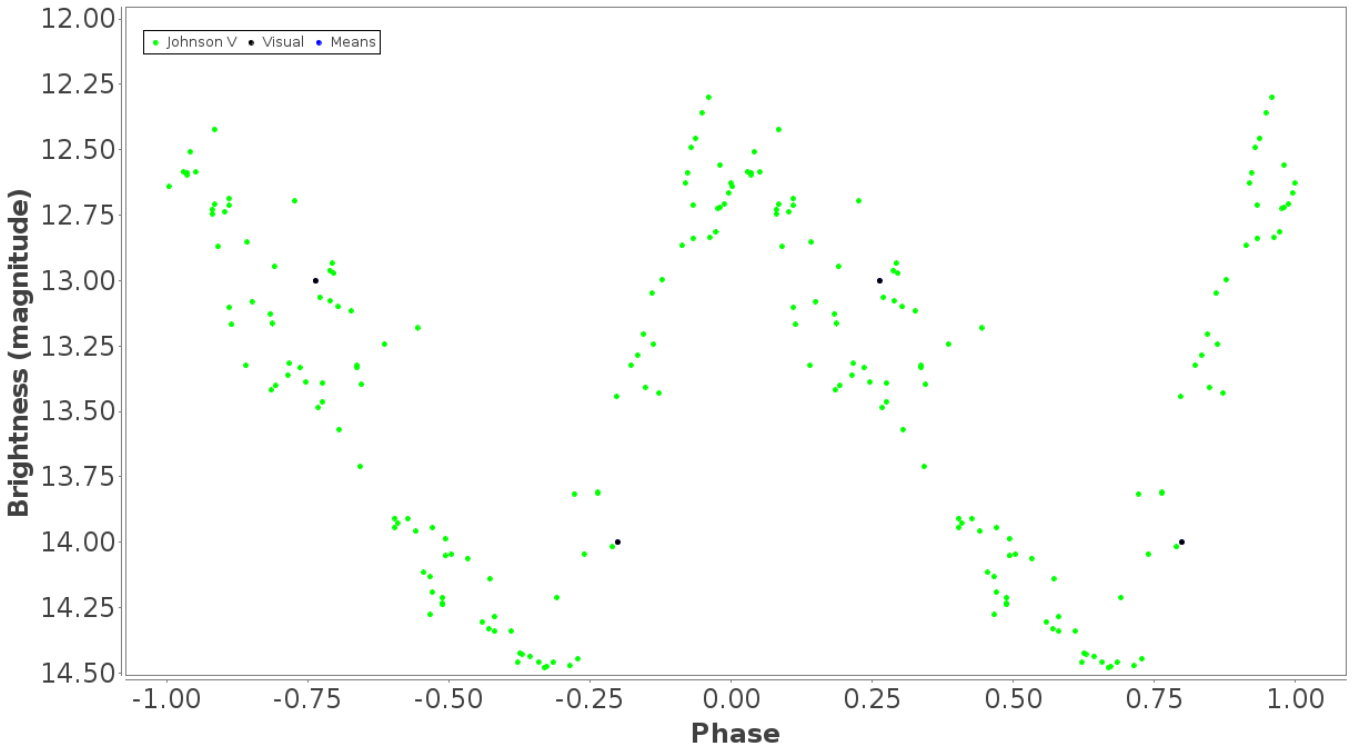

Figure 1. Phase plot for EQ And, 13 Jun 2018 (database). EQ And is classified as SR. The phase diagram using mostly Johnson V observations (green), a period of 270.48 days, and epoch 2454781.925, shown here, is quite satisfactory. The period in VSX, 211: days, does not produce a good phase diagram.

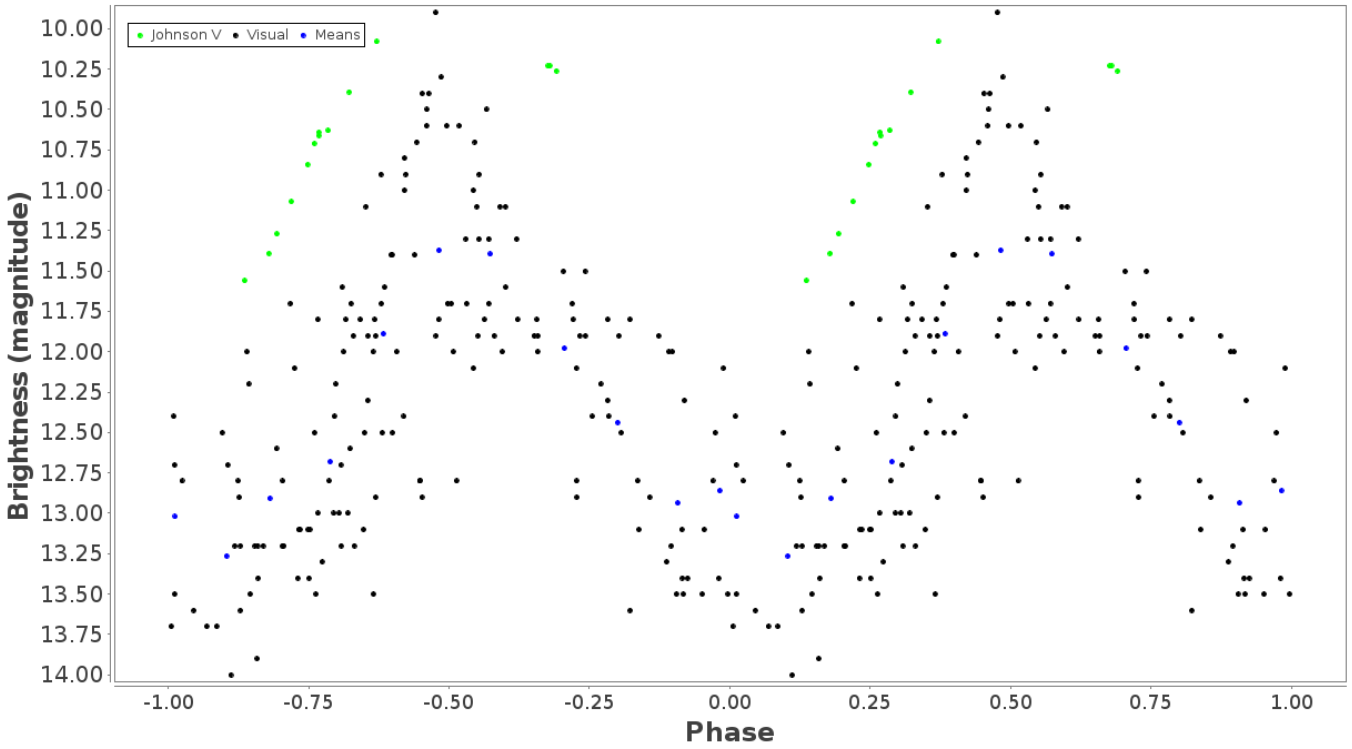

Figure 2. Phase plot for OR Cep, 13 Jun 2018 (database). OR Cep is classified as Lb (irregular). The phase diagram using mostly visual (black) and a few Johnson V (green) observations, a period of 348.5 days, and an epoch of 2454651.51, shown here, is quite satisfactory.

Table 1. Variability Properties of Some SRa Stars.

Star	*PVSX (days)*	*P (days)*	*Amp (mag)*	*Notes*
UV Aql	385.5	350 ± 30	0.17v	many peaks
LQ Ara	183.7	179.73	0.34v	1:
FX Cas	289	292.4	1.44v	data consistent with PVSX
V533 Cas	305	303.67	1.04v	1
V864 Cas	—	344	1.00V	P (vis) = 368 days
AL Cen	125	128.7	0.69v	1, ASAS P = 126.64 days
V343 Cep	525	482.9	0.93v	1
UZ Cet	121.74	203.34	0.14V	*; 1, multiperiodic?
V577 Cyg	479	478.5	0.32v	1, P (V) = 460.8 days
V659 Cyg	514	509.68	0.73v	1
V1059 Cyg	372	380 ± 10	0.18v	poor phase curve; period spurious?
AY Her	129.75	127.58	1.05v	2
IV Peg	214.0	213.8	0.95v	1, ASAS P = 210.387 days
TW Ret	217.6	225.99	—	*, 2, RVT according to SIMBAD
VV Tel	138.8	137.6	0.70V	1
UZ Vel	354	390.6	0.16v	1:, ASAS P = 353 days
NSVS J0712062+293744	106.2	106.64	0.43v	3

Table 2. Variability Properties of Some SRb Stars.

Star	*PVSX (days)*	*P (days)*	*Amp (mag)*	*Notes*
W Ara	122	119.6	0.14v	1, ASAS P = 121.8 days
V505 Car	26.5	20.266	0.02V	and/or 26.408 days
V481 Cas	158.4	159	0.07V	
R Cir	222	366.3?	0.24v	1, 3, ASAS P = 220 days
RU Crt	60.85	700:	0.39v	broad peak in Fourier spectrum
AQ Del	71.9	71.6	0.16v	1, ASAS P = 73.61 days
VY Eri	102.5	189:	0.23v	*; 1, ASAS P = 191 days, one cycle in V
V521 Ori	221	225.17	0.36V	1
X Pav	199.19	400.3	0.33v	1
V443 Per	69.5	69.9	0.17V	3, LSP ~ 400 days
RW Psc	154	154.2	0.15v	2
Z Ser	88.2	88.3	0.18v	P (ASAS) = 89.379 days
BN Ser	140.7	same	0.17V	*; ASAS P = 144.131 days
GK Vel	120:	182:	0.08v?	1, several peaks including 123.7 days

Table 3. Variability Properties of Some SR Stars.

Star	*PVSX (days)*	*P (days)*	*Amp (mag)*	*Notes*
EQ And	211:	273.6	0.82v	1; see Figure 1
KQ Aql	164.2	417	0.50v	2, PVSX gives good phase curve
V925 Aql	—	398.8	0.18v:	poor phase curve
SZ Ara	221.8	219.8	0.77v	1
UW Cam	544	523.3	0.33v	variable amplitude
AM Car	314	408	0.45v	1; also 50-day cycles
RU CrB	436	427	0.2V	*; 2, 436 days may be an LSP
V1673 Cyg	115.5	116.5	0.15v	
AE Del	260	152.5	0.67v	PVSX is an alias
V529 Her	400	197.3	0.10v	2
TZ Hor	???	35.52	0.02V	*; also 23.41 days
Y Mic	364:	180 ± 2	0.18v	4
V360 Peg	44.9	45.28	0.09V	*; 1, RV Tau evidence weak
V Pic	180	173.3	0.62v	1
SW Pic	—	25.2 ± 0.1	0.026V	*
γ Ret	25	29.87	0.034V	
DR Tuc	—	23.59	0.028V	*Hipparcos* P = 23.87 days
o Vir	—	30.50	0.036V	
NSV11453	153	296.47	0.85v	1
OGLE-BLG-LPV-062772	78.09	same	0.21V	2

Table 4. Variability Properties of Some Lb Stars.

Star	*P (days)*	*Amp (mag)*	*Notes*
KR Cep	50	0.13V	one cycle in V
KT Cep	77	0.16V	two cycles in V
KW Cep	170 ± 10	0.15v	*; complex; cycles 150 days long
OR Cep	348.5	0.97v	good phase curve; Figure 2
DV Lac	170 ± 10	0.27V	*; irregular; result uncertain
PY Lac	95	0.19V	one cycle in V; also short-period variability?
RU Leo	161	0.38V	good phase curve
VX Leo	95.6	0.16V	good phase curve, but complex, multiperiodic?
CP Leo	190:	0.07V	poor phase curve; complex, multiperiodic?
GK Leo	345 ± 5	0.16V	
Z LMi	161:	0.31V	good phase curve
RS LMi	90:	0.13V	*; poor phase curve; complex
CX Mon	385	0.35v	fair phase curve
WW Psc	25 ±	0.03V	
FL Ser	390 ± 2	0.16v	fair phase curve
TT UMa	490 ± 10	0.1v	fair phase curve
NSV 623	74 ± 2	0.25v	uncertain; $\Delta V = 0.50$

Recent Maxima of 86 Short Period Pulsating Stars

Gerard Samolyk
P.O. Box 20677, Greenfield, WI 53220; gsamolyk@wi.rr.com

Received January 16, 2018; accepted January 16, 2018

Abstract This paper contains times of maxima for 86 short period pulsating stars (primarily RR Lyrae and δ Scuti stars). This represents the CCD observations received by the AAVSO Short Period Pulsator (SPP) Section in 2017.

1. Recent observations

Table 1 contains times of maxima calculated from CCD observations made by participants in the AAVSO's Short Period Pulsator (SPP) Section. The data in this table will be web-archived and made available through the AAVSO ftp site at ftp://ftp.aavso.org/public/datasets/gsamo-461-spp86.txt. The error estimate is included. RR Lyr stars in this table, along with data from earlier AAVSO publications, are included in the GEOS database at: http://rr-lyr.irap.omp.eu/dbrr/. This database does not include δ Scuti stars. These observations were reduced by the writer using the PERANSO program (Vanmunster 2007). Column F indicates the filter used. A "C" indicates a clear filter.

The linear elements in the *General Catalogue of Variable Stars* (GCVS; Kholopov *et al.* 1985) were used to compute the O–C values for most stars. For a few exceptions where the GCVS elements are missing or are in significant error, light elements from another source are used: VY CrB (Antipin 1996); RZ Cap and DG Hya (Samolyk 2010); AM CMi, V1124 Her, and FR Psc (GEOS Database); VY LMi (Henden and Vidal-Sainz 1997); and GW UMa (Hintz *et al.* 2005).

For two δ Sct stars in the table, no published light elements were found. The following light elements were calculated using a linear regression on the times of maxima listed in this paper.

V521 And Time of maximum (JD) = 2454380.625 + 0.100960755 E (1)
±0.002 0.000000056

V2416 Cyg Time of maximum (JD) = 2453612.601 + 0.055889672 E (2)
±0.001 0.000000017

References

Antipin S. V. 1996, *Inf. Bull. Var. Stars*, No. 4343, 1.

Henden, A. A., and Vidal-Sainz, J. 1997, *Inf. Bull. Var. Stars*, No. 4535, 1.

Hintz , E. G., Bush , T. C., and Rose , M. B. 2005, *Astron. J.*, **130**, 2876.

Kholopov, P. N., *et al.* 1985, *General Catalogue of Variable Stars*, 4th ed., Moscow.

Samolyk, G. 2010, *J. Amer. Assoc. Var. Stars*, **38**, 12.

Vanmunster, T. 2007, PERANSO period analysis software (http://www.peranso.com).

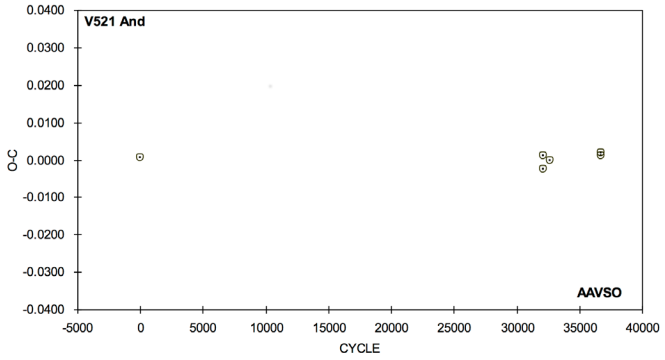

Figure 1. O–C diagram for V521 And plotted using Equation 1.

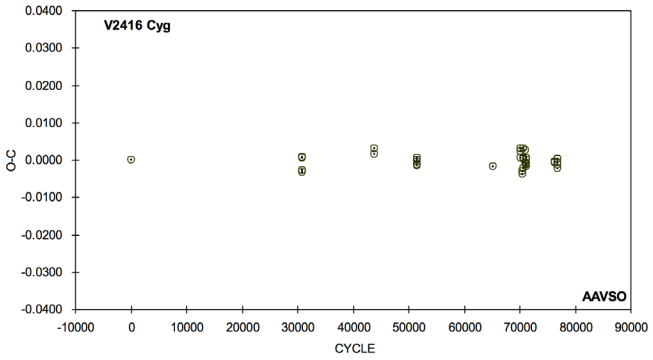

Figure 2. O–C diagram for V2416 Cyg plotted using Equation 2.

Table 1. Recent times of maxima of stars in the AAVSO Short Period Pulsator program.

Star	*JD (max) Hel. 2400000 +*	*Cycle*	*O–C*	*F*	*Observer*	*Error*
SW And	57947.6347	90023	–0.4801	V	T. Arranz	0.0006
SW And	57951.6146	90032	–0.4807	V	T. Arranz	0.0006
SW And	57970.6318	90075	–0.4815	V	T. Arranz	0.0005
SW And	57985.6688	90109	–0.4820	V	T. Arranz	0.0007
SW And	57986.5548	90111	–0.4806	V	T. Arranz	0.0007
SW And	57989.6497	90118	–0.4816	V	T. Arranz	0.0007
SW And	58009.5511	90163	–0.4828	V	T. Arranz	0.0006
SW And	58016.6275	90179	–0.4829	V	T. Arranz	0.0006
SW And	58017.5120	90181	–0.4829	V	T. Arranz	0.0006
SW And	58024.5883	90197	–0.4831	V	T. Arranz	0.0007
SW And	58025.4718	90199	–0.4842	V	T. Arranz	0.0006
SW And	58032.5488	90215	–0.4836	V	T. Arranz	0.0007
SW And	58035.6446	90222	–0.4838	V	T. Arranz	0.0006
SW And	58036.5290	90224	–0.4839	V	T. Arranz	0.0007
SW And	58039.6254	90231	–0.4835	V	T. Arranz	0.0008
SW And	58048.4704	90251	–0.4841	V	T. Arranz	0.0006
SW And	58051.5664	90258	–0.4840	V	T. Arranz	0.0007
SW And	58060.8533	90279	–0.4850	V	T. Polakis	0.0011
SW And	58079.4284	90321	–0.4856	V	T. Arranz	0.0006
XX And	57952.8620	26102	0.2789	V	G. Samolyk	0.0016
XX And	57973.8209	26131	0.2781	V	G. Samolyk	0.0013
XX And	58007.7901	26178	0.2782	V	K. Menzies	0.0011
XX And	58013.5727	26186	0.2788	V	T. Arranz	0.0010
XX And	58031.6423	26211	0.2797	V	T. Arranz	0.0010
XX And	58052.6011	26240	0.2789	V	T. Arranz	0.0011
XX And	58071.3898	26266	0.2761	V	T. Arranz	0.0008
XX And	58096.6942	26301	0.2844	V	R. Sabo	0.0027
XX And	58115.4844	26327	0.2832	V	K. Menzies	0.0014
AC And	57990.5773	13343	0.3490	V	T. Arranz	0.0013
AC And	57998.4593	13354	0.4073	V	T. Arranz	0.0011
AC And	58000.5791	13357	0.3934	V	G. Samolyk	0.0019
AC And	58000.5822	13357	0.3965	V	T. Arranz	0.0018
AC And	58003.5963	13361	0.5657	V	T. Arranz	0.0021
AC And	58005.6968	13364	0.5324	V	G. Samolyk	0.0021
AC And	58008.3813	13368	0.3720	V	T. Arranz	0.0012
AC And	58010.5031	13371	0.3601	V	T. Arranz	0.0012
AC And	58012.6183	13374	0.3415	V	T. Arranz	0.0011
AC And	58022.5859	13388	0.3518	V	T. Arranz	0.0011
AC And	58026.8261	13394	0.3245	V	G. Samolyk	0.0015
AT And	57974.7996	25338	–0.0068	V	G. Samolyk	0.0019
AT And	57989.6040	25362	–0.0084	V	T. Arranz	0.0012
AT And	58031.5571	25430	–0.0055	V	T. Arranz	0.0014
AT And	58034.6461	25435	–0.0011	V	T. Arranz	0.0016
AT And	58039.5785	25443	–0.0040	V	T. Arranz	0.0016
AT And	58070.4189	25493	–0.0093	V	T. Arranz	0.0013
DY And	57917.9144	36223	–0.1720	V	T. Polakis	0.0017
GM And	57981.8191	45759	0.0469	V	R. Sabo	0.0011
GM And	58037.6543	45838	0.0482	V	R. Sabo	0.0029
GM And	58047.5467	45852	0.0460	V	K. Menzies	0.0016
V521 And	54380.6257	0	0.0007	V	G. Samolyk	0.0019
V521 And	57623.7886	32123	0.0013	V	G. Samolyk	0.0022
V521 And	57623.8858	32124	–0.0025	V	G. Samolyk	0.0025
V521 And	57676.5896	32646	–0.0002	V	G. Samolyk	0.0034
V521 And	58083.5637	36677	0.0011	V	N. Simmons	0.0034
V521 And	58083.6655	36678	0.0019	V	N. Simmons	0.0028
SW Aqr	57904.9420	71429	–0.0019	V	T. Polakis	0.0010
SW Aqr	57951.7912	71531	–0.0017	V	G. Samolyk	0.0009
SW Aqr	58024.3615	71689	–0.0013	V	T. Arranz	0.0007
SW Aqr	58030.3324	71702	–0.0013	V	T. Arranz	0.0008
SW Aqr	58032.6288	71707	–0.0014	V	T. Polakis	0.0009
SW Aqr	58042.7334	71729	–0.0015	V	T. Polakis	0.0005
SW Aqr	58064.3200	71776	–0.0021	V	T. Arranz	0.0006
TZ Aqr	57998.8126	35802	0.0143	V	G. Samolyk	0.0018
YZ Aqr	57978.8133	40973	0.0786	V	G. Samolyk	0.0012
YZ Aqr	58077.6067	41152	0.0762	V	G. Samolyk	0.0016
AA Aqr	58035.6229	61238	–0.1740	V	G. Samolyk	0.0012
BO Aqr	58026.6792	23638	0.2155	V	G. Samolyk	0.0015
BR Aqr	58052.7095	42369	–0.2197	V	G. Samolyk	0.0009
BR Aqr	58083.5497	42433	–0.2197	V	G. Samolyk	0.0009
CY Aqr	58005.7839	388237	0.0151	V	G. Samolyk	0.0004
CY Aqr	58005.8449	388238	0.0152	V	G. Samolyk	0.0004
CY Aqr	58005.9056	388239	0.0148	V	G. Samolyk	0.0002
CY Aqr	58019.3342	388459	0.0149	V	T. Arranz	0.0002
CY Aqr	58019.3952	388460	0.0149	V	T. Arranz	0.0003
CY Aqr	58025.3771	388558	0.0151	V	T. Arranz	0.0003
TZ Aur	57768.7653	96678	0.0145	V	G. Samolyk	0.0008
TZ Aur	58029.6224	97344	0.0163	V	T. Arranz	0.0006
TZ Aur	58038.6299	97367	0.0153	V	T. Arranz	0.0006
TZ Aur	58040.5892	97372	0.0162	V	T. Arranz	0.0007
TZ Aur	58068.7891	97444	0.0155	V	K. Menzies	0.0006
TZ Aur	58102.8660	97531	0.0167	V	R. Sabo	0.0007
BH Aur	57761.5641	32910	0.0068	V	G. Samolyk	0.0009
BH Aur	58030.6591	33500	0.0088	V	T. Arranz	0.0009
BH Aur	58042.5165	33526	0.0079	V	T. Arranz	0.0009
BH Aur	58042.9719	33527	0.0072	V	T. Polakis	0.0014
BH Aur	58044.7964	33531	0.0073	V	G. Samolyk	0.0011
BH Aur	58052.5492	33548	0.0066	V	T. Arranz	0.0009
BH Aur	58073.5312	33594	0.0085	V	T. Arranz	0.0008
BH Aur	58077.6342	33603	0.0067	V	T. Arranz	0.0007
RS Boo	57807.7658	42501	–0.0073	V	G. Samolyk	0.0008
RS Boo	57861.7289	42644	–0.0037	V	G. Samolyk	0.0013
RS Boo	57875.6893	42681	–0.0049	V	T. Polakis	0.0008
RS Boo	57877.5759	42686	–0.0049	V	K. Menzies	0.0007
RS Boo	57884.7415	42705	–0.0088	V	T. Polakis	0.0008
RS Boo	57885.8735	42708	–0.0088	V	T. Polakis	0.0009
RS Boo	57887.7598	42713	–0.0092	V	T. Polakis	0.0007
RS Boo	57912.6682	42779	–0.0052	V	G. Samolyk	0.0009
RS Boo	57936.8172	42843	–0.0059	V	T. Polakis	0.0009
ST Boo	57797.8214	62055	0.0868	V	G. Samolyk	0.0015
ST Boo	57883.6999	62193	0.0892	V	R. Sabo	0.0019
ST Boo	57891.7921	62206	0.0916	V	T. Polakis	0.0011
SW Boo	57798.8881	29653	0.4794	V	G. Samolyk	0.0011
SW Boo	57875.9209	29803	0.4829	V	T. Polakis	0.0017
SZ Boo	57803.8056	57694	0.0091	V	G. Samolyk	0.0002
SZ Boo	57828.9028	57742	0.0109	V	G. Samolyk	0.0013
SZ Boo	57873.8661	57828	0.0117	V	T. Polakis	0.0011
TV Boo	57796.8628	106179	0.1075	V	R. Sabo	0.0024
TV Boo	57877.8023	106438	0.0941	V	T. Polakis	0.0014
TV Boo	57879.7084	106444	0.1249	V	R. Sabo	0.0026
TW Boo	57857.7624	58178	–0.0929	V	G. Samolyk	0.0011
TW Boo	57889.6978	58238	–0.0939	V	T. Polakis	0.0009
UU Boo	57788.9034	47501	0.3127	V	G. Samolyk	0.0013
UU Boo	57874.8073	47689	0.3156	V	T. Polakis	0.0008
UU Boo	57881.6621	47704	0.3166	V	N. Simmons	0.0011
UY Boo	57815.9180	24552	0.8863	V	G. Samolyk	0.0009
UY Boo	57907.6819	24693	0.8822	V	N. Simmons	0.0010
YZ Boo	57905.7162	151398	0.1076	V	N. Simmons	0.0007
YZ Boo	57905.8203	151399	0.1076	V	N. Simmons	0.0009
UY Cam	57811.6478	83307	–0.0874	V	G. Samolyk	0.0039
UY Cam	58008.9899	84046	–0.0896	V	T. Polakis	0.0028
UY Cam	58012.9972	84061	–0.0879	V	T. Polakis	0.0024
UY Cam	58042.9035	84173	–0.0904	V	T. Polakis	0.0011
UY Cam	58083.7579	84326	–0.0935	V	G. Samolyk	0.0027
UY Cam	58107.7935	84416	–0.0917	V	G. Samolyk	0.0033
RW Cnc	57783.7399	33310	0.2272	V	G. Samolyk	0.0015
TT Cnc	57787.7912	31668	0.1086	V	G. Samolyk	0.0021
VZ Cnc	57798.5654	100363	0.0244	V	G. Samolyk	0.0011
VZ Cnc	57798.7318	100364	0.0124	V	G. Samolyk	0.0006
AM Cnc	58108.8382	3723	0.0020	V	K. Menzies	0.0021
SS CVn	57824.8045	38039	–0.3608	V	K. Menzies	0.0010
SS CVn	57877.8913	38150	–0.3898	V	T. Polakis	0.0013
SS CVn	57926.7242	38252	–0.3661	V	T. Polakis	0.0008

Table continued on following pages

Table 1. Recent times of maxima of stars in the AAVSO Short Period Pulsator program, cont.

Star	JD (max) Hel. 2400000 +	Cycle	O–C	F	Observer	Error
RV Cap	57949.8732	53751	–0.0771	V	G. Samolyk	0.0012
RZ Cap	57998.6419	16493	0.0024	V	G. Samolyk	0.0016
YZ Cap	58006.6684	52209	0.0474	V	G. Samolyk	0.0021
RR Cet	58006.8537	44890	0.0165	V	G. Samolyk	0.0013
RR Cet	58030.6334	44933	0.0160	V	T. Arranz	0.0011
RU Cet	58088.5851	31149	0.1384	V	G. Samolyk	0.0012
RV Cet	58065.7157	30401	0.2781	V	G. Samolyk	0.0027
RX Cet	58093.5888	31319	0.3363	V	G. Samolyk	0.0019
RZ Cet	58043.7499	47271	–0.2224	V	G. Samolyk	0.0017
UU Cet	57642.9041	27116	–0.1643	V	G. Samolyk	0.0021
UU Cet	58044.7245	27779	–0.1756	V	G. Samolyk	0.0019
VY CrB	57878.8188	34782	–0.1616	V	T. Polakis	0.0012
VY CrB	58011.6807	35069	–0.1683	V	T. Polakis	0.0008
VY CrB	58043.6258	35138	–0.1673	V	T. Polakis	0.0014
XX Cyg	57881.6259	99553	0.0048	V	G. Samolyk	0.0010
XX Cyg	57881.7591	99554	0.0031	V	G. Samolyk	0.0005
XX Cyg	57902.6644	99709	0.0043	V	G. Samolyk	0.0006
XX Cyg	57902.7988	99710	0.0039	V	G. Samolyk	0.0005
XX Cyg	57928.8273	99903	0.0034	V	T. Polakis	0.0005
XZ Cyg	57886.6916	29494	–2.5982	V	G. Samolyk	0.0008
XZ Cyg	57905.8261	29535	–2.5984	V	G. Samolyk	0.0014
XZ Cyg	57912.8201	29550	–2.6049	V	H. Smith	0.0008
XZ Cyg	57928.6800	29584	–2.6128	V	G. Samolyk	0.0007
XZ Cyg	57939.4160	29607	–2.6109	V	T. Arranz	0.0006
XZ Cyg	57942.6774	29614	–2.6164	V	G. Samolyk	0.0011
XZ Cyg	57943.6154	29616	–2.6118	V	T. Arranz	0.0011
XZ Cyg	57952.4836	29635	–2.6109	V	T. Arranz	0.0005
XZ Cyg	57957.6196	29646	–2.6086	V	T. Arranz	0.0007
XZ Cyg	57960.4175	29652	–2.6109	V	T. Arranz	0.0005
XZ Cyg	57963.6827	29659	–2.6126	V	G. Samolyk	0.0007
XZ Cyg	57964.6145	29661	–2.6142	V	T. Arranz	0.0006
XZ Cyg	57972.5466	29678	–2.6160	V	T. Arranz	0.0004
XZ Cyg	57973.4787	29680	–2.6173	V	T. Arranz	0.0004
XZ Cyg	57981.4055	29697	–2.6244	V	T. Arranz	0.0007
XZ Cyg	57987.4664	29710	–2.6306	V	T. Arranz	0.0007
XZ Cyg	57998.6730	29734	–2.6248	V	G. Samolyk	0.0012
XZ Cyg	58011.7408	29762	–2.6246	V	T. Polakis	0.0016
XZ Cyg	58022.4760	29785	–2.6235	V	T. Arranz	0.0005
XZ Cyg	58031.3353	29804	–2.6315	V	T. Arranz	0.0006
XZ Cyg	58037.3943	29817	–2.6396	V	T. Arranz	0.0006
XZ Cyg	58038.3276	29819	–2.6397	V	T. Arranz	0.0006
XZ Cyg	58052.3277	29849	–2.6406	V	T. Arranz	0.0007
XZ Cyg	58074.2637	29896	–2.6395	V	T. Arranz	0.0005
DM Cyg	57923.7617	36539	0.0912	V	G. Samolyk	0.0009
DM Cyg	57971.6214	36653	0.0868	V	T. Arranz	0.0008
DM Cyg	57977.5016	36667	0.0890	V	T. Arranz	0.0007
DM Cyg	57979.6004	36672	0.0885	V	T. Arranz	0.0007
DM Cyg	57983.3785	36681	0.0878	V	T. Arranz	0.0008
DM Cyg	57998.4955	36717	0.0899	V	T. Arranz	0.0008
DM Cyg	58001.4322	36724	0.0876	V	T. Arranz	0.0008
DM Cyg	58004.3694	36731	0.0857	V	T. Arranz	0.0008
DM Cyg	58009.4110	36743	0.0890	V	T. Arranz	0.0009
DM Cyg	58021.5852	36772	0.0873	V	K. Menzies	0.0008
DM Cyg	58028.7251	36789	0.0896	V	K. Menzies	0.0011
DM Cyg	58033.3416	36800	0.0876	V	T. Arranz	0.0008
V2416 Cyg	53612.6009	0	–0.0001	V	G. Samolyk	0.0021
V2416 Cyg	55341.6604	30937	0.0006	V	G. Samolyk	0.0019
V2416 Cyg	55341.7162	30938	0.0006	V	G. Samolyk	0.0018
V2416 Cyg	55341.7687	30939	–0.0029	V	G. Samolyk	0.0017
V2416 Cyg	55341.8240	30940	–0.0034	V	G. Samolyk	0.0019
V2416 Cyg	56064.8193	43876	0.0031	V	G. Samolyk	0.0015
V2416 Cyg	56064.8737	43877	0.0016	V	G. Samolyk	0.0023
V2416 Cyg	56493.6581	51549	0.0004	V	G. Samolyk	0.0021
V2416 Cyg	56493.7136	51550	0.0001	V	G. Samolyk	0.0019
V2416 Cyg	56493.7681	51551	–0.0014	V	G. Samolyk	0.0011
V2416 Cyg	56493.8250	51552	–0.0004	V	G. Samolyk	0.0015
V2416 Cyg	56493.8797	51553	–0.0016	V	G. Samolyk	0.0016
V2416 Cyg	57257.6119	65218	–0.0018	V	N. Simmons	0.0024
V2416 Cyg	57531.6437	70121	0.0030	V	G. Samolyk	0.0017
V2416 Cyg	57531.6989	70122	0.0023	V	G. Samolyk	0.0015
V2416 Cyg	57531.8649	70125	0.0006	V	G. Samolyk	0.0016
V2416 Cyg	57557.6255	70586	–0.0039	V	G. Samolyk	0.0015
V2416 Cyg	57557.6823	70587	–0.0030	V	G. Samolyk	0.0013
V2416 Cyg	57564.6693	70712	–0.0022	V	G. Samolyk	0.0016
V2416 Cyg	57564.7303	70713	0.0029	V	G. Samolyk	0.0017
V2416 Cyg	57564.7838	70714	0.0005	V	G. Samolyk	0.0015
V2416 Cyg	57564.8393	70715	0.0002	V	G. Samolyk	0.0021
V2416 Cyg	57579.6524	70980	0.0025	V	G. Samolyk	0.0017
V2416 Cyg	57579.7052	70981	–0.0007	V	G. Samolyk	0.0016
V2416 Cyg	57595.6349	71266	0.0005	V	G. Samolyk	0.0015
V2416 Cyg	57595.6893	71267	–0.0010	V	G. Samolyk	0.0014
V2416 Cyg	57595.7448	71268	–0.0014	V	G. Samolyk	0.0017
V2416 Cyg	57595.8003	71269	–0.0017	V	G. Samolyk	0.0009
V2416 Cyg	57595.8580	71270	0.0001	V	G. Samolyk	0.0016
V2416 Cyg	57881.6770	76384	–0.0007	V	G. Samolyk	0.0022
V2416 Cyg	57881.7330	76385	–0.0006	V	G. Samolyk	0.0018
V2416 Cyg	57902.6367	76759	0.0003	V	G. Samolyk	0.0021
V2416 Cyg	57902.6899	76760	–0.0023	V	G. Samolyk	0.0016
V2416 Cyg	57902.7468	76761	–0.0013	V	G. Samolyk	0.0014
V2416 Cyg	57902.8031	76762	–0.0009	V	G. Samolyk	0.0011
V2416 Cyg	57902.8601	76763	0.0002	V	G. Samolyk	0.0014
RW Dra	57811.8438	41620	0.2473	V	G. Samolyk	0.0011
RW Dra	57886.7176	41789	0.2681	V	T. Polakis	0.0011
RW Dra	57886.7187	41789	0.2692	V	G. Samolyk	0.0008
RW Dra	57889.8125	41796	0.2626	V	T. Polakis	0.0009
RW Dra	57970.4312	41978	0.2704	V	T. Arranz	0.0007
RW Dra	57978.3771	41996	0.2438	V	T. Arranz	0.0008
XZ Dra	57861.8290	33439	–0.1282	V	G. Samolyk	0.0009
XZ Dra	57925.6771	33573	–0.1307	V	G. Samolyk	0.0010
XZ Dra	57943.7924	33611	–0.1223	V	N. Simmons	0.0008
SV Eri	58107.7016	31598	1.0540	V	G. Samolyk	0.0021
RR Gem	57788.5870	41358	–0.5898	V	G. Samolyk	0.0008
RR Gem	58037.6740	41985	–0.6165	V	T. Arranz	0.0006
RR Gem	58053.5689	42025	–0.6141	V	T. Arranz	0.0007
RR Gem	58074.6214	42078	–0.6190	V	T. Arranz	0.0005
RR Gem	58104.8201	42154	–0.6159	V	R. Sabo	0.0008
RR Gem	58108.7881	42164	–0.6210	V	K. Menzies	0.0006
TW Her	57844.8896	90840	–0.0178	V	G. Samolyk	0.0008
TW Her	57848.8866	90850	–0.0168	V	R. Sabo	0.0009
TW Her	57926.8069	91045	–0.0186	V	T. Polakis	0.0006
TW Her	57998.7346	91225	–0.0189	V	R. Sabo	0.0009
TW Her	58000.3342	91229	–0.0177	V	T. Arranz	0.0006
TW Her	58004.3297	91239	–0.0182	V	T. Arranz	0.0005
VX Her	57877.8755	79336	–0.0652	V	R. Sabo	0.0013
VX Her	57910.6624	79408	–0.0652	V	G. Samolyk	0.0007
VX Her	58012.6612	79632	–0.0699	V	T. Polakis	0.0010
VZ Her	57876.7265	47891	0.0855	V	G. Samolyk	0.0008
VZ Her	57891.6963	47925	0.0842	V	T. Polakis	0.0007
VZ Her	57923.8413	47998	0.0852	V	R. Sabo	0.0007
AR Her	57824.8657	34831	–1.0266	V	G. Samolyk	0.0011
AR Her	57857.7566	34901	–1.0376	V	G. Samolyk	0.0018
AR Her	57866.6851	34920	–1.0397	V	G. Samolyk	0.0027
AR Her	57880.8140	34950	–1.0116	V	G. Samolyk	0.0010
AR Her	57906.6743	35005	–1.0028	V	G. Samolyk	0.0019
AR Her	57911.8367	35016	–1.0107	V	G. Samolyk	0.0009
AR Her	57928.7169	35052	–1.0516	V	G. Samolyk	0.0011
AR Her	57928.7177	35052	–1.0508	V	T. Polakis	0.0028
AR Her	57936.7525	35069	–1.0064	V	G. Samolyk	0.0010
AR Her	57952.6955	35103	–1.0444	V	G. Samolyk	0.0011
AR Her	57956.4385	35111	–1.0616	V	T. Arranz	0.0008
AR Her	57965.4164	35130	–1.0142	V	T. Arranz	0.0009
AR Her	57981.3771	35164	–1.0345	V	T. Arranz	0.0007

Table continued on next page

Table 1. Recent times of maxima of stars in the AAVSO Short Period Pulsator program, cont.

Star	*JD (max) Hel. 2400000 +*	*Cycle*	*O–C*	*F*	*Observer*	*Error*
AR Her	57999.7446	35203	–0.9981	V	R. Sabo	0.0021
DL Her	57884.8465	33258	0.0589	V	R. Sabo	0.0009
DL Her	57912.6546	33305	0.0605	V	G. Samolyk	0.0015
DL Her	57969.4360	33401	0.0456	V	T. Arranz	0.0014
DL Her	57985.4252	33428	0.0609	V	T. Arranz	0.0008
DL Her	57993.6995	33442	0.0524	V	R. Sabo	0.0013
DL Her	58001.3826	33455	0.0443	V	T. Arranz	0.0015
DY Her	57881.7312	164449	–0.0327	V	G. Samolyk	0.0006
DY Her	57883.8124	164463	–0.0323	V	R. Sabo	0.0009
DY Her	57883.9597	164464	–0.0336	V	R. Sabo	0.0010
DY Her	57886.7850	164483	–0.0323	V	T. Polakis	0.0005
DY Her	57912.6469	164657	–0.0323	V	G. Samolyk	0.0008
DY Her	57912.7957	164658	–0.0321	V	G. Samolyk	0.0007
DY Her	57926.7663	164752	–0.0329	V	R. Sabo	0.0008
DY Her	57983.3957	165133	–0.0320	V	T. Arranz	0.0006
LS Her	57877.7286	129427	0.0321	V	T. Polakis	0.0017
LS Her	57916.7204	129596	0.0174	V	G. Samolyk	0.0016
V365 Her	57873.8253	47031	–0.1060	V	T. Polakis	0.0017
V1124 Her	57875.8228	11269	0.0512	V	T. Polakis	0.0012
SZ Hya	57783.8092	31838	–0.2569	V	G. Samolyk	0.0009
SZ Hya	57860.6298	31981	–0.2617	V	G. Samolyk	0.0013
UU Hya	57781.8625	34938	0.0053	V	G. Samolyk	0.0013
DG Hya	57815.6930	7214	0.0212	V	G. Samolyk	0.0013
DH Hya	57802.7900	54451	0.1050	V	G. Samolyk	0.0011
XZ Lac	57878.8780	31720	0.3940	V	T. Polakis	0.0015
XZ Lac	57936.9392	31812	0.4768	V	T. Polakis	0.0014
RR Leo	57755.8614	31964	0.1600	V	K. Menzies	0.0006
RR Leo	58101.9499	32729	0.1676	V	G. Samolyk	0.0007
RR Leo	58116.8798	32762	0.1685	V	K. Menzies	0.0008
SS Leo	57786.9014	25554	–0.1047	V	G. Samolyk	0.0018
ST Leo	57781.8214	62468	–0.0199	V	G. Samolyk	0.0009
TV Leo	57786.9103	30832	0.1289	V	G. Samolyk	0.0017
WW Leo	57811.6636	38035	0.0498	V	G. Samolyk	0.0013
WW Leo	58079.9342	38480	0.0542	V	G. Samolyk	0.0024
AA Leo	57787.8987	30387	–0.1071	V	K. Menzies	0.0009
VY LMi	57772.0176	13845	0.0193	V	R. Sabo	0.0012
VY LMi	57817.7928	13932	0.0197	V	K. Menzies	0.0015
VY LMi	57836.7392	13968	0.0248	V	R. Sabo	0.0011
SZ Lyn	57768.8532	162977	0.0353	V	G. Samolyk	0.0008
SZ Lyn	57768.9751	162978	0.0367	V	G. Samolyk	0.0008
SZ Lyn	57787.7784	163134	0.0365	V	K. Menzies	0.0011
SZ Lyn	57803.6864	163266	0.0339	V	N. Simmons	0.0005
SZ Lyn	57844.6678	163606	0.0334	V	G. Samolyk	0.0006
SZ Lyn	58011.9660	164994	0.0292	V	T. Polakis	0.0008
SZ Lyn	58035.8330	165192	0.0303	V	G. Samolyk	0.0008
SZ Lyn	58035.9539	165193	0.0306	V	G. Samolyk	0.0008
SZ Lyn	58061.0229	165401	0.0284	V	T. Polakis	0.0006
SZ Lyn	58079.7062	165556	0.0287	V	N. Simmons	0.0006
SZ Lyn	58079.8272	165557	0.0292	V	N. Simmons	0.0006
SZ Lyn	58079.9474	165558	0.0289	V	N. Simmons	0.0005
SZ Lyn	58079.9478	165558	0.0293	V	G. Samolyk	0.0006
SZ Lyn	58090.6754	165647	0.0293	V	G. Samolyk	0.0007
SZ Lyn	58090.7951	165648	0.0284	V	G. Samolyk	0.0011
SZ Lyn	58090.9163	165649	0.0291	V	G. Samolyk	0.0009
SZ Lyn	58102.9686	165749	0.0279	V	K. Menzies	0.0009
RR Lyr	57909.8036	26438	–0.4655	V	G. Samolyk	0.0016
RR Lyr	57951.7430	26512	–0.4744	V	N. Simmons	0.0016
RR Lyr	57959.6762	26526	–0.4773	V	G. Samolyk	0.0009
RZ Lyr	57876.9569	32653	–0.0639	V	T. Polakis	0.0008
RZ Lyr	57936.7800	32770	–0.0562	V	N. Simmons	0.0010
RZ Lyr	58024.7158	32942	–0.0540	V	R. Sabo	0.0011
CX Lyr	57921.7122	40300	1.5557	V	T. Polakis	0.0038
CX Lyr	58032.7404	40480	1.5878	V	T. Polakis	0.0010
CX Lyr	58068.4803	40538	1.5623	V	K. Menzies	0.0020
MW Lyr	57936.7174	55035	–0.4029	V	T. Polakis	0.0010
V340 Lyr	57919.8645	47931	–0.0210	V	T. Polakis	0.0039
ST Oph	57882.8607	65407	–0.0270	V	R. Sabo	0.0011
AV Peg	57754.5856	35771	0.1762	V	R. Sabo	0.0009
AV Peg	57990.3788	36375	0.1831	V	T. Arranz	0.0007
AV Peg	58056.3534	36544	0.1844	V	T. Arranz	0.0007
BH Peg	57928.9370	28961	–0.1413	V	T. Polakis	0.0024
BH Peg	58012.9133	29092	–0.1351	V	T. Polakis	0.0016
DY Peg	58005.5959	185167	–0.0182	V	G. Samolyk	0.0006
DY Peg	58005.6693	185168	–0.0177	V	G. Samolyk	0.0005
DY Peg	58005.7424	185169	–0.0175	V	G. Samolyk	0.0005
DY Peg	58005.8149	185170	–0.0179	V	G. Samolyk	0.0006
DY Peg	58005.8881	185171	–0.0177	V	G. Samolyk	0.0007
GV Peg	56183.6504	19872	0.2126	V	K. Menzies	0.0011
GV Peg	56260.6466	20008	0.1072	V	K. Menzies	0.0012
FR Psc	58012.7628	9439	0.0105	V	T. Polakis	0.0007
FR Psc	58043.7177	9507	–0.0211	V	T. Polakis	0.0013
FR Psc	58095.6649	9621	–0.0219	V	R. Sabo	0.0017
DF Ser	57863.8268	64317	0.1041	V	R. Sabo	0.0008
DF Ser	57877.8311	64349	0.0989	V	K. Menzies	0.0009
DF Ser	57878.7102	64351	0.1024	V	T. Polakis	0.0008
DF Ser	57909.7954	64422	0.1042	V	G. Samolyk	0.0011
DF Ser	57938.6889	64488	0.1032	V	G. Samolyk	0.0011
RV UMa	57761.9372	27104	0.1280	V	G. Samolyk	0.0009
RV UMa	57858.8259	27311	0.1282	V	K. Menzies	0.0008
RV UMa	57904.7015	27409	0.1340	V	T. Polakis	0.0009
RV UMa	58083.9696	27792	0.1351	V	G. Samolyk	0.0009
AE UMa	57754.6806	257511	0.0047	V	G. Samolyk	0.0008
AE UMa	57754.7623	257512	0.0004	V	G. Samolyk	0.0007
AE UMa	57754.8453	257513	–0.0026	V	G. Samolyk	0.0006
AE UMa	57754.9361	257514	0.0022	V	G. Samolyk	0.0009
AE UMa	57755.0237	257515	0.0038	V	G. Samolyk	0.0011
AE UMa	57759.7519	257570	0.0010	V	G. Samolyk	0.0006
AE UMa	57759.8336	257571	–0.0033	V	G. Samolyk	0.0015
AE UMa	57759.9251	257572	0.0022	V	G. Samolyk	0.0009
AE UMa	57760.0123	257573	0.0034	V	G. Samolyk	0.0007
AE UMa	57760.6137	257580	0.0027	V	G. Samolyk	0.0005
AE UMa	57760.6953	257581	–0.0017	V	G. Samolyk	0.0005
AE UMa	57760.7835	257582	0.0004	V	G. Samolyk	0.0008
AE UMa	57760.8729	257583	0.0038	V	G. Samolyk	0.0007
AE UMa	57760.9544	257584	–0.0007	V	G. Samolyk	0.0005
AE UMa	57761.7332	257593	0.0040	V	G. Samolyk	0.0008
AE UMa	57761.8163	257594	0.0010	V	G. Samolyk	0.0005
AE UMa	57761.8992	257595	–0.0021	V	G. Samolyk	0.0005
AE UMa	57761.9899	257596	0.0026	V	G. Samolyk	0.0007
GW UMa	57802.7358	28558	0.0020	V	G. Samolyk	0.0012
GW UMa	57802.9381	28559	0.0011	V	G. Samolyk	0.0009

Visual Times of Maxima for Short Period Pulsating Stars III

Gerard Samolyk
P.O. Box 20677, Greenfield, WI 53220; gsamolyk@wi.rr.com

Received January 25, 2018; accepted January 25, 2018

Abstract This compilation contains 524 times of maxima of 9 short period pulsating stars (primarily RR Lyrae stars; RW Cnc, TT Cnc, VZ Cnc, RR Cet, XZ Cyg, DM Cyg, RW Dra, XZ Dra, RR Gem). These were reduced from a portion of the visual observations made from 1966 to 2014 that are included in the AAVSO International Database.

1. Observations

This paper is the third in a series to publish of times of maxima derived from visual observations reported to the AAVSO International Database as part of the AAVSO RR Lyr Committee legacy program. The goal of this project is to fill some historical gaps in the O–C history for these stars. This list contains times of maxima for RR Lyr stars located in the constellations Cancer, Cetus, Cygnus, Draco, and Gemini (RW Cnc, TT Cnc, VZ Cnc, RR Cet, XZ Cyg, DM Cyg, RW Dra, XZ Dra, RR Gem). This list will be web-archived and made available through the AAVSO ftp site at ftp://ftp.aavso.org/public/datasets/gsamj461vismax3.txt.

These observations were reduced by the writer using the PERANSO program (Vanmunster 2007). The linear elements in the *General Catalogue of Variable Stars* (Kholopov et al. 1985) were used to compute the O–C values for all stars listed.

Figures 1, and 2 are O–C plots for two of the stars listed.

References

Kholopov, P. N., et al. 1985, *General Catalogue of Variable Stars*, 4th ed., Moscow.
Samolyk, G. 2010, *J. Amer. Assoc. Var. Star Obs.,* **38**, 12.
Samolyk, G. 2011, *J. Amer. Assoc. Var. Star Obs.,* **39**, 23.
Samolyk, G. 2012, *J. Amer. Assoc. Var. Star Obs.,* **40**, 923.
Samolyk, G. 2013, *J. Amer. Assoc. Var. Star Obs.,* **41**, 85.
Samolyk, G. 2014, *J. Amer. Assoc. Var. Star Obs.,* **42**, 124.
Samolyk, G. 2015, *J. Amer. Assoc. Var. Star Obs.,* **43**, 74.
Samolyk, G. 2016, *J. Amer. Assoc. Var. Star Obs.,* **44**, 66.
Vanmunster, T. 2007, PERANSO period analysis software (http://www.peranso.com).

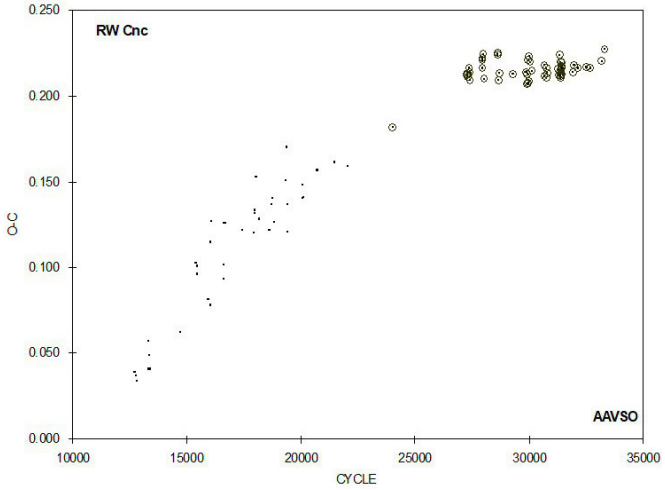

Figure 1. O–C plot for RW Cnc. The circled times of maxima are from CCD papers published in *JAAVSO* (Samolyk 2010–2016).

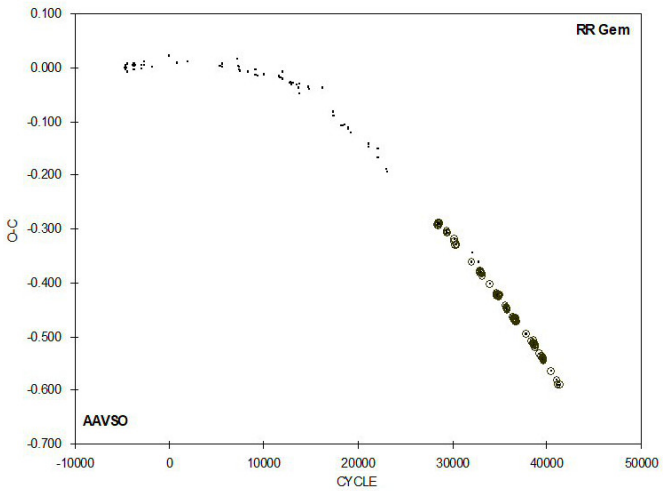

Figure 1. O–C plot for RR Gem. The circled times of maxima are from CCD papers published in *JAAVSO* (Samolyk 2010–2016).

Table 1. Recent times of minima of stars in the AAVSO short period pulsator program.

Star	*JD (max) Hel. 2400000 +*	*Cycle*	*O–C (day)*	*Observer*	*Error (day)*	*Star*	*JD (max) Hel. 2400000 +*	*Cycle*	*O–C (day)*	*Observer*	*Error (day)*
RW Cnc	46527.668	12740	0.039	M. Baldwin	0.008	TT Cnc	43219.685	5813	-0.013	M. Baldwin	0.006
RW Cnc	46550.649	12782	0.037	M. Baldwin	0.007	TT Cnc	43223.649	5820	0.006	M. Baldwin	0.009
RW Cnc	46556.665	12793	0.034	M. Baldwin	0.006	TT Cnc	43227.590	5827	0.003	M. Baldwin	0.005
RW Cnc	46829.724	13292	0.041	M. Baldwin	0.006	TT Cnc	43228.715	5829	0.001	M. Baldwin	0.005
RW Cnc	46845.609	13321	0.057	M. Baldwin	0.005	TT Cnc	43241.674	5852	0.001	M. Baldwin	0.004
RW Cnc	46858.734	13345	0.049	M. Baldwin	0.006	TT Cnc	43960.622	7128	-0.012	M. Baldwin	0.008
RW Cnc	46887.727	13398	0.041	P. Atwood	0.008	TT Cnc	44227.699	7602	-0.010	M. Baldwin	0.005
RW Cnc	47617.712	14732	0.062	R. Hill	0.012	TT Cnc	44316.728	7760	-0.006	M. Heifner	0.004
RW Cnc	47976.715	15388	0.102	M. Baldwin	0.008	TT Cnc	45026.680	9020	-0.001	M. Heifner	0.006
RW Cnc	47999.691	15430	0.096	M. Baldwin	0.009	TT Cnc	45052.585	9066	-0.014	G. Chaple	0.003
RW Cnc	48005.715	15441	0.101	M. Baldwin	0.005	TT Cnc	45079.639	9114	-0.006	G. Chaple	0.004
RW Cnc	48284.767	15951	0.082	R. Hill	0.006	TT Cnc	46150.755	11015	-0.007	M. Baldwin	0.005
RW Cnc	48318.690	16013	0.078	R. Hill	0.007	TT Cnc	46518.728	11668	0.033	M. Baldwin	0.006
RW Cnc	48335.689	16044	0.115	M. Baldwin	0.009	TT Cnc	46527.740	11684	0.030	M. Baldwin	0.008
RW Cnc	48353.759	16077	0.127	M. Baldwin	0.008	TT Cnc	46531.659	11691	0.005	M. Heifner	0.004
RW Cnc	48644.836	16609	0.093	R. Hill	0.006	TT Cnc	46531.688	11691	0.034	M. Baldwin	0.005
RW Cnc	48648.674	16616	0.102	M. Baldwin	0.003	TT Cnc	46544.616	11714	0.003	M. Baldwin	0.008
RW Cnc	48655.812	16629	0.126	M. Baldwin	0.007	TT Cnc	46553.641	11730	0.013	M. Baldwin	0.009
RW Cnc	48683.719	16680	0.126	M. Baldwin	0.008	TT Cnc	46793.692	12156	0.034	M. Baldwin	0.006
RW Cnc	49095.756	17433	0.122	M. Baldwin	0.004	TT Cnc	46833.679	12227	0.016	M. Baldwin	0.006
RW Cnc	49374.826	17943	0.120	R. Hill	0.009	TT Cnc	46850.566	12257	0.000	M. Baldwin	0.006
RW Cnc	49397.820	17985	0.132	M. Baldwin	0.006	TT Cnc	46877.647	12305	0.035	M. Baldwin	0.007
RW Cnc	49401.652	17992	0.133	M. Baldwin	0.006	TT Cnc	47232.614	12935	0.029	M. Baldwin	0.007
RW Cnc	49430.673	18045	0.153	M. Baldwin	0.005	TT Cnc	47241.637	12951	0.037	M. Baldwin	0.004
RW Cnc	49488.651	18151	0.128	M. Baldwin	0.006	TT Cnc	47268.654	12999	0.008	M. Baldwin	0.006
RW Cnc	49749.659	18628	0.122	M. Baldwin	0.006	TT Cnc	47596.618	13581	0.045	M. Baldwin	0.006
RW Cnc	49801.658	18723	0.137	M. Baldwin	0.003	TT Cnc	47921.728	14158	0.044	M. Baldwin	0.009
RW Cnc	49813.700	18745	0.140	M. Baldwin	0.006	TT Cnc	47942.570	14195	0.039	M. Baldwin	0.005
RW Cnc	49859.651	18829	0.127	M. Baldwin	0.003	TT Cnc	47978.613	14259	0.021	M. Baldwin	0.007
RW Cnc	50138.747	19339	0.151	M. Baldwin	0.007	TT Cnc	48658.739	15466	0.064	M. Baldwin	0.008
RW Cnc	50154.635	19368	0.170	M. Baldwin	0.008	TT Cnc	48675.624	15496	0.045	M. Baldwin	0.006
RW Cnc	50185.775	19425	0.121	R. Hill	0.005	TT Cnc	49843.660	17569	0.050	M. Baldwin	0.006
RW Cnc	50190.716	19434	0.137	M. Baldwin	0.003	TT Cnc	50842.637	19342	0.032	M. Baldwin	0.006
RW Cnc	50539.840	20072	0.148	M. Baldwin	0.006	TT Cnc	50896.773	19438	0.077	R. Hill	0.006
RW Cnc	50543.663	20079	0.140	G. Chaple	0.005	TT Cnc	51606.723	20698	0.080	R. Hill	0.003
RW Cnc	50573.760	20134	0.141	M. Baldwin	0.006	VZ Cnc	51212.646	63439	0.006	R. Berg	0.006
RW Cnc	50902.642	20735	0.157	M. Baldwin	0.003	VZ Cnc	51214.596	63450	-0.006	R. Berg	0.007
RW Cnc	51308.668	21477	0.161	M. Baldwin	0.003	VZ Cnc	51224.768	63507	0.000	R. Berg	0.005
RW Cnc	51633.702	22071	0.159	R. Berg	0.007	VZ Cnc	51253.646	63669	-0.017	R. Berg	0.008
TT Cnc	39139.763	-1428	0.002	M. Baldwin	0.007	VZ Cnc	51257.604	63691	0.017	R. Berg	0.009
TT Cnc	39140.902	-1426	0.014	M. Baldwin	0.010	VZ Cnc	51261.672	63714	-0.018	R. Berg	0.009
TT Cnc	39148.773	-1412	-0.003	M. Baldwin	0.006	VZ Cnc	51587.383	65540	0.001	S. Foglia	0.005
TT Cnc	39152.707	-1405	-0.014	M. Baldwin	0.003	VZ Cnc	51594.356	65579	0.018	S. Foglia	0.009
TT Cnc	39169.613	-1375	-0.011	M. Baldwin	0.004	VZ Cnc	51620.385	65725	0.006	S. Foglia	0.007
TT Cnc	39178.625	-1359	-0.014	M. Baldwin	0.007	VZ Cnc	51627.694	65766	0.002	R. Berg	0.005
TT Cnc	39200.617	-1320	0.003	M. Baldwin	0.008	VZ Cnc	51633.581	65799	0.003	R. Berg	0.006
TT Cnc	39477.841	-828	0.010	M. Baldwin	0.008	VZ Cnc	51634.648	65805	0.000	R. Berg	0.004
TT Cnc	39530.769	-734	-0.026	M. Baldwin	0.007	VZ Cnc	51639.643	65833	0.001	R. Berg	0.004
TT Cnc	39533.589	-729	-0.023	M. Baldwin	0.009	VZ Cnc	51943.401	67536	0.005	S. Foglia	0.004
TT Cnc	39556.716	-688	0.002	M. Baldwin	0.004	VZ Cnc	52024.373	67990	0.000	S. Foglia	0.005
TT Cnc	39582.642	-642	0.010	M. Baldwin	0.006	RR Cet	39169.582	10828	-0.011	M. Baldwin	0.004
TT Cnc	39894.746	-88	-0.037	M. Baldwin	0.005	RR Cet	39174.560	10837	-0.010	M. Baldwin	0.004
TT Cnc	39916.758	-49	0.000	M. Baldwin	0.008	RR Cet	39472.650	11376	-0.002	M. Baldwin	0.005
TT Cnc	39920.697	-42	-0.005	M. Baldwin	0.005	RR Cet	39477.630	11385	0.001	M. Baldwin	0.005
TT Cnc	40293.717	620	0.011	M. Baldwin	0.006	RR Cet	39492.561	11412	0.000	M. Baldwin	0.006
TT Cnc	40306.667	643	0.002	T. Cragg	0.003	RR Cet	40156.741	12613	-0.007	M. Baldwin	0.006
TT Cnc	40333.671	691	-0.040	T. Cragg	0.008	RR Cet	40186.612	12667	0.001	M. Baldwin	0.005
TT Cnc	41765.384	3232	-0.051	M. Baldwin	0.008	RR Cet	40203.758	12698	0.003	M. Baldwin	0.005
TT Cnc	42464.647	4473	-0.029	M. Baldwin	0.008	RR Cet	40208.736	12707	0.003	M. Baldwin	0.006
TT Cnc	42477.618	4496	-0.018	M. Baldwin	0.008	RR Cet	40525.614	13280	-0.004	L. Hazel	0.007
TT Cnc	42491.720	4521	-0.002	M. Baldwin	0.007	RR Cet	40562.674	13347	0.003	M. Baldwin	0.005
TT Cnc	42504.698	4544	0.017	M. Baldwin	0.009	RR Cet	42360.558	16598	-0.007	M. Baldwin	0.006
TT Cnc	42508.632	4551	0.007	M. Baldwin	0.007	RR Cet	42386.557	16645	0.000	M. Baldwin	0.006
TT Cnc	42832.588	5126	-0.021	M. Baldwin	0.006	RR Cet	42387.658	16647	-0.005	M. Baldwin	0.006
TT Cnc	42845.581	5149	0.013	M. Baldwin	0.009	RR Cet	42669.700	17157	-0.008	M. Baldwin	0.006
TT Cnc	43144.758	5680	-0.002	M. Baldwin	0.004	RR Cet	42689.618	17193	0.001	M. Baldwin	0.009

Table continued on following pages

Table 1. Recent times of minima of stars in the AAVSO short period pulsator program, cont.

Star	JD (max) Hel. 2400000 +	Cycle	O–C (day)	Observer	Error (day)	Star	JD (max) Hel. 2400000 +	Cycle	O–C (day)	Observer	Error (day)
RR Cet	42725.564	17258	0.000	M. Baldwin	0.007	DM Cyg	40147.646	-5799	0.008	M. Baldwin	0.006
RR Cet	43080.606	17900	-0.002	M. Baldwin	0.006	DM Cyg	40178.708	-5725	0.000	M. Baldwin	0.005
RR Cet	43096.647	17929	0.001	M. Baldwin	0.005	DM Cyg	40442.809	-5096	0.010	M. Baldwin	0.004
RR Cet	43101.624	17938	0.001	M. Baldwin	0.005	DM Cyg	40471.777	-5027	0.007	M. Baldwin	0.005
RR Cet	43420.717	18515	-0.003	M. Baldwin	0.006	DM Cyg	40472.612	-5025	0.002	L. Hazel	0.005
RR Cet	43446.707	18562	-0.005	M. Baldwin	0.005	DM Cyg	40524.670	-4901	-0.002	L. Hazel	0.009
RR Cet	43466.621	18598	0.000	M. Baldwin	0.004	DM Cyg	40566.664	-4801	0.006	M. Baldwin	0.003
RR Cet	43755.850	19121	-0.005	M. Baldwin	0.006	DM Cyg	41989.578	-1412	0.014	M. Baldwin	0.009
RR Cet	43780.741	19166	0.000	M. Baldwin	0.007	DM Cyg	42240.635	-814	-0.005	H. Smith	0.008
RR Cet	43815.586	19229	0.004	M. Baldwin	0.005	DM Cyg	42271.718	-740	0.008	H. Smith	0.007
RR Cet	43841.570	19276	-0.004	M. Baldwin	0.009	DM Cyg	42274.652	-733	0.003	H. Smith	0.003
RR Cet	44145.734	19826	-0.006	M. Baldwin	0.004	DM Cyg	42303.635	-664	0.016	M. Baldwin	0.007
RR Cet	44196.616	19918	-0.002	M. Baldwin	0.004	DM Cyg	42308.670	-652	0.013	M. Baldwin	0.005
RR Cet	44222.615	19965	0.004	M. Baldwin	0.008	DM Cyg	42569.818	-30	0.008	M. Baldwin	0.005
RR Cet	44227.593	19974	0.005	M. Baldwin	0.007	DM Cyg	42572.762	-23	0.013	M. Baldwin	0.007
RR Cet	44253.583	20021	0.003	M. Baldwin	0.009	DM Cyg	42598.784	39	0.003	M. Baldwin	0.005
RR Cet	44623.552	20690	-0.004	G. Hanson	0.003	DM Cyg	42632.797	120	0.008	M. Baldwin	0.003
RR Cet	44875.737	21146	0.000	M. Baldwin	0.009	DM Cyg	42637.840	132	0.012	M. Baldwin	0.003
RR Cet	45672.638	22587	-0.013	G. Chaple	0.008	DM Cyg	42658.833	182	0.012	M. Baldwin	0.003
RR Cet	45677.618	22596	-0.010	G. Chaple	0.004	DM Cyg	42662.607	191	0.008	M. Baldwin	0.007
RR Cet	46058.666	23285	0.002	M. Baldwin	0.009	DM Cyg	42669.750	208	0.013	M. Baldwin	0.004
RR Cet	46078.571	23321	-0.002	M. Baldwin	0.006	DM Cyg	42688.639	253	0.008	M. Baldwin	0.005
RR Cet	46735.576	24509	0.005	M. Baldwin	0.004	DM Cyg	42725.589	341	0.011	M. Baldwin	0.007
RR Cet	46736.665	24511	-0.012	M. Baldwin	0.006	DM Cyg	42986.736	963	0.005	M. Baldwin	0.007
RR Cet	46787.554	24603	-0.001	M. Baldwin	0.006	DM Cyg	42994.720	982	0.011	M. Baldwin	0.007
RR Cet	46793.632	24614	-0.007	M. Baldwin	0.005	DM Cyg	43036.705	1082	0.010	M. Baldwin	0.006
RR Cet	47086.742	25144	-0.002	M. Baldwin	0.005	DM Cyg	43044.674	1101	0.002	M. Baldwin	0.004
RR Cet	47111.628	25189	-0.002	M. Baldwin	0.006	DM Cyg	43337.738	1799	0.004	M. Baldwin	0.007
RR Cet	47121.583	25207	-0.001	M. Baldwin	0.009	DM Cyg	43340.674	1806	0.001	M. Baldwin	0.007
RR Cet	47425.749	25757	-0.001	M. Baldwin	0.009	DM Cyg	43350.755	1830	0.005	M. Baldwin	0.008
RR Cet	47861.540	26545	0.004	M. Baldwin	0.005	DM Cyg	43374.687	1887	0.005	M. Baldwin	0.008
RR Cet	48211.612	27178	0.009	M. Baldwin	0.007	DM Cyg	43395.689	1937	0.014	M. Baldwin	0.007
RR Cet	48571.623	27829	-0.001	M. Baldwin	0.005	DM Cyg	43398.617	1944	0.003	M. Baldwin	0.005
RR Cet	51882.594	33816	-0.010	R. Berg	0.007	DM Cyg	44131.705	3690	0.016	M. Heifner	0.006
RR Cet	54093.618	37814	0.008	R. Harvan	0.004	DM Cyg	44165.708	3771	0.010	M. Heifner	0.006
RR Cet	54350.776	38279	0.008	R. Harvan	0.005	DM Cyg	44171.585	3785	0.009	M. Heifner	0.005
RR Cet	54387.820	38346	-0.001	R. Harvan	0.003	DM Cyg	44192.573	3835	0.004	M. Heifner	0.006
RR Cet	54411.614	38389	0.013	R. Harvan	0.005	DM Cyg	44408.808	4350	0.011	G. Hanson	0.002
XZ Cyg	52634.658	18238	-1.457	R. Huziak	0.004	DM Cyg	44435.677	4414	0.009	M. Heifner	0.005
XZ Cyg	52641.655	18253	-1.460	R. Huziak	0.003	DM Cyg	44463.806	4481	0.007	G. Samolyk	0.006
XZ Cyg	52653.787	18279	-1.462	R. Huziak	0.003	DM Cyg	44463.808	4481	0.009	G. Hanson	0.004
XZ Cyg	52655.664	18283	-1.452	R. Huziak	0.002	DM Cyg	44485.651	4533	0.020	G. Samolyk	0.005
XZ Cyg	52661.713	18296	-1.470	R. Huziak	0.007	DM Cyg	44493.622	4552	0.013	G. Samolyk	0.003
XZ Cyg	52668.723	18311	-1.461	R. Huziak	0.002	DM Cyg	44503.705	4576	0.020	M. Heifner	0.003
XZ Cyg	52772.790	18534	-1.468	R. Huziak	0.004	DM Cyg	44506.632	4583	0.008	M. Heifner	0.003
XZ Cyg	52779.778	18549	-1.480	R. Hill	0.005	DM Cyg	44543.589	4671	0.017	G. Hanson	0.003
XZ Cyg	52779.787	18549	-1.471	R. Huziak	0.003	DM Cyg	44577.588	4752	0.007	M. Heifner	0.004
XZ Cyg	52806.846	18607	-1.481	R. Huziak	0.002	DM Cyg	44820.691	5331	0.011	M. Heifner	0.005
XZ Cyg	52820.845	18637	-1.483	R. Huziak	0.003	DM Cyg	44841.682	5381	0.009	M. Heifner	0.003
XZ Cyg	52848.841	18697	-1.489	R. Huziak	0.002	DM Cyg	44875.687	5462	0.006	M. Heifner	0.003
XZ Cyg	52877.748	18759	-1.517	R. Huziak	0.008	DM Cyg	44915.577	5557	0.009	G. Samolyk	0.004
XZ Cyg	52883.835	18772	-1.497	R. Huziak	0.004	DM Cyg	45258.620	6374	0.026	M. Heifner	0.006
XZ Cyg	52884.756	18774	-1.510	R. Huziak	0.003	DM Cyg	45593.668	7172	0.026	M. Heifner	0.005
XZ Cyg	52885.692	18776	-1.507	R. Huziak	0.004	DM Cyg	45614.664	7222	0.029	M. Heifner	0.006
XZ Cyg	52886.657	18778	-1.476	R. Huziak	0.009	DM Cyg	46311.614	8882	0.011	M. Baldwin	0.006
XZ Cyg	52988.338	18996	-1.535	S. Foglia	0.005	DM Cyg	46329.684	8925	0.027	M. Baldwin	0.004
XZ Cyg	53573.464	20250	-1.651	B. Wilson	0.004	DM Cyg	46355.703	8987	0.015	M. Baldwin	0.004
XZ Cyg	53620.592	20351	-1.660	G. Chaple	0.005	DM Cyg	46358.638	8994	0.011	M. Heifner	0.003
XZ Cyg	53630.367	20372	-1.685	B. Wilson	0.004	DM Cyg	46672.695	9742	0.013	M. Baldwin	0.006
XZ Cyg	53637.371	20387	-1.682	B. Wilson	0.003	DM Cyg	46682.786	9766	0.027	M. Baldwin	0.004
DM Cyg	39772.707	-6692	0.004	M. Baldwin	0.003	DM Cyg	46701.671	9811	0.019	M. Baldwin	0.007
DM Cyg	39801.687	-6623	0.014	M. Baldwin	0.005	DM Cyg	46712.585	9837	0.016	M. Baldwin	0.004
DM Cyg	39851.641	-6504	0.004	M. Baldwin	0.005	DM Cyg	46725.599	9868	0.015	M. Baldwin	0.005
DM Cyg	40070.804	-5982	0.001	M. Baldwin	0.004	DM Cyg	46735.685	9892	0.024	M. Baldwin	0.003
DM Cyg	40099.779	-5913	0.005	M. Baldwin	0.003	DM Cyg	46759.613	9949	0.020	G. Samolyk	0.004
DM Cyg	40128.752	-5844	0.008	M. Baldwin	0.005	DM Cyg	46983.805	10483	0.007	R. Hill	0.004

Table continued on following pages

Table 1. Recent times of minima of stars in the AAVSO short period pulsator program, cont.

Star	*JD (max) Hel. 2400000 +*	*Cycle*	*O–C (day)*	*Observer*	*Error (day)*	*Star*	*JD (max) Hel. 2400000 +*	*Cycle*	*O–C (day)*	*Observer*	*Error (day)*
DM Cyg	46997.676	10516	0.022	M. Baldwin	0.005	RW Dra	46210.764	15428	0.050	M. Baldwin	0.007
DM Cyg	47002.709	10528	0.017	M. Baldwin	0.005	RW Dra	46233.813	15480	0.067	M. Baldwin	0.009
DM Cyg	47023.694	10578	0.009	M. Baldwin	0.008	RW Dra	46254.633	15527	0.070	M. Baldwin	0.003
DM Cyg	47039.671	10616	0.031	M. Baldwin	0.005	RW Dra	46264.795	15550	0.045	M. Baldwin	0.006
DM Cyg	47065.694	10678	0.023	M. Baldwin	0.003	RW Dra	46269.703	15561	0.081	M. Baldwin	0.009
DM Cyg	47105.569	10773	0.011	G. Samolyk	0.005	RW Dra	46273.678	15570	0.069	M. Baldwin	0.006
DM Cyg	47358.739	11376	0.006	M. Baldwin	0.003	RW Dra	46289.607	15606	0.053	M. Baldwin	0.004
DM Cyg	47382.691	11433	0.026	M. Baldwin	0.006	RW Dra	46324.626	15685	0.082	M. Baldwin	0.004
DM Cyg	47390.659	11452	0.016	M. Baldwin	0.005	RW Dra	46327.714	15692	0.069	M. Baldwin	0.005
DM Cyg	47406.630	11490	0.033	M. Baldwin	0.009	RW Dra	46355.614	15755	0.066	M. Baldwin	0.004
DM Cyg	47419.642	11521	0.029	M. Baldwin	0.006	RW Dra	46514.594	16114	0.038	M. Baldwin	0.008
DM Cyg	47477.582	11659	0.028	M. Baldwin	0.003	RW Dra	46521.727	16130	0.085	M. Baldwin	0.008
DM Cyg	47479.675	11664	0.022	M. Baldwin	0.007	RW Dra	46556.680	16209	0.047	M. Baldwin	0.007
DM Cyg	47717.723	12231	0.009	M. Baldwin	0.006	RW Dra	46560.685	16218	0.066	M. Baldwin	0.004
DM Cyg	47733.687	12269	0.019	M. Baldwin	0.004	RW Dra	46712.576	16561	0.037	M. Baldwin	0.003
DM Cyg	47749.641	12307	0.018	M. Baldwin	0.008	RW Dra	46724.558	16588	0.060	M. Baldwin	0.004
DM Cyg	47764.754	12343	0.016	R. Hill	0.008	RW Dra	46732.548	16606	0.077	M. Baldwin	0.004
DM Cyg	47767.686	12350	0.009	M. Heifner	0.004	RW Dra	46735.646	16613	0.075	M. Baldwin	0.002
DM Cyg	47793.728	12412	0.020	M. Baldwin	0.006	RW Dra	46944.709	17085	0.081	M. Baldwin	0.005
DM Cyg	47796.676	12419	0.029	M. Baldwin	0.003	RW Dra	46948.691	17094	0.077	M. Baldwin	0.005
DM Cyg	47862.592	12576	0.027	M. Baldwin	0.004	RW Dra	46974.819	17153	0.073	M. Baldwin	0.003
DM Cyg	48150.628	13262	0.039	M. Baldwin	0.007	RW Dra	46979.710	17164	0.092	M. Baldwin	0.005
DM Cyg	48160.692	13286	0.026	M. Baldwin	0.004	RW Dra	47001.804	17214	0.040	M. Baldwin	0.003
DM Cyg	48176.638	13324	0.017	G. Samolyk	0.004	RW Dra	47022.663	17261	0.082	M. Baldwin	0.004
DM Cyg	48208.558	13400	0.028	M. Baldwin	0.005	RW Dra	47025.754	17268	0.072	M. Baldwin	0.003
DM Cyg	48213.597	13412	0.029	M. Baldwin	0.005	RW Dra	47037.713	17295	0.072	M. Baldwin	0.003
DM Cyg	48234.588	13462	0.027	M. Baldwin	0.004	RW Dra	47081.540	17394	0.051	M. Baldwin	0.002
DM Cyg	48237.516	13469	0.016	G. Samolyk	0.004	RW Dra	47231.731	17733	0.093	M. Baldwin	0.004
DM Cyg	48237.520	13469	0.020	M. Baldwin	0.004	RW Dra	47242.778	17758	0.067	M. Baldwin	0.004
DM Cyg	48469.703	14022	0.020	M. Baldwin	0.005	RW Dra	47340.646	17979	0.050	M. Baldwin	0.005
DM Cyg	48506.643	14110	0.012	M. Baldwin	0.004	RW Dra	47658.691	18697	0.081	M. Baldwin	0.005
DM Cyg	48530.586	14167	0.023	M. Baldwin	0.005	RW Dra	47670.636	18724	0.067	M. Baldwin	0.007
DM Cyg	48535.624	14179	0.023	M. Baldwin	0.006	RW Dra	47674.629	18733	0.074	M. Baldwin	0.004
DM Cyg	48543.608	14198	0.030	M. Baldwin	0.004	RW Dra	47684.833	18756	0.091	M. Baldwin	0.003
DM Cyg	48864.802	14963	0.031	M. Baldwin	0.005	RW Dra	47736.655	18873	0.091	M. Baldwin	0.005
DM Cyg	48894.617	15034	0.036	M. Baldwin	0.006	RW Dra	47747.700	18898	0.064	M. Baldwin	0.003
DM Cyg	49160.794	15668	0.022	M. Baldwin	0.005	RW Dra	47810.623	19040	0.092	M. Baldwin	0.002
DM Cyg	49203.624	15770	0.026	G. Samolyk	0.005	RW Dra	47837.609	19101	0.060	M. Baldwin	0.004
DM Cyg	49208.661	15782	0.024	M. Baldwin	0.007	RW Dra	47999.727	19467	0.071	M. Baldwin	0.008
DM Cyg	49250.651	15882	0.028	M. Baldwin	0.006	RW Dra	48007.704	19485	0.075	M. Baldwin	0.005
DM Cyg	49625.582	16775	0.024	G. Samolyk	0.007	RW Dra	48061.765	19607	0.100	M. Baldwin	0.004
DM Cyg	49722.579	17006	0.034	M. Baldwin	0.005	RW Dra	48159.598	19828	0.049	M. Baldwin	0.006
DM Cyg	49928.721	17497	0.025	M. Baldwin	0.008	RW Dra	48179.582	19873	0.101	M. Baldwin	0.005
DM Cyg	49954.769	17559	0.041	M. Baldwin	0.006	RW Dra	48190.652	19898	0.099	M. Baldwin	0.003
DM Cyg	49957.707	17566	0.040	M. Baldwin	0.004	RW Dra	48202.582	19925	0.070	M. Baldwin	0.005
DM Cyg	49989.598	17642	0.022	G. Samolyk	0.003	RW Dra	48379.749	20325	0.070	M. Baldwin	0.006
DM Cyg	50284.771	18345	0.033	G. Samolyk	0.002	RW Dra	48414.737	20404	0.068	M. Baldwin	0.005
DM Cyg	50313.755	18414	0.047	G. Samolyk	0.003	RW Dra	48452.824	20490	0.064	M. Baldwin	0.005
DM Cyg	50337.683	18471	0.043	M. Baldwin	0.005	RW Dra	48480.753	20553	0.089	M. Baldwin	0.004
DM Cyg	50373.782	18557	0.034	M. Baldwin	0.003	RW Dra	48484.737	20562	0.087	M. Baldwin	0.004
DM Cyg	50403.590	18628	0.032	G. Chaple	0.005	RW Dra	48508.668	20616	0.100	M. Baldwin	0.004
DM Cyg	50928.850	19879	0.047	M. Baldwin	0.007	RW Dra	48752.710	21167	0.095	M. Baldwin	0.004
DM Cyg	51012.823	20079	0.048	G. Samolyk	0.003	RW Dra	49089.784	21928	0.109	M. Baldwin	0.005
DM Cyg	51076.645	20231	0.051	G. Samolyk	0.007	RW Dra	49121.643	22000	0.078	M. Baldwin	0.005
DM Cyg	51100.551	20288	0.025	R. Berg	0.003	RW Dra	49124.750	22007	0.085	M. Baldwin	0.004
DM Cyg	51110.638	20312	0.036	R. Berg	0.005	RW Dra	49213.794	22208	0.102	M. Baldwin	0.006
DM Cyg	51129.530	20357	0.034	G. Chaple	0.005	RW Dra	49430.843	22698	0.122	M. Baldwin	0.005
DM Cyg	51395.727	20991	0.040	R. Berg	0.006	RW Dra	49457.834	22759	0.095	M. Baldwin	0.003
DM Cyg	51411.678	21029	0.036	M. Baldwin	0.005	RW Dra	49474.695	22797	0.125	M. Baldwin	0.004
DM Cyg	51424.702	21060	0.044	M. Baldwin	0.003	RW Dra	49614.604	23113	0.072	M. Baldwin	0.003
DM Cyg	51429.731	21072	0.035	R. Berg	0.006	RW Dra	49653.591	23201	0.083	M. Baldwin	0.006
DM Cyg	51437.712	21091	0.039	M. Baldwin	0.003	RW Dra	49868.854	23687	0.088	M. Baldwin	0.005
DM Cyg	52165.761	22825	0.050	R. Berg	0.007	RW Dra	49873.735	23698	0.097	M. Baldwin	0.003
DM Cyg	52200.600	22908	0.041	R. Berg	0.007	RW Dra	49900.750	23759	0.094	M. Baldwin	0.005
DM Cyg	52210.675	22932	0.039	R. Berg	0.007	RW Dra	49920.697	23804	0.110	M. Baldwin	0.005
DM Cyg	52548.670	23737	0.047	R. Berg	0.005	RW Dra	49958.790	23890	0.112	M. Baldwin	0.006

Table continued on following page

Table 1. Recent times of minima of stars in the AAVSO short period pulsator program, cont.

Star	JD (max) Hel. 2400000 +	Cycle	O–C (day)	Observer	Error (day)
RW Dra	50218.785	24477	0.115	R. Hill	0.005
RW Dra	50579.767	25292	0.119	M. Baldwin	0.003
RW Dra	50928.804	26080	0.138	M. Baldwin	0.003
RW Dra	50948.714	26125	0.116	M. Baldwin	0.005
RW Dra	50990.800	26220	0.125	R. Hill	0.006
RW Dra	51045.749	26344	0.153	M. Baldwin	0.003
RW Dra	51429.743	27211	0.138	M. Baldwin	0.003
RW Dra	52380.708	29358	0.160	M. Baldwin	0.004
RW Dra	52496.774	29620	0.181	M. Baldwin	0.005
RW Dra	52523.752	29681	0.142	M. Baldwin	0.004
RW Dra	52794.815	30293	0.139	R. Hill	0.008
XZ Dra	46017.665	8582	-0.006	M. Baldwin	0.005
XZ Dra	46018.628	8584	0.004	M. Baldwin	0.005
XZ Dra	46028.625	8605	-0.006	M. Baldwin	0.004
XZ Dra	46176.821	8916	0.000	M. Baldwin	0.005
XZ Dra	46205.874	8977	-0.014	M. Baldwin	0.009
XZ Dra	46269.735	9111	-0.003	M. Baldwin	0.007
XZ Dra	46279.742	9132	-0.003	M. Baldwin	0.006
XZ Dra	46311.681	9199	0.011	M. Baldwin	0.005
XZ Dra	46521.803	9640	-0.002	M. Baldwin	0.003
XZ Dra	46523.710	9644	-0.001	M. Baldwin	0.003
XZ Dra	46531.803	9661	-0.009	M. Baldwin	0.004
XZ Dra	46532.765	9663	0.000	M. Baldwin	0.006
XZ Dra	46534.678	9667	0.008	M. Baldwin	0.003
XZ Dra	46584.704	9772	0.001	M. Baldwin	0.003
XZ Dra	46968.762	10578	0.003	R. Hill	0.006
XZ Dra	46969.705	10580	-0.007	R. Hill	0.008
XZ Dra	46979.699	10601	-0.020	M. Baldwin	0.009
XZ Dra	47019.738	10685	-0.006	M. Baldwin	0.005
XZ Dra	47037.847	10723	-0.004	M. Baldwin	0.005
XZ Dra	47039.747	10727	-0.010	M. Baldwin	0.004
XZ Dra	47040.711	10729	0.001	M. Baldwin	0.006
XZ Dra	47081.683	10815	-0.006	M. Baldwin	0.006
XZ Dra	47082.640	10817	-0.002	M. Baldwin	0.008
XZ Dra	47083.588	10819	-0.007	M. Baldwin	0.005
XZ Dra	47678.735	12068	-0.005	R. Hill	0.009
XZ Dra	47769.738	12259	-0.013	M. Baldwin	0.005
XZ Dra	48004.670	12752	0.006	M. Baldwin	0.007
XZ Dra	48178.565	13117	-0.020	M. Baldwin	0.004
XZ Dra	48188.577	13138	-0.015	M. Baldwin	0.003
XZ Dra	48208.584	13180	-0.020	M. Baldwin	0.008
XZ Dra	48209.537	13182	-0.020	M. Baldwin	0.005
XZ Dra	48219.539	13203	-0.025	M. Baldwin	0.006
XZ Dra	48531.654	13858	-0.015	M. Baldwin	0.008
XZ Dra	49117.743	15088	-0.018	M. Baldwin	0.005
XZ Dra	49188.747	15237	-0.012	M. Baldwin	0.004
XZ Dra	49198.742	15258	-0.023	M. Baldwin	0.005
XZ Dra	49483.704	15856	-0.006	M. Baldwin	0.008
XZ Dra	49534.666	15963	-0.030	M. Baldwin	0.005
XZ Dra	49929.689	16792	-0.023	M. Baldwin	0.004
XZ Dra	50545.811	18085	-0.011	M. Baldwin	0.006
XZ Dra	50690.670	18389	-0.007	M. Baldwin	0.005
XZ Dra	50990.838	19019	-0.032	R. Hill	0.007
XZ Dra	50992.756	19023	-0.020	R. Hill	0.006
XZ Dra	51812.776	20744	-0.052	R. Hill	0.005
XZ Dra	52513.689	22215	-0.066	R. Berg	0.007
RR Gem	39494.612	-4688	-0.001	M. Baldwin	0.006
RR Gem	39500.578	-4673	0.005	M. Baldwin	0.005
RR Gem	39525.605	-4610	0.002	M. Baldwin	0.004
RR Gem	39530.765	-4597	-0.003	M. Baldwin	0.003
RR Gem	39532.751	-4592	-0.004	M. Baldwin	0.003
RR Gem	39556.593	-4532	0.000	M. Baldwin	0.003
RR Gem	39567.718	-4504	0.000	M. Baldwin	0.005
RR Gem	39598.701	-4426	-0.007	M. Baldwin	0.003
RR Gem	39612.622	-4391	0.008	M. Baldwin	0.003
RR Gem	39826.769	-3852	0.004	M. Baldwin	0.002
RR Gem	39890.727	-3691	-0.005	M. Baldwin	0.006
RR Gem	39892.721	-3686	0.003	M. Baldwin	0.006
RR Gem	39894.711	-3681	0.006	M. Baldwin	0.005
RR Gem	39915.768	-3628	0.006	M. Baldwin	0.005
RR Gem	40184.739	-2951	-0.002	M. Baldwin	0.003
RR Gem	40211.763	-2883	0.004	M. Baldwin	0.005
RR Gem	40323.805	-2601	0.005	M. Baldwin	0.004
RR Gem	40327.784	-2591	0.011	M. Baldwin	0.005
RR Gem	40657.543	-1761	0.002	J. Bortle	0.003
RR Gem	41380.669	59	0.023	G. Samolyk	0.007
RR Gem	41693.735	847	0.008	T. Cragg	0.004
RR Gem	42142.698	1977	0.010	T. Cragg	0.005
RR Gem	43520.565	5445	0.004	M. Baldwin	0.004
RR Gem	43578.575	5591	0.006	M. Baldwin	0.004
RR Gem	43599.627	5644	0.001	M. Baldwin	0.005
RR Gem	44216.665	7197	0.016	M. Heifner	0.005
RR Gem	44259.562	7305	0.003	M. Baldwin	0.004
RR Gem	44291.737	7386	-0.004	M. Heifner	0.004
RR Gem	44297.703	7401	0.002	M. Heifner	0.004
RR Gem	44340.604	7509	-0.006	M. Baldwin	0.004
RR Gem	44659.643	8312	-0.008	M. Heifner	0.004
RR Gem	44988.611	9140	-0.013	G. Chaple	0.005
RR Gem	45011.663	9198	-0.005	M. Heifner	0.004
RR Gem	45079.593	9369	-0.015	G. Chaple	0.004
RR Gem	45371.619	10104	-0.012	G. Chaple	0.003
RR Gem	45375.590	10114	-0.014	G. Chaple	0.003
RR Gem	45993.803	11670	-0.017	M. Baldwin	0.003
RR Gem	46005.723	11700	-0.016	M. Baldwin	0.004
RR Gem	46038.697	11783	-0.019	M. Baldwin	0.004
RR Gem	46112.595	11969	-0.021	M. Baldwin	0.005
RR Gem	46114.594	11974	-0.008	M. Baldwin	0.004
RR Gem	46458.645	12840	-0.028	M. Heifner	0.004
RR Gem	46493.610	12928	-0.026	M. Heifner	0.003
RR Gem	46514.661	12981	-0.033	M. Baldwin	0.004
RR Gem	46518.638	12991	-0.029	M. Baldwin	0.004
RR Gem	46520.622	12996	-0.032	M. Baldwin	0.003
RR Gem	46553.602	13079	-0.028	M. Baldwin	0.003
RR Gem	46744.704	13560	-0.033	M. Baldwin	0.002
RR Gem	46793.568	13683	-0.038	M. Baldwin	0.003
RR Gem	46831.699	13779	-0.049	M. Baldwin	0.005
RR Gem	46845.623	13814	-0.031	M. Baldwin	0.004
RR Gem	47226.639	14773	-0.035	M. Baldwin	0.005
RR Gem	47236.568	14798	-0.039	M. Baldwin	0.003
RR Gem	47807.903	16236	-0.037	G. Samolyk	0.004
RR Gem	48245.693	17338	-0.083	M. Baldwin	0.004
RR Gem	48261.579	17378	-0.090	M. Baldwin	0.005
RR Gem	48290.582	17451	-0.090	M. Baldwin	0.004
RR Gem	48636.622	18322	-0.108	R. Hill	0.004
RR Gem	48673.571	18415	-0.109	M. Baldwin	0.003
RR Gem	48719.661	18531	-0.107	R. Hill	0.006
RR Gem	48896.856	18977	-0.112	M. Baldwin	0.006
RR Gem	48898.841	18982	-0.114	M. Baldwin	0.006
RR Gem	49013.657	19271	-0.121	M. Baldwin	0.005
RR Gem	49746.668	21116	-0.148	R. Hill	0.005
RR Gem	49754.620	21136	-0.142	G. Samolyk	0.005
RR Gem	50129.671	22080	-0.152	R. Hill	0.005
RR Gem	50160.646	22158	-0.167	R. Hill	0.005
RR Gem	50516.615	23054	-0.189	G. Chaple	0.005
RR Gem	50543.627	23122	-0.194	G. Chaple	0.005
RR Gem	54142.713	32181	-0.344	R. Harvan	0.004
RR Gem	54387.837	32798	-0.361	R. Harvan	0.004

Recent Minima of 172 Eclipsing Binary Stars

Gerard Samolyk
P.O. Box 20677, Greenfield, WI 53220; gsamolyk@wi.rr.com

Received February 6, 2017; accepted February 6, 2017

Abstract This paper continues the publication of times of minima for eclipsing binary stars from observations reported to the AAVSO Eclipsing Binary Section. Times or minima from observations received from September 2017 thru January 2018 are presented.

1. Recent observations

The accompanying list contains times of minima calculated from recent CCD observations made by participants in the AAVSO's eclipsing binary program. This list will be web-archived and made available through the AAVSO ftp site at ftp://ftp.aavso.org/public/datasets/gsamj461eb.txt. The data in this list, along with the eclipsing binary data from earlier AAVSO publications, are also included in the Lichtenknecker database (Frank and Lichtenknecker1987) administrated by the Bundesdeutsche Arbeitsgemeinschaft für Veränderliche Sterne e. V. (BAV) at: http://www.bav-astro.eu/index.php/veroeffentlichungen/service-for-scientists/lkdb-engl. These observations were reduced by the observers or the writer using the method of Kwee and van Woerden (1956). The standard error is included when available. Column F indicates the filter used. A "C" indicates a clear filter.

The linear elements in the *General Catalogue of Variable Stars* (GCVS; Kholopov *et al.* 1985) were used to compute the O–C values for most stars. For a few exceptions where the GCVS elements are missing or are in significant error, light elements from another source are used: CD Cam (Baldwin and Samolyk 2007), AC CMi (Samolyk 2008), CW Cas (Samolyk 1992a), DF Hya (Samolyk 1992b), DK Hya (Samolyk 1990), EF Ori (Baldwin and Samolyk 2005), GU Ori (Samolyk 1985).

The light elements used for QX And, V376 And, EK Aqr, IT Cnc, VY Cet, and V1128 Tau are from (Kreiner 2004).

The light elements used for, VZ Psc, and DG Psc, are from (Paschke 2014).

The light elements used for MW And, and V731 Cep are from (Nelson 2016).

The light elements used for DG CMi, V1011 Cas, EV Lyr, and V1249 Tau are from the AAVSO VSX site (Watson *et al.* 2014). O–C values listed in this paper can be directly compared with values published in the AAVSO EB monographs.

References

Baldwin, M. E., and Samolyk, G. 2005, *Observed Minima Timings of Eclipsing Binaries No. 10*, AAVSO, Cambridge, MA.

Baldwin, M. E., and Samolyk, G. 2007, *Observed Minima Timings of Eclipsing Binaries No. 12*, AAVSO, Cambridge, MA.

Frank, P., and Lichtenknecker, D. 1987, *BAV Mitt.*, No. 47, 1.

Kreiner, J. M. 2004, "Up-to-date linear elements of eclipsing binaries," *Acta Astron.*, **54**, 207 (http://www.as.up.krakow.pl/ephem/).

Kholopov, P. N., *et al.* 1985, *General Catalogue of Variable Stars*, 4th ed., Moscow.

Kwee K. K., and van Worden, H. 1956, *Bull. Astron. Inst. Netherlands*, **12**, 327.

Nelson, R. 2016, Eclipsing Binary O–C Files (https://www.aavso.org/bob-nelsons-o-c-files).

Paschke, A. 2014, "O–C Gateway" (http://var.astro.cz/ocgate/).

Samolyk, G. 1985, *J. Amer. Assoc. Var. Star Obs.*, **14**, 12.

Samolyk, G. 1990, *J. Amer. Assoc. Var. Star Obs.* **19**, 5.

Samolyk, G. 1992a, *J. Amer. Assoc. Var. Star Obs.*, **21**, 34.

Samolyk, G. 1992b, *J. Amer. Assoc. Var. Star Obs.*, **21**, 111.

Samolyk, G. 2008, *J. Amer. Assoc. Var. Star Obs.*, **36**, 171.

Watson, C., Henden, A. A., and Price, C. A. 2014, AAVSO International Variable Star Index VSX (Watson+, 2006–2016; https://www.aavso.org/vsx).

Table 1. Recent times of minima of stars in the AAVSO eclipsing binary program.

Star	*JD (min) Hel. 2400000 +*	*Cycle*	*O–C (day)*	*F*	*Observer*	*Error (day)*	*Star*	*JD (min) Hel. 2400000 +*	*Cycle*	*O–C (day)*	*F*	*Observer*	*Error (day)*
RT And	58049.3893	26883	–0.0119	TG	I. Megson	0.0001	WZ And	58056.5028	24702	0.0788	V	T. Arranz	0.0001
RT And	58049.3894	26883	–0.0117	V	T. Arranz	0.0001	WZ And	58072.5021	24725	0.0779	V	T. Arranz	0.0001
RT And	58054.4214	26891	–0.0112	V	T. Arranz	0.0001	WZ And	58083.6334	24741	0.0787	V	N. Simmons	0.0001
RT And	58076.4329	26926	–0.0122	V	T. Arranz	0.0001	XZ And	58043.6982	25099	0.1862	V	G. Samolyk	0.0001
RT And	58078.3197	26929	–0.0122	V	T. Arranz	0.0001	XZ And	58050.4851	25104	0.1867	V	T. Arranz	0.0001
RT And	58101.5904	26966	–0.0119	V	S. Cook	0.0004	XZ And	58058.6293	25110	0.1872	V	T. Arranz	0.0001
TW And	58063.4416	4619	–0.0619	V	T. Arranz	0.0001	XZ And	58073.5593	25121	0.1872	V	T. Arranz	0.0001
UU And	58075.4919	11051	0.0948	V	T. Arranz	0.0001	XZ And	58111.5637	25149	0.1878	V	G. Samolyk	0.0001
UU And	58084.4102	11057	0.0953	V	T. Arranz	0.0001	AB And	57999.8143	65956	–0.0436	V	R. Sabo	0.0005
UU And	58121.5682	11082	0.0959	V	K. Menzies	0.0001	AB And	58051.4237	66111.5	–0.0435	V	T. Arranz	0.0001

Table continued on following pages

Table 1. Recent times of minima of stars in the AAVSO eclipsing binary program, cont.

Star	JD (min) Hel. 2400000 +	Cycle	O–C (day)	F	Observer	Error (day)	Star	JD (min) Hel. 2400000 +	Cycle	O–C (day)	F	Observer	Error (day)
AB And	58051.5891	66112	–0.0440	V	T. Arranz	0.0001	EP Aur	58035.8932	53682	0.0197	V	G. Samolyk	0.0001
AB And	58058.3943	66132.5	–0.0426	V	L. Corp	0.0002	EP Aur	58063.6706	53729	0.0198	V	T. Arranz	0.0001
AB And	58079.6336	66196.5	–0.0444	V	G. Samolyk	0.0002	EP Aur	58079.6281	53756	0.0201	V	T. Arranz	0.0001
AB And	58137.5488	66371	–0.0444	V	G. Samolyk	0.0001	EP Aur	58083.7656	53763	0.0205	V	N. Simmons	0.0001
AD And	58006.8987	19270.5	–0.0391	V	G. Samolyk	0.0002	EP Aur	58090.8579	53775	0.0207	V	G. Samolyk	0.0001
AD And	58070.5089	19335	–0.0385	V	T. Arranz	0.0001	HP Aur	58043.8308	10744.5	0.0669	V	G. Samolyk	0.0002
AD And	58071.4959	19336	–0.0377	V	T. Arranz	0.0001	HP Aur	58076.5570	10767.5	0.0684	V	T. Arranz	0.0001
AD And	58074.4533	19339	–0.0389	V	T. Arranz	0.0001	HP Aur	58132.7572	10807	0.0674	V	G. Samolyk	0.0002
AD And	58077.4113	19342	–0.0395	V	T. Arranz	0.0001	TU Boo	58132.9680	77298	–0.1571	V	B. Harris	0.0001
BD And	58044.5774	49864	0.0171	V	K. Menzies	0.0001	TZ Boo	58144.9078	62296	0.0620	V	K. Menzies	0.0001
BD And	58072.3527	49924	0.0183	V	T. Arranz	0.0002	AD Boo	58135.9287	16146	0.0357	V	G. Samolyk	0.0001
BD And	58088.5532	49959	0.0172	V	G. Samolyk	0.0001	Y Cam	58065.8061	4569	0.4806	V	G. Samolyk	0.0001
BX And	58050.5001	35275	–0.0962	V	T. Arranz	0.0001	SV Cam	58083.8837	26117	0.0606	V	G. Samolyk	0.0003
BX And	58053.5506	35280	–0.0963	V	T. Arranz	0.0001	SV Cam	58101.6747	26147	0.0595	V	S. Cook	0.0004
BX And	58058.4309	35288	–0.0969	V	T. Arranz	0.0001	CD Cam	58083.6988	6963	–0.0148	V	G. Samolyk	0.0003
BX And	58064.5325	35298	–0.0965	V	T. Arranz	0.0001	CD Cam	58107.7742	6994.5	–0.0112	V	G. Samolyk	0.0005
BX And	58075.5149	35316	–0.0961	V	T. Arranz	0.0001	WY Cnc	57849.3770	37977	–0.0433	V	T. Arranz	0.0001
BX And	58128.5915	35403	–0.0996	V	K. Menzies	0.0003	WY Cnc	57854.3534	37983	–0.0431	V	T. Arranz	0.0001
DS And	58035.8052	21665.5	0.0048	V	G. Samolyk	0.0003	IT Cnc	58114.8922	15439	0.0155	V	K. Menzies	0.0001
DS And	58079.7615	21709	0.0035	V	G. Samolyk	0.0001	SX CMa	58093.8493	18469	0.0213	V	G. Samolyk	0.0001
DS And	58111.5940	21740.5	0.0047	V	G. Samolyk	0.0001	SX CMa	58137.7050	18496	0.0220	V	G. Samolyk	0.0001
MW And	58029.8977	13561.5	–0.0084	V	K. Menzies	0.0001	UU CMa	58086.8652	6226	–0.0774	V	G. Samolyk	0.0001
QX And	58002.9325	13351	0.0001	V	R. Sabo	0.0003	UU CMa	58136.6949	6249	–0.0769	V	G. Samolyk	0.0005
QX And	58035.9103	13431	0.0042	V	G. Samolyk	0.0002	XZ CMi	58065.8944	26989	0.0031	V	G. Samolyk	0.0001
QX And	58039.8236	13440.5	0.0018	V	K. Menzies	0.0002	XZ CMi	58094.8349	27039	0.0031	V	K. Menzies	0.0001
QX And	58079.6013	13537	0.0049	V	G. Samolyk	0.0002	XZ CMi	58145.7717	27127	0.0047	V	K. Menzies	0.0001
QX And	58079.8064	13537.5	0.0040	V	G. Samolyk	0.0002	AC CMi	58070.9515	7025	0.0038	V	G. Samolyk	0.0001
QX And	58111.5402	13614.5	0.0005	V	G. Samolyk	0.0002	AK CMi	58067.9390	26447	–0.0242	V	G. Samolyk	0.0001
QX And	58111.7514	13615	0.0056	V	G. Samolyk	0.0002	DG CMi	58128.7750	5047	0.0516	V	K. Menzies	0.0001
V376 And	58044.8954	6942	0.0035	V	K. Menzies	0.0002	RZ Cas	58132.6063	12493	0.0792	V	G. Samolyk	0.0001
V376 And	58137.5414	7058	0.0033	V	K. Menzies	0.0001	TV Cas	58093.5730	7443	–0.0295	V	G. Samolyk	0.0002
RY Aqr	58006.4080	8737	–0.1378	V	T. Arranz	0.0001	TW Cas	58005.6284	11200	0.0123	V	G. Samolyk	0.0001
RY Aqr	58008.3741	8738	–0.1383	V	T. Arranz	0.0001	ZZ Cas	58020.8030	19769	0.0227	V	K. Menzies	0.0001
RY Aqr	58069.3379	8769	–0.1389	V	T. Arranz	0.0001	AB Cas	57997.6161	11181	0.1374	V	G. Samolyk	0.0002
CX Aqr	58043.6271	38832	0.0160	V	G. Samolyk	0.0001	CW Cas	58007.8209	51356.5	–0.1083	V	K. Menzies	0.0001
CX Aqr	58107.5651	38947	0.0156	V	G. Samolyk	0.0001	CW Cas	58028.8646	51422.5	–0.1096	V	K. Menzies	0.0002
CZ Aqr	58067.5571	17034	–0.0635	V	G. Samolyk	0.0001	CW Cas	58083.5482	51594	–0.1112	V	T. Arranz	0.0001
CZ Aqr	58111.5578	17085	–0.0633	V	G. Samolyk	0.0001	CW Cas	58084.6653	51597.5	–0.1101	V	S. Cook	0.0006
EK Aqr	58052.6216	18114.5	0.0146	V	G. Samolyk	0.0002	CW Cas	58136.3181	51759.5	–0.1133	V	T. Arranz	0.0001
EK Aqr	58083.5729	18215.5	0.0068	V	G. Samolyk	0.0003	CW Cas	58139.3482	51769	–0.1124	V	T. Arranz	0.0001
XZ Aql	58026.6488	7537	0.1806	V	N. Simmons	0.0004	CW Cas	58147.3193	51794	–0.1129	V	T. Arranz	0.0001
KO Aql	58046.5753	5642	0.1046	V	G. Samolyk	0.0001	DZ Cas	58043.5993	37724	–0.2074	V	G. Samolyk	0.0002
OO Aql	57980.4642	38215.5	0.0668	V	L. Corp	0.0001	DZ Cas	58084.4152	37776	–0.2059	V	T. Arranz	0.0001
V343 Aql	58045.5695	16048	–0.0364	V	K. Menzies	0.0002	IS Cas	58006.6593	15873	0.0700	V	N. Simmons	0.0001
V346 Aql	58010.4207	14545	–0.0131	V	T. Arranz	0.0001	IS Cas	58052.6978	15898	0.0707	V	G. Samolyk	0.0001
V346 Aql	58031.4415	14564	–0.0132	V	T. Arranz	0.0001	MM Cas	58093.7112	19588	0.1178	V	G. Samolyk	0.0001
SS Ari	58019.7849	46778.5	–0.3817	V	N. Simmons	0.0001	OR Cas	58052.7044	11112	–0.0319	V	G. Samolyk	0.0002
SS Ari	58064.4434	46888.5	–0.3825	V	T. Arranz	0.0001	OX Cas	58107.6241	6764	0.0746	V	G. Samolyk	0.0003
SS Ari	58066.4733	46893.5	–0.3826	V	T. Arranz	0.0001	V364 Cas	58052.5433	15371.5	–0.0245	V	G. Samolyk	0.0001
SS Ari	58074.5930	46913.5	–0.3828	V	T. Arranz	0.0001	V375 Cas	58023.6467	15869	0.2561	V	T. Arranz	0.0001
SS Ari	58079.4637	46925.5	–0.3840	V	T. Arranz	0.0001	V375 Cas	58029.5412	15873	0.2570	V	T. Arranz	0.0001
SS Ari	58124.5279	47036.5	–0.3851	V	G. Samolyk	0.0002	V375 Cas	58032.4854	15875	0.2545	V	T. Arranz	0.0002
SX Aur	58123.5755	14843	0.0196	V	G. Samolyk	0.0001	V380 Cas	58119.5460	23926	–0.0728	V	G. Samolyk	0.0003
TT Aur	57697.8840	27354	–0.0056	V	G. Samolyk	0.0001	V1011 Cas	58104.6407	3937.5	–0.0061	V	K. Menzies	0.0002
TT Aur	58065.7173	27630	–0.0072	V	G. Samolyk	0.0001	V1115 Cas	57310.5838	12132.5	–0.1011	B	G. Lubcke	0.0010
WW Aur	58123.7688	9971.5	0.0003	V	G. Samolyk	0.0002	V1115 Cas	57310.5852	12132.5	–0.0997	V	G. Lubcke	0.0001
AP Aur	58047.8474	27406	1.6600	V	K. Menzies	0.0001	V1115 Cas	57310.5859	12132.5	–0.0990	Ic	G. Lubcke	0.0044
AP Aur	58066.6361	27439	1.6614	V	T. Arranz	0.0001	V1115 Cas	57311.5524	12135.5	–0.1024	V	G. Lubcke	0.0005
AP Aur	58068.9147	27443	1.6628	V	K. Menzies	0.0001	V1115 Cas	57311.5526	12135.5	–0.1022	B	G. Lubcke	0.0003
AP Aur	58084.5761	27470.5	1.6681	V	T. Arranz	0.0001	V1115 Cas	57311.5532	12135.5	–0.1016	Ic	G. Lubcke	0.0038
AP Aur	58114.7529	27523.5	1.6713	V	G. Samolyk	0.0002	V1115 Cas	57311.7156	12136	–0.1008	Ic	G. Lubcke	0.0016
AR Aur	58132.8182	4772	–0.1295	V	G. Samolyk	0.0002	V1115 Cas	57311.7156	12136	–0.1008	V	G. Lubcke	0.0000
CL Aur	58043.8780	20152	0.1826	V	G. Samolyk	0.0001	V1115 Cas	57330.6287	12194.5	–0.1002	V	G. Lubcke	0.0006
CL Aur	58083.6977	20184	0.1826	V	T. Arranz	0.0001	V1115 Cas	57330.6289	12194.5	–0.1000	Ic	G. Lubcke	0.0010
CL Aur	58088.6750	20188	0.1825	V	G. Samolyk	0.0001	V1115 Cas	57330.6295	12194.5	–0.0994	B	G. Lubcke	0.0025
EM Aur	58065.9411	14860	–1.1147	V	G. Samolyk	0.0002	V1115 Cas	57334.6665	12207	–0.1035	B	G. Lubcke	0.0015

Table continued on following pages

Table 1. Recent times of minima of stars in the AAVSO eclipsing binary program, cont.

Star	*JD (min) Hel. 2400000 +*	*Cycle*	*O–C (day)*	*F*	*Observer*	*Error (day)*	*Star*	*JD (min) Hel. 2400000 +*	*Cycle*	*O–C (day)*	*F*	*Observer*	*Error (day)*
V1115 Cas	57334.6682	12207	–0.1018	V	G. Lubcke	0.0008	Y Leo	58093.9509	7507	–0.0678	V	G. Samolyk	0.0001
V1115 Cas	57334.6683	12207	–0.1017	Ic	G. Lubcke	0.0004	UU Leo	58136.8246	7584	0.2136	V	G. Samolyk	0.0001
V1115 Cas	57335.6375	12210	–0.1024	V	G. Lubcke	0.0010	UV Leo	58083.9457	32734	0.0442	V	G. Samolyk	0.0001
V1115 Cas	57335.6376	12210	–0.1023	Ic	G. Lubcke	0.0009	VZ Leo	58107.8308	24721	–0.0514	V	G. Samolyk	0.0003
V1115 Cas	57335.6378	12210	–0.1021	B	G. Lubcke	0.0003	XZ Leo	58132.8294	26874	0.0783	V	K. Menzies	0.0002
V1115 Cas	57336.6063	12213	–0.1034	B	G. Lubcke	0.0016	T LMi	58101.8925	4207	–0.1317	V	G. Samolyk	0.0002
V1115 Cas	57336.6077	12213	–0.1021	V	G. Lubcke	0.0003	RR Lep	58123.7393	30310	–0.0454	V	G. Samolyk	0.0001
V1115 Cas	57336.6078	12213	–0.1020	Ic	G. Lubcke	0.0005	RY Lyn	58063.8549	10576	–0.0212	V	G. Samolyk	0.0003
V1115 Cas	57361.6625	12290.5	–0.1022	V	G. Lubcke	0.0008	RY Lyn	58083.9459	10590	–0.0200	V	G. Samolyk	0.0001
V1115 Cas	57361.6632	12290.5	–0.1015	Ic	G. Lubcke	0.0011	RY Lyn	58122.6903	10617	–0.0203	V	G. Samolyk	0.0001
U Cep	58031.6976	5411	0.2145	V	G. Samolyk	0.0001	RY Lyn	58132.7360	10624	–0.0195	V	K. Menzies	0.0001
SU Cep	58066.5088	35213	0.0069	V	K. Menzies	0.0001	EV Lyr	58058.3065	3380	0.0015	V	T. Arranz	0.0001
WZ Cep	58007.6503	71787	–0.1807	V	N. Simmons	0.0001	β Lyr	57932.92	691	2.34	R	G. Samolyk	0.02
XX Cep	58031.6934	5644	0.0199	V	G. Samolyk	0.0002	β Lyr	57932.94	691	2.35	V	G. Samolyk	0.02
ZZ Cep	58080.6939	14078	–0.0175	V	S. Cook	0.0008	β Lyr	57932.94	691	2.36	B	G. Samolyk	0.02
ZZ Cep	58093.5445	14084	–0.0177	V	G. Samolyk	0.0001	β Lyr	57939.32	691.5	2.27	V	G. Samolyk	0.03
DK Cep	57997.6924	24756	0.0306	V	G. Samolyk	0.0001	β Lyr	57939.34	691.5	2.29	R	G. Samolyk	0.02
V731 Cep	58031.6900	315.5	0.2227	V	G. Samolyk	0.0002	β Lyr	57939.37	691.5	2.32	B	G. Samolyk	0.02
SS Cet	58067.7448	5251	0.0678	V	G. Samolyk	0.0001	BB Mon	58090.8907	42868	–0.0043	V	G. Samolyk	0.0001
TT Cet	58083.7357	52552	–0.0803	V	G. Samolyk	0.0001	BO Mon	58093.8921	6555	–0.0174	V	G. Samolyk	0.0001
TW Cet	58046.7417	49466	–0.0324	V	G. Samolyk	0.0001	V508 Oph	57986.3619	37425	–0.0265	R	L. Corp	0.0001
TW Cet	58086.6642	49592	–0.0332	V	G. Samolyk	0.0003	EF Ori	58081.8253	3539	0.0090	V	G. Samolyk	0.0003
TX Cet	58035.7663	20184	0.0124	V	G. Samolyk	0.0002	EQ Ori	58081.7823	15259	–0.0445	V	G. Samolyk	0.0001
VY Cet	57769.4664	15461	–0.0007	V	G. Silvis	0.0001	ER Ori	58044.8949	38777.5	0.1368	V	G. Samolyk	0.0001
RZ Com	58132.9544	68818.5	0.0567	V	G. Samolyk	0.0002	ET Ori	58132.6703	33071	–0.0039	V	G. Samolyk	0.0001
SS Com	58114.9240	80213.5	0.9309	V	G. Samolyk	0.0003	FH Ori	58046.8614	14944	–0.4606	V	G. Samolyk	0.0002
SS Com	58128.9605	80247.5	0.9325	V	K. Menzies	0.0002	FR Ori	58031.9021	34161	0.0402	V	G. Samolyk	0.0001
CC Com	58120.9672	84225.5	–0.0281	V	K. Menzies	0.0001	FT Ori	58045.9043	5300	0.0217	V	K. Menzies	0.0001
CC Com	58145.9047	84338.5	–0.0281	V	K. Menzies	0.0001	FZ Ori	58083.7548	35149.5	–0.0325	V	G. Samolyk	0.0002
TW CrB	57940.7251	34035	0.0553	V	S. Cook	0.0005	GU Ori	58046.9078	31820	–0.0646	V	G. Samolyk	0.0002
V Crt	57424.8135	22830	–0.0030	V	G. Samolyk	0.0001	GU Ori	58066.9111	31862.5	–0.0653	V	K. Menzies	0.0001
Y Cyg	58019.6090	16208.5	0.1296	V	N. Simmons	0.0001	U Peg	58039.6968	57442	–0.1668	V	K. Menzies	0.0001
BR Cyg	58000.6317	12353	0.0014	V	G. Samolyk	0.0001	U Peg	58041.3844	57446.5	–0.1658	V	L. Corp	0.0001
CG Cyg	58085.5142	29566	0.0773	V	K. Menzies	0.0001	U Peg	58081.6736	57554	–0.1656	V	S. Cook	0.0007
V704 Cyg	58079.5911	35290	0.0379	V	G. Samolyk	0.0002	U Peg	58083.5466	57559	–0.1665	V	G. Samolyk	0.0001
V836 Cyg	58005.3940	20128	0.0229	V	T. Arranz	0.0001	TY Peg	58067.7215	5697	–0.4398	V	G. Samolyk	0.0002
V836 Cyg	58020.4224	20151	0.0229	V	T. Arranz	0.0001	UX Peg	58035.6516	11401	–0.0058	V	G. Samolyk	0.0001
V836 Cyg	58039.3709	20180	0.0224	V	T. Arranz	0.0001	UX Peg	58083.5346	11432	–0.0059	V	G. Samolyk	0.0001
V836 Cyg	58056.3597	20206	0.0225	V	T. Arranz	0.0001	BX Peg	58020.5559	49302	–0.1275	V	K. Menzies	0.0001
V836 Cyg	58073.3487	20232	0.0228	V	T. Arranz	0.0001	BX Peg	58030.6519	49338	–0.1266	V	K. Menzies	0.0001
V1034 Cyg	57970.5086	15387	0.0123	V	L. Corp	0.0003	DI Peg	58114.5481	18148	0.0088	V	G. Samolyk	0.0001
V1034 Cyg	58052.5738	15471	0.0153	V	G. Samolyk	0.0002	GP Peg	58115.4866	17299	–0.0555	V	K. Menzies	0.0001
FZ Del	58065.5329	34143	–0.0239	V	G. Samolyk	0.0001	Z Per	58079.7556	4064	–0.3194	V	G. Samolyk	0.0001
TZ Eri	58139.6045	6034	0.3435	V	G. Samolyk	0.0001	RT Per	58030.8622	29026	0.1102	V	K. Menzies	0.0001
YY Eri	58043.8938	51205	0.1619	V	G. Samolyk	0.0001	RT Per	58077.5795	29081	0.1105	V	G. Samolyk	0.0001
YY Eri	58148.5422	51530.5	0.1639	V	G. Samolyk	0.0001	RT Per	58093.7186	29100	0.1110	V	G. Samolyk	0.0001
SX Gem	58082.8912	28570	–0.0547	SG	K. Menzies	0.0001	RT Per	58116.6521	29127	0.1107	V	S. Cook	0.0003
TX Gem	58135.7627	13674	–0.0407	V	G. Samolyk	0.0001	RV Per	58067.7315	8118	0.0057	V	G. Samolyk	0.0001
WW Gem	58137.6616	25976	0.0261	V	G. Samolyk	0.0001	RV Per	58148.6434	8159	0.0044	V	G. Samolyk	0.0002
AF Gem	58086.9272	24869	–0.0703	V	G. Samolyk	0.0001	ST Per	58085.7179	5909	0.3166	V	G. Samolyk	0.0002
AF Gem	58136.6655	24909	–0.0722	V	G. Samolyk	0.0001	XZ Per	58070.9673	12646	–0.0752	V	G. Samolyk	0.0001
AL Gem	58081.8410	22825	0.0930	V	G. Samolyk	0.0001	XZ Per	58106.6679	12677	–0.0753	V	S. Cook	0.0005
UX Her	58001.5794	11834	0.1348	V	K. Menzies	0.0001	XZ Per	58114.7297	12684	–0.0749	V	G. Samolyk	0.0001
WY Hya	58122.8393	24513.5	0.0385	V	G. Samolyk	0.0001	IT Per	58029.8308	18678	–0.0454	V	K. Menzies	0.0002
DF Hya	58079.9279	46255	0.0069	V	G. Samolyk	0.0001	IT Per	58054.3760	18694	–0.0398	TG	I. Megson	0.0004
DF Hya	58083.8954	46267	0.0071	V	N. Simmons	0.0001	IU Per	58114.5823	14589	0.0071	V	G. Samolyk	0.0002
DI Hya	58101.9317	43773	–0.0402	V	G. Samolyk	0.0001	KW Per	58044.8417	16795	0.0175	V	K. Menzies	0.0001
DK Hya	58131.8200	29292	0.0009	V	G. Samolyk	0.0001	KW Per	58086.7491	16840	0.0182	V	G. Samolyk	0.0001
SW Lac	58027.4548	39761	–0.0766	V	T. Arranz	0.0001	V432 Per	57997.8295	68809.5	0.0295	V	G. Samolyk	0.0002
SW Lac	58038.3599	39795	–0.0760	V	L. Corp	0.0001	V432 Per	58028.8776	68906	0.0512	V	K. Menzies	0.0001
SW Lac	58045.5748	39817.5	–0.0773	V	K. Menzies	0.0001	V432 Per	58030.7946	68912	0.0391	V	K. Menzies	0.0001
AW Lac	58066.5169	27512	0.2112	V	K. Menzies	0.0001	V432 Per	58077.5573	69057.5	0.0211	V	G. Samolyk	0.0001
CM Lac	58001.6743	19303	–0.0037	V	K. Menzies	0.0001	V432 Per	58128.5400	69216	0.0433	V	K. Menzies	0.0003
CM Lac	58025.7445	19318	–0.0038	V	K. Menzies	0.0001	β Per	58065.6732	4333	0.1302	V	G. Samolyk	0.0001
CO Lac	58046.6570	19785	0.0088	V	G. Samolyk	0.0001	Y Psc	58088.6084	3307	–0.0241	V	G. Samolyk	0.0001
CO Lac	58107.5523	19824.5	–0.0131	V	G. Samolyk	0.0001	RV Psc	58009.8061	60702	–0.0629	V	K. Menzies	0.0001

Table continued on following pages

Table 1. Recent times of minima of stars in the AAVSO eclipsing binary program, cont.

Star	JD (min) Hel. 2400000 +	Cycle	O–C (day)	F	Observer	Error (day)	Star	JD (min) Hel. 2400000 +	Cycle	O–C (day)	F	Observer	Error (day)
RV Psc	58025.8720	60731	–0.0627	V	K. Menzies	0.0001	V Tri	57997.8062	57285	–0.0073	V	G. Samolyk	0.0003
RV Psc	58090.6891	60848	–0.0626	V	G. Samolyk	0.0001	V Tri	58021.7999	57326	–0.0071	V	K. Menzies	0.0001
VZ Psc	58034.3645	54360.5	0.0027	V	L. Corp	0.0003	X Tri	58026.7877	15979	–0.0943	V	G. Samolyk	0.0001
VZ Psc	58034.4947	54361	0.0023	V	L. Corp	0.0003	X Tri	58034.5599	15987	–0.0943	V	T. Arranz	0.0001
ET Psc	58054.6918	12354	–0.0057	V	K. Menzies	0.0001	X Tri	58035.5314	15988	–0.0944	V	T. Arranz	0.0001
UZ Pup	58119.7991	16992	–0.0108	V	G. Samolyk	0.0001	X Tri	58036.5028	15989	–0.0945	V	T. Arranz	0.0001
AV Pup	58135.7783	48455	0.2459	V	G. Samolyk	0.0001	X Tri	58037.4746	15990	–0.0942	V	T. Arranz	0.0001
RW Tau	58107.6897	4487	–0.2796	V	G. Samolyk	0.0001	X Tri	58072.4496	16026	–0.0945	V	T. Arranz	0.0001
RW Tau	58132.6080	4496	–0.2809	V	K. Menzies	0.0001	X Tri	58107.4246	16062	–0.0948	V	T. Arranz	0.0001
RW Tau	58132.6081	4496	–0.2808	V	G. Samolyk	0.0001	X Tri	58108.3957	16063	–0.0952	V	T. Arranz	0.0001
RZ Tau	58031.8282	48969	0.0868	V	G. Samolyk	0.0002	X Tri	58137.5414	16093	–0.0956	V	G. Samolyk	0.0001
RZ Tau	58135.5400	49218.5	0.0878	V	G. Samolyk	0.0001	X Tri	58137.5415	16093	–0.0955	V	K. Menzies	0.0001
TY Tau	58046.8429	34208	0.2710	V	G. Samolyk	0.0002	RV Tri	58024.8530	15911	–0.0424	V	R. Sabo	0.0001
TY Tau	58086.7067	34245	0.2726	V	G. Samolyk	0.0002	W UMa	58104.8822	36984	–0.1052	V	K. Menzies	0.0001
WY Tau	58043.7516	29796	0.0643	V	G. Samolyk	0.0002	TX UMa	58148.8689	4293	0.2398	V	G. Samolyk	0.0001
WY Tau	58136.5812	29930	0.0643	V	G. Samolyk	0.0009	VV UMa	58102.8664	17876	–0.0750	V	K. Menzies	0.0001
AC Tau	58119.6188	6109	0.1670	V	G. Samolyk	0.0002	VV UMa	58104.9286	17879	–0.0749	V	K. Menzies	0.0001
AQ Tau	58047.8793	23351	0.5310	V	K. Menzies	0.0001	XZ UMa	58079.7886	9745	–0.1458	V	G. Samolyk	0.0001
CT Tau	58066.7323	18989	–0.0673	V	K. Menzies	0.0001	AH Vir	58114.8822	30183	0.2909	V	G. Samolyk	0.0001
CT Tau	58094.7381	19031	–0.0683	V	K. Menzies	0.0001	AH Vir	58145.8532	30259	0.2903	V	K. Menzies	0.0002
CT Tau	58114.7437	19061	–0.0676	V	K. Menzies	0.0001	Z Vul	58013.3935	6137	–0.0142	V	T. Arranz	0.0001
EQ Tau	58009.8334	52136	–0.0360	V	K. Menzies	0.0001	Z Vul	58040.3980	6148	–0.0139	V	T. Arranz	0.0001
EQ Tau	58025.8764	52183	–0.0363	V	K. Menzies	0.0001	AX Vul	58000.6290	6493	–0.0380	V	G. Samolyk	0.0001
EQ Tau	58057.7918	52276.5	–0.0370	V	R. Sabo	0.0002	BE Vul	58003.4504	11528	0.1062	V	T. Arranz	0.0001
EQ Tau	58066.8387	52303	–0.0358	V	K. Menzies	0.0001	BE Vul	58065.5325	11568	0.1065	V	G. Samolyk	0.0001
EQ Tau	58086.6360	52361	–0.0368	V	G. Samolyk	0.0001	BS Vul	58037.6075	31023	–0.0334	V	R. Sabo	0.0001
EQ Tau	58132.5461	52495.5	–0.0380	V	G. Samolyk	0.0001	BT Vul	58043.5939	19840	0.0059	V	G. Samolyk	0.0002
HU Tau	58124.6813	8194	0.0397	V	G. Samolyk	0.0001	BT Vul	58067.5595	19861	0.0063	V	G. Samolyk	0.0001
V1128 Tau	58058.5148	18202	–0.0020	V	L. Corp	0.0002	BU Vul	58067.5380	43118	0.0148	V	G. Samolyk	0.0001
V1128 Tau	58075.4634	18257.5	–0.0015	V	L. Corp	0.0001	CD Vul	58035.6707	17166	–0.0010	V	G. Samolyk	0.0001
V1249 Tau	58104.6566	5466	–0.0076	V	K. Menzies	0.0002							

The Variability of Young Stellar Objects: An Update

William Herbst
Astronomy Department, Wesleyan University, Middletown, CT 06419; wherbst@wesleyan.edu

Invited review paper, received May 30, 2018

Abstract A brief update is provided on the nature of the variability of young stellar objects. The emphasis is on Type III variables, also known as UXORs or "dippers," which undergo periodic or aperiodic occultation by circumstellar material.

1. Introduction

Stars form when cold clouds of gas and dust in the galaxy become gravitationally unstable and collapse, over hundreds of thousands to millions of years, to a dense central object with a surrounding "circumstellar" (CS) or "circumbinary" (CB) disk. Initially, a star's main energy source is gravitational energy, released as it collapses and heats. Eventually the star is hot enough at its core to begin turning hydrogen into helium via nuclear fusion reactions. At this point the star settles into its stable "main sequence" phase and is generally constant in its light output at a level of 0.01 mag or less. Before it gets to that point it is known as a "pre-main sequence" (PMS) star. For a star like the sun this can last 30–50 million years so there are many such objects within reach of small telescopes. They have not had time to move far from their birth sites so they cluster in regions of high gas and dust density, such as the Orion nebula or the Taurus dark clouds.

PMS stars are universally variables, for a variety of reasons—see the review by Herbst (2012) for more detail. Since they are still clustered within their nebulous birth-gas clouds, they were originally called "nebular variables." As young stars, they spin 2 to 20 times faster than the Sun and have highly convective interiors. This combination of factors generates intense magnetic fields at their surfaces. They commonly have huge spots, analogous to sunspots but covering 10% or more of their photospheres. The growth and decay of these spots results in irregular variability on a timescale of months to years, while stellar rotation imprints a periodic variation of typically 2 to 10 days. This is referred to as Type I variability (Herbst *et al.* 1994) and can reach amplitudes of 0.5 mag or larger, although <0.1 mag is most common.

The very youngest PMS stars, those with ages under 1–10 million years or so, depending on mass, have not had time to fully dissipate their surrounding disk, either by accreting it, blowing it away with stellar winds, or condensing it into planets. In these objects, gas continues to spiral in towards the star, where it encounters an intense "magnetosphere" stretching up to 10 stellar radii from the surface. In this highly magnetized zone, gas is ionized and then levitated out of the disk to crash down onto the star's surface within polar rings, analogous to auroral rings on Earth. The energy released by this accretion drives sporadic variability of these stars on a timescale of hours to days. This is referred to as Type II variability and can reach amplitudes of 1 or 2 mag in some cases, although it is commonly much less than that (<0.1 mag). An extreme form of accretion variability is exhibited by a rare class of PMS stars known as FUORs, named after the prototype FU Ori (Herbig 1977). These objects show brightness increases of many magnitudes lasting for months or years followed by a slow decline to their original levels. This is attributed to a relatively brief period of substantially enhanced accretion, the cause of which remains uncertain.

A third type of PMS variability is also limited to those objects still young enough to be embedded in CS or CB disks, but in this case it is not accretion, but occultation, of the central star by matter within the disk, that causes the observed variations. Stars of this type are characterized by rather sudden fades in brightness that occur when some piece of CS material blocks all or part of their stellar photosphere from our vantage point here on Earth. In addition to being called Type III variables, these objects are also known as UXORs (after UX Ori) and "dippers," because of their brightness dips (Stauffer *et al.* 2015). Normally the variations are aperiodic and unpredictable, but some, such as AA Tau and V582 Mon (also known as KH 15D), are periodic. In the author's opinion, these are the most interesting objects to monitor and one place where AAVSO observers can continue to make important contributions to the study of PMS variables.

2. Observing Type III pre-main sequence stars

While it is generally agreed that the variations of Type III PMS stars are caused by occultation, since their spectral types do not change even as they fade by several magnitudes, the details of the process are far from understood. A basic issue is—what causes the opacity. Hydrogen and helium gas are normally transparent at optical wavelengths (unless hot and dense) so opacity is usually attributed to dust embedded within the gas. But dust cannot survive too close to a star. It should be vaporized within the magnetosphere, so if it is sheets of gas levitated by magnetic fields within the magnetosphere that are occulting the stellar surface the opacity may come from the hot, dense gas itself, not the dust. On the other hand, far from the star, only dust seems capable of blocking the starlight, but why is the dust so non-uniformly distributed? Some astronomers have suggested that the obscuring material is in the form of giant comets that occult the stars as they orbit them. Others have suggested warps in the accretion disk, which pass over the star like waves—sometimes periodically. Another possibility is that protoplanets in the disk could have large envelopes of dust around them and could periodically pass in front of the stars, causing the fades (Stauffer *et al.* 2018). In the case of CB disks, it can actually be the stars that are moving relative to the dust,

that causes the brightness variations. V582 Mon is an excellent example of this (Aronow *et al.* 2018).

There are several features of Type III PMS objects that serve to make them particularly suitable for the attention of AAVSO observers. Important representatives of the class are sufficiently bright to be readily accessible to small telescopes. These include T Ori, SU Aur, BF Ori, CO Ori, and UX Ori, to mention a few. A more exhaustive list is provided in Herbst *et al.* (1994). The amplitude of variation is often quite large in these stars, sometimes exceeding one or two magnitudes, and the exact cause of the behaviors is still poorly described and understood, as noted above. That said, the simple observation of brightness through a single filter versus time will not do much to advance our understanding of the objects. What is needed is either multiple filters or a coordinated campaign of spectral and photometric monitoring or, ideally, both. To address the opacity issue one needs to know the wavelength dependence of the variations. Small dust grains cause a star to redden as it fades. Gas opacity from hot H gas, for example, has a distinctive spectral signature that includes a sharp break at about 360 nm, where the Balmer continuum begins. This kind of monitoring is clearly for advanced amateurs with a variety of filters and knowledge of CCD reduction techniques. B. Staels (2018) has recently been involved with multicolor monitoring of one of these objects—SU Aur—and has discovered one of the deepest dips ever recorded. There is much fertile ground for exploration here, if one has the advanced capabilities required.

A second kind of project that may interest a wider group of, still advanced, AAVSO observers is checking on PMS stars of all types that have been observed over the decades to see if they are still varying within their known ranges, or whether they have moved outside of those ranges. The actual time scales on which PMS stars change may be rather long compared to human lifetimes or to the time over which we have reasonably accurate records of their brightness. We mentioned above the FU Ori type of accretion variables and an FU Ori-type event could strike any PMS star, without warning. It is important to quantify the occurrence of large accretion outbursts on time scales much longer than has been possible so far. Simply comparing images of star forming clusters (e.g. fields in the Orion nebula and the Taurus dark clouds containing multiple PMS stars) with images taken years ago (e.g. in one of the well-known surveys such as the Palomar Sky Survey, most of which have now been digitized and are available on-line) could be a productive enterprise. Sometimes PMS stars completely change the nature of their variability and such changes may go unnoticed by professional astronomers for a long time. Famous examples include the illumination of a new nebula by a FUOR outburst in a dark cloud in Orion by an amateur astronomer (McNeil *et al.* 2004), long-term changes in the variability of the namesake of PMS variables, T Tau (Beck and Simon 2001), and the dramatic long-term changes exhibited by V582 Mon (Aronow *et al.* 2018). An interesting lesser-known example is CB 34V (Alves *et al.* 1997; Tackett *et al.* 2003) which transitioned from Type III to Type I variability.

One of the challenges for observers of PMS stars is that they are often located in young clusters, which can make it difficult to identify likely non-variable stars to serve as local flux standards. An important new resource, now available on-line to AAVSO observers and, indeed, anyone is the GAIA satellite database from the European Space Agency's (ESA) mission. These data, available at URL: https://www.cosmos.esa.int/gaia, were processed by the Gaia Data Processing and Analysis Consortium (see URL: http://gea.esac.esa.int/archive/). This extraordinary survey of about 1 billion stars provides important basic information including distance, average brightness, and a variability index. With this information one can easily look for non-variable comparison stars that are unlikely, based on their distances, to be PMS members of a young cluster. One can also, of course, find basic information on essentially every star visible on one's CCD image—a real gold mine.

3. Summary

PMS stars remain an attractive possibility for monitoring by advanced AAVSO observers with CCD equipment and knowledge of basic reduction techniques. The easiest thing to do is probably to compare recent images with older, digitized survey images to look for PMS stars that have dramatically changed their brightness levels, as some have been seen to do. Further monitoring of these cases may, then, reveal that they have completely changed the characteristics of their variability. In particular, it would be interesting to improve the statistics on the rare outbursts of FU Ori-type stars. If the Sun and other stars regularly went through such outbursts it could have an impact on our understanding of PMS disk evolution and potentially even relate to features of primitive meteorites that record early times in the solar system. Another area of interest is multi-color photometric campaigns, ideally coordinated with spectral monitoring, to study Type III PMS stars, with the hope of illuminating the cause of their variations.

References

Alves, J., Hartmann, L., Briceno, C., and Lada, C. J. 1997, *Astron. J.*, **113**, 1395.

Aronow, R. A., Herbst, W., Hughes, A. M., Wilner, D. J., and Winn, J. N. 2018, *Astron J.*, **155**, 47.

Beck, T. L., and Simon, M. 2001, *Astron. J.*, **122**, 413.

Herbig, G. H. 1977, *Astrophys. J.*, **217**, 693.

Herbst, W. 2012, *J. Amer. Assoc. Var. Star Obs.*, **40**, 448.

Herbst, W., Herbst, D. K., Grossman, E. J., and Weinstein, D. 1994, *Astron. J.*, **108**, 1906.

McNeil, J. W., Reipurth, B., and Meech, K. 2004, *IAU Circ.*, No. 8284, 1.

Staels, B. 2018, private communication.

Stauffer, J., *et al.* 2015, *Astron. J.*, **149**, 130.

Stauffer, J., *et al.* 2018, *Astron. J.*, **155**, 63.

Tackett, S., Herbst, W., and Williams, E. 2003, *Astron. J.*, **126**, 348.

Abstracts of Papers and Posters presented at the 106th Annual Meeting of the AAVSO, Held in Nashville, Tennessee, November 2–4, 2017

AAVSO Target Tool: A Web-Based Service for Tracking Variable Star Observations

Dan Burger
Keivan G. Stassun
Vanderbilt University, Department of Physics and Astronomy, 2301 Vanderbilt Place, Nashville, TN 37235; dan.burger@vanderbilt.edu

Chandler Barnes
Vanderbilt University, Department of Information Technology, 2301 Vanderbilt Place, Nashville, TN 37235

Sara Beck
Stella Kafka
AAVSO Headquarters, 49 Bay State Road, Cambridge, MA 02138

Kenneth Li
Vanderbilt University, Department of Physics and Astronomy, 2301 Vanderbilt Place, Nashville, TN 37235

Abstract The AAVSO Target Tool is a web-based interface for bringing stars in need of observation to the attention of AAVSO's network of amateur and professional astronomers. The site currently tracks over 700 targets of interest, collecting data from them on a regular basis from AAVSO's servers and sorting them based on priority. While the target tool does not require a login, users can obtain visibility times for each target by signing up and entering a telescope location. Other key features of the site include filtering by AAVSO observing section, sorting by different variable types, formatting the data for printing, and exporting the data to a CSV file. The AAVSO Target Tool builds upon seven years of experience developing web applications for astronomical data analysis, most notably on Filtergraph (Burger, D., *et al.* 2013, *Astronomical Data Analysis Software and Systems XXII*, Astronomical Society of the Pacific, San Francisco, 399), and is built using the WEB2PY web framework based on the PYTHON programming language. The target tool is available at http://filtergraph.com/aavso.

Period Variation in BW Vulpeculae

David E. Cowall
20361 Nanticoke Drive, Nanticoke, MD 21840; cowall@comcast.net

Andrew P. Odell
Department of Physics and Astronomy, Northern Arizona University, Flagstaff, AZ 86001

Abstract BW Vulpeculae (BW Vul) has the largest amplitude of the β Cephei stars. An observing campaign on this star using the AAVSOnet's Bright Star Monitor (BSM) telescopes was begun in December of 2015 and has yielded 66 nights of observations to date. A period analysis will be presented using the BSM data set in combination with unpublished data from the Lowell Observatory. Over almost 80 years of observations, BW Vul has closely followed a parabolic ephemeris (period increasing by 2.4 seconds/century) plus a light-travel-time effect. This parabola with excursions on either side also could be viewed as a sequence of straight lines (constant period) with abrupt period increases. The first paradigm predicted a necessary change in slope around 2004, which did not occur. Instead, the period decreased abruptly in 2009. That maximum occurred 250 minutes early compared to the first paradigm, and about 25 minutes early compared to the straight-line paradigm from 1982–2009.

From YY Boo (eclipsing binary) via J1407 (ringed companion) to WD 1145+017 (white dwarf with debris disk)

Franz-Josef (Josch) Hambsch
Oude Bleken 12, Mol 2400, Belgium; hambsch@telenet.be

Abstract Several years ago by accident I observed YY Boo outside of an eclipse and was very surprised to see a short term periodic variation of about 0.1 mag. That was completely unexpected and it initiated an international campaign by amateurs to identify the cause of these variations. It turned out that YY Boo showed a pulsation period of about 88 min in addition to being an Algol type eclipsing binary. Hence it turned out that YY Boo has become a new member of a class of pulsating eclipsing binary systems with, at that time, the second largest amplitude after BO Her.

Since August 2011, I have had a remote observatory (ROAD) under pristine skies in Chile. It has been a production facility since day one of operation. Via the *AAVSO Alert Notice 462* of June 25, 2012, I came to know about the interesting star 1SWASP J140747.93-394542.6 ("J1407"; V=12.3 mag), which underwent a series of deep eclipsing events during April/May 2007. The event lasted about 52 days with changes in brightness of the star by 0.5 to 3 magnitudes according to the *Alert Notice*. Nightly observations were asked for, which I started on June 27 and have continued ever since. A first paper where observations from ROAD were taken up gave a possible period in the range of 3.5 to 13.8 years. Hence the coming years will be crucial to keep up observations of this interesting object.

Finally, in 2015 I was asked by B. Gänsicke (U. Warwick) to observe the interesting object WD 1145+017. In this context I also got to know Bruce Gary who had observed this object already for some time and joined the pro-am team to contribute observations from Chile. WD 1145+017 was observed in the period 2015 November to 2016 July to characterize the transiting behavior of the white dwarf by dust clouds produced by an asteroid orbiting the star. The object was discovered by

Kepler and the observed activity was enhanced drastically during the observing period.

Keynote presentation: Looking for Zebras When There Are Only Horses

Dennis M. Conti
141 E. Bay View Drive, Annapolis, MD 21403; dennis_conti@hotmail.com

Abstract How many times have each of us thought we had made a "scientific discovery" only to realize that we were the victim of our own operational, instrumentation, or processing errors? With amateur astronomers contributing more and more to pro/am collaborations, the quality and credibility of our participation is becoming even more important.

This keynote presentation will review some of the common pitfalls in producing research-grade photometry results and will give examples of some "horses" that we thought were really "zebras." In addition, it will present some procedures and new techniques for obtaining higher precision photometry. These will be especially useful in helping amateur astronomers better identify false positives in support of the upcoming TESS exoplanet mission.

The Vega Project, Part I

Tom Calderwood
1184 NW Mt. Washington Drive, Bend, OR 97703; tjc@cantordust.net

Jim Kay
26 Steeplebush Road, Shelburne, VT 05482

Abstract Vega is a key target for spectrophotometric calibration, hence confidence in its constancy is of great importance. However, decades of claims and counter-claims in professional studies have left open the possibility that Vega is, at a significant level, a variable star. We present a plan for a new photometric study and some preliminary results.

The Exciting World of Binary Stars: Not Just Eclipses Anymore

Bert Pablo
AAVSO Headquarters, 49 Bay State Road, Cambridge, MA 02138; hpablo@aavso.org

Abstract Binary stars have always been essential to astronomy. Their periodic eclipses are the most common and efficient method for determining precise masses and radii of stars. Binaries are known for their predictability and have been observed for hundreds if not thousands of years. As such, they are often ignored by observers as uninteresting, however, nothing could be farther from the truth. In the last ten years alone the importance of binary stars, as well of our knowledge of them, has changed significantly. In this talk, I will introduce you to this new frontier of heartbeats, mergers, and evolution, while hopefully motivating a change in the collective thinking of how this unique class of objects is viewed. Most importantly, I will highlight areas in which anyone who wants can contribute to the understanding and enhancement of our astronomical knowledge base.

BV Observations of the Eclipsing Binary XZ Andromedae at the EKU Observatory

Marco Ciocca
Department of Physics and Astronomy, Eastern Kentucky State University, 521 Lancaster Avenue, New Science Building 3140, Richmond, KY 40475; marco.ciocca@eku.edu

Abstract XZ Andromedae is an Algol-type eclipsing binary. It has been the subject of many observing campaigns, all aiming at determining the mechanisms responsible for its period variation. Results have been inconsistent and the period changes did not seem to have a common explanation between authors. The latest of these observations (Y.-G. Yang, *New Astronomy*, 25, 2013, 109) concluded that a third companion may be present and that mass transfer from the secondary to the primary companion may be occurring. We performed measurements in the Bessel band passes B and V, measured several times of minimum and developed a model, using BINARY MAKER 3, that matches well the observations and includes mass transfer by adding a hot spot on the primary (the cool, more evolved companion) and a "cold" spot on the secondary (hotter, but smaller companion). The data were collected at the EKU observatory with a Celestron C14 telescope and a SBIG STL-6303 camera.

Nova Eruptions from Radio to Gamma-rays—with AAVSO Data in the Middle

Koji Mukai
Stella Kafka
Laura Chomiuk
Ray Li
Tom Finzell
Justin Linford
Jeno Sokoloski
Tommy Nelson
Michael Rupen
Amy Mioduszewski
Jennifer Weston

Address correspondence to: Goddard Space Flight Center, National Aeronautics and Space Administration, Greenbelt, MD 20771; koji.mukai@nasa.gov

Abstract Novae are among the longest-known class of optical transients. In recent years, V1369 Cen in the south reached magnitude 3.3 in late 2013, and had repeated (but not periodic) cycles of re-brightening. Earlier in 2013, V339 Del almost reached magnitude 4.0 during the northern summer. An expanding ball of gas, at about 10,000 K, expelled by a nuclear explosion on the surface of a white dwarf, can explain much of the visible light outputs of novae. But these spectacular visible light displays turn out to be just a small part of the show. Novae are also transient objects in the radio through gamma-rays—in addition to the warm, visible light-emitting gas, we need cold dust particles that emit in the infra-red, 10 million degree shock-

heated gas that emits hard X-rays, and the exposed surface of the nuclear-burning white dwarf that emits soft X-rays. Last but not least, we need an exotic process of particle acceleration to explain the gamma-rays and some radio data.

In recent years, using data from satellites (such as Swift) and ground-based telescopes (including the Jansky VLA), we have made significant progress cataloging and understanding the messy process of mass ejection in novae. But we still know very little about exactly how novae produce gamma-rays. We plan to collect more gamma-ray data using the Fermi satellite over the next several years, of course continue our multi-wavelength observations from the radio to the X-rays as well.

For that, we need the AAVSO community to (1) discover novae, as early as possible, and alert us; and (2) monitor novae, particularly brighter ones that are suitable for gamma-ray observations. Even in the era of ASAS-SN and other professional surveys, amateur astronomers are competitive in terms of nova discovery. Once discovered, the sheer number of small telescopes operated by the AAVSO community will provide the optical light curves and, increasingly, optical spectra that are the centerpiece of any study of novae.

Transits, Spots, and Eclipses: The Sun's Role in Pedagogy and Outreach

Kristine Larsen
Central Connecticut State University, 1615 Stanley Street, New Britain, CT 06050; larsen@ccsu.edu

Abstract While most people observe variable stars at night, the observers of the AAVSO Solar Section make a single observation per day, but only if it is sunny, because our variable is the Sun itself. While the Sun can play an important role in astronomy outreach and pedagogy in general, as demonstrated by the recent 2017 eclipse, it can also serve as an ambassador for variable stars. This talk will examine how our sun can be used as a tool to explain several types of variable star behaviors, including transits, spots, and eclipses.

Observations of Transiting Exoplanet Candidates Using BYU Facilities

Michael D. Joner
Eric G. Hintz
Denise C. Stephens
Brigham Young University, Department of Physics and Astronomy, N488 ESC, Provo, UT 84602; xxcygni@gmail.com

Abstract During the past five years, faculty and student observers at Brigham Young University have actively participated in observations of candidate objects as part of the follow-up network of observers for the KELT transiting exoplanet survey. These observations have made use of several small telescopes at the main campus Orson Pratt Observatory and adjacent observing deck, as well as the more remote West Mountain Observatory. Examples will be presented in this report to illustrate the wide variety of objects that have been encountered while securing observations for the KELT Follow-up Network. Many of these observations have contributed to publications that include both faculty and student researchers as coauthors.

PYTHON for Variable Star Astronomy

Matt Craig
Minnesota State University, Moorhead, Department of Physics and Astronomy, 1104 7th Avenue South, Moorhead, MN 56563; mcraig@mnstate.edu

Abstract Open source PYTHON packages that are useful for data reduction, photometry, and other tasks relevant to variable star astronomy have been developed over the last three to four years as part of the Astropy project. Using this software, it is relatively straightforward to reduce images, automatically detect sources, and match them to catalogs. Over the last year browser-based tools for performing some of those tasks have been developed that minimize or eliminate the need to write any of your own code. After providing an overview of the current state of the software, an application that calculates transformation coefficients on a frame-by-frame basis by matching stars in an image to the APASS catalog will be described.

Detecting Moving Sources in Astronomical Images

Andy Block
Minnesota State University, Moorhead, Department of Physics and Astronomy, 1104 7th Avenue South, Moorhead, MN 56563; mcraig@mnstate.edu

Abstract Source detection in images is an important part of analyzing astronomical data. This project discusses an implementation of image detection in PYTHON, as well as processes for performing photometry in PYTHON. Application of these tools to looking for moving sources is also discussed.

Variable Stars in the Field of TrES-3b

Erin Aadland
Minnesota State University, Moorhead, Department of Physics and Astronomy, 1104 7th Avenue South, Moorhead, MN 56563; mcraig@mnstate.edu

Abstract The star field around the exoplanet TrES-3b has potential for finding unknown variable stars. The field was observed over several nights using Minnesota State University Moorhead's Feder Observatory. A light curve for each star was created and are being evaluated for variability and periodicity. A PYTHON program is in development to help complete the analysis by automating some of the process. Several stars in the field appear to be variable and are being further analyzed to determine a period and to classify the type of variable.

Calculating Galactic Distances Through Supernova Light Curve Analysis

Jane Glanzer
Minnesota State University, Moorhead, Department of Physics and Astronomy, 1104 7th Avenue South, Moorhead, MN 56563; mcraig@mnstate.edu

Abstract The purpose of this project is to experimentally determine the distance to the galaxy M101 by using data that were taken on the type Ia supernova SN 2011fe at the Paul P. Feder Observatory. Type Ia supernovae are useful for determining distances in astronomy because they all have roughly the same luminosity at the peak of their outburst. Comparing the apparent magnitude to the absolute magnitude allows a measurement of the distance. The absolute magnitude is estimated in two ways: using an empirical relationship from the literature between the rate of decline and the absolute magnitude, and using sncosmo, a PYTHON package used for supernova light curve analysis that fits model light curves to the photometric data.

Discovery of KPS-1b, a Transiting Hot-Jupiter, with an Amateur Telescope Setup

Paul Benni
3 Concetta Circle, Acton, MA 01720; pbenni@verizon.net

Artem Burdanov
Vadim Krushinsky
Eugene Sokov
Space Sciences, Technologies and Astrophysics Research (STAR) Institute at the University of Liege; Artem.Burdanov@uliege.be

Abstract Using readily available amateur equipment, a wide-field telescope (Celestron RASA, 279 mm f/2.2) coupled with a SBIG ST-8300M camera was set up at a private residence in a fairly light polluted suburban town thirty miles outside of Boston, Massachusetts. This telescope participated in the Kourovka Planet Search (KPS) prototype survey, along with a MASTER-II Ural wide field telescope near Yekaterinburg, Russia. One goal was to determine if higher resolution imaging (~2 arcsec/pixel) with much lower sky coverage can practically detect exoplanet transits compared to the successful very wide-field exoplanet surveys (KELT, XO, WASP, HATnet, TrES, Qatar, etc.) which used an array of small aperture telescopes coupled to CCDs.

The RASA telescope was pointed in the direction of HIP 53535 in Ursa Major and stared at the same point in the sky every clear night from January to April 2015. The image field of view was 1.67 × 1.25 degrees, with drift corrected by autoguiding. Image exposures were 50 seconds, taken with a R_c filter. About 115 hours of data were collected and processed by K-PIPE data reduction pipeline software, consisting of sequential scripts for astrometry, instrumentation + differential photometry, and Box-fitting Least Squares (BLS) periodic transit search.

Rather serendipitously, a 13.0 magnitude star (GSC0414800138, 2MASS 11004017+6457504 at coordinates R.A. $11^h\ 00^m\ 40.150^s$, Dec. +64° 57' 50.09") with periodic 10 mmag transits was detected. Follow-up with a narrow-field telescope (Celestron 1100 EdgeHD with SBIG ST-8XME camera) confirmed the transits were real and also achromatic with different filters. The Hot-Jupiter exoplanet was validated by RV measurements from the SOPHIE spectrograph. KPS-1b is similar in mass and radius to Jupiter ($M_p = 1.14 \pm 0.15\ M_{jup}$, $R_p = 0.96 \pm 0.10\ R_{jup}$) and has an orbital period of 1.70645 ± 0.00004 days. The host star is similar to our sun with mass and radius ($M^* = 0.93 \pm 0.07\ M_\odot$, $R^* = 0.96 \pm 0.08\ R_\odot$).

From this initial success, the RASA telescope was upgraded with a larger CCD size camera, and multi-field imaging capability was added to increase the survey field of view to 8.0 × 2.5 degrees. With this setup, the Galactic Plane Exoplanet Survey (GPX) was started to survey high-density star fields of the Milky Way. Over the past year, several high quality exoplanet candidates were identified and are awaiting validation.

Searching for Variable Stars in the SDSS Calibration Fields

J. Allyn Smith
Melissa Butner
Douglas Tucker
Sahar Allam
Austin Peay State University Department of Physics, Engineering, and Astronomy, P. O. Box 4608, Clarksville TN 37044; smithj@apsu.edu

Abstract We are searching the Sloan Digital Sky Survey (SDSS) calibration fields for variable stars. This long neglected data set, taken with a 0.5-m telescope, contains nearly 200,000 stars in more than 100 fields which were observed over the course of 8+ years during the observing portion of the SDSS-I and SDSS-II surveys. During the course of the survey, each field was visited from ~10 to several thousand times, so our initial pass is just to identify potential variable stars. Our initial "quick-look" effort shows several thousand potential candidates and includes at least one nearby supernova. We present our plans for a follow-up observational program for further identification of variable types and period determinations.

Searching for Variable Stars in the Field of Dolidze 35

Jamin Welch
J. Allyn Smith
Austin Peay State University Department of Physics, Engineering, and Astronomy, P. O. Box 4608, Clarksville TN 37044; smithj@apsu.edu

Abstract We are conducting a study of the open cluster Dolidze-35. We have a data set which contains several nights and spans four years. One step of our survey is to search these data to identify candidate local standards and potential variable stars. We present early results of the variable search effort.

A Search for Variable Stars in Ruprecht 134

Rachid El Hamri
Mel Blake
University of North Alabama, Physics and Earth Science Department, Box 5065, Florence, AL 35632; rmblake@una.edu

Abstract Contact binary stars have been found in many old open clusters. These stars are useful for obtaining the distances to these star clusters and for understanding the stellar populations and evolution of the old clusters. Ruprecht 134 is a relatively neglected, old open cluster with an age of about 1 Gyr. We have obtained observations of Ruprecht 134 using the 1-meter telescope at Cerro Tololo Interamerican Observatory for the purpose of identifying candidate contact binaries. We present the preliminary results of this search and discuss future observations.

Erratum: Sloan Magnitudes for the Brightest Stars

Anthony Mallama
14012 Lancaster Lane, Bowie, MD 20715; anthony.mallama@gmail.com

In the article "Sloan Magnitudes for the Brightest Stars" (*JAAVSO*, 2014, **42**, 443), Equation 3 in section A.1. of the Appendix is incorrect; the coefficient of ((R–I) – C1) should be 0.935, rather than 0.953. The mean differences between the new and old results are 0.00 in all cases, and the standard deviations are all 0.00 or 0.01, which is less than the photometric uncertainties of the Johnson or Sloan values. A revised version of the catalog has been published at https://arxiv.org/abs/1805.09324. The revision is proposed as a bright star extension to the APASS database.